

Designing Scaffolds for Directed Cell Response in Tissue Engineering Scaffolds
Fabricated by Vat Photopolymerization

Nicholas A. Chartrain

Dissertation submitted to the faculty of the Virginia Polytechnic Institute and State
University in partial fulfillment of the requirements for the degree of

Doctor of Philosophy
In
Materials Science and Engineering

Christopher B. Williams, Co-Chair
Abby R. Whittington, Co-Chair
Timothy E. Long
E. Johan Foster
Rayne X. Zheng

10 June 2019
Blacksburg, VA

Keywords: Additive Manufacturing, 3D Printing, Tissue Engineering,
Regenerative Medicine, Biomaterials

Copyright 2019 Nicholas A. Chartrain

Designing Scaffolds for Directed Cell Response in Tissue Engineering Scaffolds
Fabricated by Vat Photopolymerization

Nicholas A. Chartrain

ABSTRACT

Vat photopolymerization (VP) is an additive manufacturing (AM) technology that permits the fabrication of parts with complex geometries and feature sizes as small as a few microns. These attributes make VP an attractive option for the fabrication of scaffolds for tissue engineering. However, there are few printable materials with low cytotoxicity that encourage cellular adhesion. In addition, these resins are not readily available and must be synthesized. A novel resin based on 2-acrylamido-2-methyl-1-propanesulfonic acid (NaAMPS) and poly(ethylene glycol) diacrylate (PEGDA) was formulated and printed using VP. The mechanical properties, water content, and high fidelity of the scaffold indicated promise for use in tissue engineering applications. Murine fibroblasts were observed to successfully adhere and proliferate on the scaffolds.

The growth, migration, and differentiation of a cell is known to dependent heavily on its microenvironment. In engineered constructs, much of this microenvironment is provided by the tissue scaffold. The physical environment results from the scaffold's geometrical features, including pore shape and size, porosity, and overall dimensions. Each of these parameters are known to affect cell viability and proliferation, but due to the difficulty of isolating each parameter when using scaffold fabrication techniques such as porogen leaching and gas foaming, conflicting results have been reported. Scaffolds with pore sizes ranging from 200 to 600 μm were fabricated and seeded with murine fibroblasts. Other geometric parameters (e.g., pore shape) remained consistent between scaffold

designs. Inhomogeneous cell distributions and fewer total cells were observed in scaffolds with smaller pore sizes (200-400 μm). Scaffolds with larger pores had higher cell densities that were homogeneously distributed. These data suggest that tissue scaffolds intended to promote fibroblast proliferation should be designed to have pore at least 500 μm in diameter.

Techniques developed for selective placement of dissimilar materials within a single VP scaffold enabled spatial control over cellular adhesion and proliferation. The multi-material scaffolds were fabricated using an unmodified and commercially available VP system. The material preferences of murine fibroblasts which resulted in their inhomogeneous distribution within multi-material scaffolds were confirmed with multiple resins and geometries. These results suggest that multi-material tissue scaffolds fabricated with VP could enable multiscale organization of cells and material into engineered constructs that would mimic the function of native tissue.

Designing Scaffolds for Directed Cell Response in Tissue Engineering Scaffolds
Fabricated by Vat Photopolymerization

Nicholas A. Chartrain

GENERAL AUDIENCE ABSTRACT

Vat photopolymerization (VP) is a 3D printing (or additive manufacturing) technology that is capable of fabricating parts with complex geometries with very high resolution. These features make VP an attractive option for the fabrication of scaffolds that have applications in tissue engineering. However, there are few printable materials that are biocompatible and allow cells attachment. In addition, those that have been reported cannot be obtained commercially and their synthesis requires substantial resources and expertise. A novel resin composition formulated from commercially available components was developed, characterized, and printed. Scaffolds were printed with high fidelity. The scaffolds had mechanical properties and water contents that suggested they might be suitable for use in tissue engineering. Fibroblast cells were seeded on the scaffolds and successfully adhered and proliferated on the scaffolds.

The growth, migration, and differentiation of cells is influenced by the environmental stimuli they experience. In engineered constructs, the scaffold provides many of stimuli. The geometrical features of scaffolds, including how porous they are, the size and shape of their pores, and their overall size are known to affect cell growth. However, scaffolds that have a variety of pore sizes but identical pore shapes, porosities, and other geometric parameters cannot be fabricated with techniques such as porogen leaching and gas foaming. This has resulted in conflicting reports of optimal pore sizes. In this work, several scaffolds with identical pore shapes and porosities but pore sizes ranging from 200 μm to 600 μm were designed and printed using VP. After seeding with cells,

scaffolds with large pores (500-600 μm) had a large number of evenly distributed cells while smaller pores resulted in fewer cells that were unevenly distributed. These results suggest that larger pore sizes are most beneficial for culturing fibroblasts.

Multi-material tissue scaffolds were fabricated with VP by selectively photocuring two materials into a single part. The scaffolds, which were printed on an unmodified and commercially available VP system, were seeded with cells. The cells were observed to have attached and grown in much larger numbers in certain regions of the scaffolds which corresponded to regions built from a particular resin. By selectively patterning more than one material in the scaffold, cells could be directed towards certain regions and away from others. The ability to control the location of cells suggests that these printing techniques could be used to organize cells and materials in complex ways reminiscent of native tissue. The organization of these cells might then allow the engineered construct to mimic the function of a native tissue.

DEDICATION

To my parents and brother.

ACKNOWLEDGEMENTS

Thank you to my two co-advisors, Prof. Abby Whittington and Prof. Christopher Williams, for providing me with exciting research opportunities, sage guidance, and encouragement. Prof. Hod Lipson and Jeff Lipton for kindling my interest in Additive Manufacturing at Cornell University ten years ago. Prof. Timothy Long for lending his expertise in polymer chemistry and readiness to pursue exciting new projects.

Thank you to a seemingly countless number of graduate students, post-docs, and collaborators who I have worked with over the years. Thanks to Viswanath Meenakshisundaram, for always being available to chat and exchange ideas. To my other colleagues working on vat photopolymerization: Daniel Rau, Keyton Feller, Donald Aduba. Andy Cohen, for being a particularly excellent and dedicated undergraduate researcher. Thank you to all of the graduate students, post-docs, and undergraduate researcher who have been part of the Design and Research for Additive Manufacturing Systems (DREAMS) Lab over the years.

Thank you to all of the members of the Bio-based Materials Lab. Shelley Cooke and André Stevenson for their assistance with mammalian cell culture. To Wyatt Surbey, for always being ready to help with seemingly impossible experiments. Thanks to Jerry Contreras for often providing a helping hand before I even knew I needed one. Jewel Cary, for her ability to empathize with anyone and her expertise in cell culture. Zuzka Han, for being a dedicated and self-motivated undergraduate researcher.

Thank you to the members of the Timothy Long lab, dozens of whom I have had the opportunity to work with. Thanks to Maruti Hegde, for his unbridled optimism and continuous flow of ideas. To Alison Schultz, Philip Scott, Justin Serrine, Clay Arrington,

and many others for their help in synthesizing new photocurable molecules that we were able to develop into high-performance resins for printing via vat photopolymerization.

Thank you to Jack Lesko and Catherine Amelink for their support of graduate students belonging to underrepresented minorities and for their recognition of the particular challenges these students face in rural Southwest Virginia. Grant Brewer, for his expertise in intellectual property protection and his appreciation of the role that graduate students play in the development of new ideas and IP. Lance Yelton, for his unwavering cheerfulness, approachability, and the rapidity with which he completed orders, scheduled reservations, and processed paperwork. Lynn Bever, for her keen insights that have helped me to more deeply understand myself and others.

Thank you to all my friends. Some are nearby (Winston Salem, Washington D.C., New York) and others are further (Minneapolis, San Francisco, Mexico, Hawaii, London, Tokyo) but they all made me feel as though they were always right beside me through thick and thin. Thank you especially to Yasmin, George, Nathan, Maggie, Greg, Mark, Mike, Matt, Ben, Luke, and David.

My greatest thanks and appreciation goes to my family. Thank you, from the bottom of my heart, to my parents, Nicole Chartrain M.S. and Michel Chartrain Ph.D., for their unwavering love, support, and encouragement. To my twin brother, Alexander Chartrain M.D., who has shown me that dedication and commitment can lead to personal fulfillment and professional success. Thanks to my grandparents and extended family for their continued support over the years.

Attribution

Prof. Abby R. Whittington

Associate Professor of Materials Science & Engineering and Chemical Engineering at Virginia Tech and research co-advisor.

Prof. Christopher B. Williams

Associate Professor of Mechanical Engineering at Virginia Tech and research co-advisor.

Andrew Cohen

Former undergraduate student in Prof. William's research group who contributed to Chapter 5.

Wyatt R. Surbey

Graduate student in Prof. Whittington's research group who contributed to Chapter 3.

Jarrold Cartwright

Former undergraduate student who conducted research in Prof. William's group through the NSF Research Experience for Undergraduates (REU) program and contributed to Chapter 3.

Table of Contents

Chapter 1. Introduction	1
1.1 Background and Motivation	1
1.2 Research Objectives and Approach	2
1.2.1 Research Aim #1: Polymeric Materials for Tissue Scaffold Fabrication with Vat Photopolymerization.....	3
1.2.2 Research Aim #2: Effects of Scaffold Pore Size on Cell Adhesion and Proliferation.....	5
1.2.3 Research Aim #3: Multi-Material Tissue Scaffolds	7
1.3 Dissertation Overview	9
Chapter 2. A Review on Fabricating Tissue Scaffolds using Vat Photopolymerization	11
2.1 Abstract	11
2.2 An Introduction to Tissue Scaffolds	12
2.2.1 The Need for Replacement Tissue and Tissue Engineering	12
2.2.2 Clinical Applications of Tissue Engineering	13
2.2.3 Tissue Scaffold Requirements	14
2.2.3.1 Biocompatibility and Biodegradability	15
2.2.3.2 Mechanical Strength	15
2.2.3.3 Porosity, Pore Size, and Interconnectivity.....	16
2.2.3.4 Incorporation and Delivery of Chemical Factors	16
2.2.3.5 The Importance of Vascularization	17
2.3 Tissue Scaffold Fabrication Techniques	18
2.3.1 Decellularization.....	18
2.3.2 Traditional Tissue Scaffold Fabrication.....	19
2.3.2.1 Solvent Casting and Particulate Leaching	20
2.3.2.2 Gas Foaming.....	20
2.3.2.3 Phase Separation.....	21
2.3.2.4 Electrospinning.....	21
2.3.3 Additive Manufacturing Techniques	22
2.3.3.1 Material Extrusion	23
2.3.3.2 Bioprinting.....	24
2.3.3.2.1 Extrusion Bioprinting.....	24
2.3.3.2.2 Inkjet Bioprinting	26

2.3.3.2.3	Laser Assisted Bioprinting	26
2.3.3.2.4	Materials for Bioprinting.....	26
2.3.3.2.5	Challenges faced by Bioprinting.....	27
2.4	Vat Photopolymerization (Stereolithography) and its Potential	28
2.4.1	Stereolithography: Principles of Operation	28
2.4.2	Microstereolithography.....	31
2.4.3	Advantages of Microstereolithography.....	34
2.4.4	Photopolymer Chemistry	35
2.4.4.1	Modeling Photocuring in SLA Systems	36
2.4.4.2	Free Radical Systems.....	37
2.4.4.3	Cationic Systems	39
2.4.5	State of the Art of Microstereolithography for Tissue Scaffolds.....	39
2.4.5.1	Resolution and Accuracy.....	39
2.4.5.2	Resins used in μ SL for Tissue Scaffolds	40
2.4.5.3	Synthetic Polymers	44
2.4.5.4	Naturally Derived Polymers	48
2.4.6	Fabrication of Parts with Multiple Materials	50
2.4.7	Photoinitiators and UV Blockers	52
2.4.8	Bioactive Additives and Cell-Containing Resins	53
2.4.9	Feature Size.....	54
2.4.10	Scaffold Architecture and Mesostructure	58
2.5	Future Directions of μSL.....	60
	References	63
Chapter 3: In Vitro Evaluation of 3D Printed NaAMPS-PEGDA Tissue Scaffolds		
Fabricated with Vat Photopolymerization		
3.1	Abstract.....	79
3.2	Introduction.....	81
3.3	Materials and Methods.....	84
3.3.1	Resin Preparation	84
3.3.2	Photorheology	84
3.3.3	Mask Projection Microstereolithography	85
3.3.4	Resin Selection and Development of Print Parameters	87
3.3.5	Equilibrium Water Content.....	88
3.3.6	Compression Testing	88
3.3.7	Fibroblast Seeding and Cytotoxicity Evaluation	89

3.3.8	Statistics	91
3.4	Results	91
3.4.1	Photorheology	91
3.4.2	Print Parameters and Tissue Scaffold Fabrication	92
3.4.3	Equilibrium Water Content of Printed Parts through TGA	94
3.4.4	Compression Testing	94
3.4.5	Cell Adhesion and Cytotoxicity.....	95
3.5	Discussion	98
3.6	Conclusions	102
	References	102
3.7	Supporting Information	107
3.7.1	Equilibrium Water Content of Printed Parts through TGA	107
3.7.2	Photorheology of Resins with and without Crosslinker	108
Chapter 4: Effects of Pore Size on Cell Proliferation and Distribution in 3D Printed Tissue Scaffolds Fabricated Using Vat Photopolymerization		
		110
4.1	Abstract	110
4.2	Introduction	111
4.3	Materials and Methods	117
4.3.1	Resin Formulation.....	117
4.3.2	Scaffold Design.....	117
4.3.3	Fabrication of Scaffolds by Vat Photopolymerization.....	118
4.3.4	Optical Microscopy and Measurement of Scaffolds.....	119
4.3.5	Sterilization and Extraction of Scaffolds	119
4.3.6	Cell Culture.....	119
4.3.7	Cell Seeding on Scaffolds.....	120
4.3.8	Fluorescence Microscopy	120
4.3.9	Image Analysis & Cell Counting.....	121
4.3.10	Statistical Analysis.....	122
4.4	Results	122
4.4.1	Scaffold Fabrication with Designed Pore Size	122
4.4.2	NIH 3T3 Proliferation Within Scaffolds.....	126
4.4.3	Cell Distribution Along Scaffold Cross-sections.....	127
4.5	Discussion	131
4.6	Conclusions	134
	References	134

4.7	Supporting Information	139
4.7.1	Image Processing	139
Chapter 5: 3D Printing of Multi-Material Tissue Scaffolds with Vat Photopolymerization for Directed Cell Response		142
5.1	Abstract	142
5.2	Introduction	143
5.3	Experimental	147
5.3.1	Resins	147
5.3.2	Scaffold Fabrication.....	150
5.3.3	Cell Culture.....	154
5.3.4	Cell Seeding and Evaluation of NaAMPS and PEGDA-C Scaffolds.....	155
5.4	Results & Discussion	157
5.4.1	Fabrication of NaAMPS and PEGDA-C Scaffolds	157
5.4.2	Cell Adhesion and Proliferation on NaAMPS and PEGDA-C.....	160
5.4.4	Cell Adhesion and Proliferation on Soy and PEGDA-B	165
5.4.5	Perfusable Scaffold Fabrication and Evaluation.....	169
5.5	Conclusions	172
References		173
Chapter 6: Overall Conclusions		177
6.1	Summary of Research, Results, and Contributions	177
6.1.1	Research Aim #1: Polymeric Materials for Tissue Scaffold Fabrication with Vat Photopolymerization.....	177
6.1.2	Research Aim #2: Effects of Scaffold Pore Size on Cell Adhesion and Proliferation.....	181
6.1.3	Research Aim #3: Multi-Material Tissue Scaffolds	186
6.2	Suggested Future Work	193
6.2.1	Investigating and Enhancing Degradation Rates of NaAMPS-based Resins 193	
6.2.2	Investigating the Effect of Large Pore Sizes on Cell Growth and Distribution Over Time	194
6.2.3	Development of Multi-Cellular Tissue Constructs from Multi-Material Tissue Scaffolds.....	194

Chapter 1. Introduction

1.1 Background and Motivation

The field of Tissue Engineering and Regenerative Medicine (TERM) has tremendous potential to change the way we treat disease, heal traumatic injuries, and age. By combining cells, a three-dimensional template on which to grow the cells, and the right stimuli, scientists, doctors, and engineers envision ‘growing’ tissue and even entire organs. Tissues created from a patient’s own cells would not require lifelong use of immunosuppressants, which is currently required of patients who have received an organ transplant. The organ transplant waiting would dramatically reduce in length and hundreds of thousands or millions of people would experience improved quality of life. Despite media reports that might suggest otherwise, substantial challenges that have persisted for nearly three decades have hampered progress towards these goals, particularly efforts to engineer thick tissue (e.g., liver, kidney). The complexity of biological systems is astounding and even overwhelming when considering the task of reverse engineering them. Many cell types, material properties, and biochemical molecules are found within a single tissue, and the locations and interactions between each of these can determine the extent to which the tissue provides function. Manufacturing techniques developed for 3D scaffold fabrication have proved inadequate for the precise placement of cells, material, and chemical cues required for engineering thick tissue. Perhaps the most challenging task in selective cell and material placement is the incorporation of a vascular (capillary) network that delivers oxygen and nutrients to every cell. In the human body, most cells must be within 200 μm (twice the thickness of a hair) of a capillary to receive sufficient oxygen and nutrients to sustain them. Engineering such complex structures requires a paradigm shift towards innovative manufacturing techniques that can mimic the complexity of nature.

Additive Manufacturing (AM), commonly referred to as 3D printing, encompasses a variety of technologies that fabricate parts from many different materials and in many different ways. However, each technique fabricates parts in an additive (as opposed to subtractive) manner, typically in a layer-by-layer fashion. Several AM methods have been used to fabricate constructs for use in tissue engineering. One of these technologies, vat photopolymerization (VP, and commonly referred to as Stereolithography, SLA, or resin printing) uses ultraviolet light to polymerize a photosensitive liquid monomer, creating a solid polymer. Exposing select areas of a thin layer of photopolymer to light in a layerwise fashion allows for the fabrication of 3D parts with complex geometries and very high resolution (features on the order of 3-200 μm depending on system configuration). The resolution and geometric complexity offered by VP make it an excellent candidate for fabricating biomimetic structures. However, drawbacks of VP include the small number of printable biocompatible materials, a lack of design rules to guide the fabrication of scaffolds that can support live, functioning cells at high densities, and a very limited ability to direct the growth or placement of multiple cell types or materials within a single printed construct. New materials, knowledge, and techniques that address each of these drawbacks of VP will help scientists, engineers, and doctors to engineer structures that may one day provide a means of fabricating patient-specific tissues.

1.2 Research Objectives and Approach

The overall goal of the work presented herein is to provide a greater understanding of the interactions that take place between cells and tissue scaffolds fabricated using VP, particularly with respect to the scaffold material and geometry. Results obtained from this work are expected

to help overcome the challenges facing the use of VP for fabricating tissue scaffolds identified in Section 1.1 (Background and Introduction).

1.2.1 Research Aim #1: Polymeric Materials for Tissue Scaffold Fabrication with Vat Photopolymerization

Research Gap #1

A large number of resins are commercially available from many vendors for use in VP systems. Several are even suitable for biomedical applications (e.g., surgical guides, dental splints) and have Class I or Class IIa biocompatibility certification. However, no resins are marketed for VP of tissue scaffolds. Commercial resins with low cytotoxicity inhibit cellular adhesion, an essential property of a suitable tissue scaffolding material. The literature contains a growing number of reports of resins that have been used to fabricate tissue scaffolds with VP and cultured with mammalian cells (see Chapters 2 and 3). Unfortunately, because these resins are not sold commercially, their major component(s) must be synthesized. Synthesis of photocurable polymers typically requires a well-equipped wet lab, more than a dozen reagents, and substantial expertise in polymer synthesis. In addition, synthesis and purification can take a week or longer. Finally, some of the resulting resins, especially those based on natural polymers that must be dissolved in substantial quantities of water, yield poor resolution and 3D printing results because water does not absorb UV light, making it difficult to fabricate thin layers. It is clear that new resin development is needed to produce resins that can be formulated without polymer synthesis, that allow high resolution VP printing, that have low cytotoxicity, and that encourage cell adhesion.

Development Objective #1

Develop a resin using commercially available components (zero-synthesis) with properties suitable for the fabrication of tissue scaffolds using VP.

To fulfill Development Objective #1, the resin must demonstrate the following properties:

- Formulation from monomers, oligomers, photoinitiators, UV absorbers, and other components that can readily be obtained by the typical university or research laboratory
- Sufficient mechanical strength after irradiation to permit the fabrication of self-supporting layers and 3D parts
- Sufficiently low viscosity to allow the recoating of thin layers of resin ($< 5 \text{ Pa}\cdot\text{s}$)
- Rapid photocuring ($< 60 \text{ s}$) of thin layers ($< 100 \mu\text{m}$) with a VP system with a UV light intensity between approximately 3 and $30 \text{ mW}/\text{cm}^2$.
- Fabrication of 3D parts with suitable resolution for tissue engineering (i.e., features smaller than $200 \mu\text{m}$)
- Low cytotoxicity and good cell adhesive properties demonstrated through a cell viability test showing an increase in cell proliferation over time on scaffolds

Development of a resin which fulfills these design requirements will allow for exploration of the impact the resin component has on the overall resin's suitability for the fabrication of tissue scaffolds. The results obtained during resin design and formulation will aid in answering Supplemental Research Question #1.1.

Supplemental Research Question #1.1

How does the NaAMPS-based resin's composition impact its printability and print resolution?

The successful development of a zero-synthesis resin that can be used to fabricate high resolution tissue scaffolds that demonstrate low cytotoxicity and good cell adhesive properties is expected to stimulate additional research into the use of VP for tissue scaffolds fabrication. In addition, an understanding of how the resin's composition can be tuned to improve or simply allow printing with VP will be acquired.

1.2.2 Research Aim #2: Effects of Scaffold Pore Size on Cell Adhesion and Proliferation

Research Gap #2

Tissue scaffolds aim to mimic the microenvironment experienced by cells *in vivo* in an effort to encourage cellular proliferation and the development of functionality (e.g., the formation of bone to provide skeletal support). The geometric parameters of the scaffold, including its overall size, the size and shape of its pores, its permeability, and its porosity, have substantial effects on cell growth. For example, in scaffolds with small pores, the diffusion of nutrients, oxygen, and cells into the center of the scaffold is low. High availability of oxygen and nutrients at the surface of the scaffold can induce rapid growth and the deposition of extracellular matrix, which further inhibits the movement of oxygen into the scaffold's center. A necrotic region can form at the core of the scaffold due to insufficient oxygen concentration. Although methods such as reducing scaffold thickness or culturing the scaffold with a perfusion bioreactor can help alleviate oxygen gradients, these have limited clinical relevance and/or associated challenges (e.g., scalability).

Previous work has studied the effects of many scaffold parameters on cell response using scaffolds fabricated with a variety of traditional means (e.g., gas foaming, particulate leaching). However, no consensus on the most optimal pore size exists in the literature. The limits imposed by

traditional scaffold fabrication technologies have prevented the study of relatively large pore sizes as well as the comparison of scaffolds with different pore sizes but otherwise identical geometric parameters. Due to their ability to fabricate a wide variety of geometries from digital models, AM technologies allow for a broader and more robust investigation into the effects of a scaffold's pore size on cells. Unlike scaffolds fabricated by traditional means or VP, bioprinting techniques (e.g., extrusion and inkjet bioprinting) incorporate cells *in situ*, trapping them in their printed locations. Cells are typically seeded after printing of scaffolds fabricated using VP, offering a more suitable AM technology for studying the effects of pore size on cell growth, proliferation, and distribution. Surprisingly, only a few studies have sought to understand the effects of pore size on cells in VP-fabricated scaffolds. Most notably, work by Melchels et al. showed that pore size can result in oxygen concentration gradients (see Section 4.2). Unfortunately, the effects of pore size on cell proliferation and resulting cell distribution within VP-fabricated scaffolds are not yet well understood. Gaining a broader understanding of pore size effects in scaffolds fabricated with VP is the subject of Research Question #2.

Research Question #2

How does pore size in a tissue scaffold fabricated with VP impact cell proliferation and cell distribution within the scaffold?

A systematic study in scaffolds with a variety of pore sizes but identical size, porosity, pore shape, and other geometric parameters will provide researchers with a more lucid understanding of the effects of pore size. The data generated (Chapter 4) will allow for more rational evidence-based tissue scaffold designs that will aid in optimizing cellular proliferation and distribution.

1.2.3 Research Aim #3: Multi-Material Tissue Scaffolds

Research Gap #3

Vascularization is often cited as the greatest challenge facing tissue engineering, despite decades of work aimed at generating vasculature in tissue engineering constructs. In thick tissue constructs, the diffusion of nutrients and oxygen into the center of the construct is insufficient to maintain cell viability. Many successes in tissue engineering have been focused on the fabrication of unvascularized flat or tubular tissue constructs in which each cell is only a few hundred microns from a surface from which nutrients and oxygen can diffuse. However, many of the tissues which provide essential functions are thick tissues (e.g., kidney, liver, muscle) and require a vascular network to provide the requisite oxygen and nutrients. Vascularization requires an inhomogeneous distribution of cells, i.e., a tubular network through which blood can flow to deliver oxygen and nutrients to all cells within a construct. For a tubular network that mimics vasculature to continue to function and permit the movement of oxygen and nutrients throughout the scaffold, its tubes must remain free of obstruction caused by cells or their extracellular matrix (ECM). In thicker tissue scaffolds made from a single material, cells typically proliferate sufficiently such that pores become blocked and the diffusion and perfusion of nutrients and oxygen is impeded. Thus, to create vasculature, as well as multi-cellular tissues whose function relies in part on the arrangement of their cell types with respect to one another, it becomes necessary to control how cells spatially arrange themselves in the tissue scaffold onto which they are seeded. Several methods might be envisioned for the spatial patterning of cells in VP-fabricated tissue scaffolds, including the *in situ* patterning of cells, however, doing so ‘traps’ them in place in the photopolymer matrix, impeding their movement and proliferation. Nor does this technique guarantee that the original location of cell types will be preserved. However, controlling cell-scaffold interactions with dissimilar

material properties within a scaffold (e.g., cell adhesion properties, biochemical differentiation factors) may permit the spatial adhesion *and proliferation* of cells in a tissue scaffold. The overall research goal of the work conducted was to gain a greater understanding in how scaffold designs impact cell response in tissue scaffolds fabricated by VP and how this knowledge can be leveraged to engineer designed responses and direct cell growth and proliferation

Research Question #3

How can multiple dissimilar materials be used to spatially control cell adhesion and proliferation in porous tissue scaffolds fabricated with VP?

The ability to spatially control cell adhesion and proliferation through multiple materials first requires the fabrication of multi-material parts with VP. A few groups have developed systems capable of multi-material parts with VP, but these are neither common nor commercially available. To answer Research Question #3, it is necessary to develop a system or techniques through which multi-material scaffolds can be fabricated.

Development Objective 3.1

Develop a system or techniques through which VP can be used to fabricate multi-material parts.

The fabrication of multi-material parts is further complicated by the need to use photopolymers with properties suitable for biomedical applications. Such materials may be hydrogels, whose large quantities of water will lower the density of photopolymerizable groups, increase the resin's depth of penetration, and permit substantial swelling of printed parts. In addition, any additives (e.g.,

photoinitiator, photo absorber) must not impart adverse properties to the resin, such as cytotoxicity. Understanding the interactions between materials with dissimilar properties and their interaction on the multi-material fabrication process will be crucial for the successful fabrication of multi-material tissue scaffolds.

Supplemental Research Question 3.2

What are the material considerations for fabricating multi-material tissue scaffolds with VP?

The development of a system capable of fabricating multi-material tissue scaffolds with suitable materials will enable spatial control over cell adhesion and proliferation in VP-fabricated structures. This would be a significant step towards creating more complex tissue engineering constructs with naturally-inspired multiscale structures that mimic vascularization or even provide the function of multi-cellular tissues.

1.3 Dissertation Overview

The efforts described in this dissertation aim to address the three drawbacks of VP identified in the motivation for this work. A more extensive review of the application of VP in tissue engineering contexts is presented in Chapter 2. The formulation, 3D printing, and characterization of a novel resin formulation designed for the fabrication of tissue scaffolds with VP is described in Chapter 3. Excellent adhesion and growth of fibroblasts (cells found in connective tissue) was observed on 3D parts printed from the resin. In contrast with other resins reported in the literature, the resin we have developed is formulated from inexpensive and readily available components that are simply mixed together. A lengthy synthesis, which often requires substantial expertise in

polymer chemistry, is thus avoided. Chapter 4 investigates the role of scaffold geometry, specifically pore size, on fibroblast growth and proliferation. Understanding how scaffold geometry affects cell density and distribution is essential for generating design guidelines for engineered constructs that will encourage tissue formation. Finally, the 3D printing of multi-material tissue scaffolds is described in Chapter 5. Our results show that the locations where cells adhere and grow in a scaffold can be controlled through the selective placement of dissimilar materials. The 3D printed constructs demonstrated in this chapter show potential for the fabrication of tubular network within a scaffold to mimic the structure and function of vasculature.

Chapter 2. A Review on Fabricating Tissue Scaffolds using Vat Photopolymerization

Published in *Acta Biomaterialia* 74 (2018) 90-111

Reprinted with permission from Elsevier

Article available at:
<https://www.sciencedirect.com/science/article/pii/S1742706118302794>

Nicholas A. Chartrain^{a,b,c}, Christopher B. Williams^{a,b,c}, Abby R. Whittington^{a,c,d*}

^aDepartment of Materials Science and Engineering, Virginia Tech, Blacksburg, VA 24061, USA.

^bDepartment of Mechanical Engineering, Virginia Tech, Blacksburg, VA 24061, USA.

^cMacromolecules Innovation Institute, Virginia Tech, Blacksburg, VA 24061, USA.

^dDepartment of Chemical Engineering, Virginia Tech, Blacksburg, VA 24061, USA.

Keywords: 3D Printing, Stereolithography, Tissue Engineering, Tissue Scaffolds, Photopolymers, Regenerative Medicine

2.1 Abstract

Vat Photopolymerization (stereolithography, SLA), an Additive Manufacturing (AM) or 3D printing technology, holds particular promise for the fabrication of tissue scaffolds for use in regenerative medicine. Unlike traditional tissue scaffold fabrication techniques, SLA is capable of fabricating designed scaffolds through the selective photopolymerization of a photopolymer resin on the micron scale. SLA offers unprecedented control over scaffold porosity and permeability, as well as pore size, shape, and interconnectivity. Perhaps even more significantly, SLA can be used to fabricate vascular networks that may encourage angio and vasculogenesis. Fulfilling this potential requires the development of new photopolymers, the incorporation of biochemical factors into printed scaffolds, and an understanding of the effects scaffold geometry have on cell viability,

proliferation, and differentiation. This review compares SLA to other scaffold fabrication techniques, highlights significant advances in the field, and offers a perspective on the field's challenges and future directions.

2.2 An Introduction to Tissue Scaffolds

The goal of tissue engineering is to bring together cells, tissue scaffolds, and a combination of electrical, mechanical, or chemical cues to stimulate the repair or regeneration of tissue. A tissue scaffold is a structure that promotes cell adhesion and the diffusion of nutrients and waste. The scaffold provides mechanical integrity to the tissue engineering construct and can also serve as a delivery vehicle for chemical factors. Tissue scaffolds have received significant attention by both the research and medical communities in the past two decades. Recent successes include the successful engineering of bladders and blood vessels using tissue scaffolds. However, traditional tissue fabrication techniques have limitations that have impeded their use in clinical settings, particularly for the regeneration of solid tissue. New techniques, particularly Additive Manufacturing (AM, also referred to as 3D Printing) technologies, are poised to solve these limitations and fabricate more complex scaffolds to allow for the engineering of solid tissue. The goal of this review is to first introduce the reader to traditional and AM scaffold fabrication techniques. The bulk of this review will then focus on apprising the reader of current research and provide a perspective on the use of Vat Photopolymerization (stereolithography, SLA) for the fabrication of complex tissue scaffolds.

2.2.1 The Need for Replacement Tissue and Tissue Engineering

In the United States alone, nearly a hundred and twenty thousand patients are currently awaiting organ transplants, yet less than thirty thousand transplants are performed each year [1]. Kidney transplant requests account for more than one hundred thousand of the patients on the organ donor transplant list [2]. There is a chronic shortage of organs available for transplant and many patients must wait several years for a transplant [1]. Part of the difficulty is finding an organ available for transplant that is compatible with the patient. The compatibility includes factors such as blood type, donor and recipient body size, and distance between the donor and recipient's hospitals. The patients that do receive organ or tissue transplants must take immunosuppressant drugs to prevent an immune response to the transplanted tissue [3]. These drugs have a variety of side effects and make patients more susceptible to infection.

The number of patients awaiting organ transplants present a daunting challenge, but even they do not account for the entire demand for replacement tissue. Millions of people suffer from tissue disease or death such as skin burns, torn ligaments, and cartilage degeneration. Although the people who suffer from these diseases are often not on the organ transplant list, they could nevertheless benefit from receiving replacement tissue. Engineered products are able to help some of these patients, such as those with severe burns, but most must rely on conventional therapies or drugs [4, 5].

2.2.2 Clinical Applications of Tissue Engineering

Tissue engineering and regenerative medicine are both relatively new disciplines, yet significant advances have been made in treating damaged or diseased tissue in the past two to three decades [6, 7]. As an example, Wake Forest Institute for Regenerative Medicine (WFIRM), led by Anthony

Atala and James Yoo, has successfully engineered and implanted a variety of tissue scaffolds in patients. Atala et. al. engineered bladders for human patients by culturing autologous urothelial and muscle cells and seeding them on collagen scaffolds or collagen and polyglycolic acid (PGA) composite scaffolds [8]. More recently, the group has reported conducting similar tests with human vaginas [9]. Patients from both groups were monitored for several years and the results of the studies were very positive overall.

Due to the widespread and expensive nature of cardiovascular disease, many research groups have focused on creating tissue engineered blood vessels. Research collaboration between several universities and Humacyte Inc. has resulted in the creation of decellularized blood vessels with very promising initial clinical trials in both non-human primates and humans [10-13]. Other groups have also shown success in creating engineered blood vessels [14-16]. However, these successes are limited to planar, tubular, or hollow tissues that require little vascularization. The regeneration of more complex solid tissue will require new techniques that incorporate vascularization.

2.2.3 Tissue Scaffold Requirements

To create a suitable environment that encourages cellular adhesion, proliferation, differentiation, and the formation of vasculature, tissue scaffolds and the materials from which they are made must satisfy several important requirements. The material(s) used should be biocompatible, degrade at a suitable rate into non-toxic products, and ideally include growth or differentiation factors to aid in tissue formation. The scaffold should have high porosity and pore interconnectivity while at the same time maintaining sufficient mechanical strength. The elastic modulus and pore size should be tuned to the tissue type being regenerated.

2.2.3.1 Biocompatibility and Biodegradability

While the term biocompatibility has no clear definition and has often been misused [17, 18], the materials used for the fabrication of tissue scaffolds should not be cytotoxic nor should they elicit a significant inflammatory response from the cells. In addition, the ideal scaffold should degrade in the body over a period of weeks to months, depending on the tissue type being regenerated. As the cells degrade the scaffold and replace it with secreted proteins, the decrease in mechanical strength of the scaffold should be balanced by the increase in strength of the extracellular matrix (ECM) produced by the cells [19]. The products into which the scaffold degrades must also be biocompatible.

2.2.3.2 Mechanical Strength

A tissue scaffold must have enough rigidity and strength to support itself in addition to any loads that might be placed on it from surrounding tissue [19, 20]. Tissue scaffolds that aim to replace ligaments or bone need significantly more strength than those intended to replace soft tissues. It is important to use a material that is tailored to the specific tissue to be replaced as greater cell viability has been observed when cells are placed on a substrate with a modulus that closely resembles that of the host tissue of the cell [21]. Further, bone resorption is a common result in joint replacements because metal implants are stiffer than the surrounding bone [22]. The compliance of the substrate, which is determined by its elastic modulus, also affects both adhesion and migration of cells on the substrate [23, 24]. Matching the mechanical properties of bone with hydrogels has proven quite challenging with extensive research focused on reinforcing hydrogels for use as bone tissue scaffolds [25-27]. Ceramics, notably hydroxyapatite and tricalcium phosphate, have been explored as substitutes as they have significantly higher elastic moduli than

hydrogels [28-33]. Mimicking the elasticity and strength of tissues such as ligament, tendon, and cartilage has also proven challenging [34-38].

2.2.3.3 Porosity, Pore Size, and Interconnectivity

Scaffold porosity, pore size, and pore interconnectivity are important factors in maintaining high cell viability and preventing apoptosis [19, 39]. Porosity is the volume of free space in a scaffold while its interconnectivity is a measure of the percent volume of pores that can be reached from the outside of the scaffold [40, 41]. The greater the porosity of a scaffold, the more cells it can potentially accommodate but at the cost of mechanical strength [19, 20]. Higher pore interconnectivity contributes to the ability of cells to migrate and proliferate through the scaffold. Pore interconnectivity, as well as the size and distribution of the interconnects, also impacts a scaffold's overall permeability and the ability for fluid to flow through it [42]. Good permeability is necessary to allow for nutrient access to cells throughout the scaffold and for the removal of cellular waste products. Pore size in tissue scaffolds fabricated via both traditional techniques and AM have been found to affect cell viability and growth [43]. One study found that preosteoblasts had the highest viability on scaffolds with pore diameters of approximately 350 μm [44]. However, different cell types tend to prefer a variety of pore sizes [43]. Researchers have also found that pore shape can also affect cell growth and viability [45, 46]. However, because traditional tissue scaffold fabrication techniques are unable to control precise pore geometry, the underlying phenomena of how pore shape impacts cell adhesion and viability are not well understood.

2.2.3.4 Incorporation and Delivery of Chemical Factors

Cells do not readily attach to most synthetic materials unless specific chemical cues are present. In practice, proteins containing the RGD (Arginylglycylaspartic acid) tripeptide sequence (found in e.g. collagen, fibronectin, elastin) are commonly incorporated into or adhered onto the tissue scaffold to improve cell adhesion and viability [47-49]. Chemical factors can also be specific to the particular type of cell being cultured. For example, scaffolds seeded with preosteoblasts often include hydroxyapatite to promote osseointegration and differentiation into osteoblasts [50-53]. Growth factors can be used to elicit a desired cell response (e.g. protein secretion, migration) and direct cell differentiation [54]. Bone morphogenetic protein 2 (BMP-2) and vascular endothelial growth factor (VEGF) have been incorporated into scaffolds to promote osteogenesis and angiogenesis [55-57].

2.2.3.5 The Importance of Vascularization

Generating vascularization in tissue engineered constructs has often been cited as the most significant challenge in creating scaffolds that can be used in clinical settings [58]. Insufficient vascularization which does not allow for nutrient diffusion to cells or for waste to be removed results in apoptosis, or programmed cell death [59]. Scaffold properties such as porosity, pore size, interconnectivity, and the incorporation of bioactive molecules will influence the degree to which a tissue engineered construct becomes vascularized.

Tissue engineered constructs that are used to repair or replace planar, tubular, or hollow tissues have been successful because cells in these constructs are never more than a few hundred micrometers away from a vascularized blood source [8]. Artificial skin constructs, bladder tissue, and vaginal tissue used in clinical settings have been successful without the incorporation of

vascularization [5, 8, 9, 60]. While hollow, tubular, and planar tissues are all composed of thin layers of cells just a few hundred micrometers thick, solid organs are composed of cells that can be centimeters away from the surface of the tissue [61]. Most of the organs which are in scarce supply for transplant, such as the kidney, liver, pancreas, and heart, are made up of thick, vascularized tissue. Tissue scaffolds used to reconstruct solid tissues must be constructed in a way that promotes vascularization and ensures that cells are within 200 μm of a capillary [58].

2.3 Tissue Scaffold Fabrication Techniques

A variety of fabrication techniques have been developed in an attempt to create scaffolds that will provide an effective structure for developing tissues. These techniques can largely be classified into three categories: decellularization processes, traditional or stochastic scaffold fabrication processes, and AM processes. Each of these is able to create scaffolds that satisfy some of the requirements described in Section 2.2.3, but no technology is currently able to satisfy them all. As a result, all three of these scaffold fabrication techniques are the subject of ongoing research. An extensive review of SLA will be presented in Section 2.4.

2.3.1 Decellularization

While the previously described techniques create tissue scaffolds using both natural and synthetic polymers, decellularization aims to create scaffolds by removing cells from existing ECM [62]. Mechanical, enzymatic and chemical techniques are used to remove cells and proteins from tissue harvested from allogenic or xenogeneic donor while leaving structural proteins of the tissue intact. These cell-removing techniques include freeze-thawing, the perfusion of enzymes such as trypsin and nucleases into the tissue, and the use of detergents and saline solutions [62, 63]. Enzymes are

used to cleave proteins (e.g. DNA, RNA) into smaller fragments, but even these can cause an immune response if a sufficient number of them remain after decellularization [64]. In addition, decellularization techniques also alter the structure of the ECM [62]. The physical alteration of ECM scaffolds as well as the unique structure of each donor organ means that no two decellularized scaffolds are quite the same. The variability between scaffolds poses a challenge for clinical trials and studies [65]. Finally, decellularization requires the use of a tissue from a donor rather than the use of synthetic means of fabrication. These donors are either in limited supply or require a suitable animal donor [66].

FDA approval has been obtained for products from a variety of source tissues and for applications in orthopedic, cardiovascular, and dental tissue repair [63]. In addition, researchers are moving towards whole organ decellularization rather than just thin tissues [66]. Improved decellularization techniques as well as a greater understanding of the remodeling process that occurs during recellularization of the ECM could eventually allow for the replacement of full organs including kidneys, livers, and hearts [66].

2.3.2 Traditional Tissue Scaffold Fabrication

Since the early 1990's, dozens of polymer processing techniques have been developed to fabricate porous polymeric scaffolds for use in regenerative medicine and tissue engineering. Some of the most popular methods for fabricating scaffolds include gas foaming, solvent casting with particulate leaching, phase separation, and electrospinning, although many other techniques and hybrid techniques have also been used successfully [67-70]. Many of the clinical successes in

tissue engineering have used these polymer processing techniques for fabricating tissue scaffolds, particularly those intended for the repair or replacement of flat, tubular, or hollow tissue [6, 8-16]. While these traditional tissue scaffold fabrication methods are adequate for planar, tubular, and hollow organs, they cannot, at present, be used to create tissue scaffolds for solid organs because they do not provide vascularity [59]. This is due to the stochastic and non-hierarchical manner in which they create pores within the scaffold [58, 71]. Despite this major shortcoming, these methods have been used to create a wide variety of scaffolds with controlled porosity, pore size, surface area to volume ratios, mechanical properties, and chemistries.

2.3.2.1 Solvent Casting and Particulate Leaching

Particulate leached scaffolds can have high porosity and, unlike many other traditional scaffold fabrication techniques, have high interconnectivity between pores [72, 73]. Cell adhesion and viability has been reported on tissue scaffolds made via solvent casting and particulate leaching using poly(L-lactic acid) (PLLA) [74], poly(lactic-co-glycolic acid) (PLGA) [73, 75], poly(L-lactic acid) poly(glycolic acid) copolymer (PLLA-PGA) [76], and polycaprolactone (PCL) [77]. Scaffolds have also been fabricated using poly(propylene fumarate) (PPF) [78], polyhydroxyalkanoates (PHA) [79], and poly(caprolactone fumarate) (PCLF) [40]. Tissue scaffolds made using this technique are often used for bone regeneration due to the relatively hard materials that can be used (e.g. PCL) [80]. The primary drawbacks of solvent casting and particulate leaching are the inability to control pore shape and pore interconnectivity [81].

2.3.2.2 Gas Foaming

Gas foaming produces highly porous scaffolds using biodegradable materials and without the use of harsh solvents [82-85]. High pressure gas (often CO₂) is used to saturate a polymer and, upon the reduction of pressure, the nucleation of gas bubbles creates pores with sizes up to 500 μm within the polymer sample [86]. Porosity of these scaffolds can be very high (greater than 90%) but it is difficult to control pore size and pore interconnectivity is often low [70, 87]. Porosity in the scaffold can be further controlled by the incorporation of particles into the polymer in a process involving both gas foaming and particulate leaching [85, 88].

2.3.2.3 Phase Separation

Phase separation is a scaffold fabrication technique capable of fabricating scaffolds with porosities up to 97% [70, 89-93]. Thermally-induced phase separation (TIPS) is performed by rapidly heating a polymer-solvent solution with a lower critical solution temperature or cooling one with an upper critical solution temperature. The instability of the solution causes it to separate into polymer-rich and solvent-rich regions [26, 94]. Hybrid scaffold fabrication techniques that employ both phase separation and particulate leaching have also been demonstrated [95, 96]. Drawbacks of phase separation include the use of organic solvents and the small pore sizes (micrometers to tens of micrometers) that are produced, which are often too small for tissue engineering applications [70].

2.3.2.4 Electrospinning

Electrospinning creates nonwoven meshes of polymeric fibers by drawing dissolved polymer solutions out of a thin syringe tip using a strong electric potential [97]. By modifying processing parameters such as the electric potential, distance to collection substrate, and syringe tip diameter, the diameter of polymer strands and mesh density can be controlled.

Electrospun scaffolds tend to have poor mechanical strengths and it is difficult to build three dimensional parts or control pore shape [81]. In addition, toxic organic solvents are often used to dissolve the polymer for electrospinning [98]. Scaffolds have been fabricated using electrospinning for applications including the engineering of nerve tissue [99], blood vessels [100], cardiovascular tissue [101], and skin [98].

2.3.3 Additive Manufacturing Techniques

AM, as defined by the joint ISO/ASTM 52900-15 standard on terminology, is a process in which material is joined, usually layer upon layer, to produce parts from 3D model data [102-104]. This is in contrast to subtractive manufacturing techniques, in which material is selectively removed, and formative manufacturing techniques, in which pressure applied to raw material is used to shape it. AM is further classified into seven processes, including vat photopolymerization, based on how material is joined together. The manufactured part's properties are determined by the class of material used, the feedstock used for adding material, the technique used to join material (e.g. curing, sintering, fusing), and the way in which the machine brings together material [102].

AM's ability to fabricate complex geometries presents a significant advantage over traditional scaffold fabrication techniques [105]. Designed scaffold geometries can be generated using Computer Aided Design (CAD) software, digitally sliced into many layers, and then fabricated layer by layer using an AM system. The digitally controlled nature of AM affords repeatability and precision to the scaffold fabrication process. This section will discuss the use of material

extrusion and bioprinting for the fabrication of tissue scaffolds while the subsequent section will explore stereolithography in more depth.

2.3.3.1 Material Extrusion

Tissue scaffolds have been fabricated using material extrusion (also known as Fused Deposition Modeling (FDM) or Fused Filament Fabrication (FFF)) as it can create objects rapidly from a growing selection of thermoplastics. In addition, both machines and the materials they use can be very inexpensive. However, the pore sizes that can be achieved with FDM are often 500 μm or greater and the geometries are typically quite simple (Fig. 2.1) [106]. In addition, the thermoplastics employed require extrusion at temperatures well above physiological temperature. For example, typical extrusion head temperatures for the extrusion of polycaprolactone range from 90-100 $^{\circ}\text{C}$ [25, 107]. This precludes simultaneous printing of cells or thermally sensitive biomolecules with the scaffold.

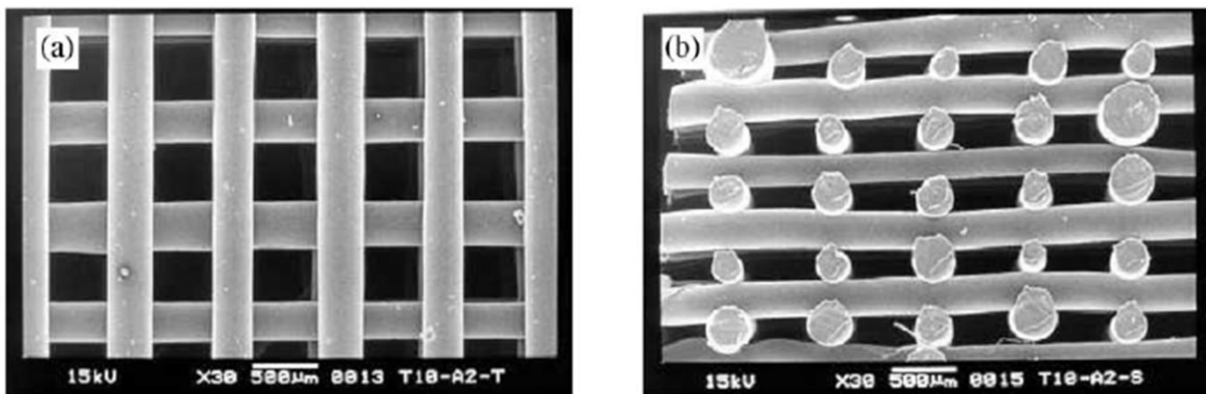


Fig. 2.1. SEM micrographs of polycaprolactone scaffolds fabricated with FDM. Reproduced from Zein et al., 2002 with permission from Elsevier [106].

2.3.3.2 Bioprinting

Bioprinting fabricates cell-containing tissue engineering constructs through the simultaneous deposition of cells and support material [108]. Bioprinting uses one or more deposition techniques including extrusion, inkjet, or laser assisted printing to selectively place material and cells [109].

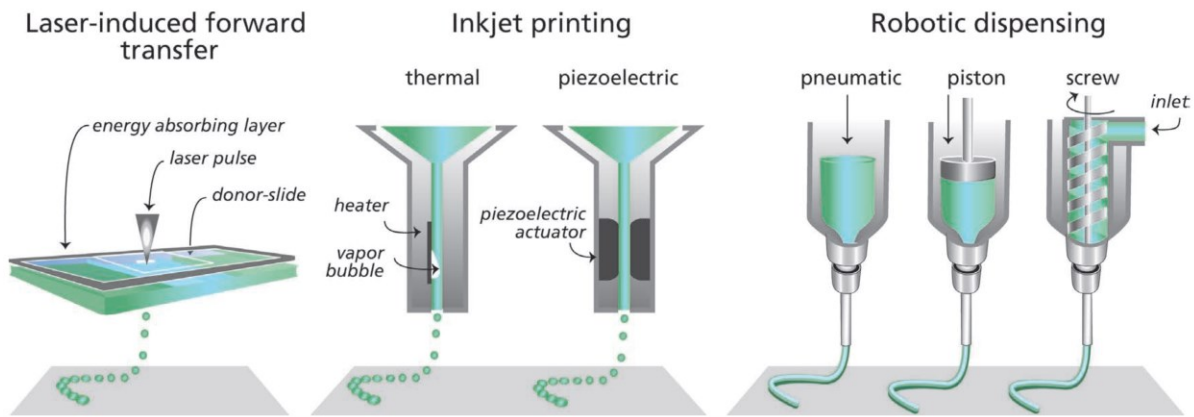


Fig. 2.2. Schematic diagrams of the three primary Bioprinting techniques. Reproduced from Malda et al., 2013 with permission from Wiley [109].

2.3.3.2.1 Extrusion Bioprinting

Extrusion bioprinters use pressure from a plunger, screw, or pneumatic system to push material and cell suspensions out of a small syringe tip. As material is laid down, it forms a scaffold and provides physical support that holds the cell suspension in place [110, 111]. Extrusion print heads are very popular as they are inexpensive and can print many cell types and materials that have a wide range of viscosities and cell densities (Fig. 2.3) [108, 112]. However, cells can experience

significant shear forces if extrusion velocities are too high and nozzle diameters too small [113]. The shear forces can destroy cell membranes and have a deleterious effect on cell viability, even after the printing process is complete [113, 114]. Increasing the printer's nozzle diameter reduces these shear forces but does so at the expense of resolution.

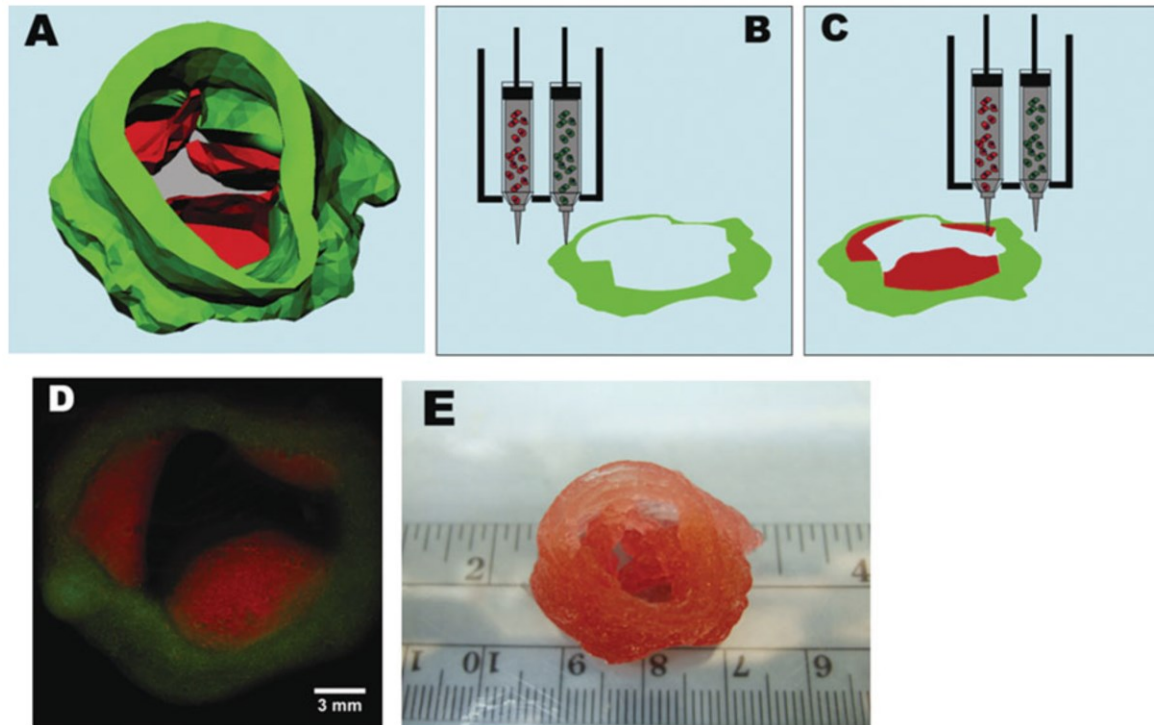


Fig. 2.3. Bioprinting of an aortic valve conduit containing both aortic root sinus smooth muscle cells (SMC) and aortic valve leaflet interstitial cells (VIC) encapsulated in an alginate and gelatin hydrogel. (a) Prior to printing, an aortic valve model was reconstructed from micro computed tomography (microCT) scan data and separated into valve root (green) and valve leaflet (red) regions; (b, c) schematic illustration of extrusion of encapsulated SMC and VIC; (d) fluorescence imaging of the first two layers of the aortic valve conduit; (e) the final printed aortic valve conduit. Reproduced from Duan et al., 2013 with permission from Wiley [112].

2.3.3.2.2 Inkjet Bioprinting

Inkjet bioprinters use a piezoelectric actuator or thermal inkjet head commonly found in conventional 2D printers to eject drops of material or cell suspensions [108]. Inkjet heads from 2D ink-based printers can be loaded with cells and placed on a 3-axis gantry. These printers tend to have slightly higher cell viability after printing than extrusion systems [113, 115]. However, achievable cell densities for inkjet printing are much lower than those observed with extrusion or laser assisted bioprinting [108, 115, 116]. In addition, inkjet bioprinters only have a small range of printable viscosities which limits the variety of materials that can be used for fabricating scaffolds [108, 117].

2.3.3.2.3 Laser Assisted Bioprinting

Laser assisted bioprinting (LAB) uses the Laser Induced Forward Transfer (LIFT) process in which a laser is used to deposit small droplets of cell-containing material off of a donor substrate onto the build area (Fig. 2.2) [109, 118]. First, a ribbon with a thin layer of the material to be deposited is prepared. It is then placed over the build surface and small droplets of material are ejected off of the ribbon using a pulsed laser beam [118]. Although it is less common than other techniques, LAB is becoming increasingly popular as it can achieve droplet sizes of less than 50 μm and very high cell densities (10^8 cells/mL) [116, 119].

2.3.3.2.4 Materials for Bioprinting

Bioinks are the polymeric materials used to encapsulate cells during bioprinting and provide mechanical support afterwards. Bioinks often have low viscosities to improve cell viability by allowing printing at lower pressures [120, 121]. They are often designed to be shear thinning [122-

124]. This allows them to be dispensed at low pressures using small diameter nozzles but self-supporting after printing. Bioinks for inkjet bioprinting must be liquids to allow for droplet formation, but must solidify after printing [108]. Cell viability can also be improved by using bioinks that can be printed at physiological temperature (e.g. 37 °C), rather than at ambient or elevated temperatures [121]. A wide range of elastic moduli can be obtained through polymer selection and by varying polymer concentration, molecular weight, and crosslink density [125, 126]. Both natural and synthetic polymers have been investigated for use in bioprinting. Polymers that have been employed in bioprinting applications include alginate [110-112, 127], collagen type I [27, 127, 128], fibrinogen [27], poly(ethylene glycol) dimethacrylate [126], gelatin [112, 129, 130], poly(ethylene glycol) diacrylate [129], and hyaluronic acid [125].

2.3.3.2.5 Challenges faced by Bioprinting

Despite the exciting results, the technology has several important barriers that may hinder clinical successes in the future. The primary difficulty is the inability to extrude very small volumes of cells without reducing their viability because of the shear forces caused by small diameter nozzles [113]. Extruding relatively large volumes of cells at a time may work well for fabricating tissues with relatively homogeneous structures, but may not be adequate for creating substructures with high complexity (e.g. kidney). This also presents a problem for creating the small vasculature necessary for solid tissues. In addition, few researchers have demonstrated the printing of cell-containing hydrogel structures taller than about 2 cm because of the mechanical properties of the inks [131]. Typically, structures printed from bioinks have moduli from about 100 Pa to 100 kPa [132-134]. Researchers are currently investigating new materials that are both bioactive and have greater mechanical strength than the polymers in use currently [131].

As the focus of this text is on the use of Stereolithography for tissue engineering, the author points the reader towards more comprehensive reviews on the use of Bioprinting that can be found in the literature [108, 135]. Further comparisons between scaffold fabrication techniques, both additive and traditional, are also available in the literature [43, 71, 105, 109, 136, 137].

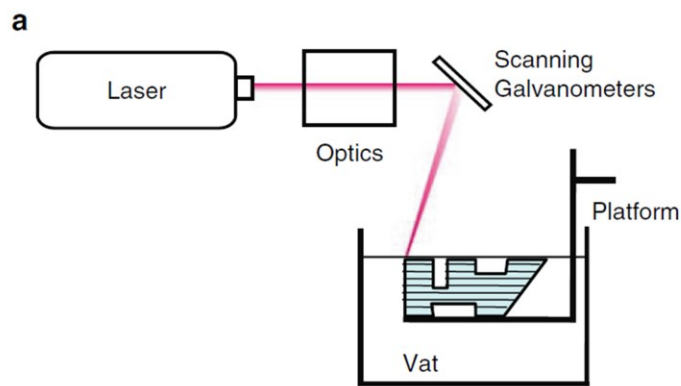
2.4 Vat Photopolymerization (Stereolithography) and its Potential

Vat photopolymerization (stereolithography, SLA) has been successfully used for the tooling and manufacturing of a number of consumer products due to its ability to create large parts with sub-millimeter details. One of the most well-known commercial applications of SLA is Invisalign®, an orthodontic treatment that uses clear, removable teeth aligners custom fabricated for each patient [138]. In conjunction with traditional manufacturing techniques, Align Technology Inc. has used SLA to manufacture and has shipped tens of millions of these individualized devices to patients. SLA is also used to fabricate the vast majority of hearing aid device shells [139]. By increasing the resolution of current SLA machines and broadening the number and variety of materials capable of being manufactured with this technique, researchers hope to achieve similar successes in the field of Tissue Engineering.

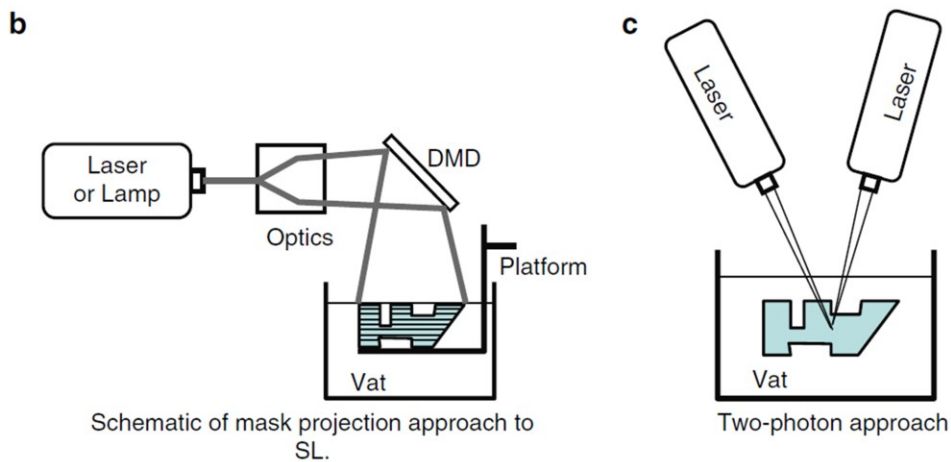
2.4.1 Stereolithography: Principles of Operation

Stereolithography uses light (often in the UV spectrum but sometimes in the visible spectrum) to selectively crosslink and thus solidify a photopolymer resin layer by layer [104]. Photopolymers were introduced in the late 1960s and are now used in a variety of industries and are particularly important in the microelectronics industry. SLA, the first Additive Manufacturing process, was

developed by Charles (Chuck) Hull in the mid-1980s. Hull scanned a laser over a photopolymer vat layer by layer to fabricate solid objects from liquid photopolymer resins. Since then, three distinct light patterning techniques have been developed for Stereolithography: vector scanning, mask projection, and two-photon (Fig. 2.4). Vector Scanning Stereolithography, (Fig. 2.4a) the technique used in most commercial machines, scans a laser over the surface of a vat filled with photopolymer resin [104]. Wherever the laser is scanned, the photopolymerization reaction occurs and the resin solidifies. Once a layer has been completed, the build stage is submerged further into the photopolymer vat and the next layer is built directly on top of the previous layer.



schematic of vector scan SL



Schematic of mask projection approach to SL.

Two-photon approach

Fig. 2.4. Schematic diagrams of the three approaches to stereolithography: a) vector scan stereolithography b) mask projection stereolithography, and c) two photon polymerization. Reproduced from Gibson et al., 2010 with permission from Springer [104].

Mask Projection Stereolithography (Fig. 2.4b) instead irradiates the entire surface of the photopolymer vat simultaneously by using a dynamic mask. The earliest systems used Liquid Crystal Displays (LCD) as their dynamic mask system [140], but most machines currently reported in the literature use Digital Micromirror Devices (DMD, a Digital Light Processing (DLP) technology developed by Texas Instruments that is widely used in projectors [104, 141]. DMDs are large arrays of micromirrors that can be rotated to be in either an ‘on’ or ‘off’ position. By doing so, light can be reflected off of a subset of the mirrors (those that are in the on position) to produce an image of patterned light. Generally, Mask Projection systems are faster than Vector Scanning systems because an entire layer is irradiated at once.

While traditional stereolithography relies on the absorption of a single photon (usually UV) by single molecules leading to initiation and crosslinking, these reactions can also be induced by the simultaneous absorption of two lower energy photons [142]. In multi-photon polymerization (MPP), an ultrafast pulsed laser is used to create a very high flux of photons in a small temporal and spatial volume to allow for the absorption of two photons by a single molecule [143-146]. The absorption of two photons produced by a Two-Photon Polymerization (2PP) system at a higher wavelength (often 780-820 nm) is energetically equivalent to the absorption of a single photon at half this wavelength. Sub-micron feature sizes can readily be achieved by 2PP due to the quadratic dependency of two photon absorption with light intensity [147-149]. Typically, parts fabricated

with 2PP systems are significantly smaller than 1 mm^3 , and are thus not practical for fabricating tissue scaffolds for implantation [150]. The fabricated structures are, however, useful for understanding cell-scaffold interactions [151].

2.4.2 Microstereolithography

Microstereolithography systems are Vector Scan or Mask Projection systems that achieve feature sizes on the micron scale. They were first demonstrated in 1993 by Ikuta et al. who used a scanning laser with a spot diameter of $5 \text{ }\mu\text{m}$ [152]. Many present systems still use Vector Scanning, but with the rapidly increasing resolution of DMDs, Mask Projection systems have become more popular in Microstereolithography.

Mask Projection Microstereolithography (MP μ SL) systems are fundamentally made up of a light source, conditioning and imaging optics, dynamic mask, build platform, a recoating system, photopolymer container, and a controller (Fig. 2.5). MP μ SL systems using UV lamps, LEDs, and lasers have been reported [141]. When choosing a light source, it is important to consider the emission spectrum of the source as well as its intensity, intensity profile, and divergence [141]. The light passes from the source through the conditioning optics, which may contain homogenizing rods, collimating lenses, filters, as well as beam expanding optics. Homogenizing rods reduce any intensity profile to help create an even light intensity across the build area. Collimating lenses are used to reduce beam divergence and increase light intensity from highly divergent sources, such as lamps. Filters remove unwanted wavelengths by allowing a single wavelength to pass through. Finally, beam expanding optics may be used to expand collimated light.

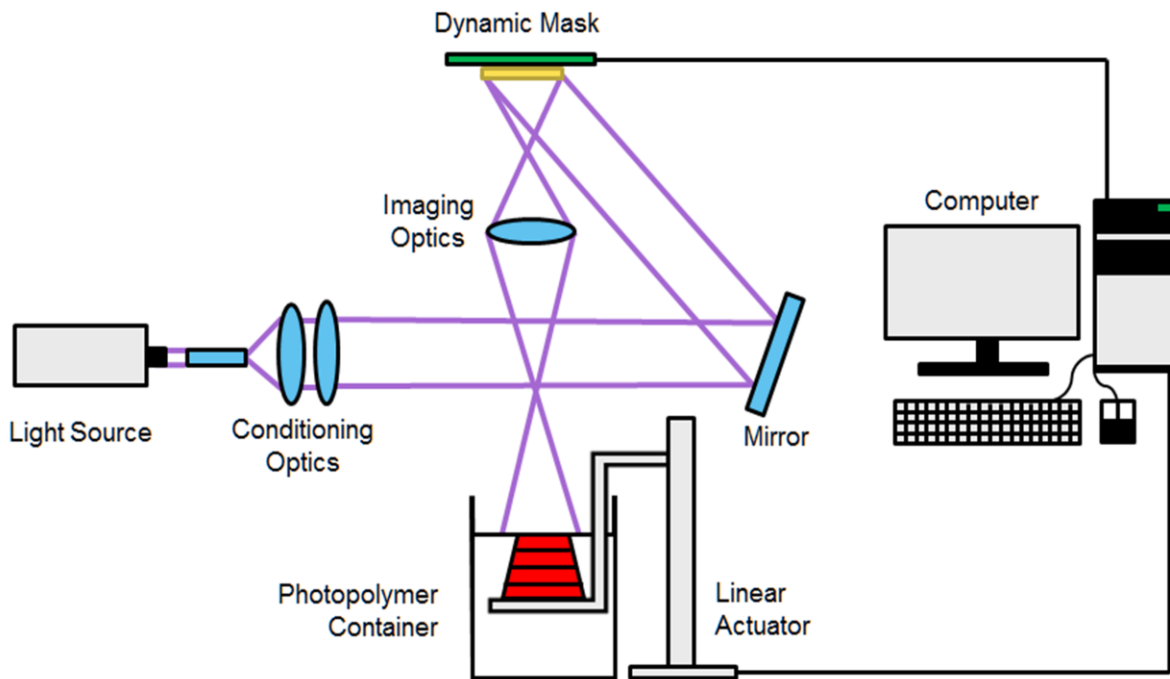


Fig. 2.5. Schematic of a Mask Projection Microstereolithography system. Reproduced from Lambert et al., 2013 [141].

The light passing through the conditioning optics is then reflected off of the dynamic mask. The efficiency of UV transmittance through LCD devices has been reported at just 12.5% [153]. Due to falling costs and higher resolutions, DMDs have become the most common dynamic mask used in MPμSL systems. The aluminum-coated micromirrors in the DMDs are designed for the reflection of light in the visible spectrum and thus have somewhat lower reflectance in the UV spectrum, but still an acceptable 88% [153]. Coatings for DMDs can be applied to increase the UV reflectance off of their micromirrors.

The imaging optics serve to focus the light reflected off the dynamic mask onto the build plane. The lenses can be used to reduce the light beam to a smaller area so that higher resolutions can be achieved. Resolution of a system can be tuned by changing the imaging optics, but image reduction will unavoidably result in a smaller build area.

Most Microstereolithography (μ SL) systems use one of two methods for recoating parts with a thin layer of liquid resin in which the next layer will be built. Top-down systems project light from above and use dipping, spreading, pumping, or a combination of these to recoat the build platform with fresh resin. Bottom-up systems project light from below and use gravity as a recoating mechanism. When projecting light from below, the window through which the light passes must be optically transparent and facilitate separation of the part from the bottom of the vat [154]. These two projection and recoating mechanisms are shown schematically in Fig. 2.6. Both systems use a build platform attached to a linear actuator. The linear actuator moves the build platform to the correct location so that the next layer can be fabricated.

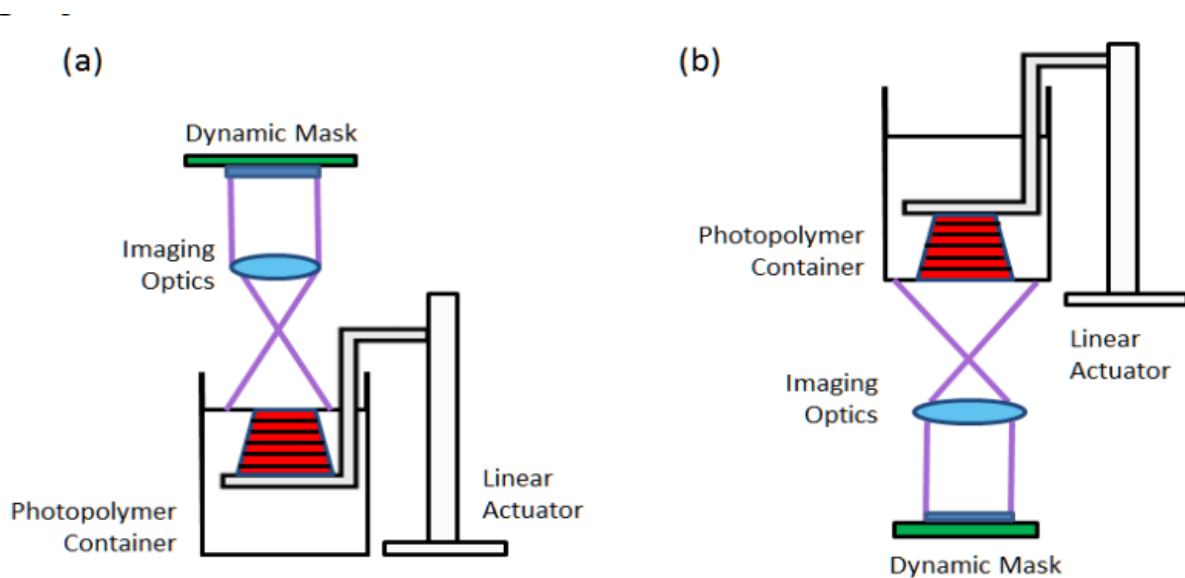


Fig. 2.6. a) Schematic of a top-down stereolithography system. b) Schematic of a bottom-up stereolithography system. Reproduced from Lambert et al., 2013 [141].

2.4.3 Advantages of Microstereolithography

μ SL offers a number of advantages both over other AM techniques as well as traditional manufacturing technologies for fabricating tissue scaffolds. Traditional fabrication techniques can only control a few of several important scaffold geometry parameters. For example, gas foaming tends to result in scaffolds with high porosity, but little pore interconnectivity [70]. Electrospinning has recently become a very popular method for fabricating tissue scaffolds, but only limited control over pore shape is possible nor can three-dimensional structures be easily fabricated [97]. AM allows for the fabrication of geometries for tissue scaffolds while maintaining complete control over pore size, shape, interconnectivity, and overall porosity simultaneously.

SLA, and μ SL in particular, allow for smaller feature sizes compared to most other AM processes as resolution is limited by a system's optics rather than an extrusion bead width or powder particle diameter. Arguably, the only AM technique that can produce smaller features is the Two Photon technique, which can produce features on the nanometer scale [155]. However, the amount of time it would take to make scaffolds of a physiologically relevant size with 2PP makes it an impractical choice. μ SL has the potential to create scaffolds with feature sizes in the tens of micrometers with overall dimensions of centimeters, making them particularly physiologically relevant. This allows the tuning of both the macrostructure and mesostructure simultaneously. Unlike melt extrusion based processes, μ SL does not require the heating of a thermoplastic to temperatures that would

cause cell death and denature peptides. Despite the toxicity of UV exposure, the incorporation of cells during the printing process with high viability has been reported [156, 157].

Through its excellent resolution and ability to control pore size, geometry, porosity, and interconnectivity simultaneously, μ SL has the potential to create complex tissue scaffolds with properties that will permit the engineering of solid tissues.

2.4.4 Photopolymer Chemistry

Photopolymers comprise monomers, oligomers, and polymers that polymerize when exposed to light [158, 159]. To photopolymerize, these molecules or mixtures of them must be in the presence of a suitable photoinitiator capable of absorbing the wavelength(s) of light to which the system is exposed (often in the UV or visible spectrum) [160]. The simplest photopolymer resin consists of a photoinitiator and a monomer, but resins can be composed of multiple photoinitiators and polymerizable molecules, light absorbers, stabilizers, anti-foaming agents, dyes, functional additives (e.g. ceramic particles and polypeptides), dispersants, and other additives [56, 161, 162]. Photopolymers have been used for decades in the microelectronics industry as photoresists, notably the epoxy-based SU-8 photoresist [163, 164]. Photopolymers are used extensively as coatings and adhesives in a wide range of industries. Photopolymer resins for SLA are almost exclusively systems that polymerize through free radical photopolymerization and cationic photopolymerization [161]. Free radical polymerization is used to polymerize acrylates, methacrylates, and acrylamides, while epoxides and vinyl ethers can be photopolymerized cationically [104].

2.4.4.1 Modeling Photocuring in SLA Systems

The curing characteristics of a resin can be described by the Jacobs Equation, which is derived from the Beer-Lambert law. First popularized by Paul Jacobs, it relates the cured depth of the polymer (C_D) and the exposure (E), to two intrinsic material (or resin) properties: depth of penetration (D_P) and critical exposure (E_C) [165, 166].

$$C_D = D_P \ln \left(\frac{E}{E_C} \right) \quad \text{Equation 2.1}$$

The cured depth is the thickness of the gelled polymer while the depth of penetration is the depth in the resin at which the irradiation intensity is equal to $1/e$ of the irradiation intensity at the surface of the resin [104, 165]. The exposure is the energy delivered to the surface of the resin. The critical exposure is the amount of exposure required for gelation of the resin to begin. While the cure depth and exposure can be readily controlled and measured in a system, the critical exposure and depth of penetration must be determined prior to processing a resin. The depth of penetration and critical exposure can be presented graphically by plotting observed cure depth and exposure delivered to the resin surface (Fig. 2.7). In the resulting “working curve”, the x-intercept of a trend line corresponds to the critical exposure while its slope represents the resin’s depth of penetration [165].

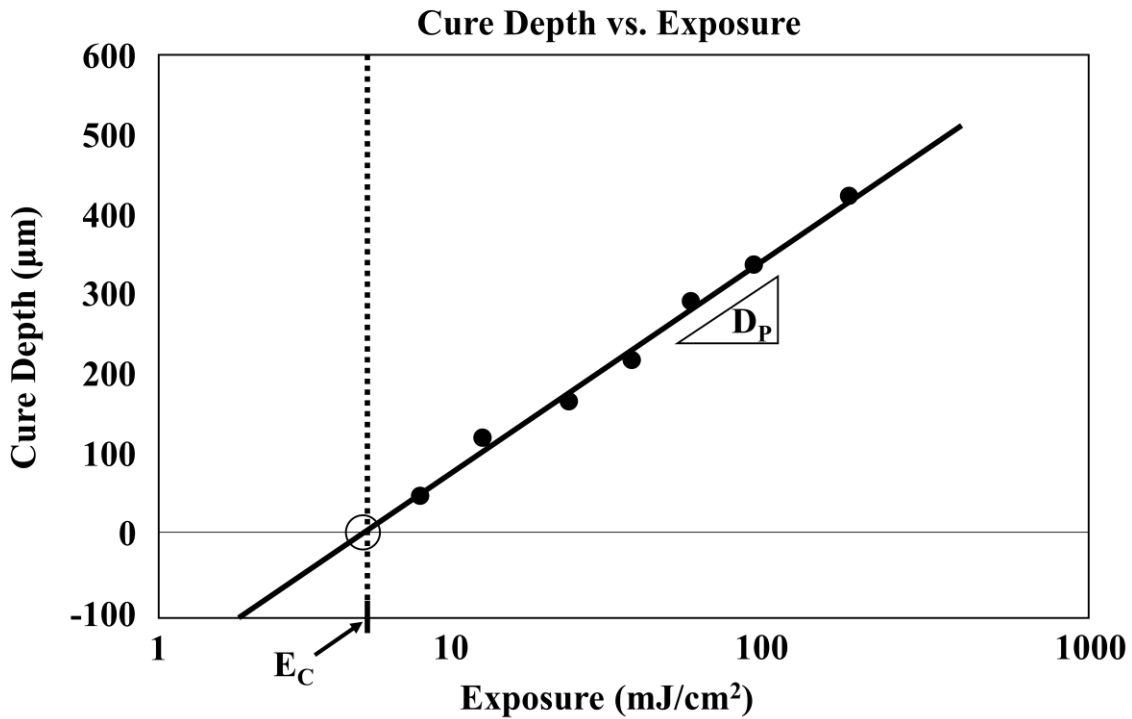


Fig. 2.7. Resin “working curve” of cure depth versus exposure.

2.4.4.2 Free Radical Systems

Free radical photopolymerization begins with the absorption of a photon (or multiple photons, in the case of MPP) by a photoinitiator molecule, resulting in the generation of a free radical [160, 167]. This radical then initiates the polymerization of the acrylate or acrylamide molecules through a carbon-carbon double bond [168]. The polymerization continues during the propagation step where hundreds or thousands of monomers are covalently linked. Polymerization terminates through either the recombination, disproportionation, or occlusion of the propagating radical. Recombination occurs when two propagating chains react and merge while in disproportionation two radicals react but the chains do not merge. Occlusion occurs when the radical on a propagating

chain gets trapped in a solidified area where all monomers have reacted to form polymer chains [145, 161, 168].

Acrylate based systems are widely used in industry and by researchers because of their fast photopolymerization [158]. However, they typically experience significant shrinkage during curing resulting in curled layers and internal stresses [104, 161]. Polymerization speed is also reduced by oxygen inhibition, which is of particular concern in top-down SLA systems where the resin being photopolymerized is in direct contact with air during printing [158, 169]. However, oxygen inhibition can be leveraged to prevent adhesion of the photopolymer to the bottom of the vat allowing for continuous printing [154, 170]. Polymerization of monoacrylate systems results in linear chains that do not form a crosslinked network. Due to the longer gel times and lower moduli of monofunctional systems, acrylate systems are based largely on di-, tri, and tetra-acrylate monomers and oligomers [161, 168]. However, the combination of acrylates and methacrylates with differing functionalities and molecular weights in a resin allows for the tuning of resin properties (e.g. viscosity, critical energy) and the final properties of printed parts (e.g. crosslink density, elastic modulus) [167]. Multifunctional oligomers or polymers permit crosslinking of the system and impart mechanical, electrical, and thermal properties to the final part [171, 172]. Because these macromolecules are typically too viscous to print on their own, resin viscosity is reduced through the addition of low molecular weight acrylates and reactive diluents [156, 173], although non-reactive diluents can be used as well [39, 171]. These lower molecular species can either be mono or multifunctional.

Free radical photopolymerization in thiol-ene and thiol-yne systems is not inhibited by oxygen and tend to have lower shrinkage than acrylate systems [150, 174]. In addition, higher conversions are required for gelation of thiol-ene systems than acrylate systems, allowing for chain rearrangement to occur at higher conversion percentages and resulting in reduced residual stresses in printed parts. However, widespread use of thiol-based systems for SLA has been hindered by their unpleasant odor and typically low moduli [161].

2.4.4.3 Cationic Systems

Although free radical systems tend to be more reactive than their cationic counterparts, epoxides and vinyl ethers that photopolymerize cationically have an important role in SLA resins [159, 175]. The reduced shrinkage of these resins during printing results in more dimensionally accurate parts. In addition, the lack of an oxygen inhibition effect during cationic polymerization allows for a reduction in the amount of photoinitiator needed [104]. Most commercially available resins are a blend of epoxies and acrylates that take advantage of the favorable properties of both types of photopolymers. Some resins even contain molecules with both acrylate and epoxy functional groups [161].

2.4.5 State of the Art of Microstereolithography for Tissue Scaffolds

2.4.5.1 Resolution and Accuracy

Resolution and accuracy of a μ SL system, and in fact all AM systems, can be defined and evaluated in many ways, however, in the context of tissue scaffolds it is most appropriate to compare systems based on the minimum feature size that they are capable of fabricating. Columns and horizontal struts are positive features while holes and pores are negative features. The diameter of smallest

feature that can be fabricated is generally defined as the minimum feature size of a machine. While this metric is quite good at assessing a μ SL system's capability for fabricating tissue scaffolds, minimum feature size can differ depending on the material being used and does not take into account the aspect ratios of the features.

The ability to fabricate scaffolds with feature sizes below 100 μ m allows for the fabrication of features just slightly larger than the average cell diameter. Resolution and minimum feature size are generally limited by optics in SLA machines, and this continues to be true for μ SL systems. Several research groups have reported the fabrication of parts with μ SL with features below 100 μ m (Table 2.1). In projection SLA systems, there is an inherent compromise between the minimum feature size that can be achieved and the projection area of the machine. The largest DMD currently available has an array of 2560 x 1600 micromirrors. Lenses can be used to reduce the projected area that a pixel exposes at the surface of the resin vat, but by doing so, the overall area that the DMD is exposing is reduced. Potential solutions might include image stitching or the use of larger DMDs when they become available [176]. On the other hand, the minimum feature size that can be achieved with laser based systems are limited by the spot size of the laser as well as the accuracy and precision of the galvanometers that raster the laser over the build surface.

2.4.5.2 Resins used in μ SL for Tissue Scaffolds

Generally, commercial resins that have been developed for stereolithography do not display adequate cytocompatibility, nor can they degrade into non-toxic products within the body. Even in the research space, creating photopolymers for μ SL with adequate biocompatibility for cell culture has remained challenging and relatively few materials have been used to fabricate tissue

scaffolds (Table 2.1) [167]. To be suitable for μ SL, resins must cure relatively quickly and have a viscosity that allows for rapid recoating of thin layers. In general, oligomers with higher molecular weights than analogous lower molecular weight oligomers or monomers have lower toxicities and impart more mechanical strength, however, they also cure more slowly and have higher viscosities. The majority of the resins reported in the literature are based on low molecular weight multifunctional acrylates that create highly crosslinked structures which are rigid and brittle.

Much of μ SL research for tissue scaffolds has focused on the use of poly(propylene fumarate) (PPF) resulting in scaffolds with a limited range of mechanical properties and degradation timelines (Table 2.1). Several other materials have been explored, but overall, the number and variety of photopolymers available for use are inadequate to fulfill the potential that μ SL holds. Because only a small number of photopolymers have been adequately characterized for use, engineers have a limited range of mechanical properties, bioresorption properties, and surface chemistries. To create scaffolds for all types of tissue replacement requires a palette of materials with a range of properties.

There are numerous examples of μ SL-fabricated tissue scaffolds being assessed for cell adhesion, viability, and proliferation *in vitro* (Table 2.1), however, few studies have been conducted *in vivo* on live animal models. Although the number of studies using μ SL-fabricated scaffolds has increased in recent years, few researchers have evaluated synthetic materials *in vivo* [177-183] and even fewer have studied natural polymers [184].

Table 2.1. Summary of literature reporting the use of Microstereolithography for the fabrication or potential fabrication of tissue scaffolds

Material	Photoinitiator	UV Blocker	Scaffold Architecture	Minimum Feature Size	Projection vs Scanning	Cell Culture	Ref
GelMA	1% Irgacure 2959	0.1% HMBS, 0.01% TEMPO	Square, hexagonal, 200-500 μm pores	50 μm	Projection	Immortalized HUVEC	[46]
HDDA	Benzoin ethyl ether	0.3% unspecified photoabsorber	Square, 150 μm pores	5-15 μm	Projection		[153, 185]
GelMA	BAPO (Irgacure 819) & Irgacure 2959				Projection & Scanning	MG63 osteoblast-like cells	[186]
PDLLA	2-6% Irgacure TPO-L	0.15-0.20% Orasol Orange G dye	Gyroid, 200-500 μm pores	250 μm	Projection	Human articular chondrocytes, MC3T3-E1, and iMSC	[39, 187, 188]
PDLLA containing up to 20% hydroxyapatite nanoparticles	4% Lucirin-TPO	0.15% Orasol Orange G dye	Gyroid, 750 μm pores		Projection	Bone marrow derived hMSC up to 21 days	[189]
PEGDA	Irgacure 819	0.5-0.8% unspecified photoabsorber	Micro bioreactor	20 μm	Projection	INVSc1 yeast cells for 45h	[190]
PEGDA	10% Irgacure 2959	0.2% Tinuvin 234	Hexagonal, 150 μm pores	50 μm	Scanning	Fibronectin surface modified. Murine marrow progenitor for 48h	[191]
PEGDA	0.1% Irgacure 2959	None	Hexagonal, square, triangle, 165-650 μm pores	100 μm shown, 20 μm claimed	Projection	Murine OP-9 marrow stromal cells encapsulated in resin, primary murine mesenchymal stem cells up to 4 weeks	[45]
PEGDA and dipentaerythritol penta-/hexa-acrylate	1.8 wt% Irgacure 784		Gyroid			hMSC for up to 7 days	[192]
PEGDA with RGDS	0.5 wt% Irgacure 2959		Multi-material parts	250 μm	Scanning	Human dermal fibroblasts up to 1 week	[193]
PPF/DEF	2% BAPO	None	Square, 100 μm pores	30 μm	Projection		[194]
PPF/DEF	1 % BAPO	None	Interpenetrating square and 'X', 125 – 500 μm pores	90 μm	Scanning	5SFB and RGD surface modified. MC3T3-E1, up to 2 weeks	[195]
PPF/DEF	1% Irgacure 819	None	Offset square, 350 μm pores	125 μm	Scanning	MC3T3-E1 up to 14 days, surface modification with RGD, cyclo RGD, or RGD-KRSR	[196]
PPF/DEF	1% BAPO	None	Offset square, 100-500 μm pores	125 μm	Projection	MC3T3-E1 up to 7 days	[44]
PPF/DEF	1% BAPO (Irgacure 819)	None		500 μm	scanning		[197]
PPF/DEF, suspended PLGA microspheres containing BMP-2	1% BAPO	None	Offset square, 200 μm and 400 μm pores	100 μm	Scanning	MC3T3-E1 showed bone formation <i>in vivo</i> after up to 11 weeks	[56]

Material	Photoinitiator	UV Blocker	Scaffold Architecture	Minimum Feature Size	Projection vs Scanning	Cell Culture	Ref
PPGDA, Pluronic L-31	2% DMPA	None	Square	57 μm	Projection	MC3T3-E1 up to 7 days	[47]
PTEGA-DMA (Poly(tri(ethylene glycol) adipate) dimethacrylate)	2% DMPA		Cylindrical		Projection	Viability of MDA-MB-231 cells after 24h	[198]
Somos 11120		Proprietary		50 μm	Projection		[199]
TMC/TMP (Trimethylene carbonate/ trimethylolpropane acrylated oligomer)	BDMK	None	Square, 300-500 μm pores	120 μm	Scanning	Primary chondrocytes from New Zealand white rabbits up to 4 weeks	[200, 201]

2.4.5.3 Synthetic Polymers

Synthetic photopolymers have mechanical properties, degradation rates, and viscosities that can be tuned over a wide range based on chemical structure, molecular weight, and processing. However, cell adhesion and viability on synthetic polymers are typically considerably lower than on natural polymers.

The most widely synthesized resin for use in fabricating tissue scaffolds with μ SL is poly(propylene fumarate) (PPF) [56, 195, 197, 202-205]. PPF was developed in the late 1980's [206] and later used to build tissue scaffolds via μ SL [78, 197]. It's printing is straightforward and its mechanical and degradation properties can be tuned by varying molecular weight and crosslinking density [56, 195, 196, 202-204, 207, 208]. The material is popular because it is biodegradable and osteoblasts have been shown to proliferate on it [44, 56, 195-197]. In addition, its hydrolytic degradation products, fumaric acid and propylene glycol, are relatively nontoxic, although they are acidic [209, 210]. While the material is not commercially available, techniques for its synthesis and purification have been meticulously reported [211]. For printing, the PPF oligomer is often blended with its monomer, diethyl fumarate (DEF), to reduce the viscosity of the resin. A free radical photoinitiator is added to allow for the photocrosslinking of the resin, however, unlike most other resins, a UV absorber is generally not included. Crosslinked PPF is a relatively hard material and thus well suited for bone, cartilage, and hard tissue repair [208, 212]. PPF-based scaffolds have been evaluated *in vivo* for use in bone regeneration. BMP-2 growth factor loaded into the resin prior to printing was found to increase bone formation and induce differentiation of hADSC seeded onto the scaffolds 11 weeks after implantation into Wistar rats [213]. In addition,

scaffolds fabricated using μ SL were found to perform better than those fabricated via particulate leaching/gas foaming [56].

Poly(D,L-lactide) (PDLLA) is a hard, biodegradable, and amorphous form of polylactic acid that has been used in resorbable bone fixation devices [187]. Although it has been FDA approved for some applications, its very slow degradation rate limits its use in tissue scaffolds to hard tissue regeneration [210]. The monomer can be modified with methacrylate groups to allow photocuring in SLA systems [187]. Adequate cell adhesion and cytotoxicity have been reported from studies conducted on scaffolds fabricated via SLA [39, 188]. In addition, researchers have shown that hydroxyapatite powder can be added to PDLLA resins to improve strength, toughness, and bone cell biocompatibility [51, 189]. They have demonstrated the viability of bone marrow derived human mesenchymal stem cells (hMSC) on such scaffolds as long as 21 days [189].

PCL is often used in bone tissue engineering and has been modified into methacrylated macromers for printing [214]. Micro-computed tomography (μ CT) demonstrated excellent geometric fidelity between the 3D computer model data and the resulting printed structure. Further, murine fibroblasts seeded on the polymerized material adhered evenly over the entire surface. Like PDLLA, PCL is approved for some clinical applications by the FDA, but also has a very slow degradation rate [209]. In addition, cell adhesion is generally low and PCL's degradation products are acidic [210].

Poly(ethylene glycol) diacrylate (PEGDA), derived from poly(ethylene glycol) (PEG), a material with low cytotoxicity that has been extensively implanted into the human body. It has been studied

extensively for use in drug delivery as cells generally do not readily attach to it. Several groups have printed tissue scaffolds from PEGDA using μ SL, but have been thwarted by low cell adhesion to the material [190, 191, 215]. However, one research group has demonstrated the encapsulation of murine marrow stromal cells in PEGDA resin prior to printing and shown relatively good viability of the cells after printing [45]. Macromers derived from both PEG and collagen I can also be used to improve cell adhesion to parts fabricated using μ SL [216].

1,6-Hexanediol diacrylate (HDDA) is a low viscosity monomer that has been used in fabricating microstructures with Microstereolithography [151, 153, 185, 217, 218]. Cell viability and proliferation studies have not been conducted on the material, however it has been found to be a potent skin sensitizer [219]. Structures with feature sizes as small as 0.6 μ m have been fabricated with μ SL using HDDA [153].

Trimethylene carbonate (TMC) based photopolymers were some of the first used in μ SL with tissue engineering applications [220, 221]. The TMC-based oligomers generally include PEG, caprolactone, or trimethylolpropane (TMP) and are biodegradable [200, 201, 222]. The viability and proliferation of cells on TMC films as well as on scaffolds both *in vitro* and *in vivo* has been demonstrated [200, 201, 221, 223, 224]. Recently, hADSC seeded onto scaffolds fabricated from a TMC-based photopolymer and exposed to transforming growth factor (TGF)- β 3 were found to efficiently differentiate towards anulus fibrosus-like cells [224]. This advance could allow for the engineering of anulus fibrous tissue for the treatment of spinal disk herniation and degeneration of intervertebral disk degeneration. Scaffolds fabricated using TMC-based resin have been used to explore the formation of bone and cartilage tissue *in vivo* [181, 200]. The inclusion of

hydroxyapatite nanoparticles into TMC resin were found to improve osteogenic differentiation of hBMSC *in vitro* and improved healing and bone formation in New Zealand white rabbit animal models after four weeks [181]. Separately, cartilage-like morphology was achieved after four weeks *in vivo* with scaffolds fabricated from TCM and injected with alginate-encapsulated chondrocytes before implantation [200].

Tube-like scaffolds mimicking arterial constructs and porous scaffolds have been fabricated using poly(tri(ethylene glycol) adipate) dimethacrylate (PTEGA-DMA), a hydrolyzable polyester (Fig. 2.8). The material was found to promote good cell adhesion of both MDA-MB-231 human breast cancer cells and MC3T3-E1 mouse preosteoblasts [198, 225].

Several commercially available SLA resins have been used for μ SL with tissue scaffold applications in mind as they are relative inexpensive, require no synthesis, and work readily with commercially available machines [31, 199, 226-230]. However, these resins are not developed with the requirements of tissue scaffold in mind and thus are not well suited for fabricating scaffolds. When crosslinked, the majority of these polymers are rigid and would have mechanical properties suitable for hard tissue engineering [231]. However, no commercial SLA resins demonstrate the requisite biodegradability or bioresorption. Despite this, cell seeding has been attempted on some of these resins, albeit with little success [226, 227].

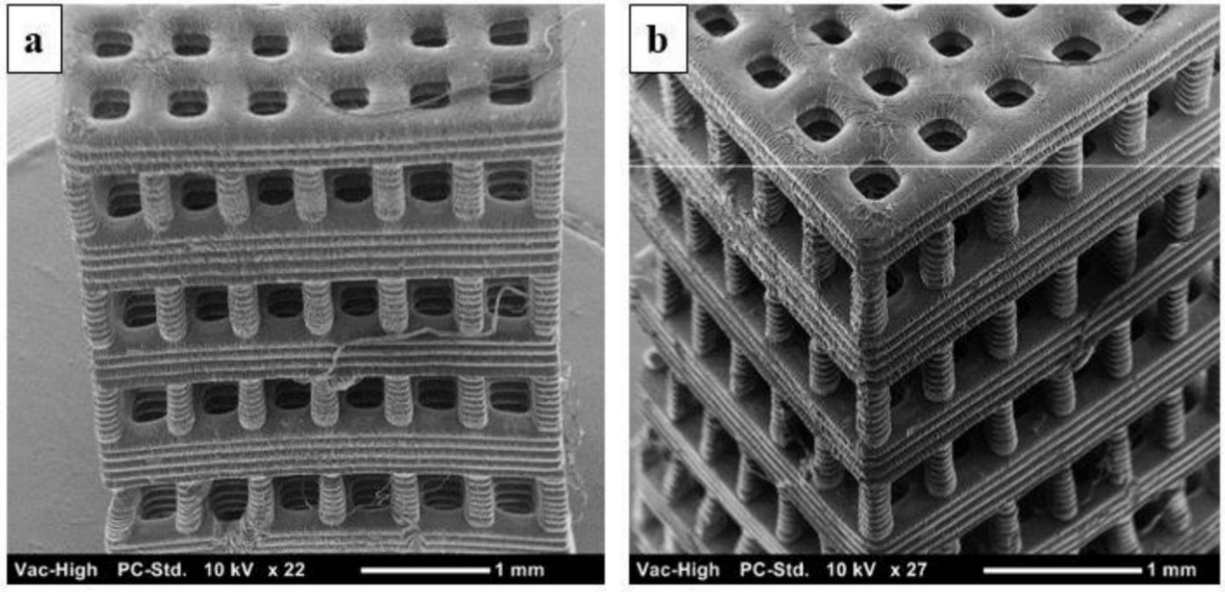


Fig. 2.8. SEM micrographs of tissue scaffolds fabricated from poly(tri(ethylene glycol) adipate) dimethacrylate (PTEGA). Reproduced from Chartrain et al., 2016 [225].

2.4.5.4 Naturally Derived Polymers

Efforts have also been made to fabricate scaffolds from naturally derived materials with μ SL as they are often biodegradable and exhibit low cytotoxicity. Arginylglycylaspartic acid (RGD) groups present on many proteins found in the ECM are recognized by attachment dependent cells and promotes their adhesion. Collagen, when combined with a μ SL fabricated β -tricalcium phosphate scaffold, has shown promise for the engineering of osteochondral tissue [232]. Gelatin, which is derived from collagen, has been modified with methacrylate endgroups (GelMA) in order to allow photopolymerization and the fabrication of three-dimensional structures via SLA [46, 186, 233]. Further, the stiffness of the GelMA can be controlled by the degree of methacrylation. The compressive modulus of GelMA can be increased by a factor of three from 10 to 30 kPa by increasing the methacrylation from 20% to 80% [234]. Mechanical properties and cell response can also be tuned by varying GelMA content in the gel. Recently, scaffolds fabricated from a

GelMA solution containing BMP-2 and encapsulated hBMSC have been tested *in vitro* and *in vivo* for bone formation [184]. Fourteen weeks after intramuscular implantation in mice, scaffolds with both BMP-2 and encapsulated hBMSC had significantly higher bone formation than scaffolds that did not contain BMP-2. The bone was localized in the scaffold and found to be primarily due to the hBMSC rather than host cells.

Chitosan can also be incorporated into resins that use PEGDA as a crosslinker either by simply blending the PEGDA with a chitosan solution [235] or by functionalizing the chitosan so that it copolymerizes with the PEGDA [236]. Researchers have also demonstrated the ability to functionalize and print hyaluronic acid using SLA [237] and photocure monolayers of alginate [238]. Epoxidized soybean oil acrylate mixed with acetone has been fabricated into scaffolds using a 355 nm laser scanning system [239]. Proliferation of hMSC on the cured material after five days was similar to proliferation on PCL and PLA substrates. This advance could pave the way for the use of renewable plant-based oils in stereolithography.

Most fabrication of tissue scaffolds with Microstereolithography has used synthetic polymers and thus the introduction of natural polymers will have significant impact in overcoming many of the limitations posed by synthetic materials. Unlike many synthetic polymers, natural polymers tend to be biocompatible, biodegradable, and promote cell adhesion. However, natural polymers have disadvantages of their own. They typically have poorer mechanical properties and can be harder to process than synthetic polymers [86, 161, 209, 210]. In addition, protein-based biopolymers derived from animal sources can have contaminants that provoke an immune response or impact material properties [86, 210]. Despite these challenges, μ SL of tissue scaffolds using natural

polymers or blends with both natural and synthetic polymers will continue to become more common because of their beneficial bioactivity and low toxicity.

2.4.6 Fabrication of Parts with Multiple Materials

Tissue scaffolds fabricated by the selective placement of more than one material hold particular promise for Tissue Engineering. Multi-material scaffolds can be used to direct cell growth and proliferation, create mechanical property gradients, and control scaffold degradation [97, 193]. For example, by selectively placing materials or growth factors, endothelial cells could be induced to attach to certain areas of a scaffold while stimulating osteoblasts to attach to other areas. This would provide exceptional control over the physical attachment, growth, and proliferation of cells in a tissue scaffold. Similar examples could be envisioned for controlling stiffness, degradation, hydrophilicity, and other properties. Researchers have reported multi-material stereolithography and even Microstereolithography. To build multi-material objects, the build platform is dipped into a vat containing a first material, one or several layers are fabricated, the platform and partially fabricated object are cleaned of unpolymerized resin, and fabrication continues in another vat containing a dissimilar material [230, 240-243]. However, these systems have not yet been used to fabricate tissue scaffolds that take advantage of the myriad new design possibilities due to the technical challenges of frequent switching between materials. The most complex multi-material μ SL-built objects to date have been fabricated by Wicker et al. using a modified 3D Systems Viper si2 (Fig. 2.9). These objects can even contain more than one material in a single layer by fabricating part of the layer in one material, switching to a second material, and fabricating the remainder of the layer. However, to create complex multi-material scaffolds that can be used to guide cell

adhesion, growth, and differentiation, it will be necessary to fabricate parts with dozens if not hundreds of material changeouts.

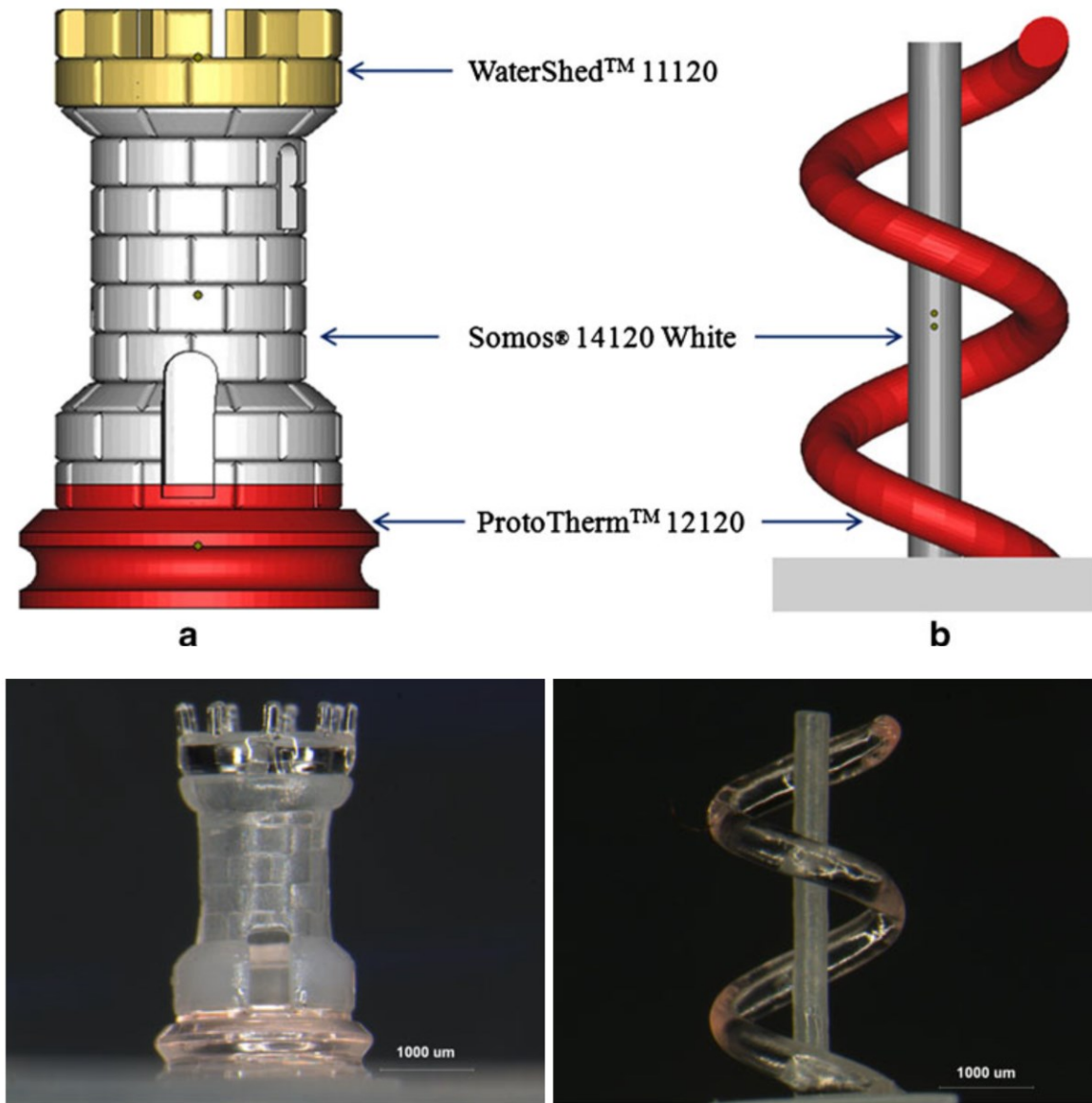


Fig. 2.9. Wicker et al. have developed the most advanced multi-material μ SL system reported to date through the modification of a 3D Systems Viper si2 [230,240,241]. CAD models of a multi-material rook (top left) and post with helix (top right). The rook (bottom left) was fabricated with

two material changeouts (from ProtoTherm 12,120 to 14,120 White and then to WaterShed 11,120 while only two were required for the post and helix (bottom right). The entire post was printed before beginning the fabrication of the surrounding helix [230,240]. Reproduced from Wicker et al., 2009 with permission from Springer [230].

2.4.7 Photoinitiators and UV Blockers

Photoinitiators are generally chosen for their absorption in the UV spectrum and low cytotoxicity, although cell viability is affected by many photoinitiators [244]. Irgacure 819 (phenylbis(2,4,6-trimethylbenzoyl)phosphine oxide) is used in SLA systems with higher wavelength (>400 nm) but it suffers from poor solubility. Irgacure 2959 (2-Hydroxy-1-(4-(2-hydroxyethoxy)phenyl)-2-methyl-1-propanone) is perhaps the most widely used photoinitiator in tissue engineering applications due to its solubility in water. However, low absorption at wavelengths >370 nm results in long cure times for SLA systems with higher wavelength light sources. Irgacure TPO (diphenyl (2,4,6-trimethylbenzoyl) phosphine oxide), and DMPA (2,2-dimethoxy-2-phenylacetophenone) are also commonly used initiators, neither is water soluble. Recently, LAP (lithium phenyl-2,4,6-trimethylbenzoylphosphinate) has gained attention for its potential in both tissue engineering and SLA [157, 245]. LAP has good absorption at both 365 nm and 405 nm light, low cytotoxicity, and is water soluble. The initiators used in commercial resins are not reported.

UV blockers are used to decrease the depth to which radiation penetrates in the resin (D_p) so that thinner layers of polymer can be polymerized to allow for overhanging structures. Increasing the quantity of UV blocker in a resin allows for the fabrication of parts with smaller feature sizes, but requires an increase in radiation [246]. A much greater variety of UV blockers (or UV absorbers)

than photoinitiators are used in Microstereolithography resins (Table 2.1). In addition, there do not appear to be any trends in UV blocker selection and as each research group appears to favor a specific UV blocker.

2.4.8 Bioactive Additives and Cell-Containing Resins

The addition of bioactive particles or peptide molecules can increase the adhesion of certain cell types and help direct differentiation. Hydroxyapatite (HA) and tricalcium phosphate (TCP), materials found in bone, can be added to μ SL resins in the form of powder or microparticles [31, 51, 189, 204]. The ceramic particles modify the scaffold's mechanical properties to allow for moduli that can mimic a variety of tissues [51]. The presence of these bioactive ceramics has been shown to improve cell adhesion and viability as well as promoting their differentiation into osteoblast-like cells [189, 204]. Optionally, the photopolymer can be burned out and the ceramic particles sintered together to create a hard, dense ceramic scaffold [31, 162]. Cellulose nanocrystals, which may have widespread applicability to tissue engineering due to their low toxicity, have been used as additives in SLA resins to improve the tensile strength and elastic moduli of printed objects [247, 248]. Peptide sequences that promote cell adhesion or differentiation can be incorporated in the resin or applied as a coating to the scaffold after it has been fabricated [191, 195, 196]. RGD is popular as it facilitates the adhesion of all adherent cell types while lysine-arginine-serine-arginine (KRSR) is used to promote the adhesion of osteoblast cells [203]. The inclusion of the growth factor bone morphogenetic protein-2 (BMP-2) encapsulated in microspheres into μ SL-fabricated scaffolds has been found to enhance bone formation *in vivo* for both human adipose derived stem cells (hADSC) and MC3T3-E1 mouse

preosteoblasts [56, 213]. Finally, naturally derived proteins, such as fibronectin, can be coated onto scaffolds to promote attachment of adherent cell types [191].

One of the greatest drawbacks of SLA is that cells are not placed into the scaffold during the printing process, but instead seeded onto the scaffold after printing. Large scaffolds intended to repair or replace entire tissues would make this quite challenging. In addition, tissues are made up of multiple cell types and the tissues function arises from the arrangement of those cell types in relation to each other. To overcome this challenge, some groups have incorporated cells into the photopolymer resin prior to printing [156, 157, 184, 249]. Tuan et al. demonstrated the stereolithographic fabrication of parts containing hADSC in a PEGDA-based resin [157]. Notably, they used lithium phenyl-2,4,6-trimethylbenzoylphosphinate (LAP), a water soluble photoinitiator with demonstrated biocompatibility at low concentrations that strongly absorbs both visible and UV light [245]. Using a live-dead assay, they demonstrated >90% viability of cells in the scaffolds after seven days. Kim et al. used a similar process to incorporate NIH 3T3 mouse fibroblasts into PEGDA/GelMA hydrogels during printing [156]. Cell viability in their constructs was in excess of 80% after five days. It could be envisioned that in future work, multi-material stereolithography could be used to print parts containing multiple cell types arranged in a way that mimics native tissue.

2.4.9 Feature Size

Microstereolithography machines are differentiated from stereolithography machines by the resolution or feature size that they can achieve. Resolution is the most commonly reported quality parameter of μ SL machines; however, the minimum feature size that can be fabricated using a

given resin is a much more informative measure of what the system is capable of building. The resolution of a machine can be a measure of many different parameters (e.g. motor step size, laser beam width, effective pixel size). Most μ SL machines can fabricate features smaller than about 150 μm but just a handful are capable of feature sizes smaller than 50 μm (Fig. 2.10, Table 2.1).

The ability to build smaller feature sizes provides a distinct advantage in fabricating tissue scaffolds with greater surface area and porosity and allow for more complex designs [19]. Micropatterning can also be used to control cell adhesion and migration [250]. The optics of a μ SL system are often the major factor in achieving smaller feature sizes [141]. In a Mask Projection μ SL system, it is possible to incorporate imaging optics that will reduce the effective pixel size at the resin surface, but the build area will be proportionally minimized. Solutions (e.g. image stitching) will be important in fabricating tissue scaffolds that have both feature sizes and overall dimensions that are physiologically relevant.

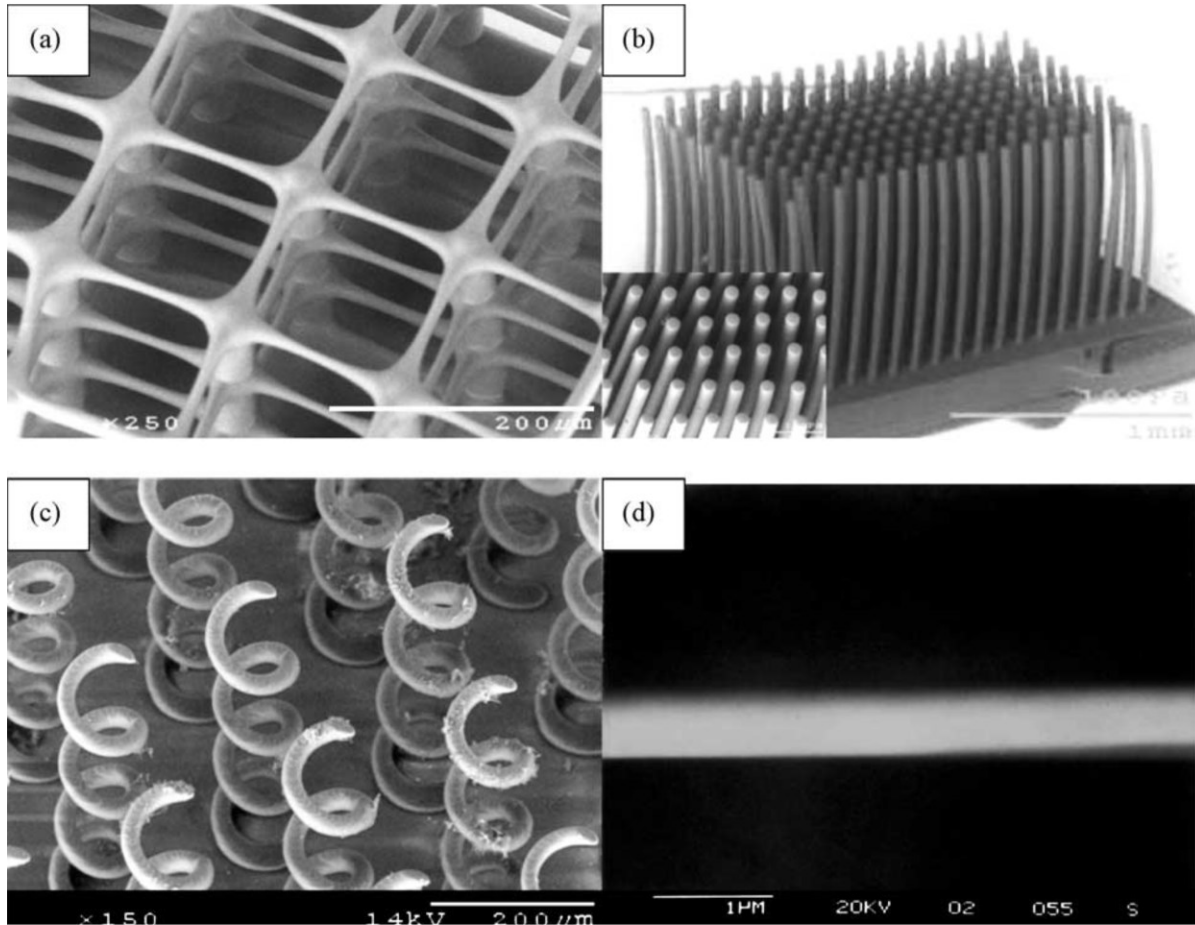


Fig. 2.10. A variety of geometries have been fabricated using a very high resolution μ SL system including (a) high porosity matrix with beam diameters of $5\ \mu\text{m}$; (b) high aspect ratio micro-rods in a 21×11 array; (c) micro springs with wire diameter of $25\ \mu\text{m}$; (d) horizontal beam with diameter of $0.6\ \mu\text{m}$. Reproduced from Sun et al., 2005 with permission from Elsevier [153].

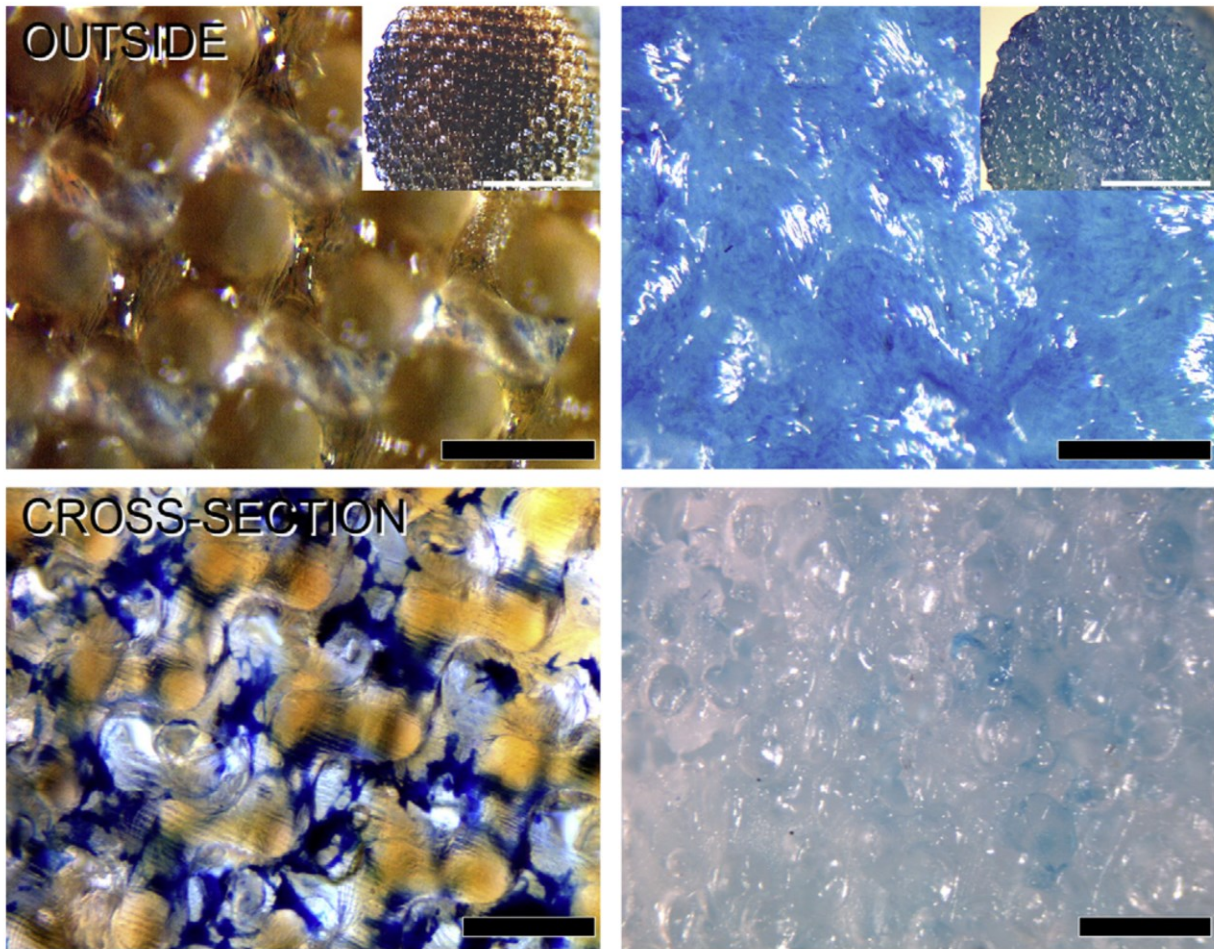


Fig. 2.11. Stereomicroscope images of the outer surface and cross-section of methylene-blue stained scaffolds fabricated in a gyroid geometry by μ SL (left) or salt-leaching (right). Scaffolds were seeded with immortalized mesenchymal stem cells and cultures under static conditions for 5 days. (top) The salt leached scaffold has significantly more cell proliferation on the scaffold's outer surfaces; (bottom) the printed scaffold has cells throughout the entire three dimensional structure while the interior of the salt- leached scaffold is nearly devoid of cells. Scale bars represent 500 μ m or 4 mm in the insets. Reproduced from Melchels et al., 2010 with permission from Elsevier [39]. (For interpretation of the references to colour in this figure legend, the reader is referred to the web version of this article.)

2.4.10 Scaffold Architecture and Mesostructure

The architecture and mesostructure of a scaffold influence cell migration and growth through it [188]. This includes the shape and size of pores as well as the struts that define their boundaries. Relatively few scaffold architectures have been explored with μ SL and other AM techniques (Table 2.1). Square (or log cabin) and offset square architectures are the most common, but hexagonal (honeycomb) and gyroid architectures have also been fabricated and others have been proposed (Fig. 2.11) [39, 188, 196, 251-253]. Tissues in the human body do not organize in such simple periodic architectures, but few researchers have fabricated biomimetic or organic scaffolds with μ SL [188]. Several studies have shown that pore size and architecture of these scaffolds affects cell viability, but the variety of materials and cell lines used makes it difficult to assert broad conclusions as to which pore sizes and architectures are optimal [39]. In fact, it is likely that each combination of material and cell type has a unique optimal pore size and architecture. While the architecture and mesostructure of the scaffold affects cell viability, the more significant impact may be on differentiation and organization into functional units. However, the impact of architecture and mesostructure on differentiation has yet to be explored using μ SL scaffolds. In addition to the three dimensional scaffold architecture, surface curvature, topography, and roughness can affect how cells adhere, align, and spread on a substrate [253-255]. Recent work has even shown that these surface characteristics can also impact cellular migration and differentiation [256]. μ SL has the potential to create powerful environmental cues to help guide tissue formation by creating tissue scaffolds with designed geometry and surface characteristics.

To supply nutrients and oxygen to all cells, thick tissue scaffolds require vascularization that cannot be fabricated with traditional scaffold fabrication techniques [58]. The fabrication of

scaffolds with μ SL that have the blueprint for cells to create vascularization has been remarkably lacking in the literature, despite the sufficient capability of several systems and research groups. A tissue scaffold that has the potential for inducing vascularization should have a biomimetic capillary-like network of tubes or some other architecture that would allow for nutrient, oxygen, and waste flow between the surface and interior of the scaffold. When the fabrication of tube-like networks has been reported, they are standalone structures [190]. To generate large functional tissues, these capillary structures must be embedded in scaffolds to promote the growth of both parenchymal and endothelial cells (Fig. 2.12).

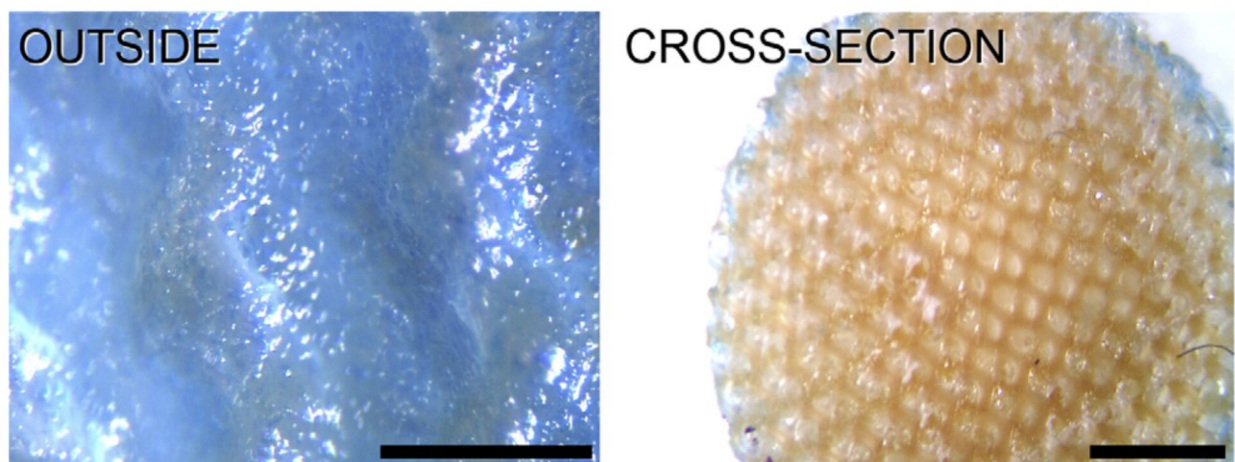


Fig. 2.12. Stereomicroscope images of methylene blue-stained cells on gyroid scaffolds after 20 days of static culture. Scale bars are 500 μ m (left) and 2 mm (right). Cell viability is markedly reduced after 20 days due to the lack of vascular structures incorporated into the tissue scaffold. Reproduced from Melchels et al., 2010 with permission from Elsevier [39]. (For interpretation of the references to colour in this figure legend, the reader is referred to the web version of this article.)

2.5 Future Directions of μ SL

The application of μ SL for the fabrication of tissue scaffolds presents a significant opportunity and will see increased development in the coming years. Future improvements in the technology will help it to overcome the limitations that prevent the fabrication of tissue scaffolds that can be used in clinical settings. While challenges remain, there are many opportunities for the development of more suitable materials, improvements in scaffold design and feature sizes, and the incorporation of vasculature.

The lack of a diverse palette of biodegradable and cytocompatible materials presents a significant impediment to fabricating clinically relevant scaffolds using μ SL. In fact, a lack of varied materials is a challenge that plagues not only SLA, but all AM technologies [161, 257]. As μ SL continues to gain traction as a viable method for creating tissue scaffolds, researchers will be looking to synthesize novel materials that are better suited for the fabrication process [198]. Some of these will be synthetic materials containing peptides, additives, or other molecules that facilitate cell adhesion, proliferation, and differentiation. Researchers will also modify a greater number of natural and renewable polymers for use in μ SL, such as recent work using soybean oil and keratin [239, 258]. Synthetic and natural photopolymers will be blended to derive beneficial properties from each, as has recently been demonstrated by Wang et al. [156]. A wider variety of suitable materials will allow for a greater range of mechanical and degradation properties in scaffolds that are essential for replicating tissues with very different properties (e.g. bone and hepatic tissue) [215]. Finally, the fabrication of multi-material scaffolds will allow for the creation of more complex multicellular tissues that could not be achieved by using single material scaffolds.

μ SL allows for unprecedented control over the architecture and mesostructure of tissue scaffolds that cannot be achieved with traditional fabrication techniques or other AM technologies. This presents researchers with a unique opportunity to explore how scaffold architecture can influence cellular adhesion and migration [39, 259, 260]. To date, only a handful of simple architectures have been investigated, and the number of biomimetic or naturally inspired scaffolds is even fewer. It is likely that the architectures that researchers fabricate will soon become more complex and begin to mimic the actual architectures of human tissue. Cell biologists may also be able to glean insight on how cells interact with their three dimensional environment [253]. Understanding the influence of architecture and mesostructure on cells will allow researchers to create design rules for tissue scaffolds that will apply not only to μ SL but to the wider field of Tissue Engineering.

The inability to generate vasculature in tissue engineering constructs has plagued researchers for more than two decades. Traditional techniques are simply unable to fabricate scaffolds that include both small pores as well as a network of larger pores that allow nutrient and oxygen perfusion through the scaffold. The fabrication of tubular networks that resemble vasculature have been demonstrated with μ SL and the next steps for determining whether vasculature can be formed from these networks by incorporating them into scaffolds should receive considerable attention.

Tissue scaffolds for the repair of bone is the focus of much current research in μ SL. Osteoblasts tend to prefer larger pore sizes in tissue scaffolds, which are easier to fabricate than small pore sizes. To fabricate tissue scaffolds suitable for cell types that prefer smaller pores will necessitate improvements in the feature sizes that μ SL machines can achieve. It is unclear the extent to which sub-micron feature sizes in tissue scaffolds would be beneficial, but features on the order of 10 μ m

are achievable and would be advantageous for certain types of cell culture and tissue organization (e.g. renal structures) [153]. Because of the advantages of fabricating such small features, more μ SL machines with similar capabilities will likely be developed despite the challenges. However, projection μ SL machines with optics that focus the light path into a very small build area are unable to build scaffolds with a large footprint. A promising solution is to use image stitching where patterned light is focused to several build areas in succession for the fabrication of a single layer. In this scenario, high resolution is retained while allowing for the fabrication of much larger objects [176].

In addition to the regeneration and repair of tissue, μ SL will find use in fabricating other three dimensional structures with micron-sized features. Researchers have fabricated scaffold structures to elucidate the underlying mechanisms of arterial thrombosis [261] and cancer metastasis and migration [262, 263]. μ SL has also been leveraged for the fabrication of microfluidics with three dimensional components that could not otherwise be fabricated [264, 265]. These structures have been used as static mixers [266, 267] and chemical reactionware [268]. μ SL made microfluidics have also been used for pathogen detection, which may suggest future use of μ SL for the fabrication of micro-sensors [269]. The geometric constraints of conventional MEMS fabrication can be circumvented with μ SL to create functioning microactuators with unique geometries [270]. Finally, future developments may allow for organ-on-a-chip devices that combine aspects of both microfluidics and tissue scaffolds to create realistic human models that could greatly accelerate drug discovery, more accurately assess their toxicity, and perhaps even eliminate the need for animal models [108, 264, 265, 271, 272].

Funding: This research did not receive any specific grant from funding agencies in the public, commercial, or not-for-profit sectors.

Conflicts of Interest: The authors declare no conflicts of interest.

References

- [1] OPTN/SRTR 2012 annual data report. Introduction, *Am. J. Transplant.* 14 Suppl 1 (2014) 8-10.
- [2] A.J. Matas, J.M. Smith, M.A. Skeans, B. Thompson, S.K. Gustafson, M.A. Schnitzler, D.E. Stewart, W.S. Cherikh, J.L. Wainright, J.J. Snyder, A.K. Israni, B.L. Kasiske, OPTN/SRTR 2012 annual data report: Kidney, *Am. J. Transplantation* 14 Suppl 1 (2014) 11-44.
- [3] C.L. Ahrens, E.M. Manno, Neurotoxicity of commonly used hepatic drugs, *Handb. Clin. Neurol.* 120 (2014) 675-682.
- [4] M.E. Furth, A. Atala, M.E. Van Dyke, Smart biomaterials design for tissue engineering and regenerative medicine, *Biomaterials* 28(34) (2007) 5068-5073.
- [5] E. Catalano, A. Cochis, E. Varoni, L. Rimondini, B. Azzimonti, Tissue-engineered skin substitutes: An overview, *J. Artificial Organs* 16(4) (2013) 397-403.
- [6] J.P. Vacanti, C.A. Vacanti, The history and scope of tissue engineering, in: R. Lanza, R. Langer, J.P. Vacanti (Eds.), *Principles of tissue engineering*, Elsevier, London, UK, 2014, pp. 3-8.
- [7] R. Langer, J.P. Vacanti, Tissue engineering, *Science* 260(5110) (1993) 920-926.
- [8] A. Atala, S.B. Bauer, S. Soker, J.J. Yoo, A.B. Retik, Tissue-engineered autologous bladders for patients needing cystoplasty, *The Lancet* 367(9518) (2006) 1241-1246.
- [9] A.M. Raya-Rivera, D. Esquiliano, R. Fierro-Pastrana, E. López-Bayghen, P. Valencia, R. Ordorica-Flores, S. Soker, J.J. Yoo, A. Atala, Tissue-engineered autologous vaginal organs in patients: A pilot cohort study, *The Lancet* 384(9940) (2014) 329-336.
- [10] S.L. Dahl, A.P. Kypson, J.H. Lawson, J.L. Blum, J.T. Strader, Y. Li, R.J. Manson, W.E. Tente, L. DiBernardo, M.T. Hensley, R. Carter, T.P. Williams, H.L. Prichard, M.S. Dey, K.G. Begelman, L.E. Niklason, Readily available tissue-engineered vascular grafts, *Sci. Transl. Med.* 3(68) (2011) 68ra69.
- [11] S.L.M. Dahl, J.L. Blum, L.E. Niklason, Bioengineered vascular grafts: Can we make them off-the-shelf?, *Trends Cardiovasc. Med.* 21(3) (2011) 83-89.
- [12] J. Lawson, S. Dahl, H. Prichard, R. Manson, S. Gage, A. Kypson, J. Blum, A. Pilgrim, W. Tente, L. Niklason, VS5 human tissue-engineered grafts for hemodialysis: Development, preclinical data, and early investigational human implant experience, *J. Vasc. Surg.* 59(6) (2014) 32S-33S.
- [13] M. Poh, M. Boyer, A. Solan, S.L.M. Dahl, D. Pedrotty, S.S.R. Banik, J.A. McKee, R.Y. Klinger, C.M. Counter, L.E. Niklason, Blood vessels engineered from human cells, *The Lancet* 365(9477) (2005) 2122-2124.
- [14] L.E. Niklason, J. Gao, W.M. Abbott, K.K. Hirschi, S. Houser, R. Marini, R. Langer, Functional arteries grown in vitro, *Science* 284(5413) (1999) 489-493.

- [15] N. L'Heureux, T.N. McAllister, L.M. de la Fuente, Tissue-engineered blood vessel for adult arterial revascularization, *N. Engl. J. Med.* 357(14) (2007) 1451-1453.
- [16] J.T. Krawiec, D.A. Vorp, Adult stem cell-based tissue engineered blood vessels: A review, *Biomaterials* 33(12) (2012) 3388-3400.
- [17] D.F. Williams, There is no such thing as a biocompatible material, *Biomaterials* 35(38) (2014) 10009-10014.
- [18] D.F. Williams, On the mechanisms of biocompatibility, *Biomaterials* 29(20) (2008) 2941-2953.
- [19] S.J. Hollister, Porous scaffold design for tissue engineering, *Nat. Mater.* 4(July) (2005).
- [20] S.J. Hollister, R.D. Maddox, J.M. Taboas, Optimal design and fabrication of scaffolds to mimic tissue properties and satisfy biological constraints, *Biomaterials* 23(20) (2002) 4095-4103.
- [21] R.G. Wells, The role of matrix stiffness in regulating cell behavior, *Hepatology* 47(4) (2008) 1394-1400.
- [22] E. Kitamura, R. Stegaroiu, S. Nomura, O. Miyakawa, Biomechanical aspects of marginal bone resorption around osseointegrated implants: Considerations based on a three-dimensional finite element analysis, *Clin. Oral Implants Res.* 15(4) (2004) 401-412.
- [23] J.Y. Wong, A. Velasco, P. Rajagopalan, Q. Pham, Directed movement of vascular smooth muscle cells on gradient-compliant hydrogels, *Langmuir* 19(5) (2003) 1908-1913.
- [24] X.Q. Brown, K. Ookawa, J.Y. Wong, Evaluation of polydimethylsiloxane scaffolds with physiologically-relevant elastic moduli: Interplay of substrate mechanics and surface chemistry effects on vascular smooth muscle cell response, *Biomaterials* 26(16) (2005) 3123-3129.
- [25] L. Shor, S. Guceri, X. Wen, M. Gandhi, W. Sun, Fabrication of three-dimensional polycaprolactone/hydroxyapatite tissue scaffolds and osteoblast-scaffold interactions in vitro, *Biomaterials* 28(35) (2007) 5291-5297.
- [26] R. Zhang, P.X. Ma, Poly(alpha-hydroxyl acids)/hydroxyapatite porous composites for bone-tissue engineering. I. Preparation and morphology, *J. Biomed. Mater. Res.* 44(4) (1999) 446-455.
- [27] T. Xu, K.W. Binder, M.Z. Albanna, D. Dice, W. Zhao, J.J. Yoo, A. Atala, Hybrid printing of mechanically and biologically improved constructs for cartilage tissue engineering applications, *Biofabrication* 5(1) (2013) 015001.
- [28] H. Seitz, W. Rieder, S. Irsen, B. Leukers, C. Tille, Three-dimensional printing of porous ceramic scaffolds for bone tissue engineering, *J. Biomed. Mater. Res., Part B* 74(2) (2005) 782-788.
- [29] S. Tarafder, V.K. Balla, N.M. Davies, A. Bandyopadhyay, S. Bose, Microwave-sintered 3D printed tricalcium phosphate scaffolds for bone tissue engineering, *J. Tissue Eng. Regen. Med.* 7(8) (2013) 631-641.
- [30] S.C. Cox, J.A. Thornby, G.J. Gibbons, M.A. Williams, K.K. Mallick, 3D printing of porous hydroxyapatite scaffolds intended for use in bone tissue engineering applications, *Mater. Sci. Eng. C Mater. Biol. Appl.* 47 (2015) 237-247.
- [31] Y.J. Seol, D.Y. Park, J.Y. Park, S.W. Kim, S.J. Park, D.W. Cho, A new method of fabricating robust freeform 3D ceramic scaffolds for bone tissue regeneration, *Biotechnol. Bioeng.* 110(5) (2013) 1444-1455.
- [32] A. Bertsch, S. Jiguet, H. Hofmann, P. Renaud, Ceramic microcomponents by microstereolithography, *MEMS 2004: 17th IEEE International Conference on Micro Electro Mechanical Systems, Technical Digest* (2004) 725-728.
- [33] S. Bose, S. Vahabzadeh, A. Bandyopadhyay, Bone tissue engineering using 3D printing, *Mater. Today* 16(12) (2013) 496-504.

- [34] J.G. Barber, A.M. Handorf, T.J. Allee, W.J. Li, Braided nanofibrous scaffold for tendon and ligament tissue engineering, *Tissue Eng., Part A* 19(11-12) (2013) 1265-1274.
- [35] C.T. Laurencin, J.W. Freeman, Ligament tissue engineering: An evolutionary materials science approach, *Biomaterials* 26(36) (2005) 7530-7536.
- [36] Z. Ge, F. Yang, J.C. Goh, S. Ramakrishna, E.H. Lee, Biomaterials and scaffolds for ligament tissue engineering, *J. Biomed. Mater. Res., Part A* 77(3) (2006) 639-652.
- [37] Y. Liu, H.S. Ramanath, D.A. Wang, Tendon tissue engineering using scaffold enhancing strategies, *Trends Biotechnol.* 26(4) (2008) 201-209.
- [38] C. Chung, J.A. Burdick, Engineering cartilage tissue, *Adv. Drug Del. Rev.* 60(2) (2008) 243-262.
- [39] F.P. Melchels, A.M. Barradas, C.A. van Blitterswijk, J. de Boer, J. Feijen, D.W. Grijpma, Effects of the architecture of tissue engineering scaffolds on cell seeding and culturing, *Acta Biomater.* 6(11) (2010) 4208-4217.
- [40] J. Kim, M.J. Yaszemski, L. Lu, Three-dimensional porous biodegradable polymeric scaffolds fabricated with biodegradable hydrogel porogens, *Tissue Eng., Part C* 15(4) (2009) 583-594.
- [41] F. Melchels, B. Rijckaert, D. Grijpma, J. Feijen, Micro-CT analysis of tissue engineering scaffold architectures, *BMTI/iBME Symposium*, Enschede, Netherlands, 2008.
- [42] F.J. O'Brien, B.A. Harley, M.A. Waller, I.V. Yannas, L.J. Gibson, P.J. Prendergast, The effect of pore size on permeability and cell attachment in collagen scaffolds for tissue engineering, *Technol. Health Care* 15(1) (2007) 3-17.
- [43] Q.L. Loh, C. Choong, Three-dimensional scaffolds for tissue engineering applications: Role of porosity and pore size, *Tissue Eng., Part B* 19(6) (2013) 485-502.
- [44] J.W. Lee, G. Ahn, J.Y. Kim, D.-W. Cho, Evaluating cell proliferation based on internal pore size and 3D scaffold architecture fabricated using solid freeform fabrication technology, *J. Mater. Sci.: Mater. Med.* 21(12) (2010) 3195-3205.
- [45] Y. Lu, G. Mapili, G. Suhali, S. Chen, K. Roy, A digital micro-mirror device-based system for the microfabrication of complex, spatially patterned tissue engineering scaffolds, *J. Biomed. Mater. Res.* 77(2) (2006) 396-405.
- [46] R. Gauvin, Y.C. Chen, J.W. Lee, P. Soman, P. Zorlutuna, J.W. Nichol, H. Bae, S. Chen, A. Khademhosseini, Microfabrication of complex porous tissue engineering scaffolds using 3D projection stereolithography, *Biomaterials* 33(15) (2012) 3824-3834.
- [47] P. Lambert, N. Chartrain, A. Schultz, S. Cooke, T. Long, A. Whittington, C. Williams, Mask projection microstereolithography of novel biocompatible polymers, *Solid Freeform Fabrication Symposium Proceedings*, University of Texas at Austin, Austin, TX, 2014, pp. 974-990.
- [48] P. Soman, S. Chen, Projection printing of three-dimensional tissue scaffolds with tunable poisson's ratio, in: G. Forgacs, W. Sun (Eds.), *Biofabrication: Micro- and nano-fabrication, printing, patterning, and assemblies*, Elsevier, Oxford, UK, 2013, pp. 47-57.
- [49] J.-h.S. Arthur, J. Kim, Effect of solid freeform fabrication-based polycaprolactone/poly(lactic-co-glycolic acid)/collagen scaffolds on cellular activities of human adipose-derived stem cells and rat primary hepatocytes, *J. Mater. Sci.: Mater. Med.* 24 (2013) 1053-1065.
- [50] J.Y. Kim, J.W. Lee, S.-J. Lee, E.K. Park, S.-Y. Kim, D.-W. Cho, Development of a bone scaffold using HA nanopowder and micro-stereolithography technology, *Microelectron. Eng.* 84(5-8) (2007) 1762-1765.
- [51] A. Ronca, L. Ambrosio, D.W. Grijpma, Preparation of designed poly(d,l-lactide)/nanosized hydroxyapatite composite structures by stereolithography, *Acta Biomater.* 9(4) (2013) 5989-5996.

- [52] C. Du, F.Z. Cui, X.D. Zhu, K. de Groot, Three-dimensional nano-hap/collagen matrix loading with osteogenic cells in organ culture, *J. Biomed. Mater. Res.* 44(4) (1999) 407-415.
- [53] L.H. Nguyen, N. Annabi, M. Nikkhah, H. Bae, S. Park, Y. Kang, Y. Yang, A. Khademhosseini, Vascularized bone tissue engineering: Approaches for potential improvement, *Tissue Eng., Part B* 18(5) (2012).
- [54] T. Dvir, A. Kedem, E. Ruvinov, O. Levy, I. Freeman, N. Landa, R. Holbova, M.S. Feinberg, S. Dror, Y. Etzion, J. Leor, S. Cohen, Prevascularization of cardiac patch on the omentum improves its therapeutic outcome, *Proc. Natl. Acad. Sci. U. S. A.* 106(35) (2009) 14990-14995.
- [55] D.H. Kempen, L. Lu, A. Heijink, T.E. Hefferan, L.B. Creemers, A. Maran, M.J. Yaszemski, W.J. Dhert, Effect of local sequential VEGF and BMP-2 delivery on ectopic and orthotopic bone regeneration, *Biomaterials* 30(14) (2009) 2816-2825.
- [56] J.W. Lee, K. Shin, S. Ho, J.-y. Kim, B.-k. Lee, D.-w. Cho, Bone regeneration using a microstereolithography-produced customized poly (propylene fumarate)/diethyl fumarate photopolymer 3D scaffold incorporating BMP-2 loaded PLGA microspheres, *Biomaterials* 32(3) (2011) 744-752.
- [57] C. Li, C. Vepari, H.J. Jin, H.J. Kim, D.L. Kaplan, Electrospun silk-BMP-2 scaffolds for bone tissue engineering, *Biomaterials* 27(16) (2006) 3115-3124.
- [58] E.C. Novosel, C. Kleinbans, P.J. Kluger, Vascularization is the key challenge in tissue engineering, *Adv. Drug Del. Rev.* 63(4-5) (2011) 300-311.
- [59] E.A. Phelps, A.J. García, Engineering more than a cell: Vascularization strategies in tissue engineering, *Curr. Opin. Biotechnol.* 21(5) (2010) 704-709.
- [60] J.H. Lawson, M.H. Glickman, M. Ilzecki, T. Jakimowicz, A. Jaroszynski, E.K. Peden, A.J. Pilgrim, H.L. Prichard, M. Guziewicz, S. Przywara, J. Szmidt, J. Turek, W. Witkiewicz, N. Zapotoczny, T. Zubilewicz, L.E. Niklason, Bioengineered human acellular vessels for dialysis access in patients with end-stage renal disease: Two phase 2 single-arm trials, *The Lancet* 387(10032) (2016) 2026-2034.
- [61] A. Atala, Engineering organs, *Curr. Opin. Biotechnol.* 20(5) (2009) 575-592.
- [62] T.W. Gilbert, T.L. Sellaro, S.F. Badylak, Decellularization of tissues and organs, *Biomaterials* 27(19) (2006) 3675-3683.
- [63] P.M. Crapo, T.W. Gilbert, S.F. Badylak, An overview of tissue and whole organ decellularization processes, *Biomaterials* 32(12) (2011) 3233-3243.
- [64] T.J. Keane, R. Londono, N.J. Turner, S.F. Badylak, Consequences of ineffective decellularization of biologic scaffolds on the host response, *Biomaterials* 33(6) (2012) 1771-1781.
- [65] T. Woods, P.F. Gratzner, Effectiveness of three extraction techniques in the development of a decellularized bone-anterior cruciate ligament-bone graft, *Biomaterials* 26(35) (2005) 7339-7349.
- [66] J.E. Arenas-Herrera, I.K. Ko, A. Atala, J.J. Yoo, Decellularization for whole organ bioengineering, *Biomed. Mater.* 8(1) (2013) 014106.
- [67] B. Subia, J. Kundu, S.C. Kundu, Biomaterial scaffold fabrication techniques for potential tissue engineering applications, in: D. Eberli (Ed.), *Tissue engineering InTech*, 2008, pp. 141-159.
- [68] P. Bartolo, B. Bidanda, *Virtual prototyping & bio manufacturing in medical applications*, Springer US, New York, 2008, p. 299.
- [69] C. Liu, Z. Xia, J.T. Czernuszka, Design and development of three-dimensional scaffolds for tissue engineering, *Chem. Eng. Res. Des.* 85(7) (2007) 1051-1064.
- [70] A.G. Mikos, J.S. Temenoff, Formation of highly porous biodegradable scaffolds for tissue engineering, *Electron. J. Biotechnol.* 3(2) (2000).

- [71] T. Lu, Y. Li, T. Chen, Techniques for fabrication and construction of three-dimensional scaffolds for tissue engineering, *Int. J. Nanomed.* 8 (2013) 337-350.
- [72] A.G. Mikos, A.J. Thorsen, L.A. Czerwonka, Y. Bao, R. Langer, D.N. Winslow, J.P. Vacanti, Preparation and characterization of poly(l-lactic acid) foams, *Polymer* 35(5) (1994) 1068-1077.
- [73] A.S. Goldstein, G. Zhu, G.E. Morris, R.K. Meszlenyi, A.G. Mikos, Effect of osteoblastic culture conditions on the structure of poly(dl-lactic-co-glycolic acid) foam scaffolds, *Tissue Eng.* 5(5) (1999) 421-434.
- [74] Y.H. Gong, Z.W. Ma, Q.L. Zhou, J. Li, C.Y. Gao, J.C. Shen, Poly(lactic acid) scaffold fabricated by gelatin particle leaching has good biocompatibility for chondrogenesis, *J. Biomater. Sci., Polym. Ed.* 19(2) (2008) 207-221.
- [75] W.L. Murphy, R.G. Dennis, J.L. Kileny, D.J. Mooney, Salt fusion: An approach to improve pore interconnectivity within tissue engineering scaffolds, *Tissue Eng.* 8(1) (2002) 43-52.
- [76] A.G. Mikos, Y. Bao, L.G. Cima, D.E. Ingber, J.P. Vacanti, R. Langer, Preparation of poly(glycolic acid) bonded fiber structures for cell attachment and transplantation, *J. Biomed. Mater. Res.* 27(2) (1993) 183-189.
- [77] N. Thadavirul, P. Pavasant, P. Supaphol, Development of polycaprolactone porous scaffolds by combining solvent casting, particulate leaching, and polymer leaching techniques for bone tissue engineering, *J. Biomed. Mater. Res.* 102(10) (2014) 3379-3392.
- [78] J.P. Fisher, T.A. Holland, D. Dean, P.S. Engel, A.G. Mikos, Synthesis and properties of photocross-linked poly(propylene fumarate) scaffolds, *J. Biomater. Sci. Polym. Ed.* 12(6) (2001) 673-687.
- [79] R. Sodian, J.S. Sperling, D.P. Martin, A. Egozy, U. Stock, J.E. Mayer, J.P. Vacanti, Fabrication of a trileaflet heart valve scaffold from a polyhydroxyalkanoate biopolyester for use in tissue engineering, *Tissue Eng.* 6(2) (2000) 183-188.
- [80] X. Liu, P.X. Ma, Polymeric scaffolds for bone tissue engineering, *Ann. Biomed. Eng.* 32(3) (2004) 477-486.
- [81] P.X. Ma, Scaffolds for tissue fabrication, *Mater. Today* 7(5) (2004) 30-40.
- [82] Y.C. Huang, D.J. Mooney, Gas foaming to fabricate polymer scaffolds in tissue engineering, in: P.X. Ma, J. Elisseeff (Eds.) *Scaffolding In Tissue Engineering*, CRC Press, Boca Raton, FL, 2006, pp. 155-167.
- [83] A. Salerno, M. Oliviero, E. Di Maio, S. Iannace, P.A. Netti, Design of porous polymeric scaffolds by gas foaming of heterogeneous blends, *J. Mater. Sci.: Mater. Med.* 20(10) (2009) 2043-2051.
- [84] D.J. Mooney, D.F. Baldwin, N.P. Suh, L.P. Vacanti, R. Langer, Novel approach to fabricate porous sponges of poly(d,l-lactic-co-glycolic acid) without the use of organic solvents, *Biomaterials* 17(14) (1996) 1417-1422.
- [85] L.D. Harris, B.S. Kim, D.J. Mooney, Open pore biodegradable matrices formed with gas foaming, *J. Biomed. Mater. Res.* 42(3) (1998) 396-402.
- [86] D. Puppi, F. Chiellini, A.M. Piras, E. Chiellini, Polymeric materials for bone and cartilage repair, *Prog. Polym. Sci.* 35(4) (2010) 403-440.
- [87] V. Keskar, N.W. Marion, J.J. Mao, R.A. Gemeinhart, In vitro evaluation of macroporous hydrogels to facilitate stem cell infiltration, growth, and mineralization, *Tissue Eng., Part A* 15(7) (2009) 1695-1707.
- [88] Y.S. Nam, J.J. Yoon, T.G. Park, A novel fabrication method of macroporous biodegradable polymer scaffolds using gas foaming salt as a porogen additive, *J. Biomed. Mater. Res.* 53(1) (2000) 1-7.

- [89] D.W. Hutmacher, Scaffolds in tissue engineering bone and cartilage, *Biomaterials* 21(24) (2000) 2529-2543.
- [90] K. Whang, C.H. Thomas, K.E. Healy, G. Nuber, A novel method to fabricate bioabsorbable scaffolds, *Polymer* 36(4) (1995) 837-842.
- [91] H. Lo, S. Kadiyala, S.E. Guggino, K.W. Leong, Poly(l-lactic acid) foams with cell seeding and controlled-release capacity, *J. Biomed. Mater. Res.* 30(4) (1996) 475-484.
- [92] H. Lo, M.S. Ponticciello, K.W. Leong, Fabrication of controlled release biodegradable foams by phase separation, *Tissue Eng.* 1(1) (1995) 15-28.
- [93] P. van de Witte, P.J. Dijkstra, J.W.A. van den Berg, J. Feijen, Phase separation processes in polymer solutions in relation to membrane formation, *J. Membr. Sci.* 117(1-2) (1996) 1-31.
- [94] V. Maquet, A.R. Boccaccini, L. Pravata, I. Notingher, R. Jerome, Preparation, characterization, and in vitro degradation of bioresorbable and bioactive composites based on bioglass-filled polylactide foams, *J. Biomed. Mater. Res., Part A* 66(2) (2003) 335-346.
- [95] X. Liu, P.X. Ma, Phase separation, pore structure, and properties of nanofibrous gelatin scaffolds, *Biomaterials* 30(25) (2009) 4094-4103.
- [96] C. Tu, Q. Cai, J. Yang, Y. Wan, J. Bei, S. Wang, The fabrication and characterization of poly(lactic acid) scaffolds for tissue engineering by improved solid-liquid phase separation, *Polym. Adv. Technol.* 14(8) (2003) 565-573.
- [97] S. Samavedi, S.A. Guelcher, A.S. Goldstein, A.R. Whittington, Response of bone marrow stromal cells to graded co-electrospun scaffolds and its implications for engineering the ligament-bone interface, *Biomaterials* 33(31) (2012) 7727-7735.
- [98] S.G. Kumbar, S.P. Nukavarapu, R. James, L.S. Nair, C.T. Laurencin, Electrospun poly(lactic acid-co-glycolic acid) scaffolds for skin tissue engineering, *Biomaterials* 29(30) (2008) 4100-4107.
- [99] L. Ghasemi-Mobarakeh, M.P. Prabhakaran, M. Morshed, M.H. Nasr-Esfahani, S. Ramakrishna, Electrospun poly(epsilon-caprolactone)/gelatin nanofibrous scaffolds for nerve tissue engineering, *Biomaterials* 29(34) (2008) 4532-4539.
- [100] C.M. Vaz, S. van Tuijl, C.V. Bouten, F.P. Baaijens, Design of scaffolds for blood vessel tissue engineering using a multi-layering electrospinning technique, *Acta Biomater.* 1(5) (2005) 575-582.
- [101] S. Heydarkhan-Hagvall, K. Schenke-Layland, A.P. Dhanasopon, F. Rofail, H. Smith, B.M. Wu, R. Shemin, R.E. Beygui, W.R. MacLellan, Three-dimensional electrospun ECM-based hybrid scaffolds for cardiovascular tissue engineering, *Biomaterials* 29(19) (2008) 2907-2914.
- [102] ISO/ASTM 52900-15, standard terminology for additive manufacturing – general principles – terminology, ASTM International, West Conshohocken, PA, 2015.
- [103] D.L. Bourell, Perspectives on additive manufacturing, *Annu. Rev. Mater. Res.* 46(1) (2016) 1-18.
- [104] I. Gibson, D. Rosen, B. Stucker, Additive manufacturing technologies rapid prototyping to direct digital manufacturing, Springer, New York, 2010.
- [105] F.P.W. Melchels, M.a.N. Domingos, T.J. Klein, J. Malda, P.J. Bartolo, D.W. Hutmacher, Additive manufacturing of tissues and organs, *Prog. Polym. Sci.* 37(8) (2012) 1079-1104.
- [106] I. Zein, D.W. Hutmacher, K.C. Tan, S.H. Teoh, Fused deposition modeling of novel scaffold architectures for tissue engineering applications, *Biomaterials* 23(4) (2002) 1169-1185.
- [107] S. van Uden, J. Silva-Correia, V.M. Correlo, J.M. Oliveira, R.L. Reis, Custom-tailored tissue engineered polycaprolactone scaffolds for total disc replacement, *Biofabrication* 7(1) (2015) 015008.

- [108] S.V. Murphy, A. Atala, 3D bioprinting of tissues and organs, *Nat. Biotechnol.* 32(8) (2014) 773-785.
- [109] J. Malda, J. Visser, F.P. Melchels, T. Jungst, W.E. Hennink, W.J. Dhert, J. Groll, D.W. Huttmacher, 25th anniversary article: Engineering hydrogels for biofabrication, *Adv. Mater.* 25(36) (2013) 5011-5028.
- [110] D.L. Cohen, E. Malone, H. Lipson, L.J. Bonassar, Direct freeform fabrication of seeded hydrogels in arbitrary geometries, *Tissue Eng.* 12(5) (2006) 1325-1335.
- [111] D.L. Cohen, W. Lo, A. Tsavaris, D. Peng, H. Lipson, L.J. Bonassar, Increased mixing improves hydrogel homogeneity and quality of three-dimensional printed constructs, *Tissue Eng.* 17(2) (2011) 239-248.
- [112] B. Duan, L.A. Hockaday, K.H. Kang, J.T. Butcher, 3D bioprinting of heterogeneous aortic valve conduits with alginate/gelatin hydrogels, *J. Biomed. Mater. Res., Part A* 101(5) (2013) 1255-1264.
- [113] R. Chang, J. Nam, W. Sun, Effects of dispensing pressure and nozzle diameter on cell survival from solid freeform fabrication-based direct cell writing, *Tissue Eng., Part A* 14(1) (2008) 41-48.
- [114] C.M. Smith, A.L. Stone, R.L. Parkhill, R.L. Stewart, M.W. Simpkins, A.M. Kachurin, W.L. Warren, S.K. Williams, Three-dimensional bioassembly tool for generating viable tissue-engineered constructs, *Tissue Eng.* 10(9-10) (2004) 1566-1576.
- [115] T. Xu, C.A. Gregory, P. Molnar, X. Cui, S. Jalota, S.B. Bhaduri, T. Boland, Viability and electrophysiology of neural cell structures generated by the inkjet printing method, *Biomaterials* 27(19) (2006) 3580-3588.
- [116] B. Guillotin, A. Souquet, S. Catros, M. Duocastella, B. Pippenger, S. Bellance, R. Bareille, M. Remy, L. Bordenave, J. Amedee, F. Guillemot, Laser assisted bioprinting of engineered tissue with high cell density and microscale organization, *Biomaterials* 31(28) (2010) 7250-7256.
- [117] B.-J. de Gans, P. C. Duineveld, U.S. Schubert, Inkjet printing of polymers: State of the art and future developments, *Adv. Mater.* 16(3) (2004) 203-213.
- [118] J.A. Barron, B.R. Ringeisen, H. Kim, B.J. Spargo, D.B. Chrisey, Application of laser printing to mammalian cells, *Thin Solid Films* 453-454 (2004) 383-387.
- [119] B. Hopp, T. Smausz, N. Kresz, N. Barna, Z. Bor, L. Kolozsvári, D.B. Chrisey, A. Szabó, A. Nógrádi, Survival and proliferative ability of various living cell types after laser-induced forward transfer, *Tissue Eng.* 11(11/12) (2005) 1817-1823.
- [120] K. Nair, M. Gandhi, S. Khalil, K.C. Yan, M. Marcolongo, K. Barbee, W. Sun, Characterization of cell viability during bioprinting processes, *Biotechnol. J.* 4(8) (2009) 1168-1177.
- [121] A. Skardal, Chapter 1 - bioprinting essentials of cell and protein viability, in: A. Atala, J.J. Yoo (Eds.), *Essentials of 3D biofabrication and translation*, Academic Press, Boston, 2015, pp. 1-17.
- [122] D.B. Kolesky, R.L. Truby, A.S. Gladman, T.A. Busbee, K.A. Homan, J.A. Lewis, 3D bioprinting of vascularized, heterogeneous cell-laden tissue constructs, *Adv. Mater.* 26(19) (2014) 3124-3130.
- [123] M. Guvendiren, H.D. Lu, J.A. Burdick, Shear-thinning hydrogels for biomedical applications, *Soft Matter* 8(2) (2012) 260-272.
- [124] C.J. Ferris, K.J. Gilmore, S. Beirne, D. McCallum, G.G. Wallace, M. in het Panhuis, Bio-ink for on-demand printing of living cells, *Biomater. Sci.* 1(2) (2013) 224-230.

- [125] A. Skardal, J. Zhang, G.D. Prestwich, Bioprinting vessel-like constructs using hyaluronan hydrogels crosslinked with tetrahedral polyethylene glycol tetracrylates, *Biomaterials* 31(24) (2010) 6173-6181.
- [126] X. Cui, K. Breitenkamp, M.G. Finn, M. Lotz, D.D. D'Lima, Direct human cartilage repair using three-dimensional bioprinting technology, *Tissue Eng., Part A* 18(11-12) (2012) 1304-1312.
- [127] T. Xu, W. Zhao, J.M. Zhu, M.Z. Albanna, J.J. Yoo, A. Atala, Complex heterogeneous tissue constructs containing multiple cell types prepared by inkjet printing technology, *Biomaterials* 34(1) (2013) 130-139.
- [128] K. Jakab, C. Norotte, B. Damon, F. Marga, A. Neagu, C.L. Besch-Williford, A. Kachurin, K.H. Church, H. Park, V. Mironov, R. Markwald, G. Vunjak-Novakovic, G. Forgacs, Tissue engineering by self-assembly of cells printed into topologically defined structures, *Tissue Eng., Part A* 14(3) (2008) 413-421.
- [129] P.S. Maher, R.P. Keatch, K. Donnelly, R.E. Mackay, J.Z. Paxton, Construction of 3D biological matrices using rapid prototyping technology, *Rapid Prototyp. J.* 15(3) (2009) 204-210.
- [130] W. Lee, V. Lee, S. Polio, P. Keegan, J.H. Lee, K. Fischer, J.K. Park, S.S. Yoo, On-demand three-dimensional freeform fabrication of multi-layered hydrogel scaffold with fluidic channels, *Biotechnol. Bioeng.* 105(6) (2010) 1178-1186.
- [131] K. Markstedt, A. Mantas, I. Tournier, H. Martinez Avila, D. Hagg, P. Gatenholm, 3D bioprinting human chondrocytes with nanocellulose-alginate bioink for cartilage tissue engineering applications, *Biomacromolecules* 16(5) (2015) 1489-1496.
- [132] A. Skardal, M. Devarasetty, H.W. Kang, I. Mead, C. Bishop, T. Shupe, S.J. Lee, J. Jackson, J. Yoo, S. Soker, A. Atala, A hydrogel bioink toolkit for mimicking native tissue biochemical and mechanical properties in bioprinted tissue constructs, *Acta Biomater.* 25 (2015) 24-34.
- [133] C. Colosi, S.R. Shin, V. Manoharan, S. Massa, M. Costantini, A. Barbetta, M.R. Dokmeci, M. Dentini, A. Khademhosseini, Microfluidic bioprinting of heterogeneous 3D tissue constructs using low-viscosity bioink, *Adv. Mater.* 28(4) (2016) 677-684.
- [134] L.A. Hockaday, K.H. Kang, N.W. Colangelo, P.Y. Cheung, B. Duan, E. Malone, J. Wu, L.N. Girardi, L.J. Bonassar, H. Lipson, C.C. Chu, J.T. Butcher, Rapid 3D printing of anatomically accurate and mechanically heterogeneous aortic valve hydrogel scaffolds, *Biofabrication* 4(3) (2012) 035005.
- [135] Y.J. Seol, H.W. Kang, S.J. Lee, A. Atala, J.J. Yoo, Bioprinting technology and its applications, *Eur. J. Cardiothorac. Surg.* 46(3) (2014) 342-348.
- [136] A.A. Chen, V.L. Tsang, D.R. Albrecht, S.N. Bhatia, 3-D fabrication technology for tissue engineering, in: M. Ferrari, T. Desai, S. Bhatia (Eds.), *BioMEMS and biomedical nanotechnology*, Springer, Boston, MA, 2006.
- [137] S.M. Peltola, F.P. Melchels, D.W. Grijpma, M. Kellomaki, A review of rapid prototyping techniques for tissue engineering purposes, *Ann. Med.* 40(4) (2008) 268-280.
- [138] B.H. Wong, Invisalign a to z, *Am. J. Orthod. Dentofacial Orthop.* 121(5) (2002) 540-541.
- [139] A. Bertsch, P. Bernhard, C. Vogt, P. Renaud, Rapid prototyping of small size objects, *Rapid Prototyp. J.* 6(4) (2000) 259-266.
- [140] A. Bertsch, J.Y. Yezequel, J.C. Andre, Study of the spatial resolution of a new 3D microfabrication process: The microstereolithography using a dynamic mask-generator technique, *J. Photochem. Photobiol., A* 107(1-3) (1997) 275-281.
- [141] P.M. Lambert, E.A. Campaigne-III, C.B. Williams, Design considerations for mask projection microstereolithography systems, *Solid Freeform Fabrication Symposium Proceedings*, University of Texas at Austin, Austin, TX, 2013, pp. 111-130.

- [142] S. Maruo, O. Nakamura, S. Kawata, Three-dimensional microfabrication with two-photon-absorbed photopolymerization, *Opt. Lett.* 22(2) (1997) 132-134.
- [143] U. Hinze, B. Chichkov, Light sources and systems for multiphoton lithography, in: J. Stampfl, R. Liska, A. Ovsianikov (Eds.), *Multiphoton lithography: Techniques, materials and applications*, Wiley-VCH Verlag, Weinheim, Germany, 2016, pp. 95-109.
- [144] E. Stratakis, A. Ranella, M. Farsari, C. Fotakis, Laser-based micro/nanoengineering for biological applications, *Prog. Quantum Electron.* 33(5) (2009) 127-163.
- [145] P.J. Bartolo, *Stereolithography: Materials, processes and applications*, Springer US, Boston, 2011.
- [146] J.F. Xing, M.L. Zheng, X.M. Duan, Two-photon polymerization microfabrication of hydrogels: An advanced 3D printing technology for tissue engineering and drug delivery, *Chem. Soc. Rev.* 44(15) (2015) 5031-5039.
- [147] A. Ovsianikov, V. Mironov, J. Stampf, R. Liska, Engineering 3D cell-culture matrices: Multiphoton processing technologies for biological and tissue engineering applications, *Expert Rev. Med. Devices* 9(6) (2012) 613-633.
- [148] S. Wu, J. Serbin, M. Gu, Two-photon polymerisation for three-dimensional micro-fabrication, *J. Photochem. Photobiol., A* 181(1) (2006) 1-11.
- [149] S.H. Park, D.Y. Yang, K.S. Lee, Two-photon stereolithography for realizing ultraprecise three-dimensional nano/microdevices, *Laser Photonics Rev.* 3(1-2) (2009) 1-11.
- [150] M.W. Tibbitt, J.A. Shadish, C.A. DeForest, Photopolymers for multiphoton lithography in biomaterials and hydrogels, in: J. Stampfl, R. Liska, A. Ovsianikov (Eds.), *Multiphoton lithography: Techniques, materials and applications*, Wiley-VCH Verlag, Weinheim, Germany, 2016, pp. 183-220.
- [151] Y.M. Ha, J.W. Choi, S.H. Lee, Mass production of 3-D microstructures using projection microstereolithography, *J. Mech. Sci. Technol.* 22(3) (2008) 514-521.
- [152] K. Ikuta, K. Hirowatari, Real three dimensional microfabrication using stereolithography and metal molding, *Proceedings IEEE Micro Electro Mechanical Systems*, Fort Lauderdale, FL, 1993, pp. 42-47.
- [153] C. Sun, N. Fang, D.M. Wu, X. Zhang, Projection micro-stereolithography using digital micro-mirror dynamic mask, *Sens. Actuators, A* 121(1) (2005) 113-120.
- [154] J.R. Tumbleston, D. Shirvanyants, N. Ermoshkin, R. Januszewicz, A.R. Johnson, D. Kelly, K. Chen, R. Pinschmidt, J.P. Rolland, A. Ermoshkin, E.T. Samulski, J.M. DeSimone, Continuous liquid interface production of 3D objects, *Science* 347(6228) (2015) 1349-1352.
- [155] H.-B. Sun, S. Kawata, Two-photon photopolymerization and 3D lithographic microfabrication, *NMR; 3D analysis; photopolymerization*, Springer-Verlag Berlin Heidelberg, New York, 2004, pp. 169-273.
- [156] Z. Wang, R. Abdulla, B. Parker, R. Samanipour, S. Ghosh, K. Kim, A simple and high-resolution stereolithography-based 3D bioprinting system using visible light crosslinkable bioinks, *Biofabrication* 7(4) (2015) 045009.
- [157] H. Lin, D. Zhang, P.G. Alexander, G. Yang, J. Tan, A.W. Cheng, R.S. Tuan, Application of visible light-based projection stereolithography for live cell-scaffold fabrication with designed architecture, *Biomaterials* 34(2) (2013) 331-339.
- [158] M.D. Soucek, X. Ren, UV-curable coating technologies, in: A. Tiwari, A. Polykarpov (Eds.), *Photocured materials*, The Royal Society of Chemistry, Cambridge, UK, 2015, pp. 15-48.
- [159] M. Sangermano, Advances in cationic photopolymerization, *Pure Appl. Chem.* 84(10) (2012).

- [160] J.P. Fouassier, X. Allonas, J. Lalevée, C. Dietlin, Photoinitiators for free radical polymerization reactions, in: N.S. Allen (Ed.), Photochemistry and photophysics of polymer materials, John Wiley & Sons, Inc., Hoboken, NJ, 2010, pp. 351-419.
- [161] S.C. Ligon, R. Liska, J. Stampfl, M. Gurr, R. Mulhaupt, Polymers for 3D printing and customized additive manufacturing, *Chem. Rev.* 117(15) (2017) 10212-10290.
- [162] J.W. Halloran, Ceramic stereolithography: Additive manufacturing for ceramics by photopolymerization, *Annu. Rev. Mater. Res.* 46(1) (2016) 19-40.
- [163] M. Gabriel Ivan, J. Cesar Scaiano, Photoimaging and lithographic processes in polymers, in: N.S. Allen (Ed.), Photochemistry and photophysics of polymer materials, John Wiley & Sons, Inc., Hoboken, NJ, 2010, pp. 479-507.
- [164] Y. Chiu, Y.-T. Cheng, SU-8 for microsystem fabrication, in: A. Tiwari, A. Polykarpov (Eds.), Photocured materials, The Royal Society of Chemistry, Cambridge, UK, 2015, pp. 220-255.
- [165] P.F. Jacobs, Fundamentals of stereolithography, Solid Freeform Fabrication Symposium Proceedings, University of Texas at Austin, 1992, pp. 196-211.
- [166] J.H. Lee, R.K. Prud'homme, I.A. Aksay, Cure depth in photopolymerization: Experiments and theory, *J. Mater. Res.* 16(12) (2001) 3536-3544.
- [167] F.P.W. Melchels, J. Feijen, D.W. Grijpma, A review on stereolithography and its applications in biomedical engineering, *Biomaterials* 31(24) (2010) 6121-6130.
- [168] G. Odian, Principles of polymerization, 4th ed., John Wiley & Sons, Inc., Hoboken, NJ, 2004.
- [169] D. Bourell, A.S. Jariwala, F. Ding, A. Boddapati, V. Breedveld, M.A. Grover, C.L. Henderson, D.W. Rosen, Modeling effects of oxygen inhibition in mask-based stereolithography, *Rapid Prototyp. J.* 17(3) (2011) 168-175.
- [170] Y. Pan, C. Zhou, Y. Chen, A fast mask projection stereolithography process for fabricating digital models in minutes, *J. Manuf. Sci. Eng.* 134(5) (2012) 051011.
- [171] M. Hegde, V. Meenakshisundaram, N. Chartrain, S. Sekhar, D. Tafti, C.B. Williams, T.E. Long, 3D printing all-aromatic polyimides using mask-projection stereolithography: Processing the nonprocessable, *Adv. Mater.* 29(31) (2017).
- [172] A.R. Schultz, P.M. Lambert, N.A. Chartrain, D.M. Ruohoniemi, Z. Zhang, C. Jangu, M. Zhang, C.B. Williams, T.E. Long, 3D printing phosphonium ionic liquid networks with mask projection microstereolithography, *ACS Macro Lett.* 3(11) (2014) 1205-1209.
- [173] J.P. Fisher, D. Dean, A.G. Mikos, Photocrosslinking characteristics and mechanical properties of diethyl fumarate/poly(propylene fumarate) biomaterials, *Biomaterials* 23(22) (2002) 4333-4343.
- [174] B.-S. Chiou, R.J. English, S.A. Khan, UV cross-linking of thiol-ene polymers: A rheological study, in: A.B. Scranton, C.N. Bowman, R.W. Peiffer (Eds.), Photopolymerization fundamentals and applications, American Chemical Society, Washington, DC, 1997, pp. 150-166.
- [175] M.U. Kahveci, A.G. Yilmaz, Y. Yagci, Photoinitiated cationic polymerization: Reactivity and mechanistic aspects, in: N.S. Allen (Ed.), Photochemistry and photophysics of polymer materials, John Wiley & Sons, Inc., Hoboken, NJ, 2010, pp. 421-478.
- [176] X. Zheng, W. Smith, J. Jackson, B. Moran, H. Cui, D. Chen, J. Ye, N. Fang, N. Rodriguez, T. Weisgraber, C.M. Spadaccini, Multiscale metallic metamaterials, *Nat. Mater.* 15(10) (2016) 1100-1106.

- [177] T.M. Chu, D.G. Orton, S.J. Hollister, S.E. Feinberg, J.W. Halloran, Mechanical and in vivo performance of hydroxyapatite implants with controlled architectures, *Biomaterials* 23(5) (2002) 1283-1293.
- [178] C. Heller, M. Schwentenwein, G. Russmueller, F. Varga, J. Stampfl, R. Liska, Vinyl esters: Low cytotoxicity monomers for the fabrication of biocompatible 3D scaffolds by lithography based additive manufacturing, *J. Polym. Sci., Part A: Polym. Chem.* 47(24) (2009) 6941-6954.
- [179] C. Heller, M. Schwentenwein, G. Russmüller, T. Koch, D. Moser, C. Schopper, F. Varga, J. Stampfl, R. Liska, Vinylcarbonates and vinylcarbamates: Biocompatible monomers for radical photopolymerization, *J. Polym. Sci., Part A: Polym. Chem.* 49(3) (2011) 650-661.
- [180] G. Russmueller, R. Liska, J. Stampfl, C. Heller, A. Mautner, K. Macfelda, B. Kapeller, R. Lieber, A. Haider, K. Mika, C. Schopper, C. Perisanidis, R. Seemann, D. Moser, 3D printable biophotopolymers for in vivo bone regeneration, *Materials* 8(6) (2015) 3685-3700.
- [181] O. Guillaume, M.A. Geven, C.M. Sprecher, V.A. Stadelmann, D.W. Grijpma, T.T. Tang, L. Qin, Y. Lai, M. Alini, J.D. de Bruijn, H. Yuan, R.G. Richards, D. Eglin, Surface-enrichment with hydroxyapatite nanoparticles in stereolithography-fabricated composite polymer scaffolds promotes bone repair, *Acta Biomater.* 54 (2017) 386-398.
- [182] V.K. Popov, A.V. Evseev, A.L. Ivanov, V.V. Roginski, A.I. Volozhin, S.M. Howdle, Laser stereolithography and supercritical fluid processing for custom-designed implant fabrication, *J. Mater. Sci.: Mater. Med.* 15(2) (2004) 123-128.
- [183] C. Heller, M. Schwentenwein, F. Varga, M. Porodec, M. Schulz-Siegmund, G. Russmueller, J. Stampfl, R. Liska, New 3D-biophotopolymers with selective surface-cell interactions for regenerative medicine, *Materials Research Society Symposium Proceedings*, Boston, MA, 2009.
- [184] H. Lin, Y. Tang, T.P. Lozito, N. Oyster, R.B. Kang, M.R. Fritch, B. Wang, R.S. Tuan, Projection stereolithographic fabrication of BMP-2 gene-activated matrix for bone tissue engineering, *Sci. Rep.* 7(1) (2017).
- [185] N. Fang, C. Sun, X. Zhang, Diffusion-limited photopolymerization in scanning microstereolithography, *Appl. Phys. A: Mater. Sci. Process.* 79(8) (2004).
- [186] M. Schuster, C. Turecek, F. Varga, H. Lichtenegger, J. Stampfl, R. Liska, 3D-shaping of biodegradable photopolymers for hard tissue replacement, *Appl. Surf. Sci.* 254(4) (2007) 1131-1134.
- [187] F.P. Melchels, J. Feijen, D.W. Grijpma, A poly(D,L-lactide) resin for the preparation of tissue engineering scaffolds by stereolithography, *Biomaterials* 30(23-24) (2009) 3801-3809.
- [188] F.P. Melchels, B. Tonnarelli, A.L. Olivares, I. Martin, D. Lacroix, J. Feijen, D.J. Wendt, D.W. Grijpma, The influence of the scaffold design on the distribution of adhering cells after perfusion cell seeding, *Biomaterials* 32(11) (2011) 2878-2884.
- [189] A. Ronca, L. Ambrosio, D.W. Grijpma, Design of porous three-dimensional PDLLA / nanoparticle composite scaffolds using stereolithography, *J. Appl. Biomater. Funct. Mater.* 10(3) (2012) 249-258.
- [190] C. Xia, N.X. Fang, 3D microfabricated bioreactor with capillaries, *Biomed. Microdevices* 11(6) (2009) 1309-1315.
- [191] L.-H. Han, G. Mapili, S. Chen, K. Roy, Projection microfabrication of three-dimensional scaffolds for tissue engineering, *J. Manuf. Sci. Eng.* 130(2) (2008) 021005-021005.
- [192] S.J. Leigh, H.T. Gilbert, I.A. Barker, J.M. Becker, S.M. Richardson, J.A. Hoyland, J.A. Covington, A.P. Dove, Fabrication of 3-dimensional cellular constructs via microstereolithography using a simple, three-component, poly(ethylene glycol) acrylate-based system, *Biomacromolecules* 14(1) (2013) 186-192.

- [193] K. Arcaute, B. Mann, R. Wicker, Stereolithography of spatially controlled multi-material bioactive poly(ethylene glycol) scaffolds, *Acta Biomater.* 6(3) (2010) 1047-1054.
- [194] J.-W. Choi, R. Wicker, S.-H. Lee, K.-H. Choi, C.-S. Ha, I. Chung, Fabrication of 3D biocompatible/biodegradable micro-scaffolds using dynamic mask projection microstereolithography, *J. Mater. Process. Technol.* 209(15-16) (2009) 5494-5503.
- [195] P.X. Lan, J.W. Lee, Y.-J. Seol, D.-W. Cho, Development of 3D PPF / DEF scaffolds using micro-stereolithography and surface modification, *J. Mater. Sci.: Mater. Med.* 20 (2009) 271-279.
- [196] J. Hwal, S. Jin, W. Lee, J. Hwa, Evaluation of cell proliferation and differentiation on a poly(propylene fumarate) 3D scaffold treated with functional peptides, *J. Mater. Sci.* 46 (2011) 5282-5287.
- [197] M.N. Cooke, J.P. Fisher, D. Dean, C. Rimnac, A.G. Mikos, Use of stereolithography to manufacture critical-sized 3D biodegradable scaffolds for bone ingrowth, *J. Biomed. Mater. Res., Part B* 64(2) (2003) 65-69.
- [198] J.M. Serrine, A.M. Pekkanen, A.M. Nelson, N.A. Chartrain, C.B. Williams, T.E. Long, 3D-printable biodegradable polyester tissue scaffolds for cell adhesion, *Aust. J. Chem.* 68(9) (2015) 1409.
- [199] J.W. Choi, Y.M. Ha, S.H. Lee, K.H. Choi, Design of microstereolithography system based on dynamic image projection for fabrication of three-dimensional microstructures, *J. Mech. Sci. Technol.* 20(12) (2006) 2094-2104.
- [200] S.-J. Lee, J.-W. Rhie, D.-W. Cho, Development of three-dimensional alginate encapsulated chondrocyte hybrid scaffold using microstereolithography, *J. Manuf. Sci. Eng.* 130(2) (2008) 021007-021007.
- [201] S.-J. Lee, H.-W. Kang, J.K. Park, J.-W. Rhie, S.K. Hahn, D.-W. Cho, Application of microstereolithography in the development of three-dimensional cartilage regeneration scaffolds, *Biomed. Microdevices* 10(2) (2008) 233-241.
- [202] J.W. Lee, P.X. Lan, B. Kim, G. Lim, D.-W. Cho, 3D scaffold fabrication with PPF/DEF using micro-stereolithography, *Microelectron. Eng.* 84(5-8) (2007) 1702-1705.
- [203] D.-W. Cho, J.H. Jung, D.S. Kim, J.W. Lee, G. Lim, Estimation of cell proliferation by various peptide coating at the PPF/DEF 3D scaffold, *Microelectron. Eng.* 86(4-6) (2009) 1451-1454.
- [204] J.W. Lee, G. Ahn, D.S. Kim, D.-W. Cho, Development of nano- and microscale composite 3D scaffolds using PPF/DEF-HA and micro-stereolithography, *Microelectron. Eng.* 86(4-6) (2009) 1465-1467.
- [205] D. Dean, J. Wallace, K. Kim, A.G. Mikos, J.P. Fisher, Stereolithographic rendering of low molecular weight polymer scaffolds for bone tissue engineering, in: P. Bartolo (Ed.), *Innovative developments in design and manufacturing: Advanced research in virtual and rapid prototyping*, CRC Press Taylor & Francis, Boca Raton, FL, 2010, pp. 37-43.
- [206] A.J. Domb, Poly(propylene glycol fumarate) compositions for biomedical applications, US patent 4888413, 19 Dec 1989.
- [207] J.W. Lee, B. Kim, G.B. Lim, D.W. Cho, Scaffold fabrication with biodegradable poly(propylene fumarate) using microstereolithography, *Key Eng. Mater.* 342-343 (2007) 141-144.
- [208] J.W. Lee, P.X. Lan, B. Kim, G. Lim, D.W. Cho, Fabrication and characteristic analysis of a poly(propylene fumarate) scaffold using micro-stereolithography technology, *J. Biomed. Mater. Res., Part B* 87(1) (2008) 1-9.

- [209] L.S. Nair, C.T. Laurencin, Biodegradable polymers as biomaterials, *Prog. Polym. Sci.* 32(8-9) (2007) 762-798.
- [210] S.C. Beck, T. Jiang, L.S. Nair, C.T. Laurencin, Chitosan for bone and cartilage regenerative engineering, in: J.A. Jennings, J.D. Bumgardner (Eds.), *Chitosan based biomaterials: Tissue engineering and therapeutics*, Woodhead Publishing, Duxford, UK, 2017, pp. 33-72.
- [211] F.K. Kasper, K. Tanahashi, J.P. Fisher, A.G. Mikos, Synthesis of poly(propylene fumarate), *Nat. Protoc.* 4(4) (2009) 518-525.
- [212] S. Pal, *Mechanical properties of biological materials, Design of artificial human joints & organs*, Springer, New York, 2014, pp. 23-40.
- [213] J.W. Lee, K.-j. Kim, K.S. Kang, S. Chen, J.-w. Rhie, D.-w. Cho, Development of a bone reconstruction technique using a solid free-form fabrication (SFF) -based drug releasing scaffold and adipose-derived stem cells, *J. Biomed. Mater. Res., Part A* 101A (2013) 1865-1875.
- [214] L. Elomaa, S. Teixeira, R. Hakala, H. Korhonen, D.W. Grijpma, J.V. Seppala, Preparation of poly(epsilon-caprolactone)-based tissue engineering scaffolds by stereolithography, *Acta Biomater.* 7(11) (2011) 3850-3856.
- [215] J. Stampfl, S. Baudis, C. Heller, R. Liska, A. Neumeister, R. Kling, Photopolymers with tunable mechanical properties processed by laser-based high-resolution stereolithography, *J. Micromech. Microeng.* 18(125014) (2009) 9-9.
- [216] V. Chan, J.H. Jeong, P. Bajaj, M. Collens, T. Saif, H. Kong, R. Bashir, Multi-material bio-fabrication of hydrogel cantilevers and actuators with stereolithography, *Lab Chip* 12(1) (2012) 88-98.
- [217] X. Zheng, J. Deotte, M.P. Alonso, G.R. Farquar, T.H. Weisgraber, S. Gemberling, H. Lee, N. Fang, C.M. Spadaccini, Design and optimization of a light-emitting diode projection micro-stereolithography three-dimensional manufacturing system, *Rev. Sci. Instrum.* 83(12) (2012) 125001.
- [218] R. Ibrahim, R. Ibrahim, M.H.H. Ramlee, M.A. Shaik Mohamed, M. Ibrahim, M.S. Wahab, Evaluation on the photoabsorber composition effect in projection microstereolithography, *Appl. Mech. Mater.* 159 (2012) 109-114.
- [219] V.A. Morgan, J.M. Fewings, 1,6-hexanediol diacrylate: A rapid and potent sensitizer in the printing industry, *Australas. J. Dermatol.* 41(3) (2000) 190-192.
- [220] T. Matsuda, M. Mizutani, Liquid acrylate-endcapped biodegradable poly(epsilon-caprolactone-co-trimethylene carbonate). II. Computer-aided stereolithographic microarchitectural surface photoconstructs, *J. Biomed. Mater. Res.* 62(3) (2002) 395-403.
- [221] I.K. Kwon, T. Matsuda, Photo-polymerized microarchitectural constructs prepared by microstereolithography (μ SL) using liquid acrylate-end-capped trimethylene carbonate-based prepolymers, *Biomaterials* 26(14) (2005) 1675-1684.
- [222] I.K. Kwon, T. Matsuda, Photo-polymerized microarchitectural constructs prepared by microstereolithography (musl) using liquid acrylate-end-capped trimethylene carbonate-based prepolymers, *Biomaterials* 26(14) (2005) 1675-1684.
- [223] A.P. Pego, C.L. Vleggeert-Lankamp, M. Deenen, E.A. Lakke, D.W. Grijpma, A.A. Poot, E. Marani, J. Feijen, Adhesion and growth of human schwann cells on trimethylene carbonate (co)polymers, *J. Biomed. Mater. Res., Part A* 67(3) (2003) 876-885.
- [224] S.B.G. Blanquer, A.W.H. Gebraad, S. Miettinen, A.A. Poot, D.W. Grijpma, S.P. Haimi, Differentiation of adipose stem cells seeded towards annulus fibrosus cells on a designed poly(trimethylene carbonate) scaffold prepared by stereolithography, *J. Tissue Eng. Regen. Med.* 11(10) (2017) 2752-2762.

- [225] N.A. Chartrain, M. Vratsanos, D.T. Han, J.M. Serrine, A. Pekkanen, T.E. Long, A.R. Whittington, C.B. Williams, Microstereolithography of tissue scaffolds using a biodegradable photocurable polyester, *Solid Freeform Fabrication Symposium Proceedings*, University of Texas at Austin, Austin, TX, 2016, pp. 1732-1748.
- [226] S.-j. Lee, B. Kim, G. Lim, S.-w. Kim, J.-w. Rhie, D.-w. Cho, Effect of three-dimensional scaffold geometry on chondrocyte adhesion, *Key Eng. Mater.* 343 (2007) 97-100.
- [227] S.J. Lee, B. Kim, J.S. Lee, S.W. Kim, M.S. Kim, J.S. Kim, G.B. Lim, D.W. Cho, Three-dimensional microfabrication system for scaffolds in tissue engineering, *Key Eng. Mater.* 326-328 (2006) 723-726.
- [228] J.S. Choi, H.-w. Kang, I.H. Lee, Development of micro-stereolithography technology using a UV lamp and optical fiber, *Int. J. Adv. Des. Manuf. Technol.* 41 (2009) 281-286.
- [229] S.H. Kim, D.J. Jung, J.Y. Joo, S.H. Jeong, Modification of the curing characteristics of the photocurable resin FA1260T for 3D microfabrication using microstereolithography, *Key Eng. Mater.* 326-328 (2006) 107-110.
- [230] J.-W. Choi, E. MacDonald, R. Wicker, Multi-material microstereolithography, *Int. J. Adv. Des. Manuf. Technol.* 49(5-8) (2009) 543-551.
- [231] A. Bens, H. Seitz, G. Bermes, M. Emons, A. Pansky, B. Roitzheim, E. Tobiasch, C. Tille, Non-toxic flexible photopolymers for medical stereolithography technology, *Rapid Prototyp. J.* 13(1) (2007) 38-47.
- [232] W. Bian, D. Li, Q. Lian, X. Li, W. Zhang, K. Wang, Z. Jin, Fabrication of a bio-inspired beta-tricalcium phosphate/collagen scaffold based on ceramic stereolithography and gel casting for osteochondral tissue engineering, *Rapid Prototyp. J.* 18(1) (2012) 68-80.
- [233] R. Liska, M. Schuster, R. Inführ, C. Turecek, C. Fritscher, B. Seidl, V. Schmidt, L. Kuna, a. Haase, F. Varga, H. Lichtenegger, J. Stampfl, Photopolymers for rapid prototyping, *J. Coat. Technol. Res.* 4(4) (2007) 505-510.
- [234] J.W. Nichol, S.T. Koshy, H. Bae, C.M. Hwang, S. Yamanlar, A. Khademhosseini, Cell-laden microengineered gelatin methacrylate hydrogels, *Biomaterials* 31(21) (2010) 5536-5544.
- [235] V.B. Morris, S. Nimbalkar, M. Younesi, P. McClellan, O. Akkus, Mechanical properties, cytocompatibility and manufacturability of chitosan: PEGDA hybrid-gel scaffolds by stereolithography, *Ann. Biomed. Eng.* 45(1) (2017) 286-296.
- [236] P.S. Timashev, K.N. Bardakova, T.S. Demina, G.I. Pudovkina, M.M. Novikov, M.A. Markov, D.S. Asyutin, L.F. Pimenova, E.A. Svidchenko, A.M. Ermakov, I.I. Selezneva, V.K. Popov, N.A. Konovalov, T.A. Akopova, A.B. Solovieva, V.Y. Panchenko, V.N. Bagratashvili, Novel biocompatible material based on solid-state modified chitosan for laser stereolithography, *Sovrem Tehnol. Med.* 7(3) (2015) 20-31.
- [237] S. Suri, L.H. Han, W. Zhang, A. Singh, S. Chen, C.E. Schmidt, Solid freeform fabrication of designer scaffolds of hyaluronic acid for nerve tissue engineering, *Biomed. Microdevices* 13(6) (2011) 983-993.
- [238] P. Zorlutuna, J.H. Jeong, H. Kong, R. Bashir, Stereolithography-based hydrogel microenvironments to examine cellular interactions, *Adv. Funct. Mater.* 21(19) (2011) 3642-3651.
- [239] S. Miao, W. Zhu, N.J. Castro, M. Nowicki, X. Zhou, H. Cui, J.P. Fisher, L.G. Zhang, 4D printing smart biomedical scaffolds with novel soybean oil epoxidized acrylate, *Sci. Rep.* 6 (2016) 27226.
- [240] J.-W. Choi, E. MacDonald, R. Wicker, Multiple material microstereolithography, *Solid Freeform Fabrication Symposium Proceedings*, University of Texas at Austin, Austin, TX, 2009, pp. 781-792.

- [241] H. Kim, C. Jae-Won, R. Wicker, Scheduling and process planning for multiple material stereolithography, *Rapid Prototyp. J.* 16(4) (2010) 232-240.
- [242] Q. Ge, A.H. Sakhaei, H. Lee, C.K. Dunn, N.X. Fang, M.L. Dunn, Multimaterial 4D printing with tailorable shape memory polymers, *Sci. Rep.* 6 (2016) 31110.
- [243] C. Zhou, Y. Chen, Z. Yang, B. Khoshnevis, Digital material fabrication using mask-image-projection-based stereolithography, *Rapid Prototyp. J.* 19(3) (2013) 153-165.
- [244] C.G. Williams, A.N. Malik, T.K. Kim, P.N. Manson, J.H. Elisseeff, Variable cytocompatibility of six cell lines with photoinitiators used for polymerizing hydrogels and cell encapsulation, *Biomaterials* 26(11) (2005) 1211-1218.
- [245] B.D. Fairbanks, M.P. Schwartz, C.N. Bowman, K.S. Anseth, Photoinitiated polymerization of PEG-diacrylate with lithium phenyl-2,4,6-trimethylbenzoylphosphinate: Polymerization rate and cytocompatibility, *Biomaterials* 30(35) (2009) 6702-6707.
- [246] J.W. Choi, R.B. Wicker, S.H. Cho, C.S. Ha, S.H. Lee, Cure depth control for complex 3D microstructure fabrication in dynamic mask projection microstereolithography, *Rapid Prototyp. J.* 15(1) (2009) 59-70.
- [247] R.M. Domingues, M.E. Gomes, R.L. Reis, The potential of cellulose nanocrystals in tissue engineering strategies, *Biomacromolecules* 15(7) (2014) 2327-2346.
- [248] S. Kumar, M. Hofmann, B. Steinmann, E.J. Foster, C. Weder, Reinforcement of stereolithographic resins for rapid prototyping with cellulose nanocrystals, *ACS Appl. Mater. Interfaces* 4(10) (2012) 5399-5407.
- [249] A.X. Sun, H. Lin, A.M. Beck, E.J. Kilroy, R.S. Tuan, Projection stereolithographic fabrication of human adipose stem cell-incorporated biodegradable scaffolds for cartilage tissue engineering, *Front. Bioeng. Biotechnol.* 3 (2015) 115.
- [250] M. Diez, V.A. Schulte, F. Stefanoni, C.F. Natale, F. Mollica, C.M. Cesa, J. Chen, M. Möller, P.A. Netti, M. Ventre, M.C. Lensen, Molding micropatterns of elasticity on PEG-based hydrogels to control cell adhesion and migration, *Adv. Eng. Mater.* 13(10) (2011) B395-B404.
- [251] K.W. Lee, S.F. Wang, B.C. Fox, E.L. Ritman, M.J. Yaszemski, L.C. Lu, Poly(propylene fumarate) bone tissue engineering scaffold fabrication using stereolithography: Effects of resin formulations and laser parameters, *Biomacromolecules* 8(4) (2007) 1077-1084.
- [252] J. Jansen, F.P.W. Melchels, D.W. Grijpma, J. Feijen, Fumaric acid monoethyl ester-functionalized poly(D,L-lactide)/n-vinyl-2-pyrrolidone resins for the preparation of tissue engineering scaffolds by stereolithography, *Biomacromolecules* 10(2) (2009) 214-220.
- [253] S.B.G. Blanquer, M. Werner, M. Hannula, S. Sharifi, G.P.R. Lajoinie, D. Eglin, J. Hyttinen, A.A. Poot, D.W. Grijpma, Surface curvature in triply-periodic minimal surface architectures as a distinct design parameter in preparing advanced tissue engineering scaffolds, *Biofabrication* 9(2) (2017) 025001.
- [254] D. Hoffman-Kim, J.A. Mitchel, R.V. Bellamkonda, Topography, cell response, and nerve regeneration, *Annu. Rev. Biomed. Eng.* 12 (2010) 203-231.
- [255] B.N. Johnson, K.Z. Lancaster, G. Zhen, J. He, M.K. Gupta, Y.L. Kong, E.A. Engel, K.D. Krick, A. Ju, F. Meng, L.W. Enquist, X. Jia, M.C. McAlpine, 3D printed anatomical nerve regeneration pathways, *Adv. Funct. Mater.* 25(39) (2015) 6205-6217.
- [256] M. Werner, S.B. Blanquer, S.P. Haimi, G. Korus, J.W. Dunlop, G.N. Duda, D.W. Grijpma, A. Petersen, Surface curvature differentially regulates stem cell migration and differentiation via altered attachment morphology and nuclear deformation, *Adv. Sci.* 4(2) (2017) 1600347.
- [257] H.N. Chia, B.M. Wu, Recent advances in 3D printing of biomaterials, *J. Biol. Eng.* 9 (2015) 4.

- [258] J.K. Placone, J. Navarro, G.W. Laslo, M.J. Lerman, A.R. Gabard, G.J. Herendeen, E.E. Falco, S. Tombllyn, L. Burnett, J.P. Fisher, Development and characterization of a 3D printed, keratin-based hydrogel, *Ann. Biomed. Eng.* 45(1) (2017) 237-248.
- [259] J.W. Lee, H.-w. Kang, Effect of pore architecture on oxygen diffusion in 3D scaffolds for tissue engineering, *J. Biomech. Eng.* 132 (2010) 1-5.
- [260] A.L. Olivares, E. Marsal, J.A. Planell, D. Lacroix, Finite element study of scaffold architecture design and culture conditions for tissue engineering, *Biomaterials* 30(30) (2009) 6142-6149.
- [261] P.F. Costa, H.J. Albers, J.E.A. Linssen, H.H.T. Middelkamp, L. van der Hout, R. Passier, A. van den Berg, J. Malda, A.D. van der Meer, Mimicking arterial thrombosis in a 3D-printed microfluidic in vitro vascular model based on computed tomography angiography data, *Lab Chip* 17(16) (2017) 2785-2792.
- [262] W. Zhu, B. Holmes, R.I. Glazer, L.G. Zhang, 3D printed nanocomposite matrix for the study of breast cancer bone metastasis, *Nanomedicine* 12(1) (2016) 69-79.
- [263] P. Soman, J.A. Kelber, J.W. Lee, T.N. Wright, K.S. Vecchio, R.L. Klemke, S. Chen, Cancer cell migration within 3D layer-by-layer microfabricated photocrosslinked PEG scaffolds with tunable stiffness, *Biomaterials* 33(29) (2012) 7064-7070.
- [264] C.M. Ho, S.H. Ng, K.H. Li, Y.J. Yoon, 3D printed microfluidics for biological applications, *Lab Chip* 15(18) (2015) 3627-3637.
- [265] R. Zhang, N.B. Larsen, Stereolithographic hydrogel printing of 3D culture chips with biofunctionalized complex 3D perfusion networks, *Lab Chip* 17(24) (2017) 4273-4282.
- [266] T.W. Lim, Y. Son, Y.J. Jeong, D.Y. Yang, H.J. Kong, K.S. Lee, D.P. Kim, Three-dimensionally crossing manifold micro-mixer for fast mixing in a short channel length, *Lab Chip* 11(1) (2011) 100-103.
- [267] A. Bertsch, S. Heimgartner, P. Cousseau, P. Renaud, Static micromixers based on large-scale industrial mixer geometry, *Lab Chip* 1(1) (2001) 56-60.
- [268] M.D. Symes, P.J. Kitson, J. Yan, C.J. Richmond, G.J. Cooper, R.W. Bowman, T. Vilbrandt, L. Cronin, Integrated 3D-printed reactionware for chemical synthesis and analysis, *Nat. Chem.* 4(5) (2012) 349-354.
- [269] W. Lee, D. Kwon, W. Choi, G.Y. Jung, S. Jeon, 3D-printed microfluidic device for the detection of pathogenic bacteria using size-based separation in helical channel with trapezoid cross-section, *Sci. Rep.* 5 (2015) 7717.
- [270] H.-W. Kang, I.H. Lee, D.-W. Cho, Development of a micro-bellows actuator using micro-stereolithography technology, *Microelectron. Eng.* 83(4-9) (2006) 1201-1204.
- [271] D. Huh, B.D. Matthews, A. Mammoto, M. Montoya-Zavala, H.Y. Hsin, D.E. Ingber, Reconstituting organ-level lung functions on a chip, *Science* 328(5986) (2010) 1662-1668.
- [272] D. Huh, G.A. Hamilton, D.E. Ingber, From 3D cell culture to organs-on-chips, *Trends Cell Biol.* 21(12) (2011) 745-754.

Chapter 3: In Vitro Evaluation of 3D Printed NaAMPS-PEGDA Tissue Scaffolds Fabricated with Vat Photopolymerization

Nicholas A. Chartrain^{1,2,3}, Jarrod Cartwright^{1,3}, Wyatt Surbey², Abby R. Whittington^{1,2,4}, Christopher B. Williams*^{1,3}

¹Macromolecules Innovation Institute, Virginia Tech, Blacksburg, VA 24061

²Department of Materials Science & Engineering, Virginia Tech, Blacksburg, VA 24061

³Department of Mechanical Engineering, Virginia Tech, Blacksburg, VA 24061

⁴Department of Chemical Engineering, Virginia Tech, Blacksburg, VA 24061

Keywords:

Tissue Scaffolds; Additive Manufacturing; 3D Printing; Biomaterials; Stereolithography; Vat Photopolymerization

3.1 Abstract

Future advances in tissue engineering depend on the ability to fabricate complex scaffolds with predesigned geometry, pore size, high permeability, and a vascular network. Additionally, scaffolds must support cellular adhesion, proliferation, and potentially influence cellular differentiation to permit the generation of *de novo* tissue. Traditional scaffold fabrication techniques can be used to process a wide variety of biodegradable materials with low cytotoxicity and a range of material properties, but have only partial control over the geometries generated. Vat photopolymerization (VP), an additive manufacturing process also known as stereolithography, fabricates three-dimensional parts by selectively curing a photopolymer resin, layer-by-layer, based on a computer aided design (CAD) model. VP allows the fabrication of complex scaffolds with tailored geometry and micrometer resolution. VP, however, has a very limited palette of materials from which to choose. No commercially available VP resins that promote cell adhesion and proliferation currently exist. Resins described in the literature require significant synthetic

expertise or yield poorer resolution than commercial VP materials. In this work, a novel resin based on 2-acrylamido-2-methyl-1-propanesulfonic acid (NaAMPS) and poly(ethylene glycol) diacrylate (PEGDA) was formulated. Its curing kinetics were investigated to develop parameters that enabled high resolution printing. High resolution scaffolds were fabricated which demonstrated physiologically relevant water contents and elastic moduli. Murine fibroblasts proliferated on films and three-dimensional tissue scaffolds, suggesting that the resin developed could be suitable for tissue engineering applications.

3.2 Introduction

Recent growth in the use of additive manufacturing (AM, 3D printing) in medicine has led to the 3D printing of biomedical implants, surgical tools and jigs, and tissue engineering constructs, to name but a few examples [1–5]. Bioprinting, the AM of three-dimensional parts for use in regenerative medicine or tissue engineering, is a promising technique in overcoming some of tissue engineering's most important challenges, particularly that of generating vascularization [6,7]. Several AM technologies have been employed for tissue scaffold fabrication, including vat photopolymerization [8], material jetting [9], material extrusion [10], powder bed fusion [11], and binder jetting [12]. Vat photopolymerization (VP, also referred to as stereolithography) is an AM technology that uses patterned UV light to selectively photopolymerize thin layers of resin one on top of another to fabricate three-dimensional parts [5]. The precise spatial and temporal control of light afforded by Digital Light Processing (DLP) technology permits the fabrication of features as small as 3 μm [13,14]. Microstereolithography systems are VP machines capable of fabricating feature sizes smaller than about 100 μm . (Multi-photon polymerization (MPP, 2PP), a related AM process, can fabricate features as small as 100 nm [15].)

Due to the high resolution that it affords, VP is gaining traction as a tool for the fabrication of tissue scaffolds [5]. However, VP has traditionally been limited to a narrow range of materials [2,13,16]. For the most part, commercial resins are based on low molecular weight synthetic acrylate, methacrylate, and epoxide monomers that result in hard but brittle parts. These resins do not have properties suitable for tissue scaffolds (e.g., low cytotoxicity, high cell adhesion) as they were developed for rapid prototyping applications rather than biomedical applications. In addition, resins were formulated with low M_w monomers and oligomers, as they typically provide low

viscosity (less than about 5 Pa·s) to allow for rapid recoating of thin layers [13,17]. Recent advances in VP have demonstrated fabrication with novel materials having unique properties including ionic conductivity [18], shape memory effect [19], Class IIA biocompatibility [20], and excellent thermomechanical properties [21]. In addition, tissue scaffolds have been fabricated using both synthetic and natural photopolymer resins that have been developed for VP. The synthetic polymers used for VP typically have poor cellular adhesion and proliferation compared to natural materials, and thus are often surface-treated prior to cell culture [22–24]. Natural polymers provide an excellent substrate for cell growth but are more challenging to build into scaffolds and result in poor resolution, particularly along the print (build) direction [25–28].

Most previous work that uses VP to fabricate tissue scaffolds has focused on poly(propylene fumarate) (PPF) diluted in its monomer, diethyl fumarate (DEF). Synthetic techniques have been thoroughly documented [29], but require a well-equipped wet lab, nearly a dozen reagents and materials, and synthesis expertise. Access to gel permeation chromatograph (GPC) equipment for the determination of molecular weight is also needed. Finally, the synthesis and purification requires several days. The techniques for synthesis of other photopolymers for scaffold fabrication using VP are not as meticulously documented in the literature, but have equipment, material, and expertise requirements nonetheless [30,31]. Commercial oligomers that do not require synthesis demonstrate inferior cellular adhesion and proliferation and thus require surface modification or the inclusion of bioactive molecules (e.g., acrylated polypeptides) [32]. Recent work has shown that epoxidized soybean oil acrylate, which requires no synthesis, can be used with VP for the fabrication of patterned structures [25]. However, scaffolds are only shown from the top surface and it is unclear whether they contained more than a single layer or whether high resolution in the

vertical axis could be obtained. Adhesion and proliferation of human bone marrow mesenchymal stem cells on the material was similar to that on polycaprolactone and polylactic acid surfaces, although adhesion and proliferation of cells on the negative control, polymerized PEGDA, was considerably higher than other literature would suggest [32,33].

Resins for VP based on functionalized natural polymers have become more prevalent in the literature due to their low cytotoxicity and excellent cell adhesion properties. Much of the recent work has focused on methacrylate functionalized gelatin (GelMA). Several groups have reported the printing of GelMA or GelMA-containing resins and the successful proliferation of cells on the printed parts [34–37]. However, the structures fabricated are either two-dimensional or lack any porosity in the direction of printing. Even with the addition of UV absorbers, the high water content and low volumetric density of crosslinking groups in GelMA resin make it very challenging to fabricate thin layers that would permit high resolution in the print direction. Advances in machine or resin development will need to be made before the fabrication of high resolution three-dimensional scaffolds from GelMA can be achieved.

Many synthetic photopolymers that show good cell adhesion and proliferation have been processed using traditional scaffold fabrication techniques but have not yet been incorporated into VP resins for biomedical applications [38]. One of these, the sodium salt of 2-acrylamido-2-methyl-1-propanesulfonic acid (NaAMPS) dissolves readily in water and forms a hydrogel when polymerized (pNaAMPS). Endothelial cells have been found to grow on hydrogels of pNaAMPS crosslinked with *N,N'*-methylenebisacrylamide without any protein surface modification [39]. Further, the negative charge of pNaAMPS hydrogels encourages cellular adhesion, proliferation

and growth to confluence, possibly due to improved adsorption of protein-containing serum onto the gel [39,40].

It is clear that developing a wider palette of resins that permit the fabrication of high resolution tissue scaffolds while simultaneously encouraging cellular adhesion and growth will greatly advance the use of VP in the fields of regenerative medicine and tissue engineering. This study describes the formulation and characterization of one such resin, based on commercially available components, including NaAMPS. Notably, no synthesis or solvents are required to prepare the resin. The incorporation of a UV absorber and the development of print parameters permit the fabrication of high resolution porous structures using a mask projection Microstereolithography system (MP μ SL). Printed parts have physiologically relevant mechanical properties and high water contents. NIH3T3 mouse fibroblasts adhered and proliferated on both cast films and 3D printed tissue scaffolds fabricated from the resin.

3.3 Materials and Methods

3.3.1 Resin Preparation

A resin for 3D printing was formulated from a NaAMPS solution (50 wt% in H₂O, Sigma Aldrich) and poly(ethylene glycol) diacrylate (PEGDA, M_w = 575, Sigma Aldrich). The NaAMPS solution and PEGDA were mixed in a 3:1 ratio by weight. NaAMPS-PEGDA resins were formulated with 1 wt% 2,2-dimethoxy-2-phenylacetophenone (DMPA, TCI Chemicals) photoinitiator and varying quantities of avobenzone (0-0.50 wt%), a UV absorber with an absorbance peak at $\lambda = 357$ nm.

3.3.2 Photorheology

Photorheology was performed on a TA Instruments DHR-2 rheometer coupled with an Omnicure S2000 light source and SmartSwap™ UV geometry. A 20 mm quartz parallel plate geometry was used to permit efficient transmission of light. Samples were loaded with a 500 μm gap, equilibrated for 1 min, and irradiated while being subjected to a 0.3% oscillatory strain at 1 Hz. The light intensity was calibrated using a Silverline radiometer with a 20 mm diameter sensor.

The experiments for avobenzene concentration selection were conducted with a UV light intensity of 5.4 mW/cm².

3.3.3 Mask Projection Microstereolithography

In VP, three-dimensional parts are fabricated by successively curing thin layers of photopolymer (Fig. 3.1). A light source creates a beam of UV light that passes through a series of optics that collimate and homogenize the light. In mask projection VP, the beam of light is selectively patterned onto the resin surface by reflecting it off of a digital micromirror device (DMD), which provides a dynamic mask for changing the projected shape. A pattern corresponding to a single layer of a CAD model is displayed on the DMD by selectively actuating mirrors to permit the reflection of light towards the build area. Alternatively, scanning VP creates patterned light by rastering a laser beam over the resin surface. In both cases, the patterned light photopolymerizes the thin layer of resin between the surface of the resin and the immersed build platform. The build platform, mounted on a linear actuator, then moves down a single layer thickness before the process repeats for each layer of the part.

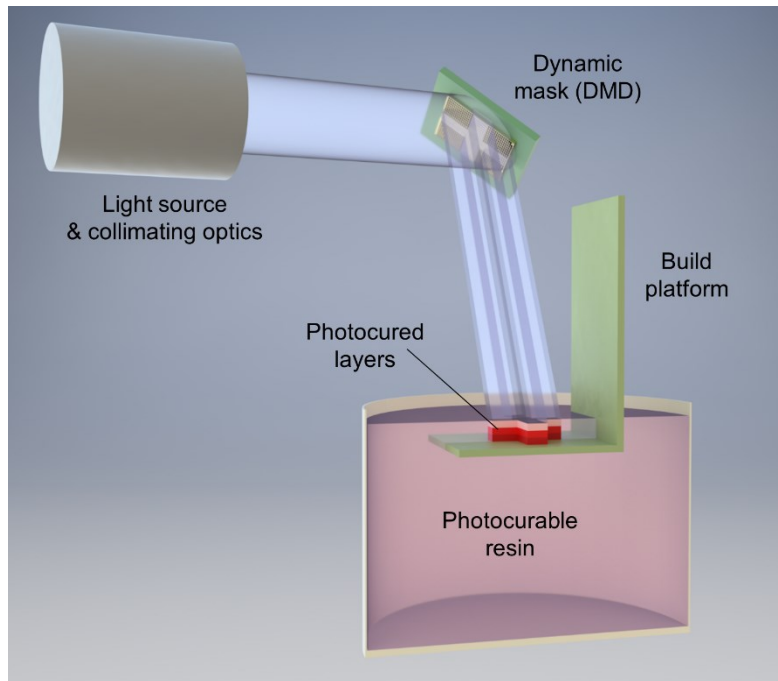


Fig. 3.1. Schematic view of mask projection vat photopolymerization. Collimated light is patterned using a dynamic mask onto the surface of the resin where photopolymerization occurs. Thin layers of photocured resin are stacked one on top of another as the build platform is further submerged into the resin.

Tissue scaffolds were fabricated using a custom lab-built mask projection Microstereolithography (MP μ SL) system. Light from a Hamamatsu LightningCure LC-L1V3 365 nm source was expanded, collimated, and homogenized through a series of optics. This light beam was reflected off a Texas Instruments DLP6500 chip to produce a patterned light beam. Additional optics reduced the size of the beam by a factor of two to create a build area measuring approximately 4 x 7 mm. This optical setup yielded an effective micromirror pitch of 3.78 μ m and a light intensity of 15.0 mW/cm² at the build plane. A build platform was actuated using a Zaber T-LSR075A motorized linear slide. All components were controlled using a custom LabView VI.

3.3.4 Resin Selection and Development of Print Parameters

The generation of a working curve, a semilog plot of cure depth and exposure for a resin, is useful for the determination of print settings (e.g., exposure time, layer thickness). The Jacobs equation (Equation 3.1), derived from the Beer-Lambert law, relates a resin's intrinsic material properties, depth of penetration (D_P) and critical exposure (E_C), with maximum cure depth (C_D) and total light exposure (E). The attenuation of light in a resin is defined by its D_P , while the exposure required to begin gelation of the polymer is the resin's E_C . A linear relationship is observed when C_D is plotted against E on a semi-log plot for a given resin. The x-intercept corresponds to E_C and the slope to D_P . This constitutes the working curve [5,41].

$$C_D = D_P \ln \left(\frac{E}{E_C} \right) \quad \text{Equation 3.1}$$

Data for working curves were collected for resins formulated with avobenzene concentrations between 0 and 0.30 wt%. First, a beaker of resin was placed in the MP μ SL system with the resin surface at the focal plane. All the DMD micromirrors were set to the 'on' position to irradiate the surface of the resin over the entire build area (4 x 7 mm) for a known exposure, E . The free-floating films produced were then retrieved from the resin surface using tweezers, blotted dry, and their thickness, corresponding to C_D , measured using a micrometer. Four samples at three different exposures were measured. The resin's D_P and E_C were calculated using the Jacobs equation and used to determine the exposure time required to cure 50 μ m layer thickness.

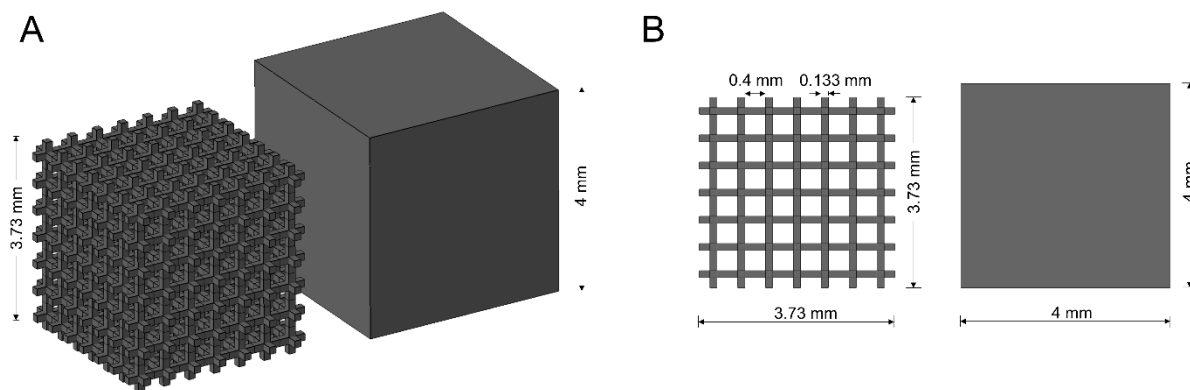


Fig. 3.2. Three-dimensional projection (A) and view along the x, y, or z axis (B) of computer aided design (CAD) models of a tissue scaffold with square pores measuring 400 μm in width and a solid cube. Both digital models were sliced into layers 50 μm thick for printing.

3.3.5 Equilibrium Water Content

Solid cubes and porous scaffolds were used to determine the equilibrium water content of printed pNaAMPS-PEGDA parts fabricated on the MP μ SL system. The scaffold and cube measured 3.73 mm and 4 mm on each side respectively and the scaffolds had 400 μm pores framed by square struts 133 μm in thickness (Fig. 3.2). Since the part was sliced into 50 μm layers, two thirds of the horizontal struts were 150 μm in height and one third were 100 μm . The scaffolds had a nominal porosity of 84.4% and 270 mm^2 of surface area. The cube's nominal surface area was 96 mm^2 .

3.3.6 Compression Testing

Unconfined compression testing was used to determine the compressive moduli of printed parts and was compared to literature values of a variety of native tissues. Scaffolds and cubes identical to those used for water content testing (Fig. 3.2) were printed, washed, post-cured, and then swollen in PBS overnight prior to testing. Samples were compressed at a rate of 1 mm/min with

an Instron 5500R tensile frame utilizing a compression geometry and 1 kN load cell. The load axis of the scaffolds and cubes was the same as the direction of print.

3.3.7 Fibroblast Seeding and Cytotoxicity Evaluation

Films of the resin were cast in circular silicone molds and photocured using a 6 W UV lamp with wavelength of 365 nm for 10 min (2 mW/cm^2 at a distance of 100 mm). The films were then swollen in deionized water overnight and a circular punch used to trim each 1 mm thick film to a diameter of 13 mm. The films were then washed three times in 70% ethanol for 1 h. Subsequently, two washes were performed in sterile PBS to remove ethanol and one wash in complete media to allow proteins to adhere to the film surface. The films were placed in an untreated 24-well polystyrene plate. NIH3T3 murine fibroblasts (ATCC) were cultured in Dulbecco's Modified Eagle Medium (Gibco) with 10% fetal bovine serum (Gibco) and 1% penicillin-streptomycin-amphotericin B (Gibco). NIH3T3 were suspended in fresh media and 1×10^4 cells seeded on each film. The same quantity of cells was seeded in wells of a 24-well tissue culture treated polystyrene (TCPS) plate as a positive control. The well plates were incubated in standard conditions and media replaced every two to three days.

After seven days, an MTS (CellTiter 96, Promega) assay containing 3-(4,5-dimethylthiazol-2-yl)-5-(3-carboxymethoxyphenyl)-2-(4-sulfophenyl)-2H-tetrazolium was performed to quantify cell proliferation using a previously described protocol [42]. The films were moved to a new plate for testing. Fresh media was placed in the wells containing the films, the wells from which the films were moved, the TCPS wells, and empty TCPS wells as an assay control. MTS assay (100 μL) was added to each well and incubated for 2 h. Solution (100 μL) was transferred to a 96 well plate

and its absorption was measured at 490 nm using a BioTek Synergy Mx plate reader. The cell density of cells cultured on pNaAMPS-PEGDA films was calculated based on the area of the film while the area of the well plate was used for TCPS calculations.

3D printed tissue scaffolds with 400 μm pores (Fig. 3.2) were washed in ethanol, PBS, and media with the same techniques used for pNaAMPS-PEGDA films. Scaffolds were placed in Costar Ultra-Low Attachment Microplates (Corning) and a suspension containing 5×10^4 cells pipetted onto the scaffold. After incubating for 4 h to permit adhesion of cells onto the scaffolds, 1 mL of media was added to each well. Media was replaced every 2-3 days and the MTS assay conducted using the same procedure as the films.

In preparation for staining, cells were fixed with a formaldehyde and Triton X-100 solution, rinsed, and post-fixed as previously reported [43]. Scaffolds were stained with 1 μM Texas Red-X Phalloidin (Invitrogen) and 150 nM DAPI (4',6-diamidino-2-phenylindole, dihydrochloride, Invitrogen) in the dark for 1 h. The scaffolds were then rinsed with PBS and stored in the dark at 4 $^{\circ}\text{C}$. A Zeiss Axio Observer.Z1 microscope with laser scanning confocal imaging capability was used to capture images of the scaffolds (Zen 2.3 blue edition, Zeiss). A Plan-Apochromat 10x objective (Zeiss) with 0.45 numerical aperture was used with two lasers and a 53 μm pinhole diameter. A three-dimensional representation showing the location of nuclei and actin around a scaffold's pore was created by collecting fluorescent images in multiple adjacent locations and at many different focal depths. To allow imaging of an entire pore, a motorized stage moved the sample while taking images in four locations (10% tile overlap). At each of these locations, images were taken at 25 focal planes (5.29 μm spacing) to permit imaging of cells along the surfaces of

the scaffold's struts. Background subtraction to remove fluorescence caused by the scaffolds' uptake of DAPI and reconstruction of the images into a three-dimensional model was completed using the Zen software package.

3.3.8 Statistics

Data were compared using ANOVA followed by Tukey's HSD post-hoc test using Origin 2019 software.

3.4 Results

3.4.1 Photorheology

Photorheology studies reveal that the addition of avobenzone to the resin results in increased time to gelation, the point at which the storage modulus becomes greater than the loss modulus. However, UV absorber concentration appears to have little effect on the plateau storage modulus of the gel, with all samples having a modulus of approximately 2 MPa after 90 s of irradiation (Fig. 3.3). The onset of gelation was delayed in samples with higher avobenzone concentrations. The formulation with 0.50 wt% avobenzone eventually reached a similar plateau modulus, but because more than a minute was required, this formulation was not considered further.

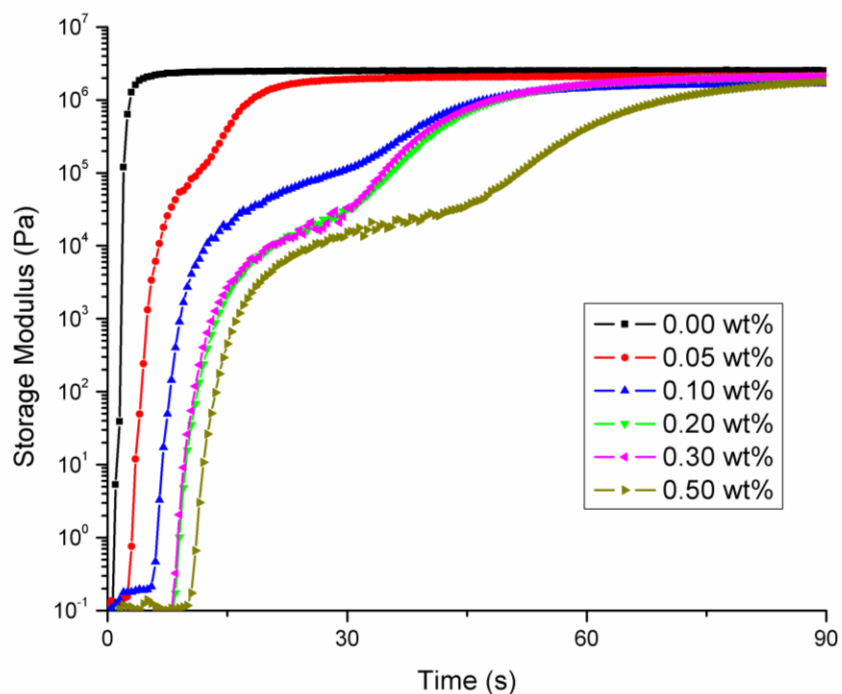


Fig. 3.3. Photorheology of resins formulated with differing avobenzene concentrations all resulted in gels with storage moduli above 10^6 Pa, although higher concentrations required more time to achieve the target modulus.

3.4.2 Print Parameters and Tissue Scaffold Fabrication

Working curves generated for each resin formulation showed that increased UV absorber concentration resulted in smaller D_P and higher E_C , as expected (Fig. 3.4). The resins formulated without avobenzene or with 0.05 wt% and 0.10 wt% concentrations had D_P values greater than $100\ \mu\text{m}$ (1060, 143, and $129\ \mu\text{m}$, respectively) which suggests curing well-defined $50\ \mu\text{m}$ layers of these resins would be difficult. The lowest concentration of avobenzene to result in a resin with a D_P of less than $100\ \mu\text{m}$ was 0.20 wt% ($92\ \mu\text{m}$). The resin with 0.30 wt% avobenzene had a D_P of just $51\ \mu\text{m}$, but the increase in E_C and decrease in D_P meant that it would take twice as long to cure $50\ \mu\text{m}$ layers than the resin containing 0.20 wt% avobenzene. To fabricate scaffolds with $50\ \mu\text{m}$

μm layers, the resin containing 0.20 wt% avobenzene was selected. Researchers who would like to build parts more quickly with thicker layers could choose to print a resin with a lower concentration of avobenzene while those who aim to create smaller feature sizes with high fidelity could instead choose to formulate a resin with 0.30 wt% of the UV absorber.

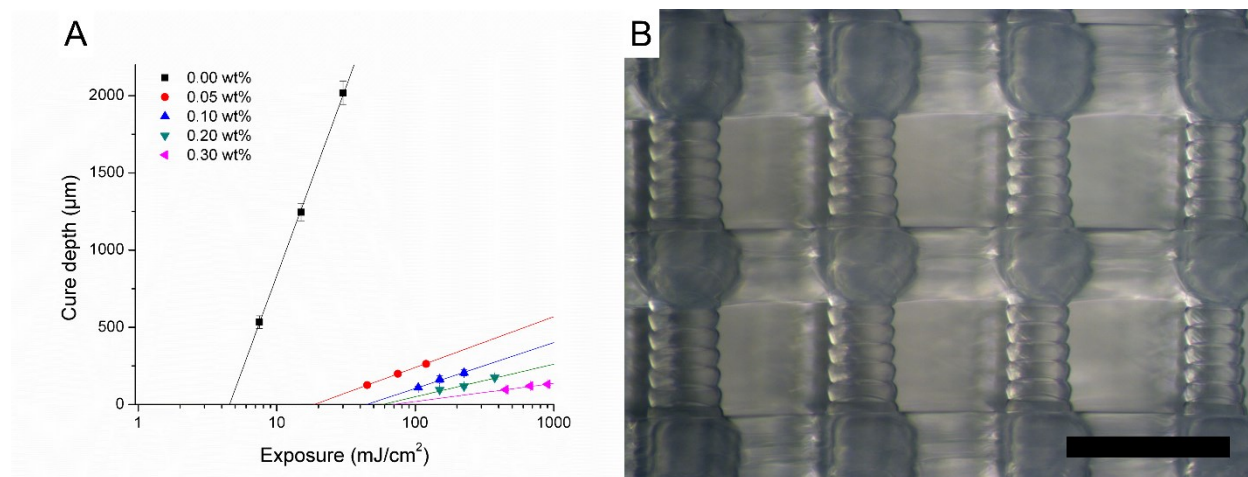


Fig. 3.4. A) Working curves of resins formulated with various concentrations of avobenzene show a decrease in the depth of penetration D_P and increase in critical exposure E_C as more UV absorber is added. B) Side view of a 3D printed tissue scaffold fabricated with a custom MP μ SL system. Scale bar represents 500 μm .

The scaffolds and cubes were printed with 50 μm layers, washed in deionized water, and post-cured. Optical microscopy of the scaffolds showed that the pores had heights and widths measuring about 350 μm rather than the 400 μm dimensions of the digital model (Fig. 3.4). In addition, the pillars were slightly wider than designed. These dimensional inaccuracies were attributed to swelling of the scaffold during cleaning with water, however, slight overexposure of the layers during printing could have been a contributing factor.

3.4.3 Equilibrium Water Content of Printed Parts through TGA

After dehydration of the PBS-swelled parts through TGA, the average water content was found to be 72 wt% (Fig. 3.S1). Even though the resin is 25 wt% water, this demonstrates a large increase in water content of the gel after washing, which is likely to be beneficial for cell adhesion and proliferation. This large water uptake caused some dimensional change in the scaffold due to swelling of the pillars, however the scaffold remained patent. The water content of the printed gels is similar to that of human cartilage (60-85%) [44]. In addition, the presence of Na⁺ ions in the gel aids in water retention, just as in the ECM. These results suggest applicability of the resin for fabricating tissue scaffolds for connective tissue.

3.4.4 Compression Testing

The bulk compressive modulus of PBS-swelled pNaAMPS-PEGDA was found to be 312 MPa ± 12 MPa, between those of mandibular trabecular and cortical bone (Table 3.1). However, printed scaffolds with 400 μm pores with 84% porosity had a substantially lower effective modulus of 902 kPa ± 165 kPa (Fig. 3.5). This is more in line with the moduli of connective tissues including cartilage and dermis. Scaffolds fractured after 11.4% compressive strain, ± 1.1% and compressive strengths of 175 kPa ± 12 kPa. These data suggest that pNaAMPS-PEGDA scaffolds would be suitable for tissue engineering of connective tissue, particularly skin and cartilage.

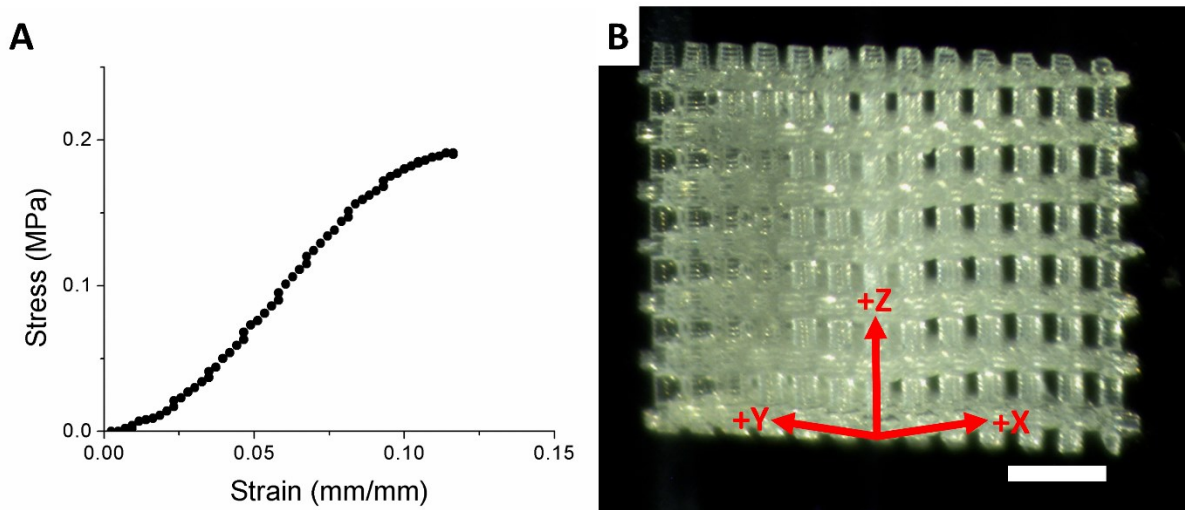


Fig. 3.5. A) Representative stress-strain curve of a printed pNaAMPS-PEGDA scaffold with 400 μm square pores and 84% porosity. B) 3D printed scaffold with a complex structure demonstrates the high resolution and fidelity that can be achieved. The scaffold was imaged at 45° so that two faces are visible simultaneously. During printing, layers photocured in the xy plane are stacked along the z-axis. The scale bar represents 1 mm.

Table 3.1. Compressive moduli of pNaAMPS-PEGDA compared with native tissues

Material	Modulus	Ref.
Cortical bone	5-10 GPa	[45]
Bulk pNaAMPS-PEGDA	312 MPa	
Mandibular trabecular bone	56 MPa	[46]
Renal capsule	7-16 MPa	[47]
Renal cortex (high strains)	1.2 MPa	[47]
Dermis	0.4-2.2 MPa	[48]
pNaAMPS-PEGDA scaffold	0.9 MPa	
Cartilage	0.3-1.5 MPa	[44,49]
Renal cortex (low strains)	15 kPa	[47]
Adipose tissue	0.4-1.7 kPa	[50]

3.4.5 Cell Adhesion and Cytotoxicity

After seven days of culture, the NIH3T3 fibroblasts were found to have adhered and proliferated both on top of the films as well as on the well plate directly below the films. The cells did not proliferate on the perimeter of the untreated well where no pNaAMPS-PEGDA was present. The fibroblasts proliferated across the entire well on the TCPS plate.

After seven days of culture, NIH3T3 cell density was nearly as high both on the top surface of the films as well as underneath them on the well plate (Fig. 3.6). The differences in cell densities between the samples and control were not significant. The excellent proliferation of NIH3T3 on pNaAMPS-PEGDA suggests this copolymer could be a suitable material for the fabrication of tissue engineering scaffolds.

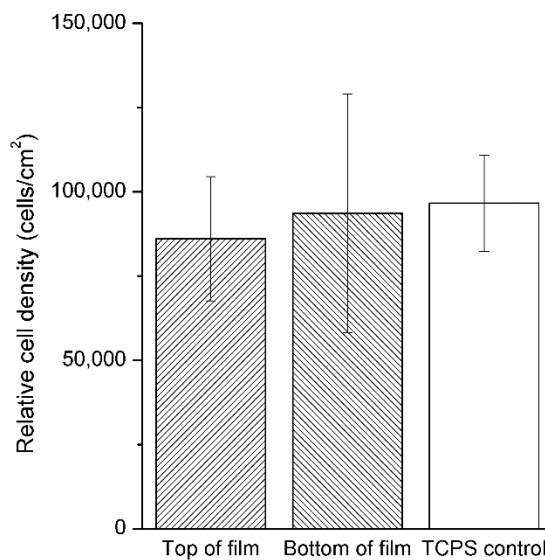


Fig. 3.6. Cell densities on the top and bottom of the pNaAMPS-PEGDA films were both slightly less than that on the TCPS well after 7 d, but this difference was not significant ($p > 0.05$).

However, the sum of the cell counts on top and underneath the film was greater than that in the TCPS wells.

Cell culture on 3D printed pNaAMPS-PEGDA tissue scaffolds with 400 μm pores showed a significant increase in total cell count on scaffolds as culture time increased (Fig. 3.7a). One-way ANOVA followed by a post-hoc Tukey's HSD test showed that the differences in cell counts at 1, 4, and 7 days of culture were significant at the $p < 0.001$ level. Fluorescence images of scaffolds stained with Texas Red and DAPI, which stain for actin and nuclear material respectively, confirmed murine fibroblast adhesion to the struts of the scaffold (Fig. 3.7b). The crosshatch pattern of the scaffold is clearly demarcated by the presence of cell nuclei. The cells were able to move along the 3D printed struts and spread across the edges of the pores. Fluorescence imaging confirms the ability of NIH3T3 fibroblasts to adhere and proliferate on three-dimensional tissue scaffolds fabricated from pNaAMPS-PEGDA using MP μ SL.

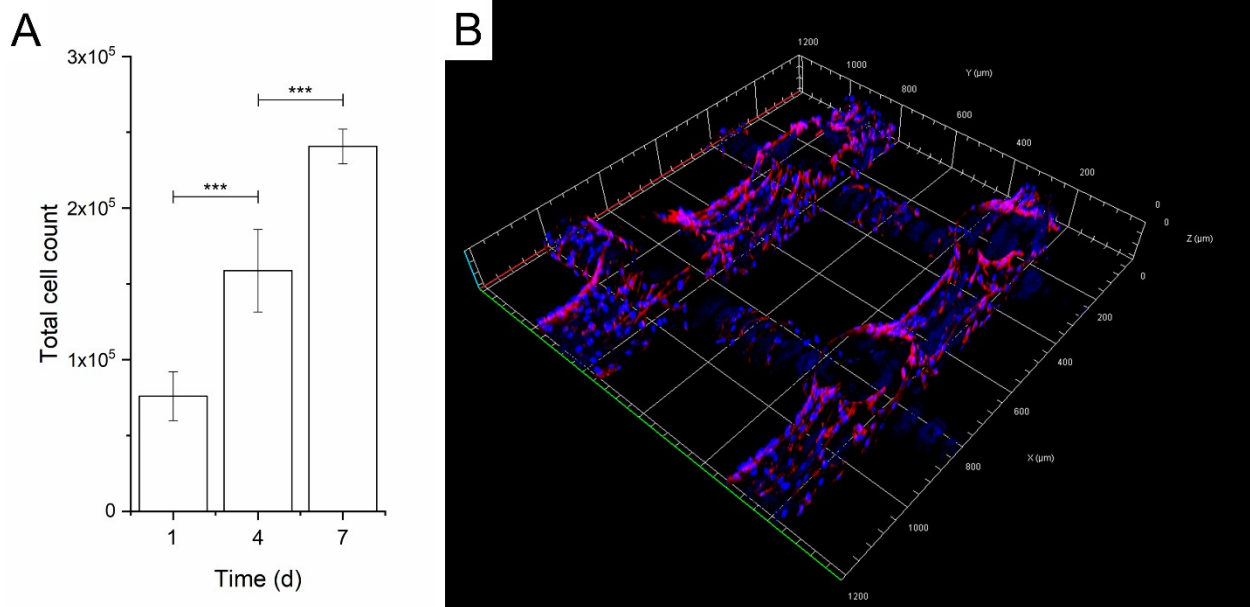


Fig. 3.7. Cell adhesion and proliferation on 3D printed pNaAMPS-PEGDA tissue scaffolds. A) The total number of cells on scaffolds, determined through an MTS assay, was significantly

different proportional to culture time ($***p < 0.001$). B) Representative stacked and tiled confocal image of DAPI (blue) and Texas Red-X (red) staining showed proliferation of fibroblasts on the scaffold after 7 d.

3.5 Discussion

In this report, a photocurable resin was developed for the fabrication of high resolution tissue scaffolds using MP μ SL. Notably, no specialized chemical synthesis was required as all components of the NaAMPS-PEGDA resin are commercially available. This is in contrast to the majority of photocurable resins reported in the literature for the fabrication of tissue scaffolds with VP. The resin reported here has substantially improved cellular adhesion compared to resins formulated from synthetic polymers that require no synthesis while simultaneously offering considerably better printing resolution, particularly in the print direction, than modified natural polymers.

NaAMPS-based hydrogels have been shown to allow fibroblast attachment and proliferation [39]. However, without the use of a crosslinking agent, pNaAMPS forms linear polymer chains resulting in a low modulus gel that does not hold its shape (Fig. 3.S2). To fabricate high resolution structures that could easily be handled after printing, PEGDA, which has previously been used to fabricate complex structures with MP μ SL, was added to NaAMPS to participate in the photopolymerization reaction as a crosslinker [22,51]. On its own, photopolymerized PEGDA forms gels that have shown success *in vivo*, however, due to the bioinert nature of the gels, cellular adhesion is extremely low [32,33]. The combination of these two monomers resulted in a printable resin whose gels promoted fibroblast attachment and proliferation.

Resins with a range of avobenzene concentrations were investigated to determine a concentration of UV absorber that facilitated efficient curing of thin layers. While DMPA and avobenzene are soluble in PEGDA, they are insoluble in a NaAMPS-H₂O solution. The lowest concentration of PEGDA that produced a miscible solution with NaAMPS-H₂O, DMPA, and avobenzene (approximately 25 wt%) was selected. Resins containing 75 wt% NaAMPS and 25 wt% PEGDA were found to be readily printable and produced photocrosslinked parts that were stable when placed in deionized water and phosphate buffered saline (PBS). Photorheology was used to characterize the curing kinetics and plateau storage modulus of resins with avobenzene concentration between 0 and 0.5 wt%. Slow curing kinetics result in print times that are excessively long. Additionally, if the modulus of the cured gel is too low, the printed part will not maintain its structural integrity during printing, cleaning, and handling. When selecting amongst the resins formulated with varying avobenzene concentrations, only those that achieved a storage modulus greater than 1×10^6 Pa with 60 s of irradiation were considered to ensure adequate strength of gels and rapid printing. The resin with the highest avobenzene concentration (0.50 wt%) was ruled out as a viable resin formulation due to its slow curing kinetics.

Three-dimensional printing of high resolution tissue scaffolds with 400 μm pores and 84% porosity was achieved with a resin containing 0.20 wt% avobenzene. Thin, accurate layers were fabricated through the development of a working curve to obtain optimized print parameters. Pore sizes were measured to be slightly smaller than designed (Fig. 3.4). This can be attributed to the printed parts' absorption of additional water during cleaning. Despite these small deviations from the intended dimensions, print fidelity was significantly better than what has been demonstrated

with modified natural polymers fabricated with MP μ SL in the direction of print (which is often not imaged) [25,37]. Because of the difficulty in fabricating scaffolds with porosity in the direction of print, MP μ SL-based fabrication of natural polymers typically is limited to fabricating high resolution 2D patterns rather than complex 3D shapes [34,36]. Even higher fidelity could be achieved with pNaAMPS-PEGDA by increasing avobenzene concentration to 0.30 wt% (or even higher), but print times would be approximately doubled. The resin's swelling ratio could be used to adjust the digital model to account for the small discrepancy in pore size between the model and printed part due to swelling of the gel.

A substrate's stiffness can have a substantial influence on adherent cell morphology and can influence proliferation, differentiation, or even cause apoptosis [52]. More favorable outcomes are achieved when cells are seeded on materials with moduli that mimic those of their native tissue [53]. The bulk compressive modulus of swelled pNaAMPS-PEGDA hydrogels has a modulus somewhat higher than that of mandibular trabecular bone, which is quite soft compared to other bone tissue [46]. The gel's bulk compressive modulus is significantly higher than that of soft tissue such as dermis and renal cortex, however, the effective moduli of porous 3D printed tissue scaffolds were approximately 1 MPa, more than two orders of magnitude lower than the solid samples. This value is comparable to the compressive moduli of connective tissues, including dermis and cartilage. The mechanical properties of NaAMPS-PEGDA scaffolds are likely particularly well suited for cartilage engineering, as it experiences relatively small strains *in vivo*. Tensile tests on tissue scaffolds, which are more difficult to carry out than compression tests, will help further evaluate NaAMPS-PEGDA's suitability for use in skin engineering. A wider range of effective moduli can be obtained by fabricating scaffolds with higher or lower porosities and by

varying crosslink density in the gel [54]. For example, the selection of a higher molecular weight PEGDA would result in decreased crosslink density and modulus, while substitution for a small molecule trifunctional or tetrafunctional acrylate would create a harder gel. A NaAMPS-PEGDA resin formulated with a higher molecular weight PEGDA could be well suited for engineering even softer tissues (e.g., kidney and liver tissue).

The modification of natural polymers, including gelatin [34], keratin [55], collagen [56], and chitosan [57], and hyaluronic acid [28] with photopolymerizable pendant groups for printing with VP has recently become more common. The low cytotoxicity, high cellular adhesion, and the opportunity for hydrolytic or enzymatic degradation all lend to the appeal of natural polymers. Unfortunately, because of the high D_P of light into these resins, fabrication of high resolution features in the print direction has proven challenging. Resins formulated with synthetic monomers and oligomers demonstrate much better fabrication results due to their high volumetric crosslinking densities and low water concentrations. However, the commercially available monomers (e.g., PEGDA) and even many of those that require synthesis, have poor cellular adhesion and proliferation *in vitro* without surface modification or addition of bioactive molecules [22]. In this work, we successfully overcame these challenges by formulating and printing a resin that combines an oligomer with demonstrated printability (PEGDA) with a monomer that encourages cellular adhesion and growth (NaAMPS) [39].

Fibroblasts seeded on films and three-dimensional scaffolds *in vitro* showed excellent proliferation after seven days. On two-dimensional films, an MTS assay showed that cellular proliferation on photopolymerized pNaAMPS-PEGDA was comparable to tissue culture treated polystyrene (Fig.

3.6). This is substantially better than other monomers suitable for MP μ SL-based fabrication of tissue scaffolds that do not require synthesis (e.g., PEGDA) and comparable to PPF/DEF, which requires a multi-day synthesis. Further, an MTS assay after 1 day of culture revealed that fibroblasts had excellent adhesion to printed scaffolds. Cell count increased significantly between 1 and 4 days of culture and again between 4 and 7 days of culture. Confocal fluorescence imaging confirmed the ability of the fibroblasts to adhere and proliferate across the 3D printed scaffolds. Three-dimensional reconstruction of a stack of fluorescence images showed that the 3T3 spread out over the pillars and struts of the scaffold after just 7 days (Fig. 3.7b). Cell proliferation was especially high in the inner corners of the pores.

3.6 Conclusions

This study shows high resolution tissue scaffolds that promote cell adhesion and proliferation can be fabricated with MP μ SL from commercially available components. An investigation into curing kinetics guided resin formulation that permitted the fabrication of scaffolds with small feature sizes and high porosities. The printed constructs had physiologically relevant compressive moduli and water contents. Further, mouse fibroblasts successfully adhered and proliferated across films and on three-dimensional printed tissue scaffolds. These results demonstrate it is possible to use commercially available components in MP μ SL systems to fabricate high resolution tissue scaffolds that also allow cell adhesion and proliferation.

References

- [1] S.M. Peltola, F.P.W. Melchels, D.W. Grijpma, M. Kellomäki, A review of rapid prototyping techniques for tissue engineering purposes, *Ann. Med.* 40 (2008) 268–280. doi:10.1080/07853890701881788.
- [2] F.P.W. Melchels, J. Feijen, D.W. Grijpma, A review on stereolithography and its

- applications in biomedical engineering., *Biomaterials*. 31 (2010) 6121–6130. doi:10.1016/j.biomaterials.2010.04.050.
- [3] S. V. Murphy, A. Atala, 3D bioprinting of tissues and organs, *Nat. Biotechnol.* 32 (2014) 773–785. doi:10.1038/nbt.2958.
- [4] B. Bidanda, P. Bártolo, eds., *Virtual prototyping & bio manufacturing in medical applications*, Springer, 2008.
- [5] N.A. Chartrain, C.B. Williams, A.R. Whittington, A review on fabricating tissue scaffolds using vat photopolymerization, *Acta Biomater.* 74 (2018) 90–111. doi:10.1016/j.actbio.2018.05.010.
- [6] E.C. Novosel, C. Kleinhaus, P.J. Kluger, Vascularization is the key challenge in tissue engineering., *Adv. Drug Deliv. Rev.* 63 (2011) 300–11. doi:10.1016/j.addr.2011.03.004.
- [7] F.P.W. Melchels, A.M.C. Barradas, C.A. Van Blitterswijk, J. De Boer, J. Feijen, D.W. Grijpma, Effects of the architecture of tissue engineering scaffolds on cell seeding and culturing, *Acta Biomater.* 6 (2010) 4208–4217. doi:10.1016/j.actbio.2010.06.012.
- [8] J.M. Serrine, A. Pekkanen, A.M. Nelson, N.A. Chartrain, C.B. Williams, T.E. Long, 3D-printable biodegradable polyester tissue scaffolds for cell adhesion, *Aust. J. Chem.* 68 (2015) 1409–1414. doi:10.1071/CH15327.
- [9] T. Xu, W. Zhao, J.M. Zhu, M.Z. Albanna, J.J. Yoo, A. Atala, Complex heterogeneous tissue constructs containing multiple cell types prepared by inkjet printing technology, *Biomaterials*. 34 (2013) 130–139. doi:10.1016/j.biomaterials.2012.09.035.
- [10] B. Duan, L.A. Hockaday, K.H. Kang, J.T. Butcher, 3D Bioprinting of heterogeneous aortic valve conduits with alginate/gelatin hydrogels, *J. Biomed. Mater. Res. - Part A*. 101 A (2013) 1255–1264. doi:10.1002/jbm.a.34420.
- [11] J.M. Williams, A. Adewunmi, R.M. Schek, C.L. Flanagan, P.H. Krebsbach, S.E. Feinberg, S.J. Hollister, S. Das, Bone tissue engineering using polycaprolactone scaffolds fabricated via selective laser sintering, *Biomaterials*. 26 (2005) 4817–4827. doi:10.1016/j.biomaterials.2004.11.057.
- [12] A. Farzadi, M. Solati-Hashjin, M. Asadi-Eydivand, N.A.A. Osman, Effect of layer thickness and printing orientation on mechanical properties and dimensional accuracy of 3D printed porous samples for bone tissue engineering, *PLoS One*. 9 (2014) e108252. doi:10.1371/journal.pone.0108252.
- [13] S.C. Ligon, R. Liska, J. Stampfl, M. Gurr, R. Mülhaupt, Polymers for 3D Printing and Customized Additive Manufacturing, *Chem. Rev.* 117 (2017) 10212–10290. doi:10.1021/acs.chemrev.7b00074.
- [14] C. Sun, N. Fang, D.M. Wu, X. Zhang, Projection micro-stereolithography using digital micro-mirror dynamic mask, *Sensors Actuators A Phys.* 121 (2005) 113–120. doi:10.1016/j.sna.2004.12.011.
- [15] V.F. Paz, M. Emons, K. Obata, A. Ovsianikov, S. Peterhänsel, K. Frenner, C. Reinhardt, B. Chichkov, U. Morgner, W. Osten, Development of functional sub-100 nm structures with 3D two-photon polymerization technique and optical methods for characterization, *J. Laser Appl.* 24 (2012). doi:10.2351/1.4712151.
- [16] K.C. Hribar, P. Soman, J. Warner, P. Chung, S. Chen, Light-assisted direct-write of 3D functional biomaterials., *Lab Chip*. 14 (2014) 268–75. doi:10.1039/c3lc50634g.
- [17] C. Hinczewski, S. Corbel, T. Chartier, Ceramic suspensions suitable for stereolithography, *J. Eur. Ceram. Soc.* 18 (1998) 583–590. doi:10.1016/S0955-2219(97)00186-6.
- [18] A.R. Schultz, P.M. Lambert, N.A. Chartrain, D.M. Ruohoniemi, Z. Zhang, C. Jangu, M.

- Zhang, C.B. Williams, T.E. Long, 3d printing phosphonium ionic liquid networks with mask projection microstereolithography, *ACS Macro Lett.* 3 (2014) 1205–1209.
- [19] Q. Ge, A.H. Sakhaei, H. Lee, C.K. Dunn, N.X. Fang, M.L. Dunn, Multimaterial 4D Printing with Tailorable Shape Memory Polymers, *Sci. Rep.* 6 (2016) 1–11. doi:10.1038/srep31110.
- [20] W.-S. Lin, B.T. Harris, J. Pellerito, D. Morton, Fabrication of an interim complete removable dental prosthesis with an in-office digital light processing three-dimensional printer: A proof-of-concept technique, *J. Prosthet. Dent.* (2018). doi:10.1016/j.prosdent.2017.12.027.
- [21] M. Hegde, V. Meenakshisundaram, N. Chartrain, S. Sekhar, D. Tafti, C.B. Williams, T.E. Long, 3D Printing All-Aromatic Polyimides using Mask-Projection Stereolithography: Processing the Nonprocessable, *Adv. Mater.* 29 (2017). doi:10.1002/adma.201701240.
- [22] L.-H. Han, G. Mapili, S. Chen, K. Roy, Projection Microfabrication of Three-Dimensional Scaffolds for Tissue Engineering, *J. Manuf. Sci. Eng.* 130 (2008) 021005. doi:10.1115/1.2823079.
- [23] P. Xuan, L.Æ. Jin, W. Lee, D. Cho, Development of 3D PPF / DEF scaffolds using microstereolithography and surface modification, *J. Mater. Sci. Mater. Med.* 20 (2009) 271–279. doi:10.1007/s10856-008-3567-2.
- [24] J. Hwal, S. Jin, W. Lee, J. Hwa, Evaluation of cell proliferation and differentiation on a poly (propylene fumarate) 3D scaffold treated with functional peptides, *J. Mater. Sci.* 46 (2011) 5282–5287. doi:10.1007/s10853-011-5467-y.
- [25] S. Miao, W. Zhu, N.J. Castro, M. Nowicki, X. Zhou, H. Cui, J.P. Fisher, L.G. Zhang, 4D printing smart biomedical scaffolds with novel soybean oil epoxidized acrylate, *Sci. Rep.* 6 (2016) 1–10. doi:10.1038/srep27226.
- [26] H. Lin, D. Zhang, P.G. Alexander, G. Yang, J. Tan, A.W.M. Cheng, R.S. Tuan, Application of visible light-based projection stereolithography for live cell-scaffold fabrication with designed architecture, *Biomaterials.* 34 (2013) 331–339. doi:10.1016/j.biomaterials.2012.09.048.
- [27] H. Lin, Y. Tang, T.P. Lozito, N. Oyster, R.B. Kang, M.R. Fritch, B. Wang, R.S. Tuan, Projection Stereolithographic Fabrication of BMP-2 Gene-activated Matrix for Bone Tissue Engineering, *Sci. Rep.* 7 (2017) 1–11. doi:10.1038/s41598-017-11051-0.
- [28] S. Suri, L.-H. Han, W. Zhang, A. Singh, S. Chen, C.E. Schmidt, Solid freeform fabrication of designer scaffolds of hyaluronic acid for nerve tissue engineering, *Biomed. Microdevices.* 13 (2011) 983–993. doi:10.1007/s10544-011-9568-9.
- [29] F.K. Kasper, K. Tanahashi, J.P. Fisher, A.G. Mikos, Synthesis of poly(propylene fumarate), *Nat. Protoc.* 4 (2009) 518–525. doi:10.1038/nprot.2009.24.
- [30] O. Guillaume, M.A. Geven, C.M. Sprecher, V.A. Stadelmann, D.W. Grijpma, T.T. Tang, L. Qin, Y. Lai, M. Alini, J.D. de Bruijn, H. Yuan, R.G. Richards, D. Eglin, Surface-enrichment with hydroxyapatite nanoparticles in stereolithography-fabricated composite polymer scaffolds promotes bone repair, *Acta Biomater.* 54 (2017) 386–398. doi:10.1016/j.actbio.2017.03.006.
- [31] A. Ronca, L. Ambrosio, D.W. Grijpma, Preparation of designed poly(D,L-lactide)/nanosized hydroxyapatite composite structures by stereolithography, *Acta Biomater.* 9 (2013) 5989–96. doi:10.1016/j.actbio.2012.12.004.
- [32] J. Zhu, Bioactive modification of poly(ethylene glycol) hydrogels for tissue engineering, *Biomaterials.* 31 (2010) 4639–4656. doi:10.1016/j.biomaterials.2010.02.044.
- [33] W. Yang, H. Yu, G. Li, Y. Wang, L. Liu, Facile modulation of cell adhesion to a

- poly(ethylene glycol) diacrylate film with incorporation of polystyrene nano-spheres, *Biomed. Microdevices*. 18 (2016). doi:10.1007/s10544-016-0133-4.
- [34] J.W. Nichol, S.T. Koshy, H. Bae, C.M. Hwang, S. Yamanlar, A. Khademhosseini, Cell-laden microengineered gelatin methacrylate hydrogels, *Biomaterials*. 31 (2010) 5536–5544. doi:10.1016/j.biomaterials.2010.03.064.
- [35] A.P. Zhang, X. Qu, P. Soman, K.C. Hribar, J.W. Lee, S. Chen, S. He, Rapid fabrication of complex 3D extracellular microenvironments by dynamic optical projection stereolithography., *Adv. Mater.* 24 (2012) 4266–70. doi:10.1002/adma.201202024.
- [36] Z. Wang, R. Abdulla, B. Parker, R. Samanipour, S. Ghosh, K. Kim, A simple and high-resolution stereolithography-based 3D bioprinting system using visible light crosslinkable bioinks, *Biofabrication*. 7 (2015). doi:10.1088/1758-5090/7/4/045009.
- [37] R. Gauvin, Y.C. Chen, J.W. Lee, P. Soman, P. Zorlutuna, J.W. Nichol, H. Bae, S. Chen, A. Khademhosseini, Microfabrication of complex porous tissue engineering scaffolds using 3D projection stereolithography, *Biomaterials*. 33 (2012) 3824–3834. doi:10.1016/j.biomaterials.2012.01.048.
- [38] L.S. Nair, C.T. Laurencin, Biodegradable polymers as biomaterials, *Prog. Polym. Sci.* 32 (2007) 762–798. doi:10.1016/j.progpolymsci.2007.05.017.
- [39] Y.M. Chen, N. Shiraishi, H. Satokawa, A. Kakugo, T. Narita, J.P. Gong, Y. Osada, K. Yamamoto, J. Ando, Cultivation of endothelial cells on adhesive protein-free synthetic polymer gels, *Biomaterials*. 26 (2005) 4588–4596. doi:10.1016/j.biomaterials.2004.11.025.
- [40] A. Kishida, H. Iwata, Y. Tamada, Y. Ikada, Cell behaviour on polymer surfaces grafted with non-ionic and ionic monomers, *Biomaterials*. 12 (1991) 786–792. doi:10.1016/0142-9612(91)90031-5.
- [41] P.F. Jacobs, *Fundamentals of Stereolithography*, in: *Solid Free. Fabr. Symp.*, 1992: pp. 196–211.
- [42] A.T. Stevenson, L.M. Reese, T.K. Hill, J. Mcguire, A.M. Mohs, R. Shekhar, L.R. Bickford, A.R. Whittington, Fabrication and Characterization of Medical Grade Polyurethane Composite Catheters for Near-Infrared Imaging, *Biomaterials*. 54 (2015) 168–176. doi:10.1016/j.biomaterials.2015.03.020.
- [43] A.W. Morgan, K.E. Roskov, S. Lin-Gibson, D.L. Kaplan, M.L. Becker, C.G. Simon, Characterization and optimization of RGD-containing silk blends to support osteoblastic differentiation, *Biomaterials*. 29 (2008) 2556–2563. doi:10.1016/J.BIOMATERIALS.2008.02.007.
- [44] V.C. Mow, A. Ratcliffe, A. Robin Poole, Cartilage and diarthrodial joints as paradigms for hierarchical materials and structures, *Biomaterials*. 13 (1992) 67–97. doi:10.1016/0142-9612(92)90001-5.
- [45] Y.-C. Fung, *Bone and Cartilage*, in: *Biomech. Mech. Prop. Living Tissues*, Springer New York, New York, NY, 1993: pp. 500–544. doi:10.1007/978-1-4757-2257-4_12.
- [46] C.E. Misch, Z. Qu, M.W. Bidez, Mechanical properties of trabecular bone in the human mandible: Implications for dental implant treatment planning and surgical placement, *J. Oral Maxillofac. Surg.* 57 (1999) 700–706. doi:10.1016/S0278-2391(99)90437-8.
- [47] S. Umale, C. Deck, N. Bourdet, P. Dhumane, L. Soler, J. Marescaux, R. Willinger, Experimental mechanical characterization of abdominal organs: Liver, kidney & spleen, *J. Mech. Behav. Biomed. Mater.* 17 (2012) 22–33. doi:10.1016/j.jmbbm.2012.07.010.
- [48] O.A. Shergold, N.A. Fleck, D. Radford, The uniaxial stress versus strain response of pig skin and silicone rubber at low and high strain rates, *Int. J. Impact Eng.* 32 (2006) 1384–

1402. doi:10.1016/j.ijimpeng.2004.11.010.
- [49] S. Pal, *Mechanical Properties of Biological Materials*, in: *Des. Artif. Hum. Joints Organs*, Springer US, Boston, MA, 2014: pp. 23–40. doi:10.1007/978-1-4614-6255-2_2.
- [50] K. Comley, N. Fleck, The compressive response of porcine adipose tissue from low to high strain rate, *Int. J. Impact Eng.* 46 (2012) 1–10. doi:10.1016/j.ijimpeng.2011.12.009.
- [51] C. Xia, N.X. Fang, 3D microfabricated bioreactor with capillaries, *Biomed. Microdevices.* 11 (2009) 1309–1315. doi:10.1007/s10544-009-9350-4.
- [52] H. Wang, S.M. Haeger, A.M. Kloxin, L.A. Leinwand, K.S. Anseth, Redirecting valvular myofibroblasts into dormant fibroblasts through light-mediated reduction in substrate modulus, *PLoS One.* 7 (2012). doi:10.1371/journal.pone.0039969.
- [53] A. Skardal, D. Mack, A. Atala, S. Sokern, Substrate elasticity controls cell proliferation, surface marker expression and motile phenotype in amniotic fluid-derived stem cells, *J. Mech. Behav. Biomed. Mater.* 17 (2012) 307–316. doi:10.1016/j.jmbbm.2012.10.001.
- [54] P. Soman, J.A. Kelber, J.W. Lee, T.N. Wright, K.S. Vecchio, R.L. Klemke, S. Chen, Cancer cell migration within 3D layer-by-layer microfabricated photocrosslinked PEG scaffolds with tunable stiffness, *Biomaterials.* 33 (2012) 7064–7070. doi:10.1016/j.biomaterials.2012.06.012.
- [55] J.K. Placone, J. Navarro, G.W. Laslo, M.J. Lerman, A.R. Gabard, G.J. Herendeen, E.E. Falco, S. Tomblin, L. Burnett, J.P. Fisher, Development and Characterization of a 3D Printed, Keratin-Based Hydrogel, *Ann. Biomed. Eng.* 45 (2017) 237–248. doi:10.1007/s10439-016-1621-7.
- [56] W. Bian, D. Li, Q. Lian, X. Li, W. Zhang, K. Wang, Z. Jin, Fabrication of a bio-inspired beta-Tricalcium phosphate/collagen scaffold based on ceramic stereolithography and gel casting for osteochondral tissue engineering, *Rapid Prototyp. J.* 18 (2012) 68–80. doi:10.1108/13552541211193511.
- [57] V.B. Morris, S. Nimbalkar, M. Younesi, P. McClellan, O. Akkus, Mechanical Properties, Cytocompatibility and Manufacturability of Chitosan:PEGDA Hybrid-Gel Scaffolds by Stereolithography, *Ann. Biomed. Eng.* 45 (2017) 286–296. doi:10.1007/s10439-016-1643-1.

3.7 Supporting Information

3.7.1 Equilibrium Water Content of Printed Parts through TGA

After printing, scaffolds were washed in deionized water and then swelled in PBS overnight. For testing, parts were removed from the PBS, briefly blotted to remove excess liquid, and placed on a platinum pan for thermogravimetric analysis (TGA). Analysis was conducted with a TA Instruments TGA 2950 with a N₂ atmosphere heated to 250 °C at 20 °C/min and held for 30 min to completely dehydrate the part. An autosampler was not used to ensure that no drying occurred while parts were waiting to be analyzed.

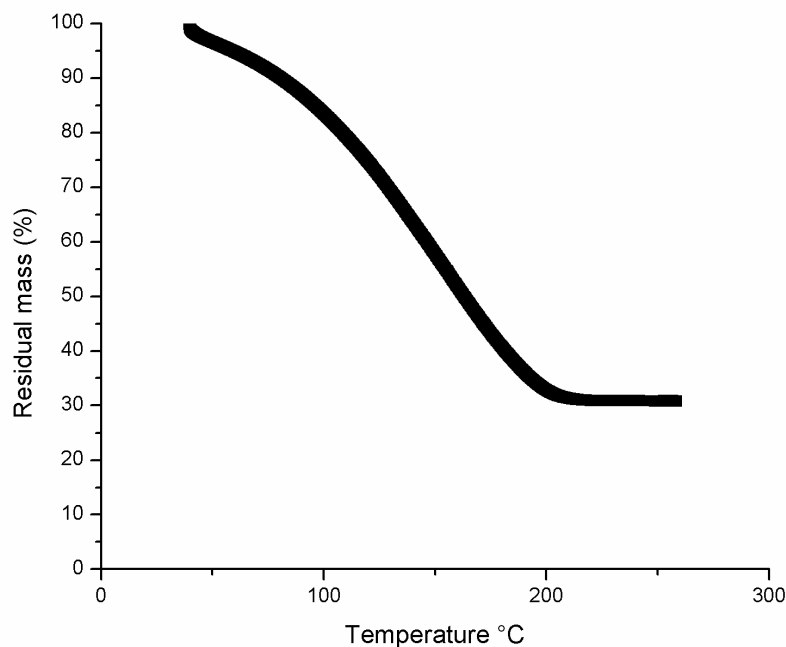


Fig. 3.S1. Representative thermogram showing water removal from a pNaAMPS-PEGDA scaffold.

3.7.2 Photorheology of Resins with and without Crosslinker

Photorheology revealed that NaAMPS resin (50 wt% in H₂O) formed very weak gels that could not be handled and were not self-supporting (Fig. 3.S2.). The resin was formulated with 1 wt% Irgacure 2959 (Sigma Aldrich), a water soluble photoinitiator that could be dissolved in the NaAMPS solution. Even after exposure to 250 mW/cm² of UV light for 10 minutes, the storage modulus of the gel was less than 10⁵ Pa. The addition of a crosslinking agent was necessary to form strong gels. The incorporation of 25 wt% PEGDA crosslinker into the resin resulted in quicker gel formation and storage moduli that exceeded 10⁶ Pa. Except for changes in light intensity and photoinitiator, photorheology parameters were identical to those used to evaluate the effect of UV blocker on NaAMPS-PEGDA photopolymerization.

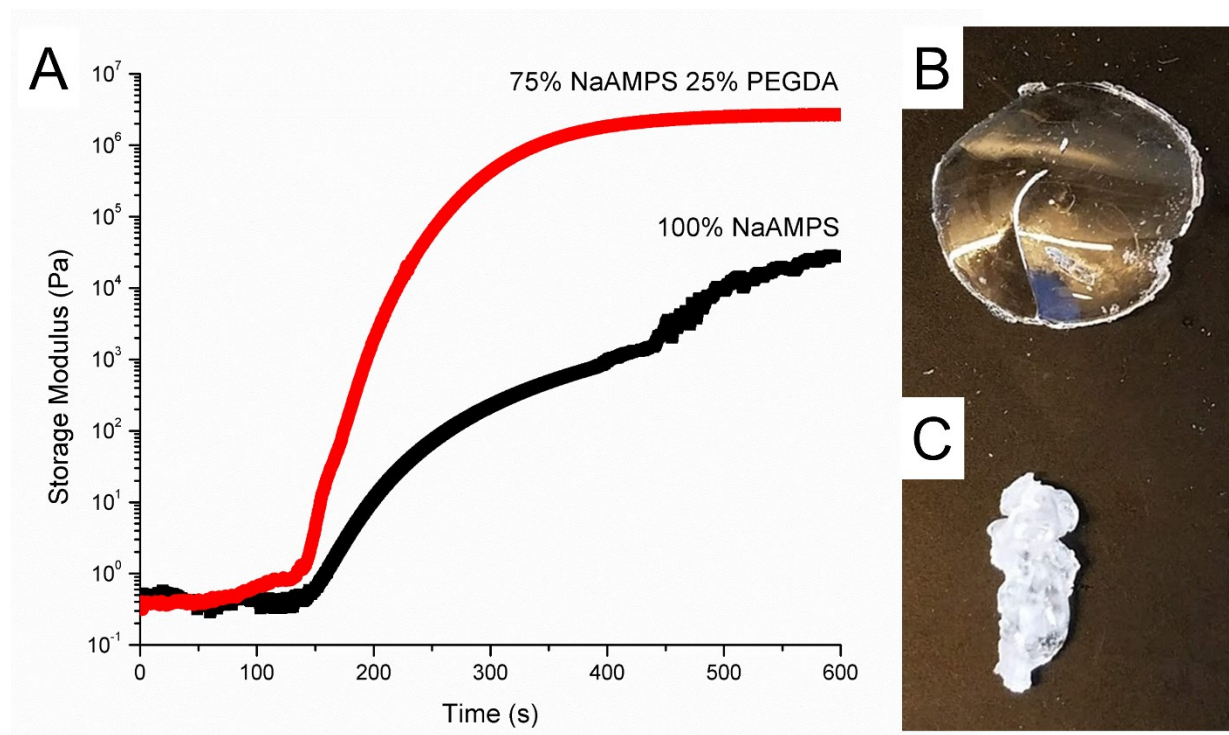


Fig. 3.S2. (A) Photoreology demonstrates that the addition of PEGDA to NaAMPS results in gels with storage moduli more than two orders of magnitude higher than NaAMPS alone.

Photopolymerized NaAMPS-PEGDA (B) formed disks that could be handled with tweezers;
NaAMPS alone (C) formed gels too soft to hold their shape during handling.

Chapter 4: Effects of Pore Size on Cell Proliferation and Distribution in 3D Printed Tissue Scaffolds Fabricated Using Vat Photopolymerization

Nicholas A. Chartrain^{1,2,3}, Christopher B. Williams^{1,3}, Abby R. Whittington^{1,2,4}

¹Macromolecules Innovation Institute, Virginia Tech, Blacksburg, VA 24061

²Department of Materials Science & Engineering, Virginia Tech, Blacksburg, VA 24061

³Department of Mechanical Engineering, Virginia Tech, Blacksburg, VA 24061

⁴Department of Chemical Engineering, Virginia Tech, Blacksburg, VA 24061

4.1 Abstract

The microenvironment created by a tissue scaffold plays a large role in determining the growth, migration, and differentiation of the cells attached to it. Creating more effective and clinically relevant tissue engineering constructs requires careful control over environmental characteristics such as scaffold material and geometry, growth and differentiation factors, and cell-cell interactions. Control over scaffold geometry, including pore size and shape, porosity, and overall pore shape can be achieved with Additive Manufacturing (AM or 3D printing). Unlike other fabrication techniques, each of these parameters can be tuned independently of one another with 3D printing. Here, we isolated and investigated the effect of pore size on cell proliferation and distribution in 3D printed scaffolds. NIH 3T3 murine fibroblasts were seeded on scaffolds with pore sizes ranging from 200 to 600 μm and cultured for 7 days. Confocal imaging along interior cross sections of the scaffolds revealed significant differences in distribution and proliferation between scaffolds. Automated nuclei counting showed that proliferation was greatest on scaffolds with 500 μm pores and that significant inhomogeneity in cell distribution occurred on scaffolds with pore sizes smaller than 400 μm . These data suggest that scaffolds should be designed with larger pore sizes to improve NIH 3T3 proliferation and the formation of homogeneous tissue engineering constructs.

4.2 Introduction

The cellular microenvironment has an essential role in determining cell growth and function [1,2]. In tissue engineering, the microenvironment experienced by cells is created mainly by the characteristics of the tissue scaffold they are grown on [3]. Tissue scaffolds can be engineered to create environments that promote (or prevent) cellular adhesion, growth, or differentiation through the selection of fabrication technique, material, and scaffold geometry [4,5]. While the cell response to certain scaffold properties can be investigated with relative ease (e.g., material selection), the effects of others can be more difficult to elucidate. In particular, the roles played by pore size, pore geometry, and permeability have proven difficult to isolate and evaluate due to the irregular and stochastic nature of the structures produced by fabrication techniques such as electrospinning [6], particulate leaching [7], and gas foaming [8]. In contrast, AM techniques can fabricate tissue scaffolds with defined geometries. One of these AM techniques, vat photopolymerization (VP, also referred to as stereolithography), can fabricate scaffolds with features smaller than 100 μm that allow investigations into the effects of scaffold parameters such as pore size and geometry [9,10]. Tissue scaffolds are typically designed to mimic the *in vivo* microenvironment, as a physiologically-relevant environment is thought to aid in the development of tissue functionality [11,12]. However, the vastly different ways in which tissues form *in utero* versus on tissue scaffolds provides a strong justification for further investigation into the effects certain scaffold features have on cell response.

Cell proliferation across a tissue engineering scaffold is a fundamental requirement and a basic metric of the scaffold's success. Scaffold pore size is known to play a significant role in cell proliferation and distribution in scaffolds fabricated with techniques such as particulate leaching

[13] and freeze drying [14–16]. However, literature values for pore sizes that result in the greatest number of cells vary and the effect on proliferation in scaffolds fabricated with VP has not been systematically investigated. Large pore sizes enable the diffusion of nutrients and oxygen throughout the scaffold, but have the drawback of reducing the total surface area on which cells can be cultured. Surface area can be increased with smaller pore size, but at the expense of nutrient and oxygen diffusion, particularly to the scaffold's center.

The total number of cells on a scaffold is an important metric for measuring the effectiveness of a tissue scaffold; however, it does not reveal a complete picture of cell response to a scaffold on its own. Ideally, cells should be distributed evenly throughout the entire scaffold. When a scaffold's pores are very small, the diffusion of oxygen and movement of cells towards the center of the scaffold is inhibited. The lack of oxygen at the center of the scaffold can be so severe that cells experience hypoxia and undergo apoptosis [17,18]. This can be exacerbated by closed pores, tortuous diffusion pathways, and the rapid growth and proliferation of cells at the oxygen and nutrient-rich surface of the scaffold [18]. Rapid cell growth at the surface of the scaffold can obstruct pores and lead to the formation of a barrier or 'skin' of cells that further prevents the diffusion of nutrients towards the center of the scaffold [19,20]. This causes an inhomogeneous distribution of cells in the scaffold and a tissue engineering construct with reduced functionality. The challenges posed by diffusion limits can be successfully avoided by fabricating extremely thin scaffolds. These, however, have limited clinical relevance. Perfusion bioreactors, which push nutrients through the scaffold to overcome diffusion limits, have been shown to improve cell viability and homogeneity of cells throughout scaffolds [21,22]. Although lessened, oxygen gradients continue to persist [17]. A broader understanding of the effects of pore size, along with

pore shape, porosity, and their interactions will allow for the rational design of complex tissue scaffold designs that encourage cell proliferation and tissue formation.

Many researchers have investigated how pore size impacts cell proliferation with scaffolds fabricated with traditional techniques (e.g., freeze drying, solvent casting and porogen leaching) [16]. For example, Murphy *et al.* found that proliferation of MC3T3-E1 murine preosteoblasts was greater in scaffolds with 325 μm pores than in those fabricated with a lyophilization process that had smaller pores, although pores larger than 325 μm were not investigated [14]. They later showed that rat mesenchymal stem cells behaved similarly with respect to pore size, but again did not use scaffolds with pores larger than 325 μm in diameter [15]. In another study with scaffolds fabricated by freeze drying by Mandal *et al.*, fibroblasts proliferated more extensively in scaffolds with larger pore sizes, but the largest studied pores were only 250 μm in diameter [16]. Human mesenchymal stem cells were found to have significantly higher proliferation on marine coral exoskeleton derived scaffolds with 500 μm pores than those fabricated with 200 μm pores [19]. Articular chondrocytes seeded on scaffolds fabricated via solvent casting and porogen leaching showed greater proliferation on scaffolds with 175 μm pores when compared to those with 125 μm and 75 μm pores [13]. In contrast, scaffolds with pore sizes ranging from 150-500 μm seeded with chondrocytes and implanted subcutaneously in mice showed no differences in proliferation after 8 weeks [7]. Despite some conflicting reports, many of these studies suggest that larger pore sizes improve proliferation, but scaffolds with pores larger than 500 μm have received little attention [16,23]. It is clear the pore size maximizing proliferation will be dependent on the cell type selected, but the optimal pore size for any single cell type continues to elude researchers [15]. This could be due to the drawbacks of using traditional scaffold fabrication techniques for this sort

of study. These techniques create stochastic scaffold geometries that make it difficult or impossible to isolate the effects of pore size on cellular proliferation from the effects of pore shape, interconnectivity, and porosity. In addition, each scaffold geometry is unique and cannot be replicated. A more complete understanding of how cells respond to pore size requires the repeatable fabrication of scaffolds with designed geometries that can effectively isolate pore size from other scaffold parameters.

Additive manufacturing methods fabricate parts in a layer-by-layer fashion from data provided by a digital model [10,24]. By modifying the digital model, scaffolds with precise and repeatable geometries can be fabricated with AM [25]. These unique capabilities of AM enable the fabrication of tissue scaffolds with a range of pore sizes while maintaining constant porosity, pore shape, and other scaffold parameters between samples [26]. Taniguchi *et al.* rigorously isolated and studied the effects of pore size on *in vivo* bone growth into porous titanium scaffolds implanted in rabbits [27]. They found that 600 μm pores improved fixation ability and bone ingrowth over 300 μm scaffolds. Unfortunately, the significant material differences between polymeric hydrogel scaffolds that are useful for engineering a wide variety of tissue types and the titanium scaffolds used by Taniguchi *et al.* prevent generalization of their conclusions. Sobral *et al.* showed that reducing pore size in extrusion-fabricated scaffolds (Bioplotter, EnvisionTec) can improve seeding efficiency of human osteosarcoma SaOs-2 cells, but did not investigate time points longer than 12 hours [28].

Bioprinting, especially extrusion and inkjet-based techniques, have become common for the fabrication of polymeric tissue scaffolds [29,30]. Some studies have used extrusion and inkjet

bioprinting to fabricate scaffolds with varying pore sizes, but did not systematically isolate pore size to study its effects on cell proliferation and distribution after culture [31]. Extrusion and inkjet-based bioprinting can pattern cell-laden inks directly into 3D shapes, avoiding the need to subsequently seed cells onto scaffolds [29]. However, pressure and temperature limitations imposed by the presence of cells limits the resolution and feature sizes that can be achieved [32]. Other drawbacks of these bioprinting techniques include the adverse impact of shear stress on cell viability, relatively low porosities, and, in some instances, limitations on part height due to material properties [33,34].

Vat photopolymerization is an AM technique that uses patterned light to selectively cure a photopolymer in a layer-by-layer manner [10,35]. Unlike other bioprinting technologies, VP can fabricate scaffolds with features as small as 5-50 μm , small or large pores, and high porosities [36,37]. The resolution and the geometric flexibility afforded by VP make it well suited for investigating the effects of pore size in 3D printed tissue scaffolds [10,38]. While some success has been made in understanding the effects of pore shape on cell response [10,39,40], little work has been conducted on pore size. In one study, researchers used VP to fabricate tissue scaffolds with a range of pore lengths and widths, but maintained a constant pore height throughout [41]. As the scaffolds were mainly imaged from the top surface, it is unclear if good interconnectivity was achieved between pores or if print-through obstructed cell migration and nutrient diffusion. Notably, Melchels *et al.* showed that O_2 concentration in VP-fabricated scaffolds with 270 μm pores was lower than in similar scaffolds with 350 μm pores, suggesting that scaffolds with pore sizes that are too small cause hypoxic conditions [18]. In another study, Melchels *et al.* also showed that pore size has a substantial effect on cell distribution in scaffolds after perfusion seeding [42].

However, distributions were only evaluated after 16 hours and cell density was determined by counting pixels in fluorescence images rather than identifying and counting individual nuclei. Despite these drawbacks, these two studies by Melchels *et al.* offer compelling evidence that pore size is a key factor affecting cell adhesion and proliferation in 3D printed tissue scaffolds. In addition, they provide motivation to investigate how pore size can be optimized in scaffolds to enhance proliferation and promote homogeneous cell distributions.

While VP does allow the fabrication of tissue scaffolds with excellent resolution and geometric flexibility, technical limitations have made it a less popular technique for bioprinting than extrusion or inkjet printing [29,43]. Cells are generally not incorporated into the photopolymer resin during printing because the UV light and cytotoxic monomer components risk damaging DNA and negatively impacting cell viability. However, recent work has demonstrated high viability of cells suspended in a resin and printed using visible light rather than UV light [44,45]. In addition, resins containing less cytotoxic water soluble photoinitiators have been developed [46]. Finally, only a few materials have been developed for VP that enable the printing of high resolution tissue scaffolds (particularly resolution in the vertical axis) that also encouraging high cellular adhesion and proliferation [10,47]. These resins are not commercially available and require substantial expertise, effort, and expense to synthesize [48]. However, recently, our group has developed a zero-synthesis resin based on 2-acrylamido-2-methyl-1-propanesulfonic acid sodium salt (NaAMPS) that does permit high resolution fabrication of tissue scaffolds that allow excellent proliferation of NIH 3T3 murine fibroblasts. This has allowed us to use VP to fabricate tissue scaffolds that can be used to investigate the effects of pore size on cell proliferation and distribution.

In this work, we explore the effects of pore size on cell proliferation and distribution in 3D printed scaffolds fabricated with VP. Designs with pore sizes ranging from 200 μm to 600 μm and constant porosity were fabricated. Murine fibroblasts were seeded and cultured *in vitro* on scaffolds for up to 7 days. Cells were fluorescently labeled and imaged using laser scanning confocal fluorescence microscopy to determine their quantity and distribution within the scaffold. Three-dimensional reconstructions of the imaged volume were used to count each cell and determine its coordinates. These data showed that pore size impacted cell distribution within scaffolds and affected cell proliferation in a statistically significant way.

4.3 Materials and Methods

4.3.1 Resin Formulation

A resin based on the sodium salt of 2-acrylamido-2-methyl-1-propanesulfonic acid (NaAMPS, Sigma Aldrich) and poly(ethylene glycol) diacrylate (PEGDA, Sigma Aldrich, $M_w=575$) that has been previously reported was selected for the fabrication of scaffolds. The resin has been shown to provide excellent print results with VP, results in gels with high water contents, and permits the adhesion and proliferation of fibroblasts. The photopolymer solution contained 37.5 wt% NaAMPS, 37.5 wt% H_2O , and 25 wt% PEGDA. The resin was formulated by adding 1 wt% 2,2-dimethoxy-2-phenylacetophenone photoinitiator (DMPA, TCI America) and 0.20 wt% avobenzene (Sigma Aldrich) UV absorber to the photopolymer solution.

4.3.2 Scaffold Design

To explore the effects of pore size on cell proliferation, scaffolds with square pores measuring 200, 300, 400, 500, or 600 μm were designed in CAD and printed (Fig. 4.2). The range of pore sizes was selected based on literature suggesting that an optimal pore size may fall within these limits (200-600 μm) [16,18,19,41]. The effect of pore size on cell response was isolated from the effects of pore shape and porosity. All scaffolds were designed with approximately 84.3% porosity and rectangular beams framing square pores. Porosity was kept constant between the different designs by varying the thickness of the pillars and struts (Fig. 4.2). Digital scaffold models were sliced into 50 μm layers to create a stack of monochrome images for projection.

4.3.3 Fabrication of Scaffolds by Vat Photopolymerization

A custom Mask Projection Microstereolithography (MP μ SL) system was used for the fabrication of scaffolds. The full description of this system, which can achieve printed features as small as 30 μm , is discussed in Hegde *et al.* [49]. Briefly, a LightningCure LC-L1V3 365 nm light source (Hamamatsu Photonics) was expanded, collimated, and homogenized with a set of optics to create a uniform beam of light with a diameter of approximately 40 mm. The beam of light was reflected off of a Texas Instruments DLP6500 digital micromirror device (DMD) controlled by a custom LabView VI to create a patterned beam of light. Resin was placed in a 20 mL beaker and a build platform, actuated by a Zaber T-LSR075A linear stage, was positioned 50 μm below the resin surface. The image for the first layer was projected on the DMD and the patterned light allowed to irradiate the resin surface for 20 s with an intensity of 15 mW/cm^2 . The build platform was then dipped into the resin to ensure complete recoating with fresh resin and positioned 50 μm below its initial position. This process was repeated for each layer until complete fabrication of the part.

After printing, parts were removed from the build stage, cleaned in deionized water, and post-cured in a UV chamber to ensure complete polymerization.

4.3.4 Optical Microscopy and Measurement of Scaffolds

Printed scaffolds were rinsed in deionized water, blotted dry, and immediately imaged with a stereo microscope equipped with an 18 megapixel complementary metal–oxide–semiconductor (CMOS) camera (AmScope) calibrated using a calibration slide. Pore and strut sizes were measured and compared to the designed dimensions.

4.3.5 Sterilization and Extraction of Scaffolds

The effective removal of unreacted monomer in printed parts is essential as these species are highly cytotoxic. After cleaning in deionized water, scaffolds were post-cured with a UV lamp and swelled in deionized water overnight. Three 70% ethanol washes, lasting an hour each, were performed to sterilize the scaffolds and extract unreacted monomer. Two additional 1 hour washes with sterile phosphate buffered saline (PBS) were used to remove the ethanol and a final wash of complete media performed to adsorb proteins onto the scaffold surface.

4.3.6 Cell Culture

NIH 3T3 murine fibroblasts were cultured on tissue culture treated polystyrene using minimum essential medium (α MEM 1X) supplemented with 10% fetal bovine serum (FBS) and 1% penicillin-streptomycin-amphotericin B solution (all from MediaTech CellGro). Cells were incubated using standard cell culture conditions (37 °C and 4.9% CO₂) and passaged when 70-80% confluent.

4.3.7 Cell Seeding on Scaffolds

Cells were seeded at 1×10^5 cells per scaffold, which had been placed in super low adhesion 24-well Nunclon Sphera plates (ThermoFisher Scientific). The cells were permitted to attach for 4 h before additional media was added to each well (1 mL total volume). Media was changed every two to three days. After 7 days, the scaffolds were removed and placed in 1 mL of 10% formalin (ThermoFisher Scientific) for cell fixation and then stored at 4 °C in PBS.

4.3.8 Fluorescence Microscopy

Seeded scaffolds were cut in half with a razor blade to reveal an interior cross-section for imaging (Fig. 4.1). A light microscope was used to orient the scaffolds before cutting so the cut direction was perpendicular to the printed layers (i.e., so that a XZ or equivalent YZ plane could be imaged). One half of each scaffold was stained using 5.7 μ M DAPI (4',6-diamidino-2-phenylindole dihydrochloride, Invitrogen) and 100 nM Texas Red-X Phalloidin (Invitrogen) in the dark for 1 h. After staining, the scaffolds were rinsed and stored in the dark at 4 °C in preparation for imaging.

The cells along the cross-section of the scaffolds were imaged using a laser scanning confocal fluorescence microscope (Zeiss Axio Observer.Z1) with 10x objective (Plan-Apochromat 10x/0.45 M27, Zeiss) and 53 μ m diameter pinhole. A volume, shown schematically in Fig. 4.1, was imaged by tiling and stacking many images. Briefly, this was done in an automated fashion using Zeiss' Zen 2.3 blue edition software which captured images at 14-16 tile locations (approximately 600 x 600 μ m each) by moving the scaffold using a three-axis motorized stage. In addition, at each of the tile locations, images were captured at a range of focal depths to allow imaging of cells along the curved features of the scaffold. Approximately 40 images were captured

at each tile location to image a depth of about 220 μm (5.48 μm vertical spacing). Three-dimensional reconstructions of the imaged volume were reconstructed in the Zen imaging software.

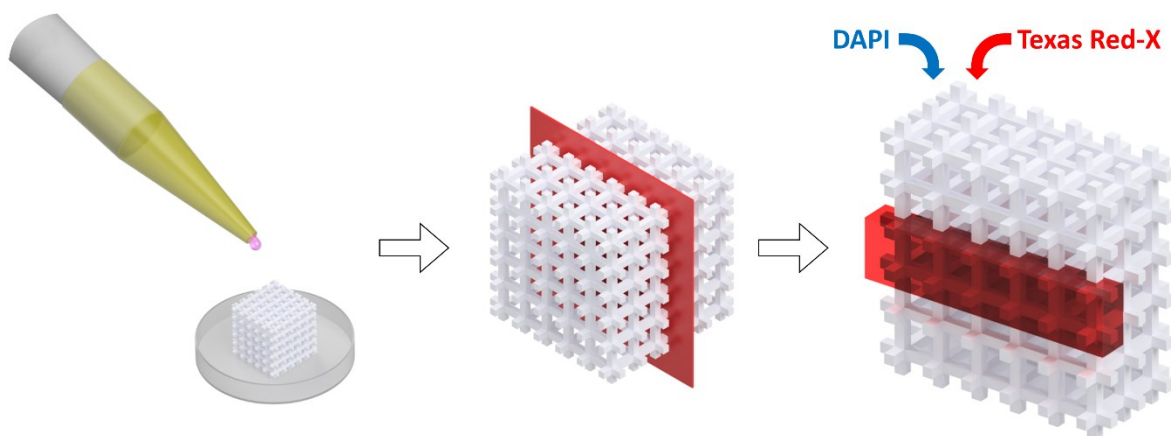


Fig. 4.1. Schematic illustration of the process of seeding, slicing, staining, and imaging murine fibroblasts on 3D printed tissue scaffolds. A cell suspension was pipetted onto a scaffold fabricated using MP μ SL which has been previously washed and sterilized. The scaffolds were cultured for 7 days under static conditions before fixing the cells and slicing the scaffold in half along the plane shown. The cells were stained with DAPI and Texas Red-X fluorescent dyes and a volume along the sliced plane imaged using laser scanning confocal fluorescence microscopy.

4.3.9 Image Analysis & Cell Counting

Image stacks were processed and analyzed in a consistent fashion to count cells and determine their distribution in scaffolds using Zen 2.3 and ImageJ (see Supplemental Information, Fig. 4.S1). Briefly, the Zen software was used to acquire images and remove background fluorescence resulting from the absorption of DAPI by the scaffold and scaffold autofluorescence. ImageJ was

used to remove any remaining background fluorescence and to split nuclei whose fluorescence profiles were contiguous. The BoneJ plugin [50] was used to identify, count, and tabulate the coordinates of each nucleus. Three dimensional reconstructions were visually compared with their original fluorescence image stacks to ensure accurate counting. Additional details and parameters used for cell counting are provided in the Supplemental Information and in Fig. 4.S1.

4.3.10 Statistical Analysis

Data comparisons were made using one-way ANOVA followed by Tukey's HSD post hoc test in the Origin 2019 software package.

4.4 Results

4.4.1 Scaffold Fabrication with Designed Pore Size

After briefly washing in RO water to remove unpolymerized monomer, scaffolds were imaged using light microscopy and the size of both pores and struts were measured to determine printing accuracy (Fig. 4.2). Swelling of the scaffolds was apparent during cleaning. Despite this, pore height and pore width in scaffolds of all pore sizes were very similar to the designed dimensions (Fig. 4.3a). In contrast, pillar and strut thickness were substantially larger than designed in all samples due to water uptake (Fig. 4.3b). If the pillars and struts had only thickened during swelling, the pores would have become partially occluded and would have been found to be smaller than their intended dimensions. Since this was not the case, pillars and struts must have also lengthened to account for the pore sizes observed. In general, strut height was larger than pillar width. We attribute this to "print-through" occurring during fabrication of the part. During curing of the struts, a sufficient amount of UV light was able to penetrate through the strut to the top of the pore below

and initiate polymerization. Additional UV absorber could have been incorporated into the resin to reduce “print-through”, however, this would have substantially increased print durations.

The total surface area and porosity of each scaffold were calculated from the pore, pillar, and strut measurements. While pore sizes were very close to their designed dimensions, the swelling of pillars and struts caused a reduction in scaffold porosity. Porosities were reduced to between 65% and 74% (Fig 4.3c), compared with 84.4% in the designed CAD models. Although this is a relatively large range of porosity, porosity of scaffolds with 300 μm to 600 μm pores fell within a 5% range (69.2-74.0%). Overall scaffold porosity is known to have an effect on cell proliferation, however, the differences in porosity studied tend to be much larger than the range of porosities in this work [51,52]. Trends in porosity between scaffolds with different pore sizes (peaking in scaffolds with 400 μm pores) were not reflected in the cell proliferations observed. As expected, the calculated total surface area of the scaffolds increased with decreasing pore size. Surface area in printed scaffolds was greater than in the CAD models due to swelling that increased the overall scaffold dimensions. Surface area of the scaffolds increased at a relatively uniform rate (i.e., between 40 and 53%).

Our findings of the impact that pore size has on cell growth and proliferation must be viewed in light of deviations in scaffold geometries that occurred due to swelling and fabrication errors. Swelling in particular had substantial effects on the printed geometries but the effects on pillar thickness, porosity, and total surface area were relatively consistent for all pore sizes. This consistency, in addition to the similarity between designed and measured pore size, resulted in a

set of scaffolds suitable for a rigorous investigation on the effect of pore size on cell growth and proliferation.

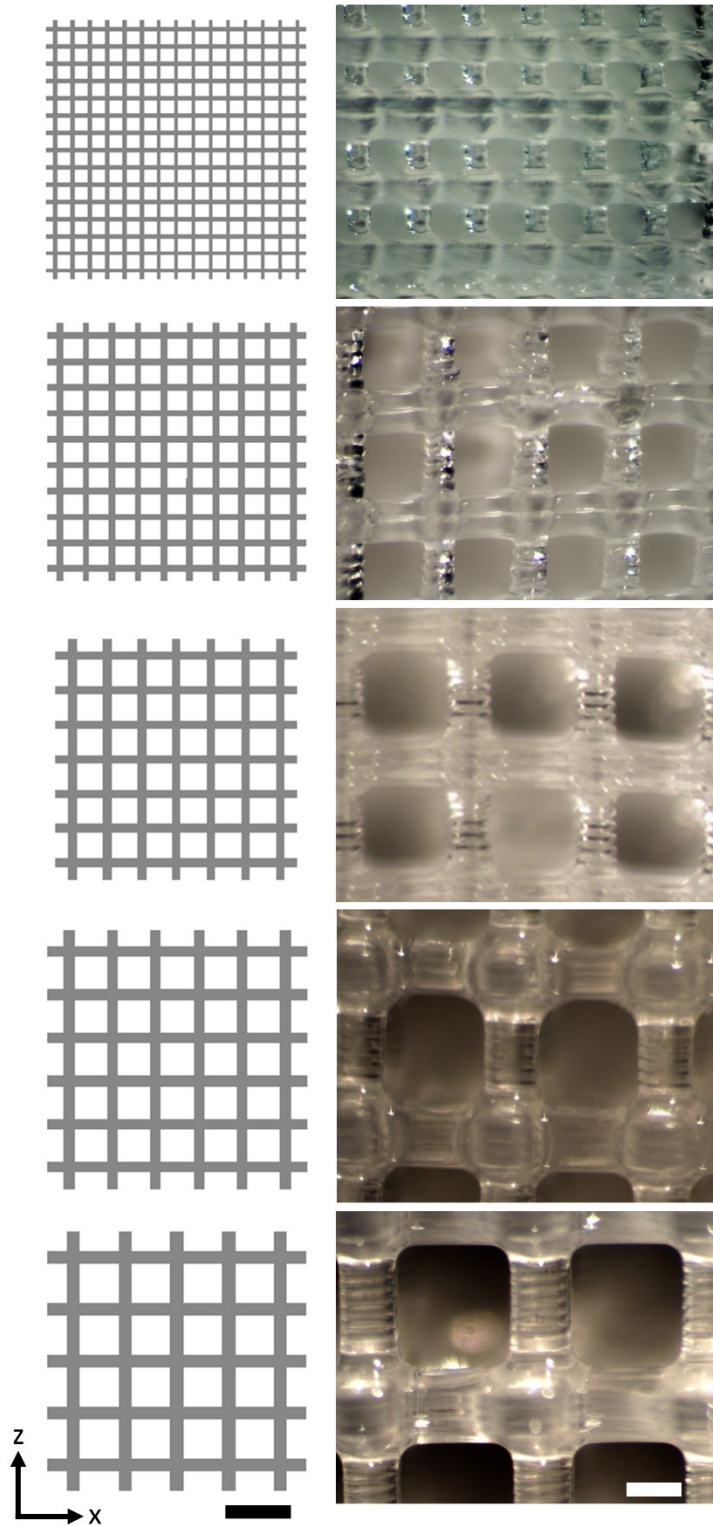


Fig. 4.2. Side view of digital CAD models and printed scaffolds with pore sizes ranging from 200 μm to 600 μm . The black scale bars represent 1 mm and white scale bars represent 250 μm .

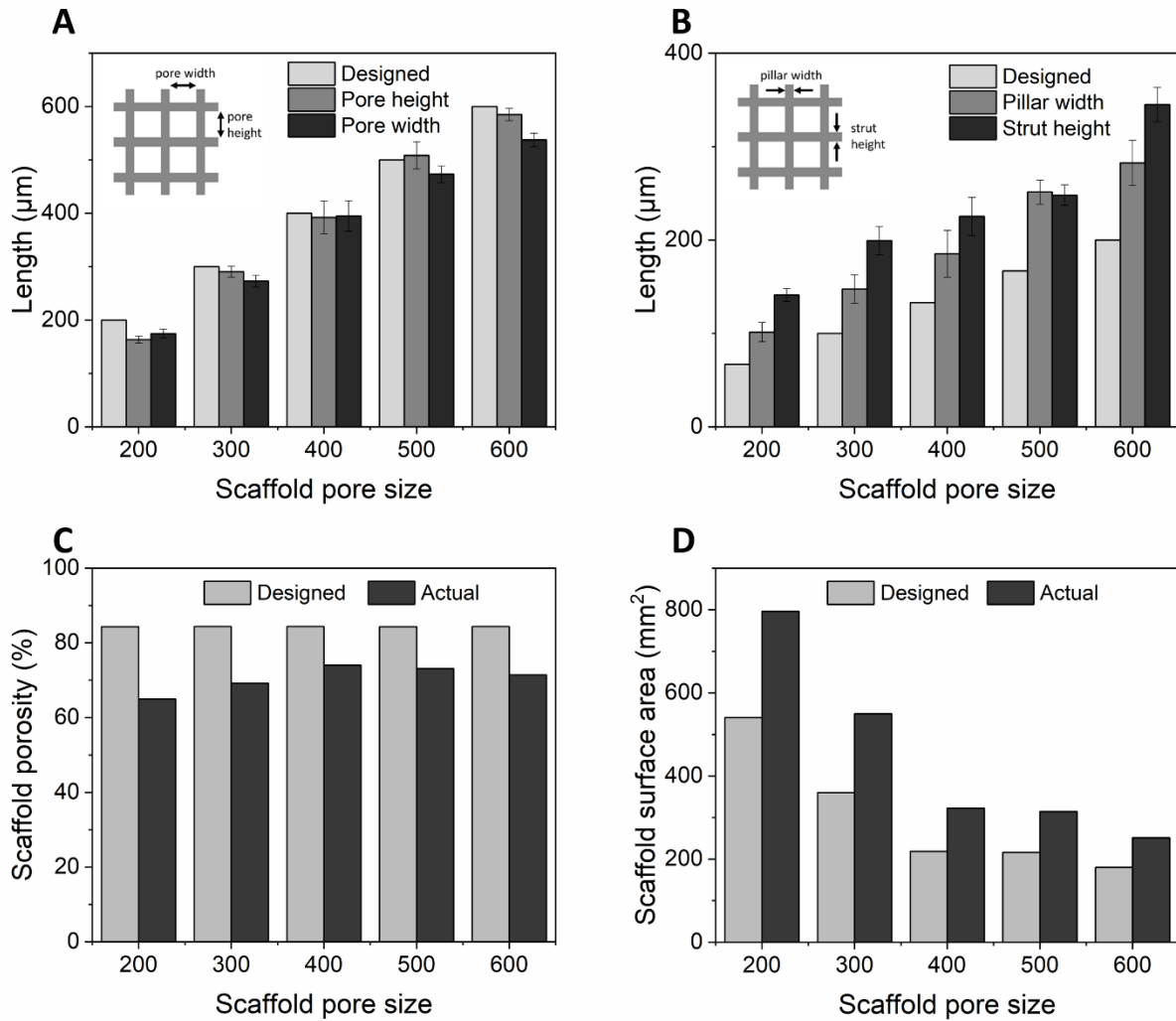


Fig. 4.3. A) The pore height and width as measured by optical microscopy are compared with their designed dimensions B) Pillar width and strut height were thicker than designed due to water uptake of the material. C) Scaffold porosity was calculated using pore and pillar dimensions and compared to designed porosity (84.4%). Calculated porosity of scaffolds ranged from 65% in scaffolds with 200 μm pores to 74% in scaffolds with 400 μm pores. D) Total surface area of each scaffold, also calculated using pore and pillar dimensions, were larger than expected due to an

increase in the overall dimensions of the scaffolds from swelling. Error bars represent standard deviations with $n = 3-6$ scaffolds for each pore size.

4.4.2 NIH 3T3 Proliferation Within Scaffolds

Laser scanning confocal fluorescence microscopy and BoneJ allowed for the counting of all cell nuclei present in the imaged volume (Fig. 4.1 and Fig. 4.S1). Nuclei counting provided a direct measurement of proliferation in the scaffolds, rather than relying on an indirect measurement of proliferation through metabolic activity (e.g. MTS assay) or actin coverage. The average total cell count was highest in the scaffolds with 500 μm pores and lowest in those with 200 μm pores (Fig. 4.4). Total cell count in 500 μm pore scaffolds was significantly higher than that of scaffolds with 200, 300, and 400 μm pores ($p < 0.01$ for 200, 300 μm ; $p < 0.05$ for 400 μm), while total cell count in 600 μm pore scaffolds was significantly higher ($p < 0.05$) than cell count in 200 and 300 μm pore scaffolds.

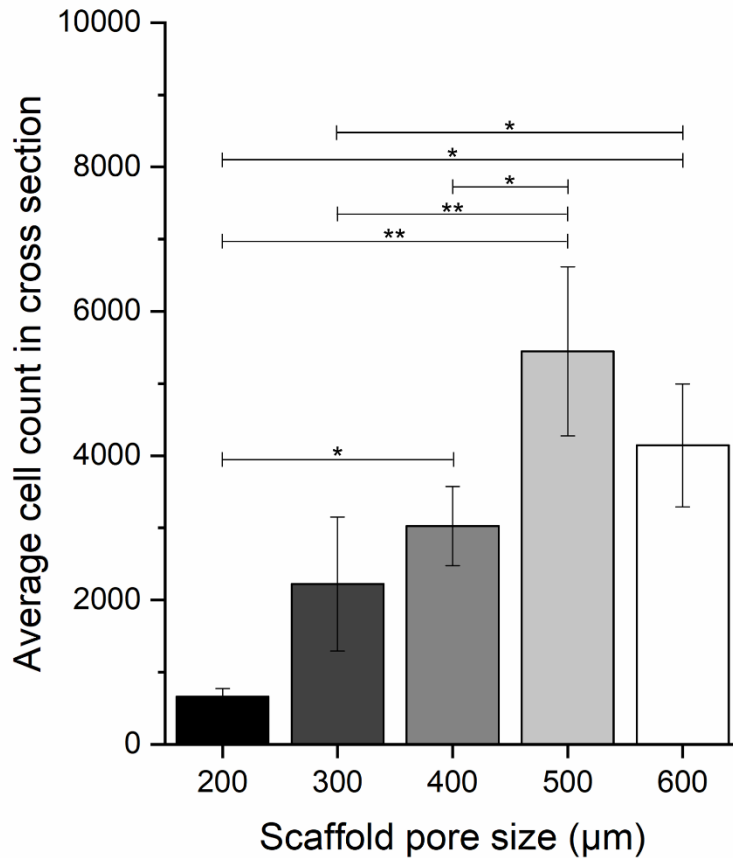


Fig. 4.4. Total cell count in the imaged volume. Cell count was significantly higher in scaffolds with 500 µm pores than in scaffolds with 200, 300, and 400 µm pores (*p < 0.05, **p < 0.01). Error bars represent the standard deviations.

4.4.3 Cell Distribution Along Scaffold Cross-sections

The coordinates of each nucleus was recorded during counting in BoneJ. These data were used to create 3D reconstructions containing each of the nuclei, which offered a visually compelling representation of the distribution of cells throughout each scaffold (Fig. 4.5a-b). The distribution of cells can also be visualized by plotting the distance of each cell from the center of the scaffold. The average number of cells in 100 µm thick slices beginning at the center of the scaffold and moving out towards the edges are shown in Fig. 4.5c. A curve superimposed on the histogram

shows the aggregate fraction of cells counted while moving away from the scaffold center (i.e., the fraction of cells within a certain distance of the scaffold center). A scaffold with perfectly uniform cell distribution would generate a histogram with bars of equal height and the curve representing aggregate fraction of cells counted would be linear.

The cell distribution histogram for scaffolds with 300 μm pores shows a greater number of cells at the surface of scaffolds and a reduced number towards their centers. This trend is greatly exaggerated in scaffolds with 200 μm pores. The lack of cells at the center of these two scaffold geometries is apparent in the 3D reconstructions of cell nuclei obtained from fluorescence imaging. Scaffolds with 400 μm pores have a much more uniform distribution of cells. However, the most uniform distributions are found in the scaffolds with 500 μm and 600 μm pores. These results show a clear correlation between cell distribution homogeneity and pore size.

The cell distribution and surface area of the scaffolds (Fig. 4.3d) were used to determine the average cell density along the scaffold cross section (Fig. 4.6). Density of cells was highest on scaffolds with 500 μm and 600 μm pores, averaging about 1,000-1,250 cells/ mm^2 . As pore size was reduced to 400 μm , cell density drops to an average of about 550 cells/ mm^2 and was even lower for scaffolds with 300 μm and 200 μm pores.

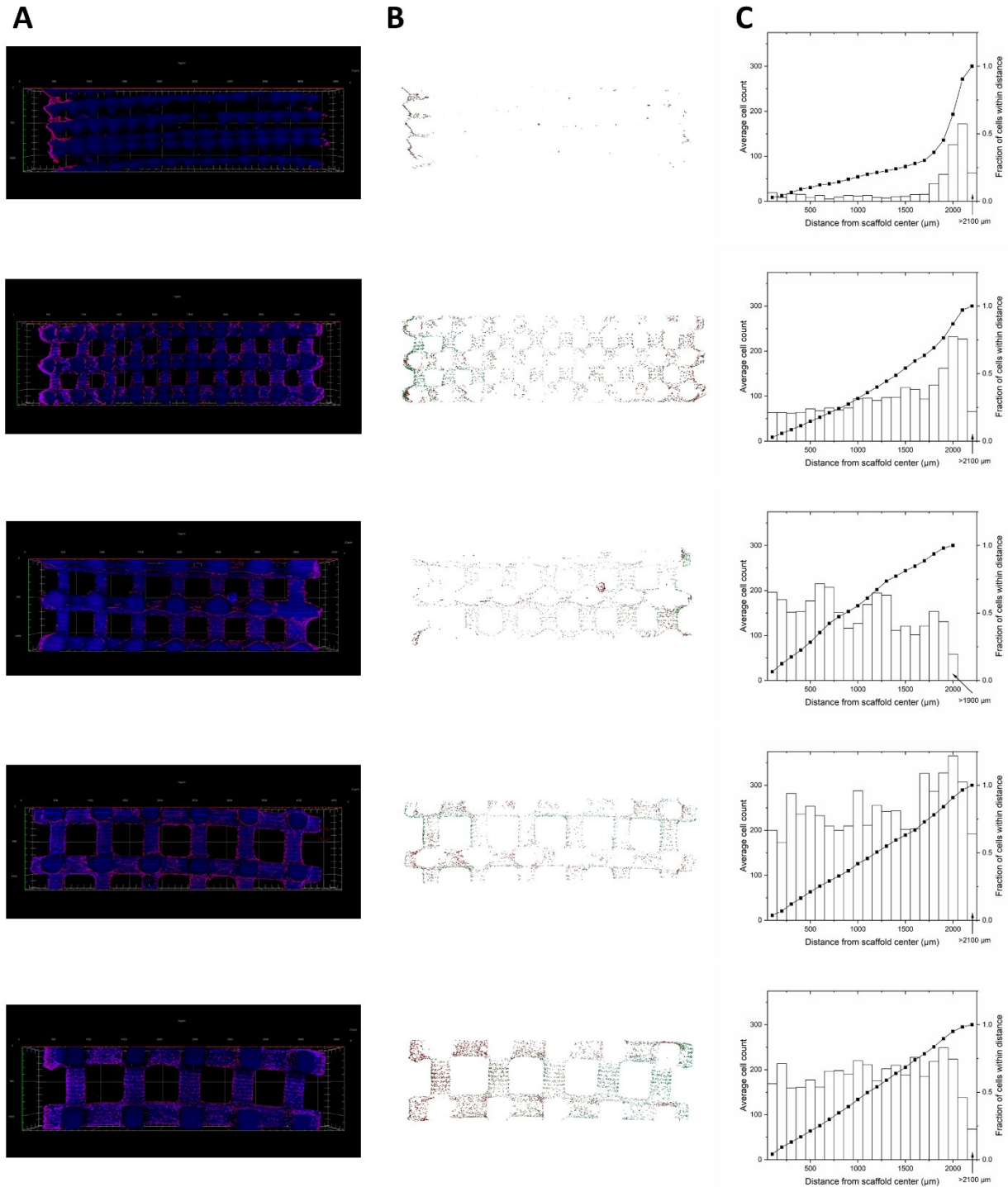


Fig. 4.5. A) Laser scanning confocal fluorescence microscopy images 7 days after seeding murine fibroblasts on scaffolds with pore sizes ranging from 200 μm (top) to 600 μm (bottom). DAPI staining (blue) reveals cell nuclei, but also caused background fluorescence of the scaffold. Texas

Red-X stained actin. Additional images are shown in Fig. 4.S1. B) 3D models showing cell nuclei were generated after removal of background fluorescence and nucleus detection. C) Average cell count from scaffold center to scaffold surface reveal their distribution within the scaffolds (n = 3-6 scaffolds for each pore size).

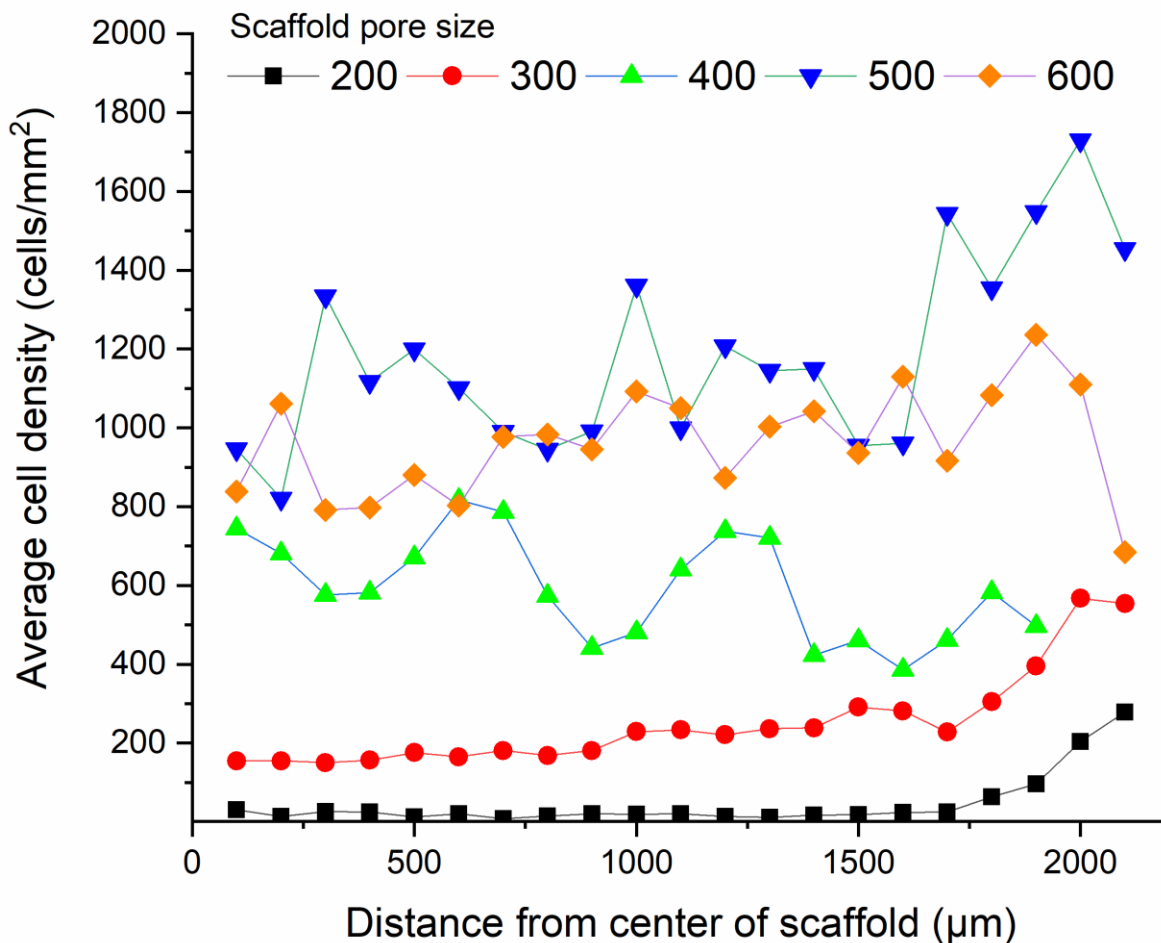


Fig. 4.6. Cell density along scaffold cross sections. Density was highest on scaffolds with 500 µm and 600 µm pores, while scaffolds with smaller pores had lower densities. Surface area of the imaged volume was defined as the proportion of the scaffold volume imaged multiplied by the scaffold's total surface area calculated from measured dimensions.

4.5 Discussion

A cell's microenvironment can have major ramifications on its fate and will help determine its differentiation, migration, and even survival [53,54]. Creating tissue engineering constructs with large populations that perform tissue-specific functions requires careful engineering of the cellular microenvironment, including the physical environment and chemical stimuli [4,11,29]. Pore size, one of the most important parameters of a tissue scaffold, has been shown to have a significant effect on the proliferation of cells in scaffolds fabricated using multiple techniques, including freeze drying [16], porogen leaching [13], and additive manufacturing methods [18]. However, many of these studies do not isolate the effects of pore size from other geometrical factors or test a sufficiently wide variety of pore sizes [15,16,31]. Thus, it is not surprising that the literature contains conflicting reports on the most ideal pore size for a specific cell type (e.g., chondrocytes) [23,55,56] and even for cell types from the same animal model (e.g., bovine articular chondrocytes) [7,13,57]. Further, the stochastic geometries created by techniques such as freeze drying, porogen leaching, and electrospinning are very different from the designed architectures and repeatable fabrication results afforded by AM. These geometrical differences have been shown to affect proliferation [18], and as a result, conclusions from traditional scaffold fabrication techniques likely cannot be generalized to AM scaffolds.

In this work, we successfully quantify the effects of pore size on cell proliferation, density, and distribution in 3D printed tissue scaffolds. The scaffolds used for these comparisons had similar porosities, pore shapes, and overall scaffold shape so as to isolate the effect of pore size to the greatest extent possible. After seven days of culture, significantly lower proliferation of murine fibroblasts was observed on scaffolds with pore sizes between 200 μm and 400 μm than on those

with 500 μm . Cell densities on scaffolds with 500 μm and 600 μm pores were quite similar, but dropped substantially on scaffolds with pore sizes 400 μm or smaller. Differences in proliferation between 500 μm and 600 μm pore scaffolds were not statistically significant, but scaffolds with 500 μm pores had substantially higher surface area available for cell adhesion. This suggests that 500 μm pores are slightly better suited for enhancing cell proliferation than 600 μm pores.

Scaffolds with 200 μm and 300 μm pores displayed inhomogeneous distribution of cells with a high distribution of cells on the surface with far fewer cells towards the center of the scaffold. This is consistent with previous work. Despite the high surface area available for cell attachment on these scaffolds, the small pores hindered cell migration into the center or prevented the diffusion of nutrients and oxygen creating hypoxic conditions. This result may suggest that tissue scaffolds with pore sizes of about 200-300 μm might be suitable when the scaffold thickness is no more than a few hundred microns thick. Unfortunately, thin scaffolds have more limited clinical relevance and cannot be used for the generation of solid *de novo* tissue. Cells were more homogeneously distributed on scaffolds with 400 μm pores, but proliferation and cell density were lower than on scaffolds with larger pores. This suggests that pores below about 400 μm are too small for the proliferation of murine fibroblasts in static culture with the size of scaffolds used (4 mm). Pore sizes of about 500 μm were most successful in maximizing the growth of murine fibroblast and generating homogeneous cell distributions because the pores were large enough so as not to impede nutrient and oxygen diffusion while simultaneously providing a large surface area for cell attachment and growth. While the sheer number of parameters governing scaffold geometry prevents us from asserting an optimal pore size for all situations, our results, in conjunction with previous studies, provides convincing evidence that large pores (400-600+ μm)

are better suited for maximizing cell growth and generating homogeneous cell distributions than smaller pores ($\leq 300 \mu\text{m}$) in tissue scaffolds more than a few hundred microns thick.

The cell growth results in this study corroborate previous findings showing that greater cell proliferation occurs in scaffolds with larger pore sizes ($> 300 \mu\text{m}$) [14–16,19]. However, we expand upon previous research by showing that an ideal pore size is even larger than previously reported, likely in the vicinity of $500 \mu\text{m}$. In fact, future studies should even include scaffolds with pore size even larger than those studied here (e.g., $700\text{-}800 \mu\text{m}$) to ascertain a narrower range of pore sizes that can maximize cell growth while also producing homogeneous distributions of cell. Unfortunately, it is challenging to fabricate highly porous tissue scaffolds ($> 60\%$ porosity) with pore sizes larger than about $400 \mu\text{m}$ using traditional scaffold fabrication methods. This difficulty has likely contributed to the absence of scaffolds with pore sizes larger than $500 \mu\text{m}$ in most previous studies. Further investigations that include additional time points will allow researchers to understand how, and when, cell distributions form in scaffolds with smaller pore sizes. These methods can also be used to understand how various cell types respond differently to pore size [15].

Our work in this study demonstrates that the choice of pore size in 3D printed tissue scaffolds has a considerable effect on the resulting cell proliferation and distribution. These results provide valuable information that, along with results from studies on the effects of other scaffold parameters such as porosity and pore shape, can be used to improve tissue scaffold design. It is important to note that changes in scaffold porosity and material, cell type, and culture technique (static versus dynamic cell culture) will likely affect the pore size that promotes the greatest cell

growth. However, the novel techniques for cell counting and distribution mapping presented in this work can be applied to future studies to help understand how proliferation is impacted by the interaction of several scaffold fabrication parameters.

4.6 Conclusions

In this report, we demonstrated the effect of tissue scaffold pore size on fibroblast proliferation and density in static culture. Pore sizes smaller than 400 μm resulted in statistically significant reductions in cell proliferation and inhomogeneous distributions. Larger pores (i.e., greater than 400 μm) resulted in higher proliferation and homogeneous distributions due to improved diffusion of nutrients and oxygen to the center of the scaffold. Cell density in scaffolds with the larger 500 μm and 600 μm pores were similar, but due to their higher surface area, 500 μm scaffolds had the greatest proliferation of cells. These data suggest that the most favorable outcomes will result when NIH 3T3 fibroblasts are seeded on tissue scaffolds with pores of about 500 μm .

References

- [1] M.P. Lutolf, J.A. Hubbell, Synthetic biomaterials as instructive extracellular microenvironments for morphogenesis in tissue engineering, *Nat. Biotechnol.* 23 (2005) 47–55. doi:10.1038/nbt1055.
- [2] A. Khademhosseini, R. Langer, J. Borenstein, J.P. Vacanti, Microscale technologies for tissue engineering and biology, *Proc. Natl. Acad. Sci.* 103 (2006) 2480–2487. doi:10.1073/pnas.0507681102.
- [3] C.M. Metallo, J.C. Mohr, C.J. Detzel, J.J. De Pablo, B.J. Van Wie, S.P. Palecek, Engineering the Stem Cell Microenvironment, *Biotechnol. Prog.* 23 (2007) 18–23. doi:10.1021/bp060350a.
- [4] J.A. Burdick, G. Vunjak-Novakovic, Engineered Microenvironments for Controlled Stem Cell Differentiation, *Tissue Eng. Part A.* 15 (2009) 205–219. doi:10.1089/ten.tea.2008.0131.
- [5] K. Arcaute, B. Mann, R. Wicker, Stereolithography of spatially controlled multi-material bioactive poly(ethylene glycol) scaffolds., *Acta Biomater.* 6 (2010) 1047–54. doi:10.1016/j.actbio.2009.08.017.

- [6] J. Rnjak-Kovacina, S.G. Wise, Z. Li, P.K.M. Maitz, C.J. Young, Y. Wang, A.S. Weiss, Tailoring the porosity and pore size of electrospun synthetic human elastin scaffolds for dermal tissue engineering, *Biomaterials*. 32 (2011) 6729–6736. doi:10.1016/j.biomaterials.2011.05.065.
- [7] Q. Zhang, H. Lu, N. Kawazoe, G. Chen, Pore size effect of collagen scaffolds on cartilage regeneration, *Acta Biomater.* 10 (2014) 2005–2013. doi:10.1016/j.actbio.2013.12.042.
- [8] T. Lu, Y. Li, T. Chen, Techniques for fabrication and construction of three-dimensional scaffolds for tissue engineering., *Int. J. Nanomedicine*. 8 (2013) 337–50. doi:10.2147/IJN.S38635.
- [9] J.M. Kempainen, S.J. Hollister, Differential effects of designed scaffold permeability on chondrogenesis by chondrocytes and bone marrow stromal cells, *Biomaterials*. 31 (2010) 279–287. doi:10.1016/j.biomaterials.2009.09.041.
- [10] N.A. Chartrain, C.B. Williams, A.R. Whittington, A review on fabricating tissue scaffolds using vat photopolymerization, *Acta Biomater.* 74 (2018) 90–111. doi:10.1016/j.actbio.2018.05.010.
- [11] L.S. Wray, E.J. Orwin, Recreating the Microenvironment of the Native Cornea for Tissue Engineering Applications, *Tissue Eng. Part A*. 15 (2009) 1463–1472. doi:10.1089/ten.tea.2008.0239.
- [12] B.N. Johnson, K.Z. Lancaster, G. Zhen, J. He, M.K. Gupta, Y.L. Kong, E.A. Engel, K.D. Krick, A. Ju, F. Meng, L.W. Enquist, X. Jia, M.C. McAlpine, 3D Printed Anatomical Nerve Regeneration Pathways, *Adv. Funct. Mater.* 25 (2015) 6205–6217. doi:10.1002/adfm.201501760.
- [13] M.M. Nava, L. Draghi, C. Giordano, R. Pietrabissa, The effect of scaffold pore size in cartilage tissue engineering, *J. Appl. Biomater. Funct. Mater.* 14 (2016) e223–e229. doi:10.5301/jabfm.5000302.
- [14] C.M. Murphy, M.G. Haugh, F.J. O’Brien, The effect of mean pore size on cell attachment, proliferation and migration in collagen-glycosaminoglycan scaffolds for bone tissue engineering, *Biomaterials*. 31 (2010) 461–466. doi:10.1016/j.biomaterials.2009.09.063.
- [15] C.M. Murphy, G.P. Duffy, A. Schindeler, F.J. O’Brien, Effect of collagen-glycosaminoglycan scaffold pore size on matrix mineralization and cellular behavior in different cell types, *J. Biomed. Mater. Res. - Part A*. 104 (2016) 291–304. doi:10.1002/jbm.a.35567.
- [16] B.B. Mandal, S.C. Kundu, Cell proliferation and migration in silk fibroin 3D scaffolds, *Biomaterials*. 30 (2009) 2956–2965. doi:10.1016/j.biomaterials.2009.02.006.
- [17] E. Volkmer, I. Drosse, S. Otto, A. Stangelmayer, M. Stengele, B.C. Kallukalam, W. Mutschler, M. Schieker, Hypoxia in Static and Dynamic 3D Culture Systems for Tissue Engineering of Bone, *Tissue Eng. Part A*. 14 (2008) 1331–1340. doi:10.1089/ten.tea.2007.0231.
- [18] F.P.W. Melchels, A.M.C. Barradas, C.A. Van Blitterswijk, J. De Boer, J. Feijen, D.W. Grijpma, Effects of the architecture of tissue engineering scaffolds on cell seeding and culturing, *Acta Biomater.* 6 (2010) 4208–4217. doi:10.1016/j.actbio.2010.06.012.
- [19] T. Mygind, M. Stiehler, A. Baatrup, H. Li, X. Zou, A. Flyvbjerg, M. Kassem, C. Bünger, Mesenchymal stem cell ingrowth and differentiation on coralline hydroxyapatite scaffolds, *Biomaterials*. 28 (2007) 1036–1047. doi:10.1016/j.biomaterials.2006.10.003.
- [20] I. Martin, R.F. Padera, G. Vunjak-Novakovic, L.E. Freed, In vitro differentiation of chick embryo bone marrow stromal cells into cartilaginous and bone-like tissues, *J. Orthop. Res.*

- 16 (1998) 181–189. <https://onlinelibrary-wiley-com.ezproxy.lib.vt.edu/doi/pdf/10.1002/jor.1100160205> (accessed January 29, 2019).
- [21] D. Pazzano, K.A. Mercier, J.M. Moran, S.S. Fong, D.D. DiBiasio, J.X. Rulfs, S.S. Kohles, L.J. Bonassar, Comparison of chondrogenesis in static and perfused bioreactor culture, *Biotechnol. Prog.* 16 (2000) 893–896. doi:10.1021/bp000082v.
- [22] A. Tocchio, M. Tamplenizza, F. Martello, I. Gerges, E. Rossi, S. Argenti, S. Rodighiero, W. Zhao, P. Milani, C. Lenardi, Versatile fabrication of vascularizable scaffolds for large tissue engineering in bioreactor, *Biomaterials.* 45 (2015) 124–131. doi:10.1016/j.biomaterials.2014.12.031.
- [23] S.-M. Lien, L.Y. Ko, T.J. Huang, Effect of pore size on ECM secretion and cell growth in gelatin scaffold for articular cartilage tissue engineering, *Acta Biomater.* 5 (2009) 670–679. doi:10.1016/j.actbio.2008.09.020.
- [24] D.L. Bourell, Perspectives on Additive Manufacturing, *Annu. Rev. Mater. Res.* 46 (2016) 1–18. doi:10.1146/annurev-matsci-070115-031606.
- [25] S.C. Ligon, R. Liska, J. Stampfl, M. Gurr, R. Mühlaupt, Polymers for 3D Printing and Customized Additive Manufacturing, *Chem. Rev.* 117 (2017) 10212–10290. doi:10.1021/acs.chemrev.7b00074.
- [26] J. An, J.E.M. Teoh, R. Sun, C.K. Chua, Design and 3D Printing of Scaffolds and Tissues, *Engineering.* 1 (2015) 261–268. doi:10.15302/J-ENG-2015061.
- [27] N. Taniguchi, S. Fujibayashi, M. Takemoto, K. Sasaki, B. Otsuki, T. Nakamura, T. Matsushita, T. Kokubo, S. Matsuda, Effect of pore size on bone ingrowth into porous titanium implants fabricated by additive manufacturing: An in vivo experiment, *Mater. Sci. Eng. C.* 59 (2016) 690–701. doi:10.1016/j.msec.2015.10.069.
- [28] J.M. Sobral, S.G. Caridade, R.A. Sousa, J.F. Mano, R.L. Reis, Three-dimensional plotted scaffolds with controlled pore size gradients: Effect of scaffold geometry on mechanical performance and cell seeding efficiency, *Acta Biomater.* 7 (2011) 1009–1018. doi:10.1016/j.actbio.2010.11.003.
- [29] S. V. Murphy, A. Atala, 3D bioprinting of tissues and organs, *Nat. Biotechnol.* 32 (2014) 773–785. doi:10.1038/nbt.2958.
- [30] D.B. Kolesky, R.L. Truby, A.S. Gladman, T.A. Busbee, K.A. Homan, J.A. Lewis, 3D bioprinting of vascularized, heterogeneous cell-laden tissue constructs, *Adv. Mater.* 26 (2014) 3124–3130. doi:10.1002/adma.201305506.
- [31] M. Domingos, F. Intranuovo, T. Russo, R. De Santis, A. Gloria, L. Ambrosio, J. Ciurana, P. Bartolo, The first systematic analysis of 3D rapid prototyped poly(ϵ - caprolactone) scaffolds manufactured through BioCell printing: The effect of pore size and geometry on compressive mechanical behaviour and in vitro hMSC viability, *Biofabrication.* 5 (2013) 045004. doi:10.1088/1758-5082/5/4/045004.
- [32] J. Shim, J. Lee, J.Y. Kim, Bioprinting of a mechanically enhanced three-dimensional dual cell-laden construct for osteochondral tissue engineering using a multi-head tissue / organ building system, *J. Micromechanics Microengineering* 2. 085014 (2012). doi:10.1088/0960-1317/22/8/085014.
- [33] K. Nair, M. Gandhi, S. Khalil, K.C. Yan, M. Marcolongo, K. Barbee, W. Sun, Characterization of cell viability during bioprinting processes, *Biotechnol. J.* 4 (2009) 1168–1177. doi:10.1002/biot.200900004.
- [34] I.T. Ozbolat, M. Hospodiuk, Current advances and future perspectives in extrusion-based bioprinting, *Biomaterials.* 76 (2016) 321–343. doi:10.1016/j.biomaterials.2015.10.076.

- [35] J.M. Serrine, A.M. Pekkanen, A.M. Nelson, N.A. Chartrain, C.B. Williams, T.E. Long, 3D-Printable Biodegradable Polyester Tissue Scaffolds for Cell Adhesion, *Aust. J. Chem.* 68 (2015) 1409–1414. doi:10.1071/CH15327.
- [36] X. Zheng, W. Smith, J. Jackson, B. Moran, H. Cui, D. Chen, J. Ye, N. Fang, N. Rodriguez, T. Weisgraber, C.M. Spadaccini, Multiscale metallic metamaterials, *Nat. Mater.* 15 (2016) 1100–1106. doi:10.1038/nmat4694.
- [37] C. Sun, N. Fang, D.M. Wu, X. Zhang, Projection micro-stereolithography using digital micro-mirror dynamic mask, *Sensors Actuators A Phys.* 121 (2005) 113–120. doi:10.1016/j.sna.2004.12.011.
- [38] F.P.W. Melchels, J. Feijen, D.W. Grijpma, A review on stereolithography and its applications in biomedical engineering., *Biomaterials.* 31 (2010) 6121–6130. doi:10.1016/j.biomaterials.2010.04.050.
- [39] Y. Lu, G. Mapili, G. Suhali, S. Chen, K. Roy, A digital micro-mirror device-based system for the microfabrication of complex , spatially patterned tissue, *J. Biomed. Mater. Res. A.* 77 (2006) 396–405. doi:10.1002/jbm.a.30601.
- [40] R. Gauvin, Y.C. Chen, J.W. Lee, P. Soman, P. Zorlutuna, J.W. Nichol, H. Bae, S. Chen, A. Khademhosseini, Microfabrication of complex porous tissue engineering scaffolds using 3D projection stereolithography, *Biomaterials.* 33 (2012) 3824–3834. doi:10.1016/j.biomaterials.2012.01.048.
- [41] J.W. Lee, G. Ahn, J.Y. Kim, D.-W. Cho, Evaluating cell proliferation based on internal pore size and 3D scaffold architecture fabricated using solid freeform fabrication technology., *J. Mater. Sci. Mater. Med.* 21 (2010) 3195–3205. doi:10.1007/s10856-010-4173-7.
- [42] F.P.W. Melchels, B. Tonnarelli, A.L. Olivares, I. Martin, D. Lacroix, J. Feijen, D.J. Wendt, D.W. Grijpma, The influence of the scaffold design on the distribution of adhering cells after perfusion cell seeding., *Biomaterials.* 32 (2011) 2878–84. doi:10.1016/j.biomaterials.2011.01.023.
- [43] A. Atala, J.J. Yoo, eds., *Essentials of 3D Biofabrication and Translation*, Academic Press, London, UK, 2015. doi:10.1016/C2013-0-18665-5.
- [44] H. Lin, D. Zhang, P.G. Alexander, G. Yang, J. Tan, A.W.M. Cheng, R.S. Tuan, Application of visible light-based projection stereolithography for live cell-scaffold fabrication with designed architecture, *Biomaterials.* 34 (2013) 331–339. doi:10.1016/j.biomaterials.2012.09.048.
- [45] A.X. Sun, H. Lin, A.M. Beck, E.J. Kilroy, R.S. Tuan, Projection Stereolithographic Fabrication of Human Adipose Stem Cell-Incorporated Biodegradable Scaffolds for Cartilage Tissue Engineering, *Front. Bioeng. Biotechnol.* 3 (2015) 1–9. doi:10.3389/fbioe.2015.00115.
- [46] B.D. Fairbanks, M.P. Schwartz, C.N. Bowman, K.S. Anseth, Photoinitiated polymerization of PEG-diacrylate with lithium phenyl-2,4,6-trimethylbenzoylphosphinate: polymerization rate and cytocompatibility, *Biomaterials.* 30 (2009) 6702–6707. doi:10.1016/j.biomaterials.2009.08.055.
- [47] J.P. Fisher, D. Dean, A.G. Mikos, Photocrosslinking characteristics and mechanical properties of diethyl fumarate/poly(propylene fumarate) biomaterials, *Biomaterials.* 23 (2002) 4333–4343. doi:10.1016/S0142-9612(02)00178-3.
- [48] F.K. Kasper, K. Tanahashi, J.P. Fisher, A.G. Mikos, Synthesis of poly(propylene fumarate), *Nat. Protoc.* 4 (2009) 518–525. doi:10.1038/nprot.2009.24.
- [49] M. Hegde, V. Meenakshisundaram, N. Chartrain, S. Sekhar, D. Tafti, C.B. Williams, T.E.

- Long, 3D Printing All-Aromatic Polyimides using Mask-Projection Stereolithography: Processing the Nonprocessable, *Adv. Mater.* 29 (2017). doi:10.1002/adma.201701240.
- [50] M. Doube, M.M. Klosowski, I. Arganda-Carreras, F.P. Cordelières, R.P. Dougherty, J.S. Jackson, B. Schmid, J.R. Hutchinson, S.J. Shefelbine, BoneJ: Free and extensible bone image analysis in ImageJ, *Bone*. 47 (2010) 1076–1079. doi:10.1016/j.bone.2010.08.023.
- [51] V. Karageorgiou, D. Kaplan, Porosity of 3D biomaterial scaffolds and osteogenesis., *Biomaterials*. 26 (2005) 5474–91. doi:10.1016/j.biomaterials.2005.02.002.
- [52] M.E. Gomes, H.L. Holtorf, R.L. Reis, A.G. Mikos, Influence of the Porosity of Starch-Based Fiber Mesh Scaffolds on the Proliferation and Osteogenic Differentiation of Bone Marrow Stromal Cells Cultured in a Flow Perfusion Bioreactor, *Tissue Eng.* 12 (2006) 801–809. doi:10.1089/ten.2006.12.801.
- [53] Q.L. Loh, C. Choong, Three-Dimensional Scaffolds for Tissue Engineering Applications: Role of Porosity and Pore Size, *Tissue Eng. Part B Rev.* 19 (2013) 485–502. doi:10.1089/ten.teb.2012.0437.
- [54] R.A. Perez, G. Mestres, Role of pore size and morphology in musculo-skeletal tissue regeneration, *Mater. Sci. Eng. C*. 61 (2016) 922–939. doi:10.1016/j.msec.2015.12.087.
- [55] D.J. Griffon, M.R. Sedighi, D. V. Schaeffer, J.A. Eurell, A.L. Johnson, Chitosan scaffolds: Interconnective pore size and cartilage engineering, *Acta Biomater.* 2 (2006) 313–320. doi:10.1016/j.actbio.2005.12.007.
- [56] S. Yamane, N. Iwasaki, Y. Kasahara, K. Harada, T. Majima, K. Monde, S.I. Nishimura, A. Minami, Effect of pore size on in vitro cartilage formation using chitosan-based hyaluronic acid hybrid polymer fibers, *J. Biomed. Mater. Res. - Part A*. 81 (2007) 586–593. doi:10.1002/jbm.a.31095.
- [57] M.L. Alves da Silva, A. Crawford, J.M. Mundy, V.M. Correlo, P. Sol, M. Bhattacharya, P. V Hatton, R.L. Reis, N.M. Neves, Chitosan/polyester-based scaffolds for cartilage tissue engineering: Assessment of extracellular matrix formation, *Acta Biomater.* 6 (2010) 1149–1157. doi:10.1016/j.actbio.2009.09.006.

4.7 Supporting Information

4.7.1 Image Processing

Image stacks were processed and analyzed in a consistent fashion to count cells and determine their distribution in scaffolds using Zen 2.3 and ImageJ (1.52e with Fiji plugin package). The Zen 2.3 software used during acquisition was used to subtract background fluorescence (radius = 15) and export images as TIFF files. The stack of images was then loaded in ImageJ and the blue channel isolated for counting of cell nuclei stained with DAPI. Contrast was enhanced (0.1% saturated pixels, normalized) and background fluorescence from the uptake of DAPI by scaffolds further reduced using the Background Subtraction function (radius = 15). An intensity threshold was then applied which varied between samples. The threshold was chosen to eliminate as much remaining background as possible while preserving the cells. In some samples, it was necessary to manually remove background fluorescence (Fig. 4.S1c). Next, the Remove Outliers function (radius = 7) was used to eliminate noise. Cell nuclei that appeared contiguous in the images were split using Watershed Split 3D (BoneJ 1.4.3 plugin, radius = 3). Each nucleus was then counted and its coordinates tabulated using BoneJ. Three-dimensional reconstructions of the nuclei were also created. Each 3D reconstruction was visually compared to its original image stack in Zen 2.3 to ensure that neither overcounting nor undercounting occurred.

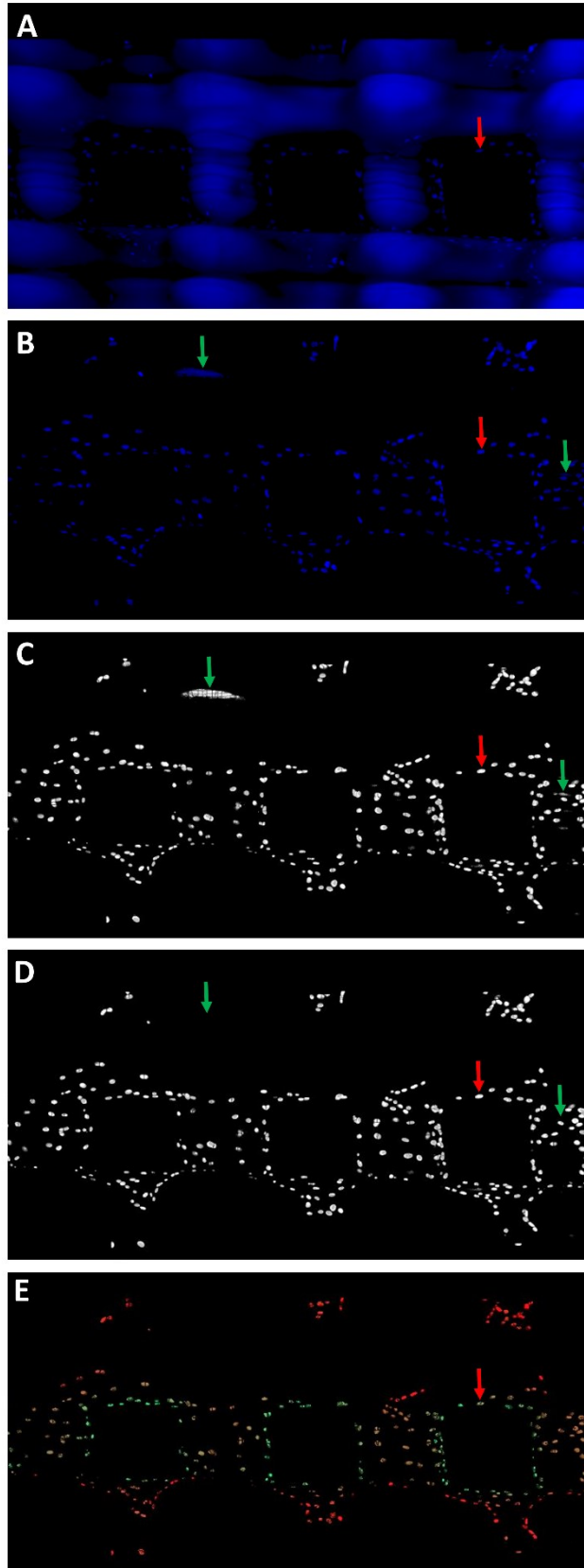


Fig. 4.S1. The processing of fluorescence images and the identification and of nuclei using Zen and ImageJ software packages. A) A stack of fluorescence images of scaffold and cells is shown before any processing. The scaffold is readily apparent and prevents the automated counting of cells. The red arrow points to a cell nucleus that can be seen in each image throughout the processing steps. B) After background subtraction in Zen, nearly all background fluorescence has been removed. The green arrows show background fluorescence that required manual removal. C) Many individual cells can be seen in the 3D reconstruction from the stack of images processed in ImageJ, but green arrows show some areas where background fluorescence from the scaffold persist. D) The same 3D reconstruction after manual removal of background fluorescence. E) The final 3D reconstruction where each nucleus has been identified. Red nuclei are closer to the viewer while green nuclei are further away.

Chapter 5: 3D Printing of Multi-Material Tissue Scaffolds with Vat Photopolymerization for Directed Cell Response

Nicholas A. Chartrain^{1,2,3}, Andrew Cohen³, Abby R. Whittington^{2,4}, Christopher B. Williams^{1,2,3}

¹Macromolecules Innovation Institute, Virginia Tech, Blacksburg, VA 24061

²Department of Materials Science & Engineering, Virginia Tech, Blacksburg, VA 24061

³Department of Mechanical Engineering, Virginia Tech, Blacksburg, VA 24061

⁴Department of Chemical Engineering, Virginia Tech, Blacksburg, VA 24061

5.1 **Abstract**

The fabrication of tissue engineering constructs that will mimic the structure and function of tissue found in nature requires the development of manufacturing techniques with precise control over the placement of multiple cell types and materials. Techniques traditionally used for scaffold fabrication, such as particulate leaching and freeze drying, can support cell growth, but the homogeneity of the engineered constructs preclude the development of more complex functional structures (e.g., vasculature, nephrons). Vat photopolymerization (VP), an additive manufacturing (3D printing) technology, can fabricate tissue scaffolds with complex geometries and precise material placement, but generally, parts are printed from a single material. In this work, we demonstrate the fabrication of multi-material tissue scaffolds using a commercially available low-cost VP system without any mechanical modifications or custom code. Four resins were formulated, two of which encouraged NIH 3T3 murine fibroblast adhesion, and two that permitted only small quantities of fibroblasts to adhere and grow. Fibroblast adhesion to scaffolds fabricated from a single material was evaluated with a viability assay and fluorescence imaging. Simple multi-material scaffolds were fabricated by partially fabricating a scaffold, pausing the build, cleaning the part and exchanging the material before allowing the build to finish. Fibroblasts seeded on multi-material scaffolds fabricated from materials with dissimilar adhesion properties

showed a strong preference for regions fabricated from adhesion-encouraging material after 4 and 7 days. Finally, more complex multi-material scaffolds with an embedded perfusable network of tubes were fabricated through multiple material exchanges. The tubes were fabricated from a material that discouraged fibroblast adhesion. After 7 days in static culture, the tubes remained clear of cells and matrix while cells were observed to be proliferating in the scaffold's other regions. These results indicate that multi-material tissue scaffolds fabricated with VP could contain tubular networks that remain patent and perfusable at extended time points to provide structure and function similar to that of vasculature.

5.2 Introduction

Tissue engineering aims to use scaffolds, in conjunction with cells and various stimuli, to fabricate engineered constructs that mimic the complex structure and functions of biological tissues [1]. Traditional techniques used for scaffold fabrication such as particulate leaching, gas foaming, and electrospinning are unable to produce hierarchical structures akin to those found in nature [2]. This limitation has hindered the engineering of vasculature, which is necessary to support long term viability of most cell types in thick tissue constructs [3]. Bulk constructs without perfusable vasculature develop hypoxic conditions and necrotic cores due to insufficient access to nutrients, oxygen, and waste removal [4]. Precise patterning or placement of materials, cells, and vasculature would enable the fabrication of engineered constructs that overcome the current size constraints imposed by diffusion limits [4].

Recent efforts have employed additive manufacturing (AM, or “3D printing”) techniques, such as extrusion bioprinting, inkjet bioprinting, and vat photopolymerization (VP, stereolithography) to

engineer tissue constructs with complex architectures that more closely resemble the tissues they are intended to replace [5–7]. VP is an AM technique that uses ultraviolet (UV) light to selectively polymerize a liquid photopolymer. Two primary embodiments of VP exist: a ‘top-down’ method where light is projected from above the resin vat and polymerization occurs at the surface of the vat and a ‘bottom-up’ method where light is projected from below through a transparent window in the vat and polymerization occurs at the window-resin interface. (Two photon polymerization is another VP process which builds microscale parts within the photopolymer resin and requires no recoating process [2]). VP bioprinting systems can fabricate scaffolds measuring several millimeters to more than a centimeter in length while also containing features as small as 5-100 μm [2,8]. Recent work has greatly expanded the number of cytocompatible materials that can be used with VP [9–12]. Many instances of complex geometries fabricated from VP that support cell growth have been reported in the literature [4,13]. However, most traditional VP systems reported do not precisely place more than one material or cell type within a single scaffold.

Several researchers have successfully fabricated multi-material parts with VP using custom-built systems or by modifying existing ones. Nearly all of this work has been quite recent, which reflects growing interest in 3D printing of multi-functional parts. Early work by Wicker *et al.* in 2009 utilized a modified commercial VP system that employed several vats containing different materials which were rotated into the build area depending on the material needed for the fabrication of a given layer [14,15]. The top-down approach they used requires precise control over the resin level to ensure accurate fabrication results, but the scaffolds successfully demonstrated spatial control over cell adhesion [16]. Some more recent custom-built VP systems (2011-2018) using both top-down and bottom-up systems have been used to fabricate more

complex multi-material geometries, but have either not been used with materials suitable for tissue engineering scaffolds or have only been used to fabricate 2D multi-material structures [17–21]. Most recently, at least three groups have developed systems that have spatial control over the placement of multiple materials and/or cell types in complex 3D tissue engineering constructs fabricated using VP [22–24]. However, poly(ethylene glycol) diacrylate (PEGDA), a material which is not conducive to cell adhesion, is used in most of this work. In addition, these groups focus on encapsulating cells into the hydrogel scaffold matrix during printing, which can impede the cell's migration and proliferation within the scaffold.

The accelerating pace of developments in VP systems to enable the fabrication of multi-material constructs, particularly for tissue engineering applications, underscores the anticipated benefits of these advanced capabilities. With the exception of the system used by Wicker *et al.*, which is a highly modified commercial system, the other VP systems capable of multi-material fabrication are custom-built. The development of these custom machines entails substantial costs and requires expertise in machine design, optics, material science, microfluidics. In the work presented here, the authors used an unmodified low-cost commercial VP system to fabricate multi-material tissue scaffolds using materials with dissimilar cell adhesion properties. In addition, the use of dissimilar materials within a single scaffold granted insight into the material considerations that must be considered for successful multi-material scaffold fabrication.

In contrast with previous studies, the work demonstrated here aimed to build multi-material tissue scaffolds that would grant spatial control over cell adhesion and proliferation post printing, rather than encapsulating cells during scaffold fabrication. The authors' previous work has shown NIH

3T3 fibroblasts adhere and proliferate on 3D printed scaffolds fabricated from a resin based on 2-acrylamido-2-methyl-1-propanesulfonic acid sodium salt (NaAMPS) with a VP system (see Chapter 3). Further, that work demonstrated that cells are able to proliferate homogeneously throughout the entirety of a scaffold with the geometry used in this work (600 μm pores, 4 mm scaffold dimensions). In contrast, substrates fabricated using PEGDA are known to have poor cell adhesion properties, permitting their use in applications requiring bioinert materials [25]. Here, we aimed to spatially modulate fibroblast adhesion in scaffolds by printing different regions of a single scaffold from either NaAMPS or a poly(ethylene glycol) diacrylate based resin (PEGDA). In doing so, we hypothesized that cell adhesion and proliferation in multi-material scaffolds would occur only in areas fabricated from NaAMPS, while areas fabricated from PEGDA would be devoid of cells. We aimed to demonstrate the potential of multi-material tissue scaffolds fabricated with VP by printing structures with perfusable channels that would remain cell-free during culture. Thick tissues require vascularization to deliver oxygen and nutrients to every cell within them. The lack of vascularization in tissue scaffolds, which endures as the most significant challenge in the field of tissue engineering, limits the size of scaffolds on which cells can be kept viable [2,3,26]. Incorporating a network of perfusable channels within a scaffold that mimics a tissue's vascular network may help overcome the current size limits of scaffolds [4]. However, the network must remain patent to allow for fluid to pass through. Studies have shown that cells grown on scaffolds can proliferate to such an extent that pores become completely blocked by cells and their extracellular matrix [27,28]. We aimed to keep the perfusable network of channels clear by fabricating it with a material that discourages cellular adhesion (see Fig. 5.1c,d).

5.3 Experimental

5.3.1 Resins

Two separate multi-material systems were formulated for the fabrication of multi-material tissue scaffolds. Each multi-material system was composed of one photocurable resin intended to promote fibroblast adhesion and proliferation and one designed to prevent cell adhesion. Selective placement of the dissimilar materials in a single tissue scaffold was hypothesized to permit spatial control over cell adhesion and proliferation. The resin compositions are shown in Table 5.1.

The first multi-material system used in this work included a resin ('NaAMPS') based on 2-acrylamido-2-methyl-1-propanesulfonic acid sodium salt (NaAMPS). Our previous work has demonstrated excellent adhesion and proliferation of NIH 3T3 fibroblasts on scaffolds 3D printed with a NaAMPS-based resin (see Chapter 3). NaAMPS is available as a 50 wt% solution in water (Sigma Aldrich). As in our previous work, the prepolymer solution was formulated with 75 wt% NaAMPS solution and 25 wt% PEGDA. A photocurable resin was created from the prepolymer by adding 1 wt% photoinitiator (TPO, diphenyl(2,4,6-trimethylbenzoyl)phosphine oxide, Sigma Aldrich). A UV absorber, Sudan Black B (TCI Chemicals), which aids in curing thin layers and preventing print-through was added to the mixture at 0.20 wt%, producing a black resin. Sudan Black B has previously been shown to have negligible cytotoxicity at concentrations similar to those used in this study [29].

The first multi-material system also included a resin, 'PEGDA-C' (C designates a clear resin), based on poly(ethylene glycol) diacrylate (PEGDA, $M_w = 575$ g/mol, Sigma Aldrich) that was designed to prevent cellular adhesion. PEGDA has been shown in the literature to have low

cytotoxicity but very low cellular adhesion [2]. In addition, previous studies have shown that PEGDA can be fabricated into high resolution structures using VP [2]. The prepolymer mixture designed to prevent fibroblast adhesion contained 90 wt% PEGDA ($M_w = 575$ g/mol, Sigma Aldrich) and 10 wt% 2-Hydroxyethyl methacrylate (HEMA). HEMA, which also helps prevent cell adhesion, was incorporated to increase the swelling in water of the PEGDA-based resin [30,31].

Like the NaAMPS resin, it also included 1 wt% TPO. However, an alternative UV absorber was used so as to create a clear resin, which allowed the regions of multi-material scaffolds fabricated from either NaAMPS or PEGDA-C to be differentiated from one another. The UV absorber, BBOT (2,5-bis(5-tert-butyl-benzoxazol-2-yl)thiophene, TCI Chemicals), was incorporated at 0.20 wt%.

Table 5.1. Compositions of the prepolymer solutions used for multi-material tissue scaffold fabrication. Photoinitiators and UV absorbers were subsequently added to these formulations. All quantities are in wt %.

	Resin name	NaAMPS (50 wt% solution in H ₂ O)	Epoxidized soybean oil acrylate (ESOA)	PEGDA	HEMA
Multi-material system #1	NaAMPS	75		25	
	PEGDA-C			90	10
Multi-material system #2	Soy		50	50	
	PEGDA-B			100	

A second multi-material system, consisting of two additional resin formulations, was designed to overcome the limitation posed by a swelling mismatch between NaAMPS and PEGDA-C that prevented the fabrication of some multi-material geometries. The first resin, ‘Soy’, was designed to promote fibroblast adhesion and proliferation *in vitro*. Work by Miao *et al.* showed that epoxidized soybean oil acrylate (ESOA) can be selectively photopolymerized with UV light [11]. The parts were shown to support human mesenchymal stem cell (hMSC) adhesion and growth for periods up to five days. However, ESOA’s relatively high viscosity makes it difficult to print, which may have contributed to the lack of tall or geometrically complex structures in Miao *et al.*’s work [11,32].

The viscosity was reduced by creating a mixture of 50 wt% ESOA and 50 wt% PEGDA, which permitted rapid recoating of thin layers and lower peel forces [33]. PEGDA contributes to very low cellular adhesion, but we hypothesized that a sufficient quantity of Soy in the resin would still serve to encourage cellular adhesion, as was found to be true with the NaAMPS resin (see Chapter 3). Solvent (e.g., acetone) could have been used to reduce the resins viscosity, but removal of solvent after printing was likely to lead to severe distortions of the 3D printed scaffold’s shape and size and would have affected the swelling ratio of the resin [34]. Heating the resin is another approach that could have been used to recoat thin layers of pure ESOA, as the material demonstrates a substantial drop in viscosity at elevated temperatures [35]. However, this would have required hardware modifications to the Ember VP system. The resin was prepared by adding 1 wt% TPO and 0.20 wt% BBOT to the mixture of ESOA and PEGDA. The Soy resin was transparent with a slightly yellow color.

The final resin, 'PEGDA-B' (B designates a black colored resin) contained PEGDA as its only photopolymerizable component and was designed to prevent cellular adhesion. The PEGDA-B resin was formulated by adding 0.20 wt% Sudan Black B and 1 wt% TPO.

5.3.2 Scaffold Fabrication

An Autodesk Ember VP 3D printer was used to fabricate tissue scaffold structures. The printer has a build area of approximately 40 x 64 mm with a maximum part height of 134 mm and a projected pixel size of 50 μm . The resin vat's PDMS window was coated with an adhesive-backed fluorinated ethylene propylene (FEP) film to reduce adhesion of the polymerized resin to the window and reduce the peel forces required for recoating. This was done to help enable the printing of small features and softer resins which would otherwise be damaged by the large peel forces. Scaffolds fabricated entirely from a single resin had 600 μm square pores, 200 μm wide pillars, and 84% porosity (Fig. 5.1a). The model was sliced into 100 μm layers. In the first multi-material system, NaAMPS layers were exposed for 8 s per layer and PEGDA-C layers for 3.6 s each. In the second system, Soy layers were exposed for 1.5 s and PEGDA-B layers for 8 s. The Autodesk Ember VP system has a nominal intensity of 20 mW/cm^2 at 405 nm.

Block multi-material scaffolds (Fig. 5.1b) containing two materials and a single material change were fabricated using the same design. After printing the first half of the scaffold, the print was paused to allow for material exchange. The build platform was removed and the partially printed scaffold cleaned using compressed air and Kimwipes. Any resin that remained on the build platform after the use of compressed air was carefully wiped away. Attempts to use solvent for part cleaning were thwarted by slight swelling of the scaffold, which caused it to delaminate from

the build platform. The first resin was removed from the resin vat and the window cleaned with ethanol. The second resin was added and the print resumed to allow for completion of the multi-material print. Printed scaffolds were cleaned in ethanol, post-cured in a UV chamber for 10 min, and then stored in deionized (DI) water. The fabrication process is shown schematically in Fig. 5.2.

More complex multi-material scaffolds (Fig. 5.1c,d) with vascular-like structures were fabricated with multiple material exchanges. The scaffold design measures 8 mm wide, 12 mm long, and 7 mm tall. The perfusion network forms a double cross (when viewed from above) with the single channel extending the length of the scaffold. The inside of the channels measure 600 μm in height and 1 mm in width. Their wall thickness is 100 μm . The design was intended as a proof-of-concept to demonstrate the ability to fabricate multi-material scaffolds that provide additional function and utility compared to single material scaffolds. In this case, the network of tubes that extends through the scaffold could be used as a means of perfusing the scaffold with a growth medium to mimic the function of a vascular network in a living tissue. We envision that this sort of design could help overcome the size limitations of tissue scaffolds on which cells can be kept viable for an extended period of time. In contrast with scaffolds fabricated from a single adhesion-promoting material, this design would prevent growth in certain areas (the channels) to maintain a path for fluid flow and delivery of nutrients to all areas of the scaffold, especially to the center. This is analogous to the vascular network in a tissue which must remain patent to allow blood to flow. Scaffold layers containing both materials were fabricated by exposing and curing certain areas of the slice with a first material (e.g., with the material promoting cell adhesion), exchanging for a second material, and subsequently exposing other areas of the slice (e.g., the areas of the tubular network with the

material preventing cell adhesion). Partially printed scaffolds and the resin vat were cleaned in the same manner as the block multi-material scaffolds that had a single interface. While the cleaning and material exchange processes were not automated like in some previously reported systems (e.g., [19,23]), it was not necessary to build any custom hardware or write control software.

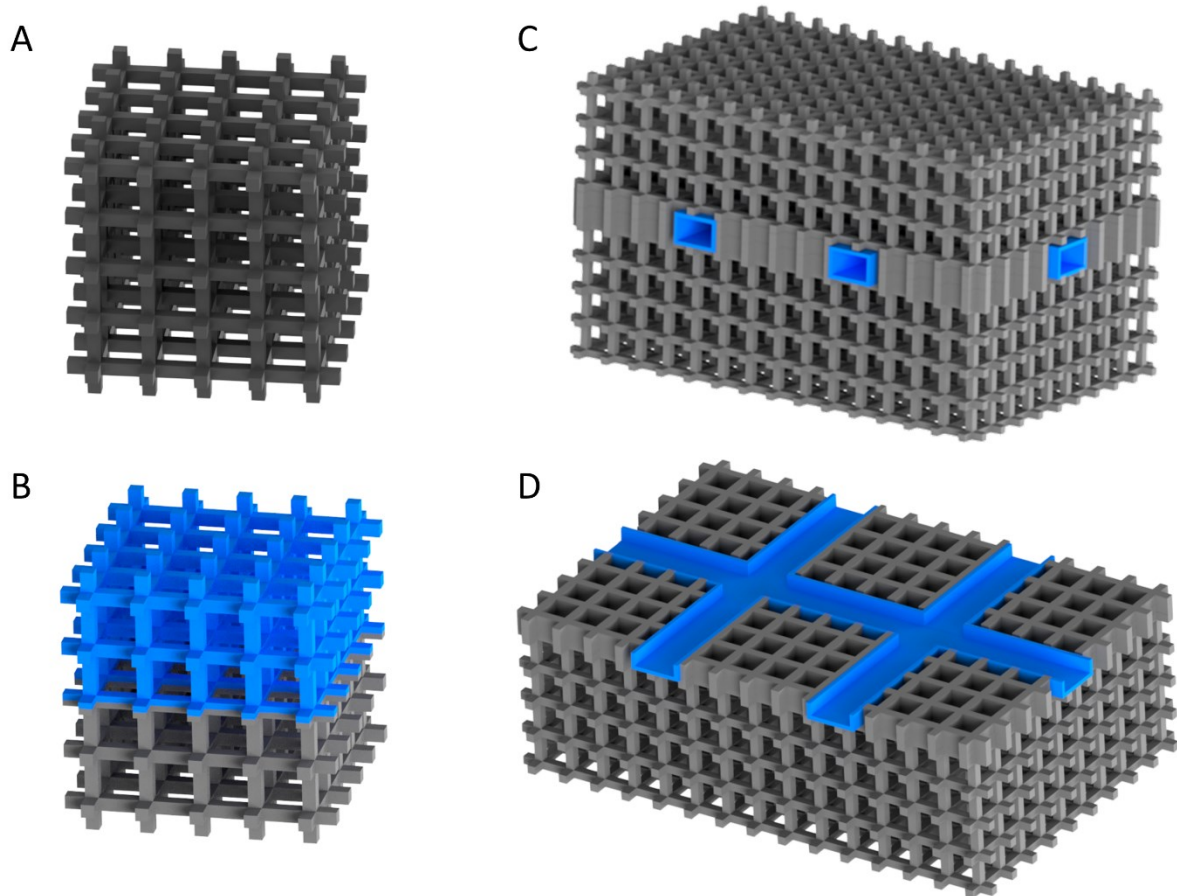


Fig. 5.1. Digital models of the tissue scaffolds fabricated using VP. A) Model used to fabricate ‘single material’ tissue scaffolds. The scaffold, with side lengths of 4 mm, contains square pores measuring 600 μm and 200 μm wide pillars. B) The model for ‘block’ multi-material tissue scaffolds is identical to that used for single material scaffolds except for a single material change that occurs half way through the print. The grey and blue areas of the scaffold represent areas

fabricated from dissimilar materials. C) The ‘complex’ multi-material scaffold model is much larger (8 mm wide, 12 mm long, and 7 mm tall) and contains several material exchanges during the print. The areas intended for cell adhesion (dark grey) also have 600 μm pores and 200 μm pillar widths. D) A sectioned view of the complex multi-material model shows the tubular network designed to prevent cell adhesion (blue) running horizontally through the part. In this area, the cell adherent material is patterned into only horizontal pillars rather than both horizontal and vertical pillars to improve the part’s strength.

The printed scaffolds were evaluated and imaged using an optical microscope equipped with an 18-megapixel complementary metal–oxide–semiconductor (CMOS) camera (AmScope). Measurements of the printed scaffolds were compared against the as-designed dimensions. In addition, the interfaces between different materials in the multi-material scaffolds were imaged to identify potential cross-contamination. The complex multi-material scaffold was imaged to determine whether the channels in the part remained patent.

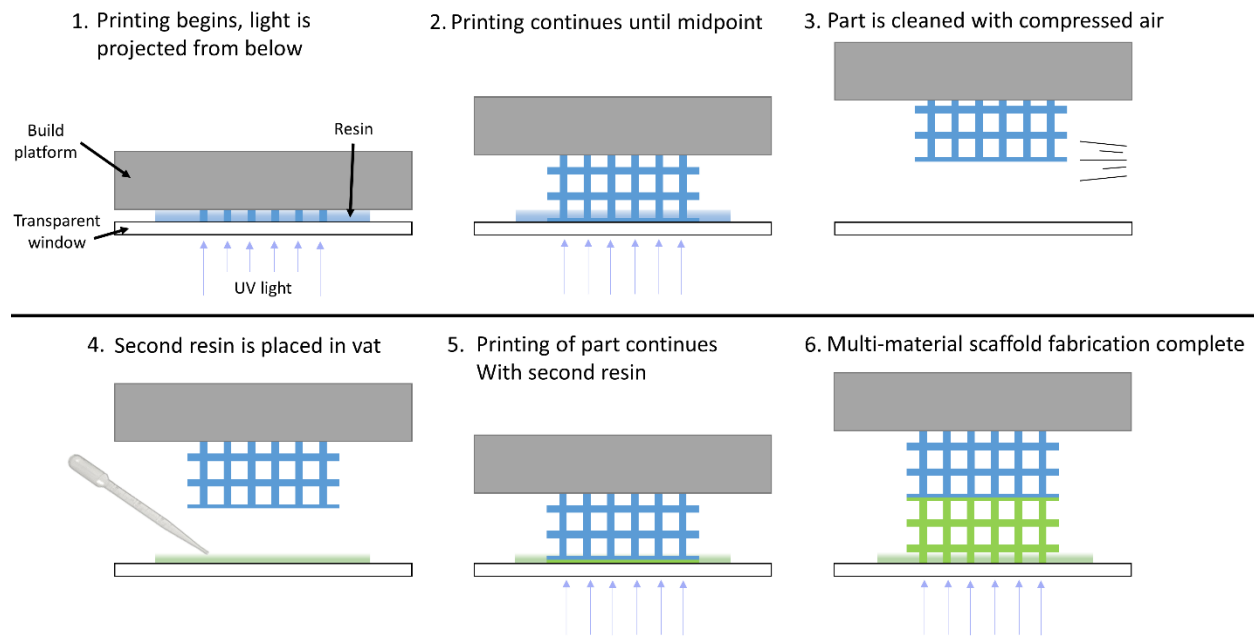


Fig. 5.2. The printing process of a ‘block’ multi-material tissue scaffold with a single material exchange is shown. The digital model of the scaffold is shown in Fig. 5.1b. The printing begins with a first resin (1) and proceeds as it would for a single material scaffold until the print is half completed (2). The fabrication process is paused, the resin is removed from the vat, and the part cleaned with compressed air (3). The second resin is added to the vat (4) and printing continues with the new material (5) until the entire part has been fabricated (6). Iteration of steps 3-5 occurs for the fabrication of parts with additional material exchanges.

5.3.3 Cell Culture

NIH 3T3 murine fibroblasts were grown in tissue cultured treated polystyrene flasks in alpha minimum essential media (MEM- α 1X, ThermoFisher Scientific) supplemented with 10% fetal bovine serum (ThermoFisher Scientific) and 1% penicillin-streptomycin-amphotericin B (MediaTech CellGro). The NIH 3T3 were grown under standard culture conditions (37 °C and 5% CO₂) and subcultured when 70 - 80% confluent [36].

5.3.4 Cell Seeding and Evaluation of NaAMPS and PEGDA-C Scaffolds

Prior to seeding cells on the 3D printed scaffolds, it was necessary to remove any cytotoxic unreacted monomer from the gels. This was done by washing the scaffolds in 70 wt% ethanol three times for 1 h per wash. This also served to sterilize the scaffolds. The ethanol was removed from the scaffolds with two washes in sterile phosphate buffered saline (PBS, ThermoFisher Scientific), also for 1 h per wash. Finally, scaffolds were placed in complete media to allow the adsorption of proteins to the scaffolds to aid cell adhesion.

In preparation for seeding, the NIH 3T3 were lifted from flasks using 0.50% trypsin, centrifuged, resuspended, and counted using a hemocytometer. Scaffolds were placed in 24-well Corning Costar ultra-low attachment well plates and the cell suspension pipetted on top of the scaffold. NaAMPS, PEGDA-C, and multi-material scaffolds fabricated from these two resins were seeded with 1.75×10^5 cells and cultured for 4 or 7 d ($n = 3-6$ per treatment group). The cell suspension volume pipetted onto each scaffold was approximately 30 μL . This volume was sufficiently small to ensure that the entirety of the suspension was absorbed into the scaffold via capillary forces rather than spreading across the ultra-low attachment well plate. After 4 h, sufficient time for the NIH 3T3 to adhere to the scaffolds, additional media was added to each well (1 mL total volume). Media was exchanged every 2-3 d.

In preparation for fluorescence staining, the cells were fixed using 10% neutral buffered formalin (ThermoFisher Scientific). After washing with PBS, cells were stained in the dark for 1 h with 5.7 μM DAPI (4',6-diamidino-2-phenylindole dihydrochloride, Invitrogen) and 100 nM Texas Red-X (Invitrogen). This allowed for visualization of cellular nuclei and actin respectively. The scaffolds

were then stored in PBS at 4 °C in the dark prior to imaging. A laser scanning confocal fluorescence microscope (Zeiss Axio Observer.Z1) was used to image cells on the scaffolds and qualitatively evaluate cell proliferation by region in the multi-material scaffolds.

5.3.5 Cell Seeding and Evaluation of Soy and PEGDA-B Scaffolds

Scaffold preparation to remove unreacted monomer was performed in the same way as those made from the first multi-material system. Single material Soy and PEGDA-B, as well as multi-material scaffolds made from these two materials were seeded with 5×10^4 cells suspended in a volume of 30 μ L and cultured for either 1 or 4 d. Previous work has shown cells can be cultured on structures made from epoxidized soybean oil acrylate, but this had not been demonstrated on a resin containing half ESOA and half PEGDA [11]. A quantitative MTS assay was used to verify that fibroblasts would adhere to and grow on single material scaffolds made from the Soy resin and compared to cell culture on PEGDA-B scaffolds. Fibroblast proliferation was determined after 1 and 4 d of culture using a colorimetric MTS assay (3-(4,5-dimethylthiazol-2-yl)-5-(3-carboxymethoxyphenyl)-2-(4-sulfophenyl)-2H-tetrazolium, Celltiter 96, Promega) as previously described (see Chapter 3). The scaffolds (n = 3-6) were moved to new well plates and immersed in 500 μ L media and 100 μ L MTS reagent. The plates were incubated for two hours in the dark, solution (100 μ L) pipetted from each well into a separate 96 well plate, and the absorption of the solution at 490 nm measured immediately using a plate reader (BioTek Synergy Mx). Cell quantity was calculated by comparing absorption values to a standard curve.

In addition, single interface multi-material Soy/PEGDA-B scaffolds (n = 3) were cultured for 4 d and stained in the manner described in the previous section. This allowed the evaluation into

whether scaffolds made from the second multi-material system would enable spatial control over cell adhesion and proliferation.

Larger ‘complex’ multi-material scaffolds fabricated from Soy/PEGDA-B with perfusion channels ($n = 2$), which had a much larger volume than the single interface multi-material scaffolds, were seeded with 2×10^5 fibroblasts. Cells on these scaffolds were cultured for 7 d and then stained and imaged using the same protocols.

5.3.6 Statistics

Statistical significance between samples was determined using ANOVA followed by Tukey’s HSD post-hoc test using Origin 2019. Values are reported as averages \pm standard deviation.

5.4 Results & Discussion

5.4.1 Fabrication of NaAMPS and PEGDA-C Scaffolds

Single material tissue scaffolds were printed to assess the VP system’s ability to fabricate porous structures with the formulated resins and to evaluate the propensity for NIH 3T3 to adhere and proliferate on the individual materials. Optical images of printed scaffolds (Fig. 5.3a-d) revealed accurate fabrication results, although NaAMPS scaffolds experienced a relatively large uptake of water. Swelling caused the pillars of the NaAMPS scaffolds to enlarge to approximately 350-400 μm in width, which was much larger than the PEGDA-C pillars, which were only 200 μm wide.

Following fabrication of single material scaffolds, multi-material scaffolds were fabricated to investigate whether cell response could be spatially modulated in a tissue scaffold made from

dissimilar materials. Multi-material scaffolds were fabricated using the same geometry with a material exchange and part cleaning at the mid-point of the print (Fig. 5.1b). A sharp interface between the two materials was observed between the two layers that make up the horizontal beams in Fig. 5.3a. Despite the transparency of the PEGDA-C, a clear layer can be distinguished from the underlying black layer in the isometric view. These images suggest that contamination between the two resins had not occurred during fabrication.

The isometric view of the multi-material scaffold in Fig. 5.3f reveals the differences between the two resin's water uptake. The swelling of NaAMPS regions was particularly large. In fact, initial formulations of PEGDA-C did not contain HEMA; however, the swelling disparities between the two materials caused the parts to fracture when immersed in water. HEMA was incorporated into the PEGDA-C resin in an attempt to more closely match the swelling ratio of NaAMPS.

Unfortunately, the more complex scaffold design (Fig. 5.1c) with multiple material exchanges could not be successfully printed on the Autodesk Ember when using the NaAMPS and PEGDA-C resin combination due to their swelling mismatch. The mismatch caused stress to accumulate at the material interface, ultimately leading to part failure. Delamination between NaAMPS and PEGDA-C regions of the scaffolds occurred during the recoating step of printing due to the peel forces experienced by the part during recoating. Reduced peel forces could be obtained with a VP system that uses an oxygen-permeable window [8,37]. These systems create a thin oxygen-rich layer of photopolymer directly above the UV transparent window, inhibiting photopolymerization in this 'dead zone'. Use of a VP system with an oxygen inhibition zone might sufficiently reduce peel forces during printing to allow the fabrication of more complex multi-material geometries

with NaAMPS and PEGDA-C. However, doing so would not prevent the additional accumulation of stresses at the material interfaces induced during storage of parts in water from potentially causing part failure.

These results demonstrate the importance of accounting for swelling ratios when choosing resins for 3D printing multi-material tissue scaffolds. Past work in printing multi-material scaffolds with VP has generally either avoided the use of hydrogels (which span a large range of swelling ratios) or used a single bulk hydrogel material [17,19]. The single hydrogel material chosen (e.g., GelMA, PEGDA) was modified in various ways by incorporating different cell types, colored particles, or bioactive molecules to create multiple dissimilar resins [24]. These additives affect certain properties of the resin, but were present in quantities too small to cause a substantial change in swelling ratio. When fabricating multi-material scaffolds with VP, it is clearly important to consider the swelling of each resin to ensure their compatibility. To overcome the challenge posed by the swelling mismatch between the NaAMPS and PEGDA-C resins, a new set of resins with more compatible swelling ratios was formulated (Soy and PEGDA-B).

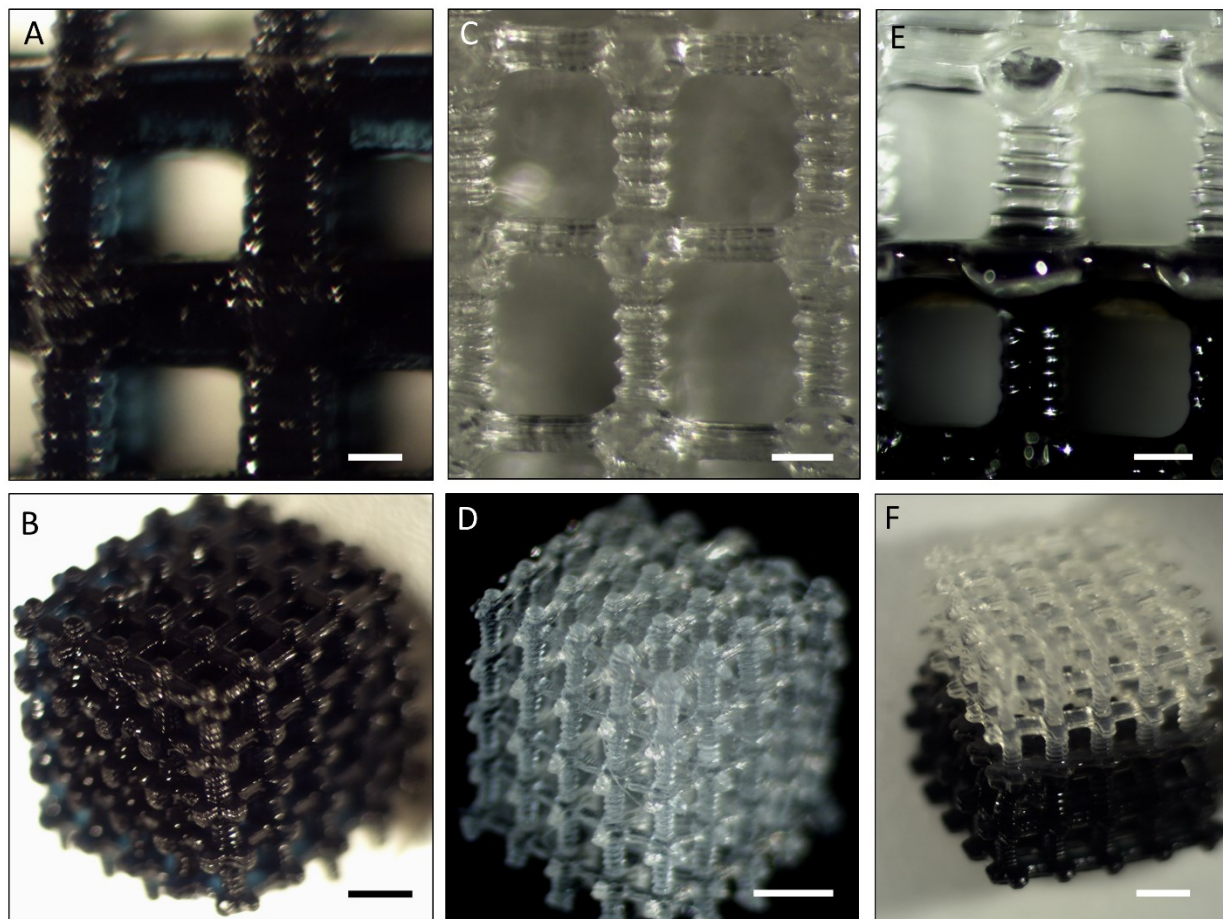


Fig. 5.3. Representative optical images of single material 3D printed scaffolds fabricated using NaAMPS (a,b) or PEGDA-C (c,d) and multi-material scaffolds fabricated using both materials (e, f). In the isometric view of the NaAMPS/PEGDA-C multi-material scaffold (f), the lower half of the scaffold made from NaAMPS has swollen more than the PEGDA-C upper half due to water uptake. Scale bars represent 250 μm in the side view images of the scaffolds (a,c,e) and 1 mm in the isometric views (b,d,f).

5.4.2 Cell Adhesion and Proliferation on NaAMPS and PEGDA-C

Fibroblasts covered much of the 3D printed NaAMPS scaffolds after 4 days of culture (Fig. 5.4a), confirming that photocured parts fabricated from this resin provide a suitable substrate for NIH 3T3 adhesion and proliferation. Conversely, while cells were present on the PEGDA-C scaffolds at this time point, the fibroblasts were clumped together rather than spread across the scaffold surfaces (Fig. 5.4b). There appeared to be only a small number of adhesion sites between cells and scaffold, with many cells adhered only to other cells. This result suggests that parts fabricated from PEGDA-C are poor substrates for NIH 3T3 fibroblast adhesion.

After 7 days, additional proliferation of NIH 3T3 and coverage of the NaAMPS scaffolds was observed (Fig. 5.4c), indicating that NaAMPS scaffolds continued to provide a favorable substrate with minimal cytotoxicity. Surprisingly, cell number on PEGDA-C scaffolds also increased (Fig. 5.4d). Past literature suggests that without surface coating, functionalization of PEGDA with RGD moieties, or other modifications, the material is bioinert and does not favor cell adhesion [2,25]. We hypothesize that the incorporation of 10 wt% HEMA in the resin, which does not encourage cellular adhesion but can permit protein adsorption, could have facilitated cell adhesion to the scaffolds. Despite this, the fibroblasts were clumped together and did not form a monolayer of cells on the scaffold's surfaces, as would be expected for a favorable substrate (e.g., tissue culture treated polystyrene).

Cell culture on multi-material tissue scaffolds fabricated using NaAMPS and PEGDA-C provided strong evidence for the use of such scaffolds to engineer a spatially modulated cell response. After 4 days, nearly all cells were observed to be on the NaAMPS section of the scaffold (Fig. 5.4e). The PEGDA-C section contained small regions with cells, but like the PEGDA-C single material

scaffolds, the fibroblasts appeared clumped together. These results were even more exaggerated after 7 days (Fig. 5.4f). A confluent layer of fibroblasts covered the NaAMPS section of the scaffold while almost no cells were identified on the PEGDA-C areas. Proliferation of cells even resulted in a slight reduction in pore size due to cells beginning to fill them in. In addition, cell number was markedly lower on the PEGDA-C regions of the multi-material scaffolds than on the single material PEGDA-C scaffolds. We attribute the lower quantity of cells on the PEGDA-C regions to the migration of cells from an unfavorable substrate to a more favorable one. This suggests the fibroblast's strong preference for NaAMPS over PEGDA-C.

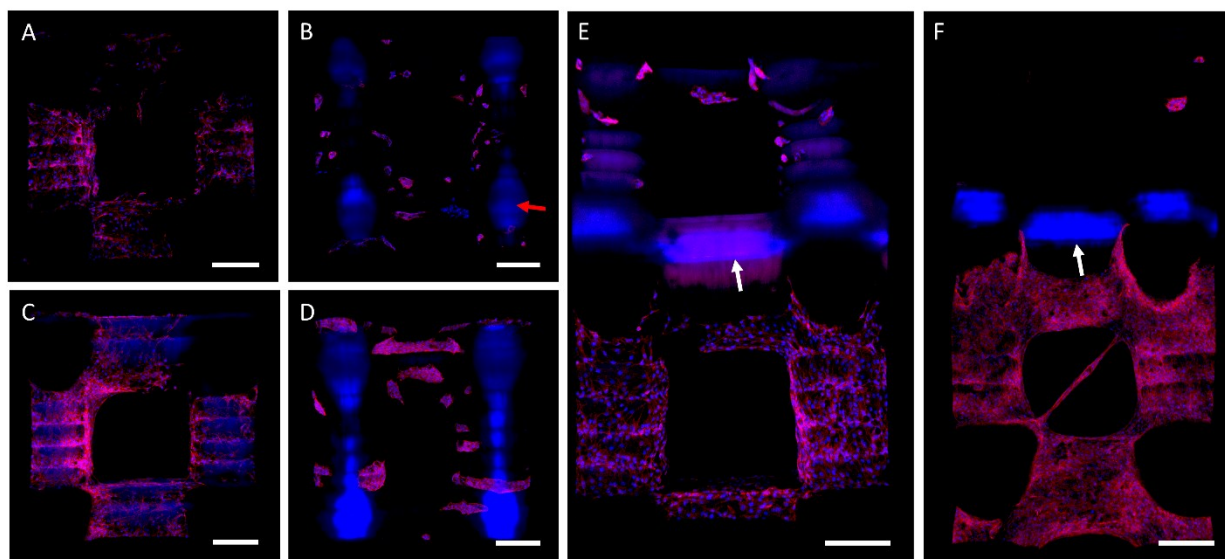


Fig. 5.4. Representative three dimensional reconstructions of confocal fluorescence images taken on scaffolds fabricated from NaAMPS (a,c), PEGDA-C (b,d), and on multi-material scaffolds made from both materials (e,f) show murine fibroblasts attachment and proliferation after 4 d (a,b,e) and 7 d (c,d,f) of culture. Cells were stained for actin (red) and nuclear material (blue). Scaffolds, especially those fabricated from PEGDA-C, autofluoresce in the blue spectrum (b, indicated by red arrow). After 4 d of culture, fibroblasts have adhered and spread on the NaAMPS

scaffold (a), but are clumped together on the PEGDA-C scaffold (b). After 7 d, cells appear to be proliferating and spreading further across the scaffold and in the pore of the NaAMPS scaffold (c). An increase in cell number is also apparent on the PEGDA-C scaffolds at this time point, but they continue to clump together rather than spread across the material (d). Selective fibroblast adhesion and proliferation occurred on multi-material scaffolds after 4 d (e) and 7 d (f). The top half of each image shows a PEGDA-C pore while the lower pore is fabricated from NaAMPS. The white arrows indicate the location of the interface between NaAMPS and PEGDA-C. At the 7 d time point, virtually no fibroblast remain on the PEGDA-C regions of the scaffold, while fibroblasts are confluent on the NaAMPS region. Some cells have even spanned the diagonal of the pore shown, although this was not observed on most pores. Samples were stained ($n = 3-5$) and imaged at each time point and scaffold type. All scale bars represent 250 μm .

5.4.3 Fabrication of Soy and PEGDA-B Scaffolds

Single material scaffolds were fabricated from the Soy and PEGDA-B resins were then evaluated for accuracy and whether they had sufficiently close swelling ratios to permit multi-material scaffold fabrication. Printed scaffolds are shown in Fig. 5.5a-d. Some swelling of pillars from water uptake was observed in the PEGDA-B scaffolds and, to a lesser extent, in the Soy scaffolds. However, the resulting differences in pillar width (250 μm for Soy and 300 μm for PEGDA-B) was substantially smaller than that between NaAMPS and PEGDA-C. Consequently, the resin pair was expected to be more conducive to the fabrication of multi-material tissue scaffolds than the NaAMPS/PEGDA-B resin system.

Tissue scaffolds fabricated from the block multi-material model are shown in Fig. 5.5e,f. A sharp interface can again be seen between the Soy (clear) and PEGDA-B (black) indicating a lack of contamination between the two materials. During fabrication of the simple multi-material scaffolds from NaAMPS/PEGDA-C, a black resin was exchanged for a clear resin. In the scaffolds made from Soy/PEGDA-B, the opposite exchange of colors was made. The transparency of the regions fabricated from the clear resins validated the quality of the cleaning process employed and indicated that the process was not impacted by the fabrication order of resins. The PEGDA-B area of the multi-material scaffolds swelled to a greater degree than the Soy region (Fig. 5.5f), but the difference between the two was not so large as to cause part failure. Fabrication of the more complex scaffold design (Fig. 5.1c) with Soy/PEGDA-B is discussed in a subsequent section.

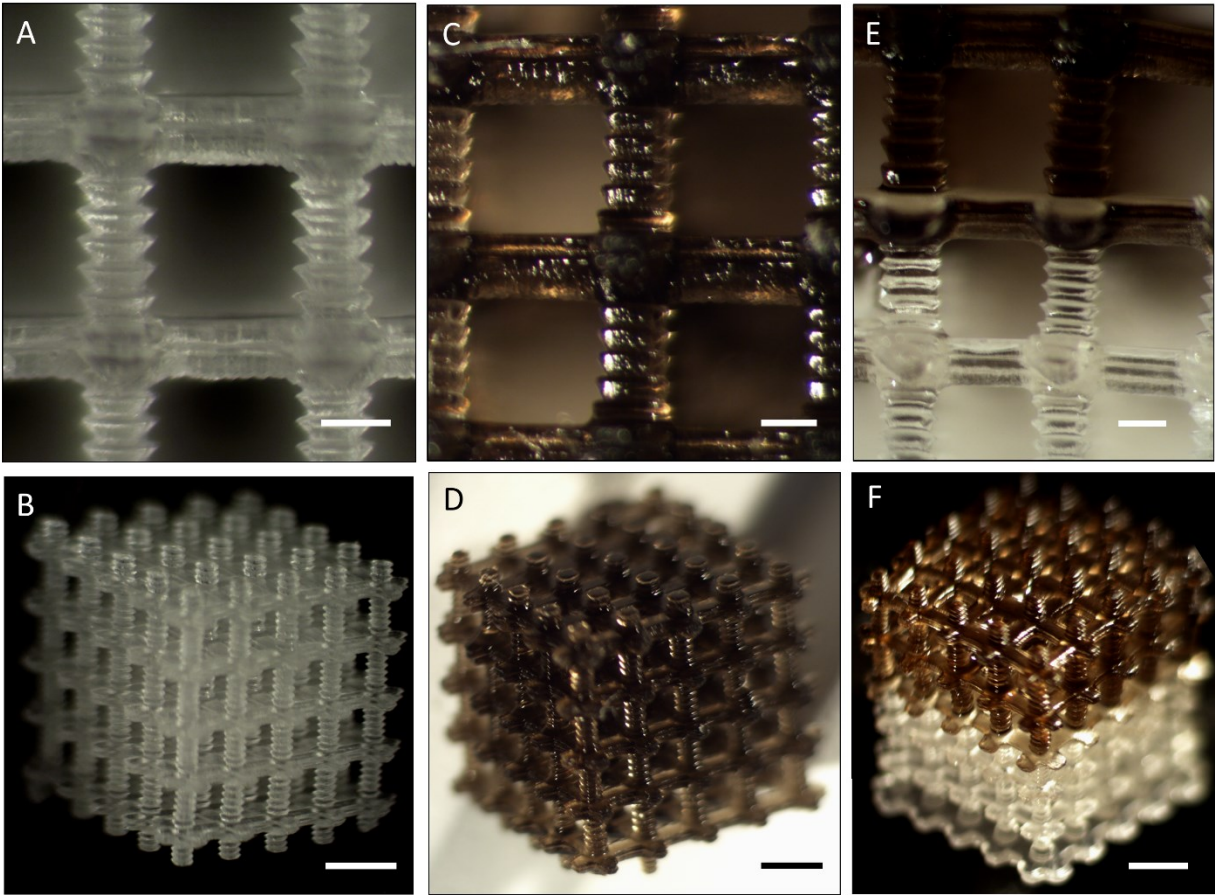


Fig. 5.5. Representative optical images show tissue scaffolds fabricated from a single material, either Soy (a,b) or PEGDA-B (c,d). Pillar widths after swelling in water were approximately 250 μm in the scaffolds fabricated from the Soy resin and 300 μm in the PEGDA-B scaffolds. Multi-material scaffolds (e,f) show a sharp interface between the areas printed from Soy (clear) and PEGDA-B (black). Slightly greater swelling was observed in the PEGDA-B part of the scaffold than the Soy region. Scale bars represent 250 μm (a,c,e) or 1 mm (b,d,f).

5.4.4 Cell Adhesion and Proliferation on Soy and PEGDA-B

The MTS assay was used to evaluate the propensity of NIH 3T3 to attach and proliferate on pure PEGDA-B and Soy scaffolds. It was surprising to find a relatively large number of the 5×10^4 cells seeded onto the PEGDA-B scaffolds ($34.4\% \pm 3.4\%$) had successfully attached. Their number also increased slightly over the next three days. Cell seeding efficiency on Soy scaffolds was very high, at $91.4\% \pm 5.1\%$. A statistically significant increase in cell number was also observed on the Soy scaffolds between 1 and 4 days of culture (Fig. 5.6, $p < 0.05$). Although the adhesion and proliferation of cells on the PEGDA-B was greater than expected, we hypothesized that a migration of cells from PEGDA-B regions of multi-material scaffolds to Soy regions might occur in the same way as was observed in the NaAMPS/PEGDA-C scaffolds.

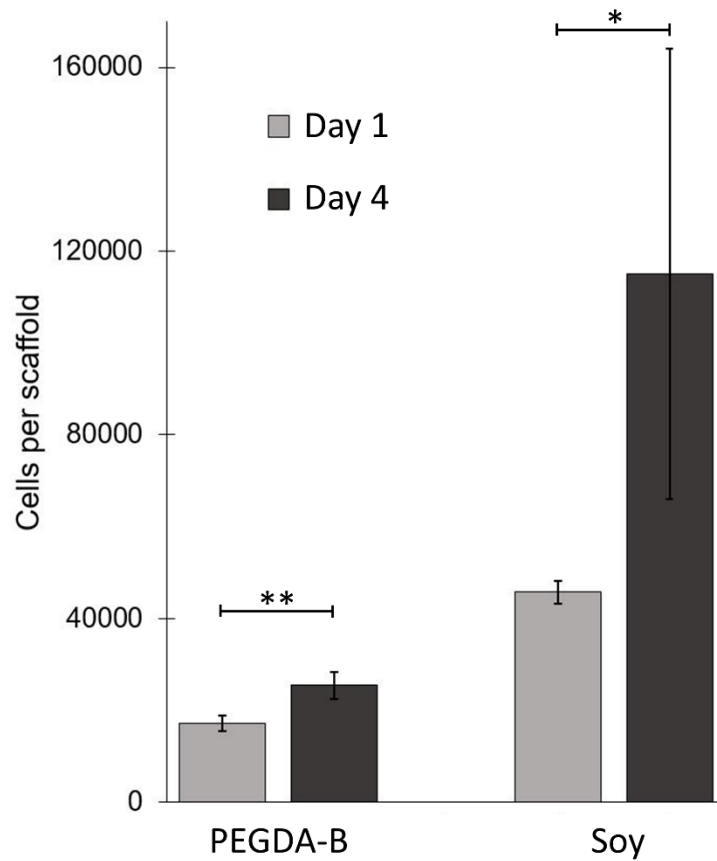


Fig. 5.6. MTS assay conducted on scaffolds fabricated entirely from either PEGDA-B or Soy, seeded with 5×10^4 NIH 3T3 fibroblasts, and cultured for 1 or 4 d. Unexpectedly, cell number increased slightly on PEGDA-B over the course of the study. However, cell count was higher on Soy scaffolds, which also showed a statistically significant increase between 1 and 4 d. One-way ANOVA followed by Tukey's HSD (* $p < 0.05$, ** $p < 0.01$, $n = 3-6$).

Soy/PEGDA-B multi-material tissue scaffolds were seeded with NIH 3T3 and cultured for 4 d to investigate whether spatially-selective adhesion and proliferation would result. Fluorescence staining and microscopy of the scaffolds revealed some proliferation of the fibroblasts on the Soy areas of the scaffold, but no discernible adhesion to the PEGDA-B areas (Fig. 5.7). Slight autofluorescence of the PEGDA-B areas helps to reveal its location in the upper half of the image (Fig. 5.7a). Areas of stronger fluorescence, exclusively in the lower half of the image, show that the fibroblasts have partially coated the Soy region. After background subtraction to remove fluorescence imparted by the PEGDA-B and the addition of the blue (DAPI) channel, the region fabricated using Soy is easily distinguished. Unfortunately, the Soy resin's autofluorescence is much stronger than the fluorescence of the DAPI-stained nuclear material, preventing the identification of cell nuclei. Isolation of the red (Texas Red-X) channel after background subtraction confirms the localization of fibroblasts exclusively on the Soy areas of the scaffold (Fig. 5.7c).

The proliferation of fibroblasts on the Soy areas was insufficient to result in a confluent layer on the material, but the multi-material scaffolds displayed selective cellular adhesion. These results, in addition to those obtained with NaAMPS/PEGDA-C multi-material scaffolds, provide

conclusive evidence that multi-material scaffolds fabricated with VP can be used to create heterogeneous cell distributions that arise directly from the design of the CAD model employed and the use of resins with dissimilar cell adhesion properties. More complex designs that would benefit from spatial modulation of cell adhesion were subsequently explored to demonstrate the value of our approach.

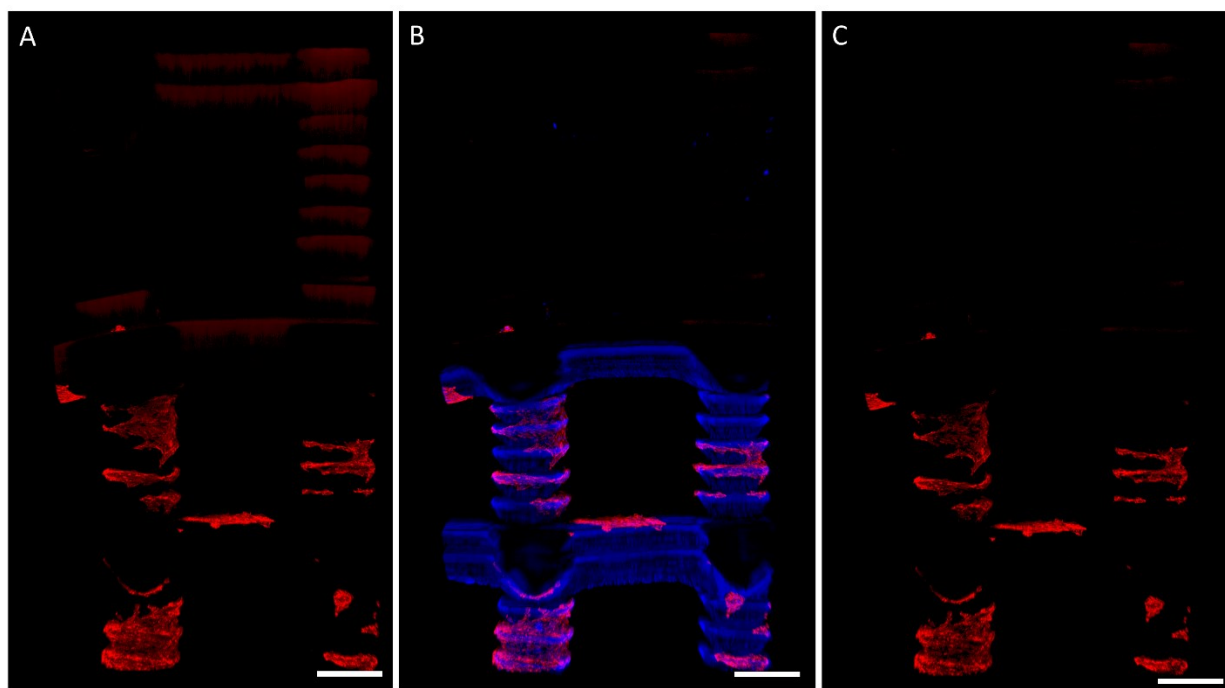


Fig. 5.7. Representative fluorescence images of a multi-material scaffold fabricated from Soy (lower half) and PEGDA-B (upper half) after 4 d of culture. A) Red staining shows that cells are located almost entirely on the Soy areas of the scaffold. The PEGDA-B regions fluoresce very lightly in the red spectrum. B) Background subtraction and the addition of the blue channel show the outline of the Soy scaffold, however, autofluorescence in the blue spectrum prevent nuclei detection. C) Actin staining is visible only in the lower half of the image after background subtraction. Scale bars represent 250 μm .

5.4.5 Perfusable Scaffold Fabrication and Evaluation

A large scaffold design with 600 μm pores and a perfusable network of channels (Fig. 5.1c) was successfully printed using the Soy and PEGDA-B resins (Fig. 5.8). The tubes, which were fabricated from PEGDA-B to prevent cell adhesion, were clear of any photopolymerized resin (Fig. 5.9a). Water uptake by the PEGDA-B tubes was greater than the scaffolding regions fabricated from Soy, as was expected based on earlier results. The swelling of the tubes also caused them to lengthen, resulting in slight protrusions from the rest of the scaffold (Fig. 5.9b). In this case, the tube lengthening may be beneficial as it may facilitate the attachment of tubing for media perfusion.

Two multi-material scaffolds with perfusable channels were seeded with 2×10^5 NIH 3T3 fibroblasts and cultured for 7 days. The scaffolds were stained in the same manner as previously described and a region at the opening of a channel imaged (Fig. 5.10). Selective adhesion of fibroblasts was observed, in accord with the results obtained from Soy/PEGDA-B multi-material scaffolds. The PEGDA-B tube, which autofluoresces weakly in the red spectrum, is located in the upper left hand corner (Fig. 5.10a). Except for one small area, the tube is devoid of fibroblasts. The Soy regions autofluoresce very strongly in the blue spectrum, allowing for easy identification. However, as mentioned above, the Soy's autofluorescence is much greater than that of the DAPI-stained nuclei, preventing their observation. Fibroblasts, whose presence can be detected by their Texas Red-X-stained actin, coat the scaffolds surface near the bottom of the image. Isolation of the red channel and background subtraction to remove autofluorescence of PEGDA-B is shown in Fig. 5.10b). This result indicates that multi-material tissue scaffolds fabricated with VP could contain tubular networks that remain patent and perfusable at extended time points and provide

structure and function similar to that of vasculature. Additional culture time or higher seeding density (the seeding density used was much lower than on the block multi-material scaffolds) may have allowed for greater cellular proliferation and coverage of the Soy regions.

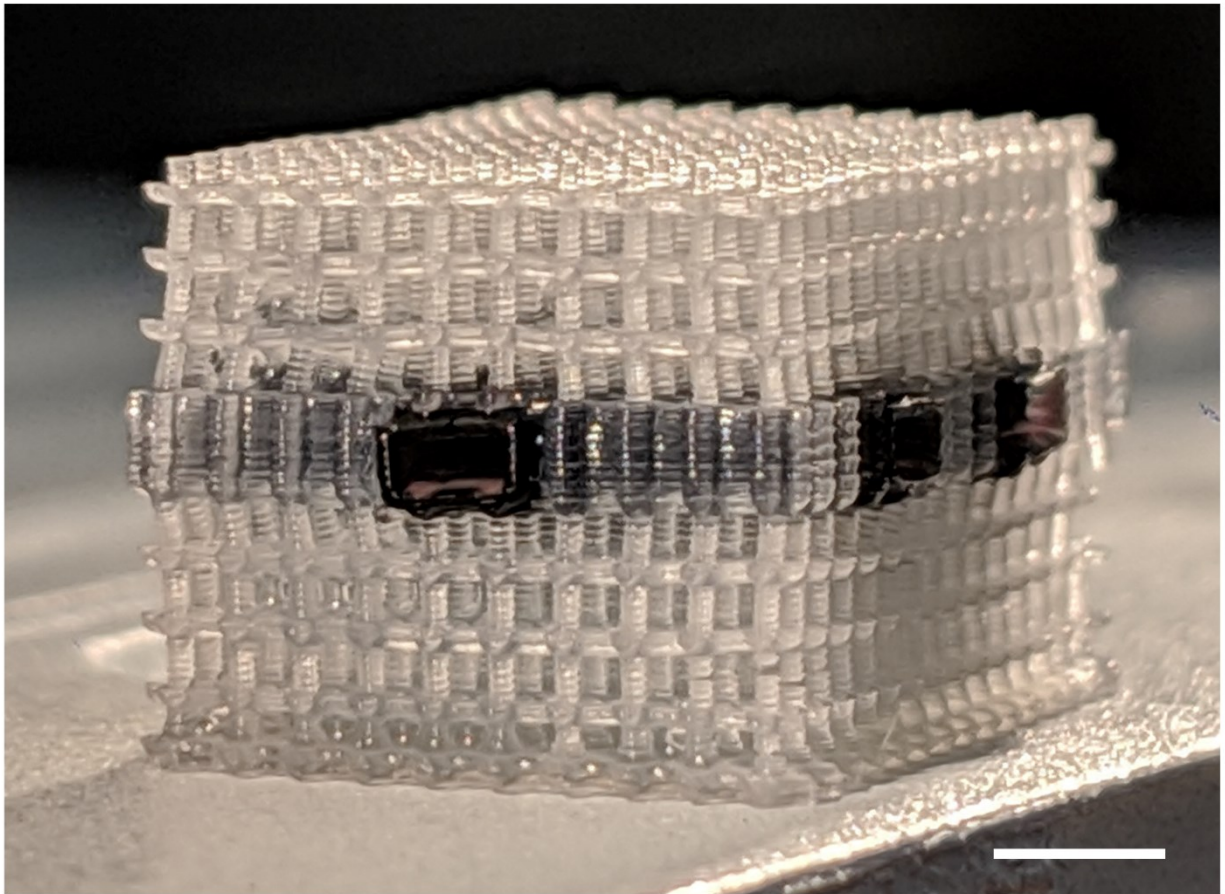


Fig. 5.8. Complex multi-material scaffold 3D printed from Soy and PEGDA-B. The Soy (clear) regions provide a conventional scaffold for adhering cells. The PEGDA-B (black) tubes, which extend through the entire part and do not demonstrate cell growth, may allow perfusion of the scaffold with growth media and a potential means of introducing vascularization into a large tissue scaffold. Scale bar = 2 mm.

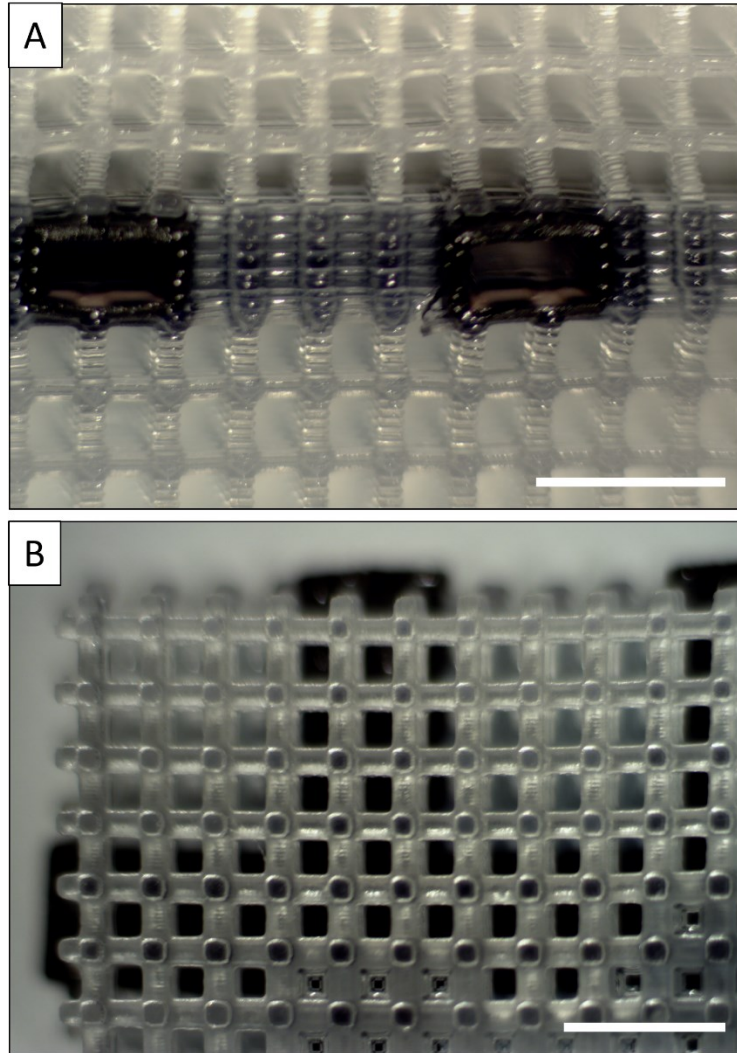


Fig. 5.9. Side (a) and top (b) views of a complex multi-material tissue scaffold fabricated from Soy (clear) and PEGDA-B (black). A) The 3D printed tubes are clear of photopolymer and provide a template for vascularization. B) Greater swelling of the PEGDA-B than the Soy is seen from the top view. The vascular-like tubes extend beyond the Soy scaffold. Scale bars represent 2 mm.

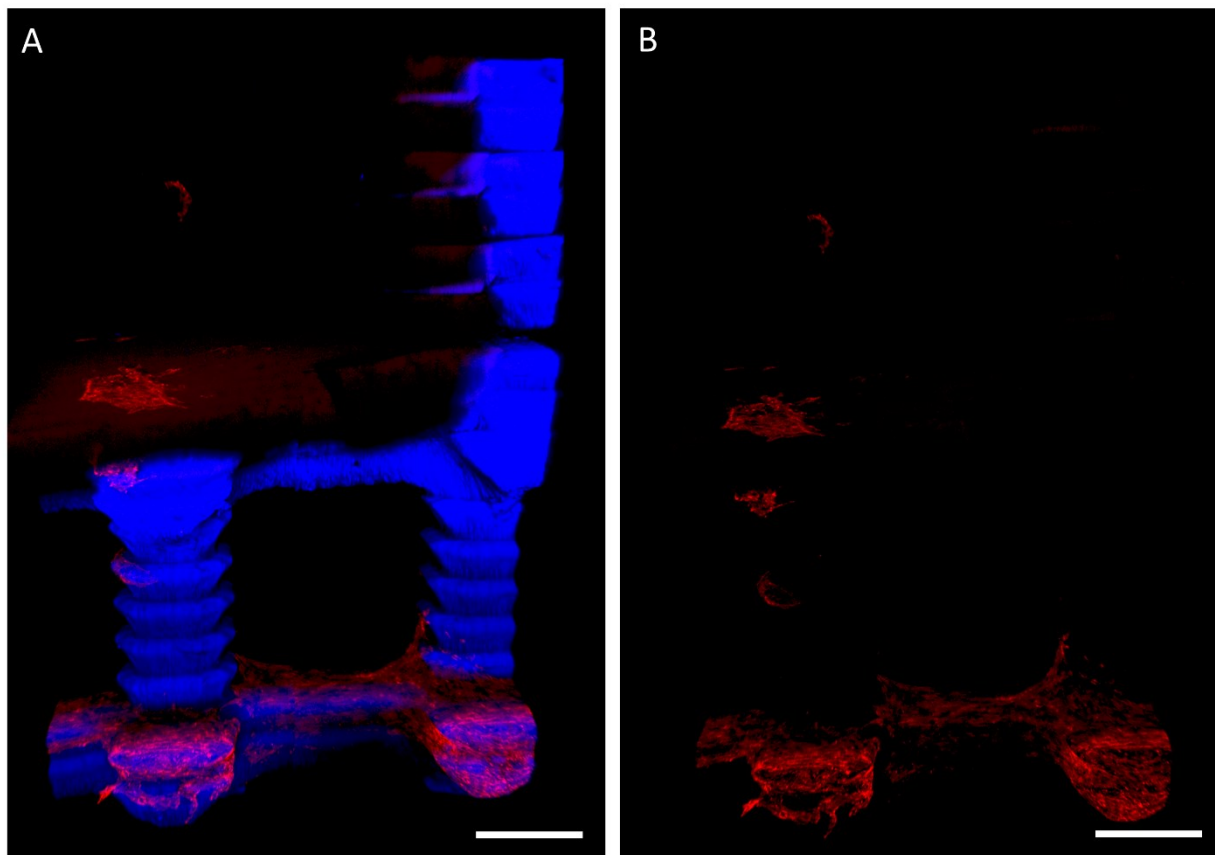


Fig. 5.10. 3D reconstructions of confocal fluorescence image stacks taken of a complex multi-material scaffold after 7 days. In the upper left is a PEGDA-B tube. The remainder of the scaffold, fabricated from Soy, is easily discernable due to its strong autofluorescence in the blue spectrum, preventing the identification of cell nuclei. A) Red stained actin is visible primarily at the bottom of the scaffold. B) After background subtraction and removal of the blue (DAPI) channel, the selective localization of cells on Soy regions is apparent. Scale bars represent 250 μm .

5.5 Conclusions

In this report, we demonstrated the use of multi-material tissue scaffolds in spatially controlling cell adhesion and proliferation. Sharp interfaces between the dissimilar materials were observed, suggesting the absence of cross-contamination between resins. The localization of fibroblasts

arising directly from selective material placement was confirmed using multiple resins and geometries. These results illustrate the potential our methods, which require no custom hardware, have for fabricating complex engineered tissue constructs with enhanced function compared to single-material constructs. The precise localization of cells by such constructs could aid in the formation of vascular networks or hierarchical structures similar to those found in the kidney. This suggests that multi-material scaffolds 3D printed with VP could be used to help overcome size limitations of engineered constructs because of diffusion constraints. We 3D printed a large (> 10 mm) multi-material scaffold using an epoxidized soybean oil-based resin that contained a network of tubes fabricated from a PEGDA-based resin that discouraged fibroblast adhesion. After 7 days, fibroblasts had proliferated on regions of the scaffold fabricated from soybean oil-based resin, but not on the perfusable network. In fabricating scaffolds from dissimilar materials, we found that material properties, especially swelling ratio mismatch, can have substantial effects on fabrication outcomes. Finally, we fabricated these tissue scaffolds using a commercial VP system, which obviated the need to develop a custom system. We hope that techniques we have developed for multi-material 3D printing will encourage scientists and engineers from many disciplines to explore the new design freedoms and biomimicry that multi-material tissue scaffold can provide.

References

- [1] R. Langer, J.P. Vacanti, Tissue Engineering, *Science* (80-.). 260 (1993) 920–926.
- [2] N.A. Chartrain, C.B. Williams, A.R. Whittington, A review on fabricating tissue scaffolds using vat photopolymerization, *Acta Biomater.* 74 (2018) 90–111. doi:10.1016/j.actbio.2018.05.010.
- [3] E.C. Novosel, C. Kleinhans, P.J. Kluger, Vascularization is the key challenge in tissue engineering., *Adv. Drug Deliv. Rev.* 63 (2011) 300–11. doi:10.1016/j.addr.2011.03.004.
- [4] F.P.W. Melchels, A.M.C. Barradas, C.A. Van Blitterswijk, J. De Boer, J. Feijen, D.W. Grijpma, Effects of the architecture of tissue engineering scaffolds on cell seeding and culturing, *Acta Biomater.* 6 (2010) 4208–4217. doi:10.1016/j.actbio.2010.06.012.
- [5] B. Grigoryan, S.J. Paulsen, D.C. Corbett, D.W. Sazer, C.L. Fortin, A.J. Zaita, P.T.

- Greenfield, N.J. Calafat, J.P. Gounley, A.H. Ta, F. Johansson, A. Randles, J.E. Rosenkrantz, J.D. Louis-Rosenberg, P.A. Galie, K.R. Stevens, J.S. Miller, Multivascular networks and functional intravascular topologies within biocompatible hydrogels, *Science* (80-.). 364 (2019) 458–464. doi:10.1126/science.aav9750.
- [6] N. Noor, A. Shapira, R. Edri, I. Gal, L. Wertheim, T. Dvir, 3D Printing of Personalized Thick and Perfusable Cardiac Patches and Hearts, *Adv. Sci.* 6 (2019) 1900344. doi:10.1002/advs.201900344.
- [7] S. V. Murphy, A. Atala, 3D bioprinting of tissues and organs, *Nat. Biotechnol.* 32 (2014) 773–785. doi:10.1038/nbt.2958.
- [8] S.C. Ligon, R. Liska, J. Stampfl, M. Gurr, R. Mülhaupt, Polymers for 3D Printing and Customized Additive Manufacturing, *Chem. Rev.* 117 (2017) 10212–10290. doi:10.1021/acs.chemrev.7b00074.
- [9] R. Gauvin, Y.C. Chen, J.W. Lee, P. Soman, P. Zorlutuna, J.W. Nichol, H. Bae, S. Chen, A. Khademhosseini, Microfabrication of complex porous tissue engineering scaffolds using 3D projection stereolithography, *Biomaterials.* 33 (2012) 3824–3834. doi:10.1016/j.biomaterials.2012.01.048.
- [10] M.N. Cooke, J.P. Fisher, D. Dean, C. Rimnac, A.G. Mikos, Use of stereolithography to manufacture critical-sized 3D biodegradable scaffolds for bone ingrowth., *J. Biomed. Mater. Res. B. Appl. Biomater.* 64 (2003) 65–9. doi:10.1002/jbm.b.10485.
- [11] S. Miao, W. Zhu, N.J. Castro, M. Nowicki, X. Zhou, H. Cui, J.P. Fisher, L.G. Zhang, 4D printing smart biomedical scaffolds with novel soybean oil epoxidized acrylate, *Sci. Rep.* 6 (2016) 1–10. doi:10.1038/srep27226.
- [12] J.K. Placone, J. Navarro, G.W. Laslo, M.J. Lerman, A.R. Gabard, G.J. Herendeen, E.E. Falco, S. Tomblyn, L. Burnett, J.P. Fisher, Development and Characterization of a 3D Printed, Keratin-Based Hydrogel, *Ann. Biomed. Eng.* 45 (2017) 237–248. doi:10.1007/s10439-016-1621-7.
- [13] F.P.W. Melchels, B. Tonnarelli, A.L. Olivares, I. Martin, D. Lacroix, J. Feijen, D.J. Wendt, D.W. Grijpma, The influence of the scaffold design on the distribution of adhering cells after perfusion cell seeding., *Biomaterials.* 32 (2011) 2878–84. doi:10.1016/j.biomaterials.2011.01.023.
- [14] J.-W. Choi, E. MacDonald, R. Wicker, Multi-material microstereolithography, *Int. J. Adv. Manuf. Technol.* 49 (2009) 543–551. doi:10.1007/s00170-009-2434-8.
- [15] K. Arcaute, B. Mann, R. Wicker, Stereolithography of spatially controlled multi-material bioactive poly(ethylene glycol) scaffolds., *Acta Biomater.* 6 (2010) 1047–54. doi:10.1016/j.actbio.2009.08.017.
- [16] V. Chan, J.H. Jeong, P. Bajaj, M. Collens, T. Saif, H. Kong, R. Bashir, Multi-material bio-fabrication of hydrogel cantilevers and actuators with stereolithography, *Lab Chip.* 12 (2012) 88–98. doi:10.1039/C1LC20688E.
- [17] D. Chen, X. Zheng, Multi-material Additive Manufacturing of Metamaterials with Giant, Tailorable Negative Poisson’s Ratios, *Sci. Rep.* 8 (2018) 9139. doi:10.1038/s41598-018-26980-7.
- [18] Q. Ge, A.H. Sakhaei, H. Lee, C.K. Dunn, N.X. Fang, M.L. Dunn, Multimaterial 4D Printing with Tailorable Shape Memory Polymers, *Sci. Rep.* 6 (2016) 1–11. doi:10.1038/srep31110.
- [19] K. Kowsari, S. Akbari, D. Wang, N.X. Fang, Q. Ge, High-Efficiency High-Resolution Multimaterial Fabrication for Digital Light Processing-Based Three-Dimensional Printing,

- 3D Print. Addit. Manuf. 5 (2018) 185–193. doi:10.1089/3dp.2018.0004.
- [20] P. Zorlutuna, J.H. Jeong, H. Kong, R. Bashir, Stereolithography-based hydrogel microenvironments to examine cellular interactions, *Adv. Funct. Mater.* 21 (2011) 3642–3651. doi:10.1002/adfm.201101023.
- [21] C. Zhou, Y. Chen, Z. Yang, B. Khoshnevis, Digital material fabrication using mask-image-projection-based stereolithography, *Rapid Prototyp. J.* 19 (2013) 153–165. doi:10.1108/13552541311312148.
- [22] A.K. Miri, D. Nieto, L. Iglesias, H. Goodarzi Hosseinabadi, S. Maharjan, G.U. Ruiz-Esparza, P. Khoshakhlagh, A. Manbachi, M.R. Dokmeci, S. Chen, S.R. Shin, Y.S. Zhang, A. Khademhosseini, Microfluidics-Enabled Multimaterial Maskless Stereolithographic Bioprinting, *Adv. Mater.* 30 (2018) 1800242. doi:10.1002/adma.201800242.
- [23] D. Han, C. Yang, N.X. Fang, H. Lee, Rapid Multi-Material 3D Printing with Projection Micro-Stereolithography Using Dynamic Fluidic Control, *Addit. Manuf.* 27 (2019) 606–615. doi:10.1016/j.addma.2019.03.031.
- [24] R. Raman, B. Bhaduri, M. Mir, A. Shkumatov, M.K. Lee, G. Popescu, H. Kong, R. Bashir, High-Resolution Projection Microstereolithography for Patterning of Neovasculature, *Adv. Healthc. Mater.* 5 (2016) 610–619. doi:10.1002/adhm.201500721.
- [25] W. Yang, H. Yu, G. Li, Y. Wang, L. Liu, Facile modulation of cell adhesion to a poly(ethylene glycol) diacrylate film with incorporation of polystyrene nano-spheres, *Biomed. Microdevices.* 18 (2016). doi:10.1007/s10544-016-0133-4.
- [26] D.B. Kolesky, R.L. Truby, A.S. Gladman, T.A. Busbee, K.A. Homan, J.A. Lewis, 3D bioprinting of vascularized, heterogeneous cell-laden tissue constructs, *Adv. Mater.* 26 (2014) 3124–3130. doi:10.1002/adma.201305506.
- [27] T. Mygind, M. Stiehler, A. Baatrup, H. Li, X. Zou, A. Flyvbjerg, M. Kassem, C. Bünger, Mesenchymal stem cell ingrowth and differentiation on coralline hydroxyapatite scaffolds, *Biomaterials.* 28 (2007) 1036–1047. doi:10.1016/j.biomaterials.2006.10.003.
- [28] I. Martin, R.F. Padera, G. Vunjak-Novakovic, L.E. Freed, In vitro differentiation of chick embryo bone marrow stromal cells into cartilaginous and bone-like tissues, *J. Orthop. Res.* 16 (1998) 181–189. <https://onlinelibrary-wiley-com.ezproxy.lib.vt.edu/doi/pdf/10.1002/jor.1100160205> (accessed January 29, 2019).
- [29] L. Qi, E.K. Knapton, X. Zhang, T. Zhang, C. Gu, Y. Zhao, Pre-culture Sudan Black B treatment suppresses autofluorescence signals emitted from polymer tissue scaffolds, *Sci. Rep.* 7 (2017) 8361. doi:10.1038/s41598-017-08723-2.
- [30] B.R. McAuslan, G. Johnson, Cell responses to biomaterials I: Adhesion and growth of vascular endothelial cells on poly(hydroxyethyl methacrylate) following surface modification by hydrolytic etching, *J. Biomed. Mater. Res.* 21 (1987) 921–935. doi:10.1002/jbm.820210708.
- [31] T.W. Minnett, B.J. Tighe, M.J. Lydon, D.A. Rees, Requirements for cell spreading on polyHEMA coated culture substrates, *Cell Biol. Int. Rep.* 8 (1984) 151–159. doi:10.1016/0309-1651(84)90082-1.
- [32] D. Behera, A.K. Banthia, Synthesis, characterization, and kinetics study of thermal decomposition of epoxidized soybean oil acrylate, *J. Appl. Polym. Sci.* 109 (2008) 2583–2590. doi:10.1002/app.28350.
- [33] P.M. Lambert, E.A.C. III, C.B. Williams, Design Considerations for Mask Projection Microstereolithography Systems, in: *Solid Free. Fabr. Symp.*, Austin, Texas, 2013: pp. 111–130.

- [34] M. Hegde, V. Meenakshisundaram, N. Chartrain, S. Sekhar, D. Tafti, C.B. Williams, T.E. Long, 3D Printing All-Aromatic Polyimides using Mask-Projection Stereolithography: Processing the Nonprocessable, *Adv. Mater.* 29 (2017). doi:10.1002/adma.201701240.
- [35] C. Hinczewski, S. Corbel, T. Chartier, Ceramic suspensions suitable for stereolithography, *J. Eur. Ceram. Soc.* 18 (1998) 583–590. doi:10.1016/s0955-2219(97)00186-6.
- [36] R.I. Freshney, *Culture of Animal Cells: A Manual of Basic Technique and Specialized Applications: Sixth Edition*, John Wiley and Sons, 2011. doi:10.1002/9780470649367.
- [37] J.R. Tumbleston, D. Shirvanyants, N. Ermoshkin, R. Januszewicz, A.R. Johnson, D. Kelly, K. Chen, R. Pinschmidt, J.P. Rolland, A. Ermoshkin, E.T. Samulski, J.M. Desimone, Continuous liquid interface production of 3D objects, *Science* (80-.). 347 (2015) 1349–1352. doi:10.1126/science.aaa2397.

Chapter 6: Overall Conclusions

6.1 Summary of Research, Results, and Contributions

The overall research goal of the work conducted was to gain a greater understanding in how scaffold designs impact cell response in tissue scaffolds fabricated by VP and how this knowledge can be leveraged to engineer designed responses and direct cell growth and proliferation. Three distinct research aims were designed to probe the interactions between scaffold design and resulting cell adhesion and proliferation. These three research aims simultaneously sought to develop materials, knowledge, and techniques to help overcome the primary limitations of VP in tissue scaffold fabrication. These limitations of VP include a small number of printable resins with low cytotoxicity and good cell adhesion, a lack of design guidelines for tissue scaffolds that will support high densities of cells, and very limited spatial control over the adhesion and proliferation of cells within a tissue scaffold construct necessary for the development of vascularized or multi-cellular tissues (See Chapter 2 for additional details). Each strategy generated results that contributed valuable knowledge and methods to the body of literature.

6.1.1 Research Aim #1: Polymeric Materials for Tissue Scaffold Fabrication with Vat Photopolymerization

The goal of the first research aim was to develop a resin formulation to maximize cell adhesion and proliferation while simultaneously enabling the printing of high resolution scaffolds with small features, as described in Development Objective #1.

Development Objective #1

Develop a resin using commercially available components (zero-synthesis) with properties suitable for the fabrication of tissue scaffolds using VP.

Specific properties of a suitable resin were defined (Section 1.2.1). These included the use of commercially available components, rapid photocuring of thin layers, and low viscosity. It was also necessary that parts fabricated with the resin have sufficient mechanical strength, small feature sizes, low cytotoxicity, and good cellular adhesion. Previous reports suggested that the sodium salt of 2-acrylamido-2-methyl-1-propanesulfonic acid (NaAMPS) might fulfill the desired specifications. However, initial experiments showed that a resin formulated with NaAMPS as its only photopolymeric component was not a viable one due to the gel's insufficient mechanical strength. This result led to the formulation of a research question complementary to the Development Objective which aimed to understand how the composition of a resin based on the NaAMPS molecule would impact the resin's printability and print resolution.

Supplemental Research Question #1.1

How does the NaAMPS-based resin's composition impact its printability and print resolution?

Photorheology of a NaAMPS-based resin containing 25 wt% PEGDA crosslinker improved photoreactivity and increased the gel's storage modulus by more than two orders of magnitude to more than 10^6 Pa, permitting the printing of self-supporting structures (see Section 3.8.2). Photorheology and working curve tests on resin formulations containing varying quantities of UV-absorbing avobenzene showed that a formulation containing 0.20 wt% avobenzene permitted rapid

photocuring (< 20 s) of thin layers (50 μm) on a lab-built VP system with a light intensity of 15 mW/cm^2 , fulfilling the desired specifications. The tissue scaffolds that were built with the resin formulation developed demonstrated feature sizes of approximately 100 μm , suitable for the fabrication of fine features needed for tissue scaffolds with high surface areas.

- These results show a NaAMPS-based resin cannot be fabricated into complex self-supporting structures without the incorporation of a crosslinking agent (e.g., PEGDA) due to the insufficient strength of the gels formed.

In the work conducted, a commercially available 50 wt% NaAMPS solution in water was used. A more concentrated NaAMPS solution with a higher density of acrylamide groups might result in the formation of a gel with a stronger gel strength. However, such a photopolymer system was not pursued because even small quantities of water loss through evaporation caused the crystallization of NaAMPS out of solution.

The successful development of a printable resin that could be fabricated into high resolution scaffolds led to the testing of the biological properties of the scaffolds, specifically their mechanical properties, cytotoxicity, cell adhesion, and cell proliferation. While the bulk modulus of the material was slightly more than 300 MPa, similar to that of soft bone, the effective modulus of a scaffold with 400 μm pores and 84% porosity was approximately 1 MPa (see Section 3.4.4). The similarity of the scaffold's effective modulus to that of dermis and cartilage suggested that they might be suitable for the engineering of connective tissues. Fibroblasts showed similar growth on films of the NaAMPS-based resin when compared to tissue culture treated polystyrene after 1

week. Evaluation of the quantity of cells adhered to scaffolds after 24 hours showed an adhesion rate of approximately 75%. A statistically significant increase in the quantity of fibroblasts on the scaffolds was found between 1 and 3 days of culture and then again between 3 and 7 days. The good adhesion of cells to the scaffolds and excellent growth over the course of one week validates the NaAMPS-based resin as a suitable tissue scaffold material.

- The NaAMPS-based resin represents a substantial improvement over other resins reported in the literature due to the combination of its commercially available components, zero-synthesis formulation, high resolution printability, low cytotoxicity, and the good adhesion and growth of cells seeded on scaffolds made from it.

The development of a photocurable resin with such a combination of attributes marks a significant contribution to the literature and the tissue engineering field as a whole. Despite its many advantages, unlike many natural resins and some synthetic ones, a NaAMPS-based resin is expected to degrade very slowly when exposed to *in vivo* conditions. Further, acrylamide-acrylamide linkages are known to have increased stability when compared to acrylate-acrylate ones. Future work should aim to address this primary limitation by increasing the degradation rate of the resin or including degradable moieties.

The development of the NaAMPS-based resin has the potential for broad impact on the use of VP-fabricated tissue scaffolds to address challenges in the fields of tissue engineering and regenerative medicine. The ease of obtaining and formulating the resin will encourage researchers to more closely consider VP as a suitable technique for the fabrication of their tissue scaffolds. The resin's

low cost is an additional benefit. While Chapter 3 only demonstrated the fabrication of tissue scaffolds with a custom ‘top-down’ VP system, the fabrication of tissue scaffolds with a NaAMPS-based resin with a commercially available VP system was shown in Chapter 5. The availability of a new resin that overcomes many of the limitations of commercially available resins and those reported in the literature will help to accelerate tissue engineering research that uses VP.

6.1.2 Research Aim #2: Effects of Scaffold Pore Size on Cell Adhesion and Proliferation

The goal of the second research aim was to gain a greater understanding of the ways in which cell proliferation and distribution within a VP-fabricated scaffold are affected by the scaffold’s geometry, namely its pore size. The effect of geometric parameters on cell response have been studied for decades using scaffolds made with traditional fabrication techniques, but little work has focused on VP scaffolds. Like other AM techniques, VP fabricates structures from computer models and can thus make scaffolds with highly regular and repeatable geometries that are pre-designed. However, VP is unique among AM techniques in its ability to fabricate tissue scaffolds with very small feature sizes, high aspect ratios, and large porosities. This gap in the literature led to the development of Research Question #2.

Research Question #2

How does pore size in a tissue scaffold fabricated with VP impact cell proliferation and cell distribution within the scaffold?

A scaffold's geometry is governed by a large number of parameters, including porosity, pore size, pore shape, overall shape and size of the scaffold, surface area, permeability, porosity, pore size distribution, and pore interconnectivity. Traditional scaffold fabrication techniques are unable to fabricate scaffolds with all but one geometric parameter being held constant between samples, making effective testing difficult. Even with AM, some tradeoffs exist. For example, scaffolds with varying pore sizes with other parameters being identical cannot be made, as surface area will inevitably increase with decreasing pore size. (It is possible to design a scaffold with varying pore sizes and constant surface area, but it would then be impossible to hold constant other parameters such as porosity or overall size). In the study performed and in contrast with some previous work, the greatest number of parameters were held constant so as to more effectively elucidate the effects of pore size on cell proliferation and distribution.

Scaffolds with pore sizes ranging from 200 μm to 600 μm were designed and fabricated from a NaAMPS-based resin using a lab built VP system. Mouse fibroblasts were seeded on scaffolds and cultured for one week and then both the total quantity of cells and their distributions within the scaffold evaluated. The results revealed the largest quantity of cells on scaffolds with 500 μm pores, although the number was not statistically significant when compared to the quantity of cells found on scaffolds with 600 μm pores (See Fig. 4.4). However, it was very clear that below 500 μm , total cell count decreased with decreasing pore size. Cell density was highest on scaffolds with 500 μm pores. Further, as pore size was reduced, cell distribution became inhomogeneous, particularly in scaffolds with 200 and 300 μm pores.

The data, which showed that scaffolds with 500 μm pores had the high cell density and largest quantity of cells and that scaffolds with pore sizes as large as 300 μm had inhomogeneous cell distributions, was somewhat surprising. While previous literature had shown that pore sizes larger than 300 μm resulted in greater cell growth, an ‘optimal’ pore size was hypothesized to lie in the vicinity of 400 μm (see Section 4.2). It is difficult to fabricate highly porous ($> 60\%$) tissue scaffolds with pore sizes larger than about 400 μm using traditional fabrication methods. Few studies investigated scaffolds with pore sizes in the range of 400-600 μm . Although several studies using scaffolds with smaller pores revealed greatest cell growth on the scaffolds with the largest pores studied, a higher cell count on scaffolds with 500 μm pores than on those with 400 μm pores was unexpected. Further, one would expect that scaffolds with regular repeating structures, such as those used in this work, rather than the more tortuous stochastic structures formed by traditional scaffold fabrication techniques would have led to the larger diffusion of oxygen and nutrients in scaffolds with small pores. The ‘optimal’ pore size in scaffolds fabricated with AM would thus be smaller than that in scaffolds fabricated through traditional means.

Scaffolds with 500 μm pores performed the best in the work shown here because 500 μm pores were large enough to permit the diffusion of oxygen and nutrients as well as the movement of cells in a 4 mm thick scaffold. While distribution of cells was still relatively homogeneous in scaffolds with 400 μm pores, the decreased diffusion and mobility led to lower overall cell growth. This effect was exacerbated in scaffolds with 300 and 200 μm pores. The difference in total cell count between scaffolds with 500 μm and 600 μm pores was not significantly different and their cell densities were relatively similar. However, the larger surface area of the scaffolds with 500 μm

pores suggests that additional growth could be expected on these scaffolds before complete coverage of the scaffold by cells was achieved.

- Scaffolds with 500 μm pores were most effective in maximizing cell growth and generating homogeneous cell distributions because the sufficiently large pores did not impede nutrient diffusion or cell movement while simultaneously providing ample surface area for cell growth.

It must be noted that the results of previous work (as well as the results of this study) should be analyzed with regard to the parameters other than pore size which were not or could not be held constant as well as the differences between scaffolds in various studies that make them dissimilar to each other. For example, as previously noted, total surface area and pore size are negatively correlated. This could benefit scaffolds with smaller pore sizes, a result which was not observed in either this work or previous studies.

There are some additional inherent limitations of this work that prevent the generalization of the conclusion about scaffolds with 500 μm pores to all tissue scaffolds in all situations. The choice of material will impact cell adhesion, viability, and growth, thus the use of different materials in separate studies makes it difficult to compare their results. Mesenchymal stem cells (MSC) and cell types differentiating from MSC (e.g., fibroblasts, osteoblasts, and chondrocytes) constitute the majority of cell types investigated in the literature with respect to the effects of pore size. Neurons, which experience a vastly different microenvironment *in vivo* may respond quite differently to scaffolds with 500 μm pores. In this work, cell growth and distribution were evaluated at a single

time point (7 days). Future work should investigate multiple time points as cell growth and distribution are likely to change over time. The use of perfusion culture is likely to impact results on the effect of pore size as the inherent limitations on diffusion posed by scaffold geometry can be at least partially overcome. Further, the implementation of perfusion culture would introduce a plethora of additional variables, which could each significantly impact cell growth and distribution (e.g., flow rate, shear rates experienced by cells, pulsatile versus continuous flow). Finally, the overall size/thickness of a tissue scaffold will help determine whether sufficient nutrients and oxygen can reach the areas furthest from the scaffold surface. The results presented here show that the quantity of cells near the surface of the tissue scaffolds with 200 and 300 μm pores was nearly as large as that seen throughout scaffolds with 500 μm pores (although density was lower). This may suggest that tissue scaffolds with 200-300 μm pore sizes could be suitable in situations where the scaffold is only a few hundred microns thick. Thin scaffolds, however, have more limited clinical relevance than thicker ones. Despite the limitations on the applicability of the conclusions generated herein to all tissue scaffolds in all situations, it is possible to establish a guideline on pore size that is useful in many situations.

- While it is not possible to declare a certain pore size to be optimal due to the sheer number of variables involved in scaffold geometry, this work, in conjunction with previous literature, provides strong evidence that larger pores (400-600+ μm) are better suited than smaller pores ($\leq 300 \mu\text{m}$) at augmenting cell growth and creating homogenous cell distributions in thick ($> 1 \text{ mm}$) scaffolds due to improved diffusion of oxygen and nutrients.

Future studies should include scaffolds with pores of 700 and 800 μm in an effort to more conclusively identify a specific range of pore sizes that provides the best conditions for cell growth and homogeneous cell distribution. The insights gained from this work provide some scaffold design guidelines for all researchers working in the field of tissue engineering. These results will guide researchers in selecting an appropriate pore size for their tissue scaffolds that will help maximize cell growth and homogeneity and ultimately aid in delivering effective tissue engineering products to clinics and patients.

The techniques presented in this work for evaluation of the effect of pore size on cell growth and distribution are both novel and widely applicable in the field of tissue engineering.

- The novel techniques developed in this work for cell counting and location mapping allow for quantitative evaluation of cell number and distribution within a tissue scaffold.

The techniques for cell counting and distribution mapping could be used to study some of the limitations of this work, such as the effect of pore size on cell growth when using various cell types. More generally, they could be used to study cell ingrowth into scaffolds implanted *in vivo* after explantation or the effect of the incorporation of a growth factor on cell proliferation.

6.1.3 Research Aim #3: Multi-Material Tissue Scaffolds

The goal of the third research aim was to use the selective placement of dissimilar materials in a single scaffold to allow spatial control over the adhesion and proliferation of cells within the

scaffold. Spatial control over the placement of cells within a scaffold is essential for the generation of vasculature. While true vasculature requires the formation of tubular networks coated with a thin layer of endothelial cells, spatial control over cell adhesion and proliferation could be used more simply to mimic the effects of vasculature. In addition, the function of complex multi-cellular tissues depends on the location of various cell types with respect to one another. These two challenges, along with a growing interest in multi-material structures fabricated by AM, present a strong case for an approach to spatial control of cell adhesion and proliferation based on multi-material tissue scaffolds.

Research Question #3

How can multiple dissimilar materials be used to spatially control cell adhesion and proliferation in porous tissue scaffolds fabricated with VP?

The approach to spatial control over cell adhesion and proliferation consisted of fabricating multi-material tissue scaffolds from one material which encouraged cell adhesion and a second which prevented adhesion. Initially, a NaAMPS-based resin was selected as the cell adherent material (see Chapter 3) and PEGDA chosen to prevent cell adhesion. Both resins were known to be printable with VP and could be fabricated into tissue scaffolds with small feature sizes. The basic approach for multi-material VP is simple: print material #1, clean and change materials, print material #2, repeat. The unfortunate reality is that multi-material VP is not presently a trivial endeavor and no commercially available solutions exist. However, there is growing interest in developing multi-material VP systems. Several groups have recently published reports on the development of such systems, some with the specific intent to fabricate multi-material tissue

scaffolds (see Section 5.2). The lack of commercially available solutions for fabricating multi-material tissue scaffolds with VP led to the formation of Development Objective 3.1.

Development Objective 3.1

Develop a system or techniques through which VP can be used to fabricate multi-material parts.

A lab-built VP system designed for the fabrication of tissue scaffolds used in Chapters 3 and 4 was available, but its design presented significant challenges for the fabrication of multi-material tissue scaffolds. The lab-built VP system fabricates on an unconstrained surface ('top-down'), thus it is essential for the resin level to be controlled very precisely during the entire print to ensure the layers fabricated are of the intended thickness. This does not present a challenge in single material printing, however, substantial difficulties arise when switching between materials. In fact, significant efforts were made in controlling resin level during multi-material prints before the use of a constrained surface ('bottom-up') system became favored. Rather than develop an entirely new constrained surface VP system, the Autodesk Ember, a commercial system, was selected due to the control over a large number of both basic and advanced fabrication parameters available to the user. In addition, this system is capable of relatively high resolution and small feature sizes.

The multi-material printing process with the system chosen requires three datasets of information from the user: a stack of images for projection, the print parameters, and information for when the print parameters for a given layer should diverge from the original parameters. These first two are common to all mask projection VP systems. The third dataset instructs the printer to use, for example, a long exposure time for a second material. This data also permits two materials to be

printed in the same layer. After part of the layer is printed with a first material, the process is paused to permit cleaning and material exchange. The dataset simply indicates that the next layer will have zero thickness, returning the build platform to the identical location where the first part of the layer was printed. The remainder of the layer is then exposed and fabricated. Procedures in Chapter 5 also explain the cleaning and material exchange processes that were developed. While the steps and parameters detailed here are not part of the Autodesk Ember's graphical user interface, all of the techniques described can be performed by the relatively advanced user.

The process for multi-material tissue scaffold fabrication developed in this work has several advantages over other systems reported in the literature. The cost of the hardware used in the techniques developed here is perhaps an order of magnitude smaller than that of lab-built systems. In addition, no physical modifications were made to the printer. Other systems require substantial expertise in machine building and optics. They may also require sophisticated pumping systems or the development of microfluidics chips. Finally, no custom code was written for the machine. Using these methods, both simple and complex multi-material geometries were printed from resins with either strong or weak cell adhesive properties.

- Techniques were developed that allowed for the successful fabrication of complex multi-material tissue scaffold using the Autodesk Ember VP system. The techniques developed with the commercially available system offer several advantages over other multi-material VP systems reported in the literature: a substantial reduction in cost, the avoidance of complex machine building, and the absence of custom code or software.

I expect that these developments will help foster the more widespread use of VP for multi-material fabrication, particularly for applications in tissue engineering. While these techniques were successful in permitting the fabrication of multi-material parts, there are important material limitations. Not all photocurable materials will be compatible with the multi-material process and, perhaps more importantly, dissimilar materials will not always be compatible with each other. Challenges arising from the properties of the materials used for multi-material scaffold fabrication led to a Supplemental Research Question aimed at helping to elucidate the effects that material properties have on the fabrication process.

Supplemental Research Question 3.2

What are the material considerations for fabricating multi-material tissue scaffolds with VP?

Multi-material tissue scaffold fabrication imparts additional material constraints to those that already exist for VP. As in all constrained surface VP systems, the photopolymerized material must be sufficiently strong to withstand peel forces generated during layer recoating. Many materials used for the fabrication of tissue scaffolds are hydrogels, which are often much weaker than the acrylate-epoxy photopolymer systems sold for use with commercial VP systems. More significantly, it was found that swelling of photopolymerized gels and the swelling ratio between dissimilar materials used for the fabrication of a single part had substantial effects on fabrication outcomes. Swelling of partially printed scaffolds during cleaning typically caused complete delamination of the part from the build platform. This was due to an uptake of solvent (e.g., water, ethanol) by the part, causing the buildup of shear stresses between the part and platform. Solvents were eschewed in preference of cleaning with compressed air and absorbent wipes. It is also

possible to clean the partially printed part with the resin which will be used for subsequent layers. If swelling during cleaning did not cause print failure, it would subsequently affect build quality as swollen pillars were no longer in the same place nor the same size. However, fabrication would continue as if the part geometry were unchanged. A swelling mismatch between the materials used for multi-material fabrication can also cause part failure or distortions. Evidence of this can be seen in parts fabricated with NaAMPS and PEGDA (Chapter 5). Substantially greater swelling of the sections fabricated from NaAMPS caused a change in shape and placed stress on the interface between the two materials. In fact, the swelling mismatch between the two materials was so significant that more complex parts could not be fabricated using the two resins. In an effort to fabricate more complex multi-material tissue scaffolds, additional resins were formulated that had more comparable swelling ratios. The addition of HEMA to a PEGDA-based resin was used to achieve similar swelling to a resin based on soybean oil epoxidized acrylate ('Soy'). While a mismatch nonetheless persisted, the swelling of the two materials were sufficiently similar so as to permit the fabrication of both simple and complex multi-material geometries. These results highlight the importance that material properties, particularly material swelling ratios, play in the multi-material fabrication process.

- Swelling ratio mismatch between materials used in multi-material tissue scaffold fabrication with VP cause deviations from intended part geometry or part failure. Swelling of partially fabricated scaffolds in solvent during cleaning steps while material exchange is taking place can cause part delamination from the build surface and print failure.

The successful fabrication of both simple and complex geometries from materials suitable for multi-material tissue scaffolds permitted an investigation into whether spatial control of cell adhesion and proliferation could be achieved. Seeding and culturing murine fibroblasts on simple multi-material tissue scaffolds showed that the overwhelming majority of cell adhesion and proliferation occurred on the material designed to encourage adhesion and proliferation. A subsequent study was conducted on a more complex tissue scaffold containing tubular networks embedded within a porous tissue scaffold made from a separate material. This experiment successfully demonstrated the spatially selective proliferation of cells in a structure mimicking vasculature.

- Spatial patterning of multiple materials with VP can successfully be used to control cellular adhesion and proliferation in tissue scaffolds. The control over adhesion and proliferation permitted the generation of acellular tubular networks within scaffolds upon which substantial cellular adhesion and growth had occurred, mimicking vasculature.

The generation of vasculature in thick tissue engineering constructs remains the greatest challenge facing the field of tissue engineering. The strategies developed for multi-material scaffold fabrication and resulting spatial control over cell adhesion and proliferation they provide present a substantial step in addressing this challenge. The use of multi-material VP tissue scaffolds to control cell adhesion and proliferation in porous tissue scaffolds, which has not been previously demonstrated, will enable the fabrication of more complex constructs that will mimic the structure and function of native tissue.

6.2 Suggested Future Work

While investigating the ways in which scaffolds can be designed to direct cell response in VP-fabricated tissue scaffolds, several limitations were encountered and new areas of interest identified. Potential avenues for further development were identified and are described in this section.

6.2.1 Investigating and Enhancing Degradation Rates of NaAMPS-based Resins

While the NaAMPS-based resin reported in this work has many advantageous properties, especially when compared to some other resins reported in the literature, its primary drawback is its lack of rapid degradability. Stability of the scaffolding material is required to support cells during their growth and proliferation, but after a period of between several weeks to a year (depending on the size and tissue type), cells will have secreted structural proteins and the scaffold will no longer be needed. At this point, it is desirable for bioabsorption of the scaffold to occur. This allows cells to remodel their environment and in effect create *de novo* tissue. Unfortunately, hydrolytic degradation of PEGDA is slow and the acrylamide linkages formed during the photopolymerization of NaAMPS are known to be quite stable.

Future work should investigate the long term degradation rates of the NaAMPS-PEGDA gels in a physiologically relevant environment. This rate is expected to be insufficient for the generation of ‘scaffold-free’ tissues of many types. A possible approach to accelerate this rate is to incorporate moieties into the resin which impart additional degradability, for example, through hydrolysis. The viability of this technique was recently demonstrated by our group. Similarly, the addition of small quantities of natural polymers to the resin could also help to increase degradation and bioabsorption without significantly impacting the resin’s print properties. It is also important that the cytotoxicity of any molecules released during degradation should be evaluated. Molecules into which materials degrade can sometimes impart cytotoxicity, even when the material in its stable form does not display such character.

6.2.2 Investigating the Effect of Large Pore Sizes on Cell Growth and Distribution Over Time

Our results show that larger pore sizes are more effective in promoting cell proliferation and the generation of homogeneous cell densities in thick tissue scaffolds. However, the generalizability of this result is constrained by certain limitations of the study performed, as described in Section 6.1.2. Additional studies should include even larger pore sizes (e.g., 700-800 μm) to determine a more specific range at which growth and proliferation are maximized. In addition, useful insights on how distributions in cell densities form over time could be gleaned from a study that incorporates multiple time points (e.g., 1, 2, and 4 weeks).

6.2.3 Development of Multi-Cellular Tissue Constructs from Multi-Material Tissue Scaffolds

In this work, the ability to use multi-material tissue scaffolds to control the spatial adhesion and proliferation of cells was successfully demonstrated. This success opens up many new possibilities related to the development of vasculature and the generation of tissue constructs with multiple cell types. Future work should investigate whether multiple materials can be used to spatially pattern more than one cell type in a single scaffold. For example, the spatial separation of endothelial cells into tube-like structures within a matrix populated with osteoblasts would result in a tissue construct that approximates the physiology and structure of natural bone tissue. Of course, this would still be somewhat simpler than natural bone, which contains many cell types. Despite this, such a development would be extremely significant and have wide ranging effects on the entire field of tissue engineering.

A second approach to creating tissue constructs with many cell types leverages the pluripotency or multipotency of stem cells. Rather than pattern terminally differentiated cells, a stem cell would be seeded across the entire tissue scaffold. The multi-material tissue scaffold, rather than having materials that influence cell adhesion, would contain materials or molecules that influence cell differentiation. For example, basic fibroblastic growth factor (bFGF) and bone morphogenetic protein 2 (BMP-2) are known to mediate the differentiation of bone marrow stromal cells (BMSC) into osteoblasts and stimulate bone formation. However, upon exposure to a variety of other growth factors, BMSCs have been shown to differentiate into neuronal and glial-like cells. While the use of growth factors in mediating stem cell differentiation is an area of active research, significant potential exists for their use in spatially controlling the differentiation of stem cells in multi-material tissue scaffolds to generate tissue constructs with multiple cell types.